LARGE PORE MESOPOROUS SILICAS FOR APPLICATION IN PROTEIN ADSORPTION, ENZYME IMMOBILISATION AND DRUG DELIVERY

Lyndsey Kay Ritchie

A Thesis Submitted for the Degree of PhD
at the
University of St Andrews

2009

Large Pore Mesoporous Silicas for Application in Protein Adsorption, Enzyme Immobilisation and Drug Delivery

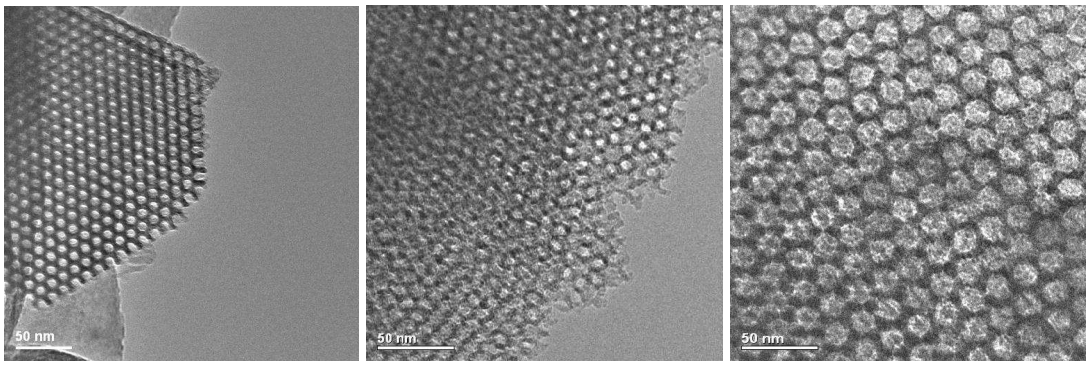

A thesis presented for the degree of
Doctor of Philosophy
in the faculty of science of the University of St. Andrews
by Lyndsey Kay Ritchie, BSc (Hons) AMRSC

September 2008

University
of
St Andrews

Declarations

I, Lyndsey Kay Ritchie, hereby certify that this thesis, which is approximately 49 000 words in length, has been written by me, that it is the record of work carried out by me and that it has not been submitted in any previous application for a higher degree.

I was admitted as a research student in October 2004 and as a candidate for the degree of PhD in October 2005; the higher study for which this is a record was carried out in the University of St Andrews between 2004 and 2008.

Date …… signature of candidate ……

I hereby certify that the candidate has fulfilled the conditions of the Resolution and Regulations appropriate for the degree of PhD in the University of St Andrews and that the candidate is qualified to submit this thesis in application for that degree.

Date …… signature of supervisor ……

In submitting this thesis to the University of St Andrews we understand that we are giving permission for it to be made available for use in accordance with the regulations of the University Library for the time being in force, subject to any copyright vested in the work not being affected thereby. We also understand that the title and the abstract will be published, and that a copy of the work may be made and supplied to any bona fide library or research worker, that my thesis will be electronically accessible for personal or research use unless exempt by award of an embargo as requested below, and that the library has the right to migrate my thesis into new electronic forms as required to ensure continued access to the thesis. We have obtained any third-party copyright permissions that may be required in order to allow such access and migration, or have requested the appropriate embargo below.

The following is an agreed request by candidate and supervisor regarding the electronic publication of this thesis:

Embargo on both the printed copy and electronic copy for the fixed period of 1 year on the following ground:

publication would preclude future publication

Date …… signature of candidate …….

signature of supervisor ……

Acknowledgements

I would first like to take this opportunity to thank my supervisor Dr. Paul A. Wright for his support, encouragement and continual enthusiasm throughout this project and for allowing me to undertake this project.

In learning new characterisation techniques I would like to thank: Mrs. Sylvia Williamson (University of St. Andrews) for training in Gas sorption measurements; Drs. Robbie Hodgkins, Wuzong Zhou and Calum Dickinson for all their help in electron microscopy.
For all their help with enzyme immobilisation Drs. Graham Smith and Nigel Botting (University of St Andrews) and drug release studies Prof Maria Vallet-Regí and Dr Miguel Manzano (Universidad Complutense de Madrid).

I would like to thank past and present members of the Wright group, especially Rob, Jorge and Stuart and also my friends in the chemistry department for keeping me sane. So in no particular order, thank you to: Lynn, Lynzi, Dave, Jono, John, Ilaria, Michael, Jen, Ed, Ben, Luke, Neil, Aoife, Natalie, Matt, Neal, Charlotte, Gavin and Lydia (an honorary ‘c word’)

Special thank you to Stephen, for never letting me give up and for always being there.

Finally I would like to thank my family for their support throughout my studies.

Dedication

This thesis is dedicated to David Ritchie.

Abstract

A range of mesoporous materials based on SBA-15, KIT-6 and FDU-12 have been prepared using neutral block copolymers Pluronic P123 and F127 and characterised using methods including electron microscopy and nitrogen adsorption. Typically the materials have a hexagonal (p6mm) or cubic (Fm3m and Ia-3d) symmetry and pore geometry and are rendered porous by either calcination or solvent extraction. Organic functional groups were incorporated into the silica walls of the materials by co-condensation in the form of propyl thiols and additives in the form of alkanes were added to control pore size and geometry.

The effects of temperature, additives, organic functionalisation, synthesis time and sol-gel composition were investigated and the resulting materials were tested as supports for protein adsorption, enzyme immobilisation, and drug delivery.

Two FDU-12 materials of differing entrance and cavity sizes were used to adsorb a range of proteins with molecular weight 17 to 160 kDa to determine if there was a size exclusion effect. It was seen that the larger pore material was able to adsorb proteins of a larger size (molecular weight 105 kDa) and an exclusion effect was observed when the dimension of the proteins became too great (larger than 130 kDa). There was no clear trend for the smaller pore material where each protein was adsorbed to some extent by the material but apart from the smallest protein, myoglobin, mainly on the surface and not within the pores.

The adsorption of the lipase B from Candida Antartica, CALB, was studied on a range of mesoporous supports with their templates removed by either calcination or extraction. The effect of pore size and functionalisation was investigated in terms of maximum loading and rate of loading. By functionalising the KIT-6 material the maximum loading of CALB was reduced from 45.5 to 32 mg/g whereas functionalising the FDU-12 material increased the maximum from 33 to 42.5 mg/g. The activity of the immobilised CALB was measured by enantioselective transesterification of (R)-1-phenylethanol in methyltetrabutyl ether (MTBE). The effect of loading, surface functionalisation and reusability in organic media

were investigated. Functionalisation with propyl thiol was seen to increase the rate of conversion after 30 minutes for both KIT-6 and FDU-12 materials.

Selected FDU-12 and KIT-6 materials with window sizes from 6 to 12 nm and with and without functionalisation were used to carry out a drug release study using Bovine serum albumin (BSA). BSA was loaded onto the material and the uptake quantified using nitrogen adsorption, elemental analysis, and thermogravimetric analysis. The release of BSA into simulated body fluid at 37 ^{o}C was measured using HPLC. Functionalisation was seen to have little effect. The type of cubic morphology controlled the rate at which the BSA was released. The KIT-6 3D channel material exhibited a burst release initially followed by a steady release of BSA whereas the mesocage FDU-12 material had a slower and more linear release profile, closer to that desired.

Abbreviations

1D	1-dimensional
2D	2-dimensional
3D	3-dimensional
µL	Microlitre (1 x 10^{-6} L)
a	Unit cell parameter
Å	Angstroms (10^{-10} m)
ABAB	Hexagonal stacking sequence of close packed spheres
ABCABC	Cubic stacking sequence
BET	Brunauer-Emmett-Teller calculation of surface area (m^2g^{-1})
BJH	Barrett-Joyner-Halenda calculation of pore size distribution
c	Unit cell parameter
℃	Degrees celsius
CALB	Candida Antarctica Lipase B
CLEA	Cross-linked Enzyme Aggregate
CCD	Charge coupled devices
ccp	Cubic close packed
CHN	Elemental analysis (wt%) for carbon, hydrogen and nitrogen
CMC	Critical micelle concentration
CMK	Carbon mesostructured materials (from KAIST)
Cn-s-1	Divalent quaternary ammonium surfactant of n carbons within the tail and s carbon atoms between the ammonium groups
CTAB	Cetyltrimethylammonium bromide (16 carbons in the surfactant tail)
d_{hkl}	Interplanar spacing
DDS	Drug delivery system
eV	Electron volts
F127	Pluronic F127 (triblock polymer PEO-PPO-PEO)
fcc	Face centred cubic
FDU	Fudan University
FFT	Fourier Transform
FSM	Folded sheet mesoporous materials
g	Surfactant packing parameter

g	Gram
GC	Gas chromatography
GI	Glucose Isomerase
GOx	Glucose Oxidase
h	Hour
hcp	Hexagonal close packed
HRTEM	High Resolution Transmission Electron Microscopy
IGA	Intelligent gravimetric analysis
IR	Infra red spectroscopy
K	Kelvin (temperature unit)
LCT	Liquid crystal template mechanism
m	Meter
MCF	Meso-cellular foam
MCM-	Mobil Composition of Matter –
mg	Milligram (1×10^{-3} g)
min	Minute
MPTES	3-Mercaptopropyltriethoxysilane
nm	Nanometre
P123	Pluronic 123 (triblock polymer PEO-PPO-PEO)
P	Pressure (bar)
Po	Saturated vapour pressure (bar)
PEO	Polyethylene oxide
PPO	Polypropylene oxide
PSD	Pore Size Distribution
SBA-	Santa Barbara–
SBF	Simulated Body Fluid
SDA	Structure directing agent
SEM	Scanning electron microscopy
STA-	St Andrews-
STAC-1	St Andrews Cambridge–1
STP	Standard temperature and pressure (0 °C, 1 atm)
TEOS	Tetraethylorthosilicate, $Si(OEt)_4$
TGA	Thermal gravimetric analysis
TMB	Trimethylbenzene

UV-Vis	UV-Visible spectroscopy
V	Volume (dm^3 or ml)
V_m	Monolayer volume
XRD	X-ray Diffraction

Contents

Aims

The aim of this project was to investigate the structural chemistry and possible applications of mesoporous solids templated by non-ionic triblock copolymers and functionalised *in situ* during their synthesis. To achieve this aim we set out the following objectives:

- To synthesise a range of mesoporous silicates based on SBA-15, KIT-6 and FDU-12, including those functionalised *in-situ* by the co-condensation with mercaptopropyl triethoxysilane;

- To characterise fully the materials, once rendered porous, using a combination of techniques including electron microscopy and porosity measurements;

- To determine the effect on performance in protein adsorption, enzyme immobilisation protein release of
    - Structure type
    - Particle Morphology
    - Functionalisation of internal surface

- To adsorb a range of proteins of varying molecular weights ranging from 17 to 160 kDa onto FDU-12 materials to examine their pore entrance sizes and compare these with nitrogen adsorption results.

- To utilise the mesoporous materials as supports for the immobilisation of CALB and investigate their catalytic properties in organic solvent.

- To carry out a ‘drug release’ study using Bovine serum albumin as a model protein compound on a range of FDU-12 and KIT-6 materials with different pore sizes and with and without thiol functionalisation.

1. Introduction

1.1 Porous Silicas: Natural Inspiration and limitations of zeolites

Silica can be found in nature in open frameworks with porosities from the ‘micro’ scale (pore sizes less than 2 nm) to the ‘macro’ scale (pores greater than 50 nm) : the ability to reproduce these synthetically in the form of micro, meso or macroporous solids is of great benefit to the development of technologies. On the macroscale in nature, for example, diatoms are microscopic single-celled algae that inhabit fresh- and saltwater bodies throughout the world. Tens of thousands of different diatom types exist with beautiful symmetric geometries and intricate nanoscopic features in their porous silica shells (seen in Figure 1.1). A characteristic feature of diatom cells is that they are encased within a unique cell wall made of silica (hydrated silicon dioxide) giving beautiful and ornate structures. Diatoms generate their cell walls by silica biomineralization. The cell walls are composed of silica and organic macromolecules and show a complex structure with porosity in the 100 nm range.

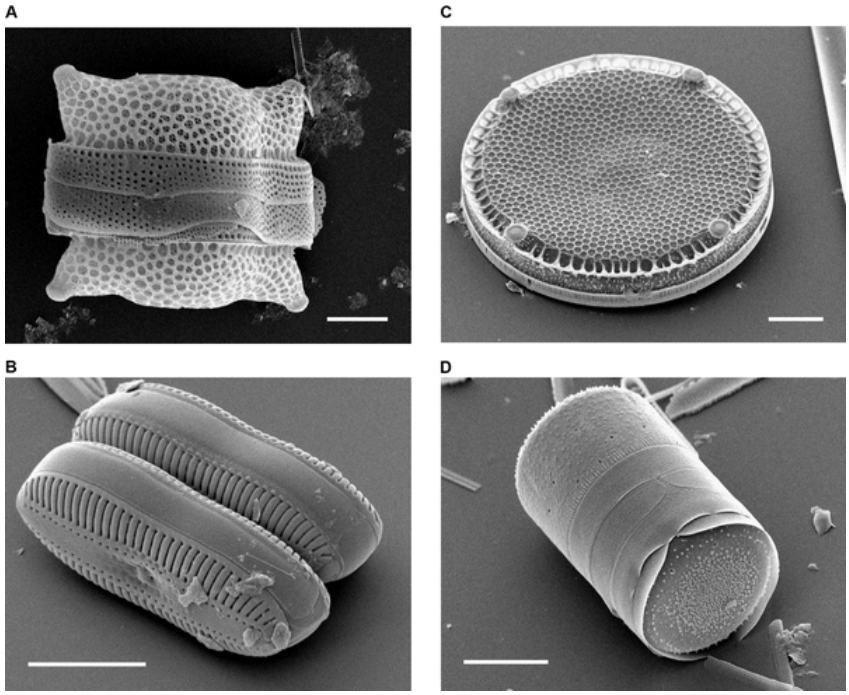

Figure 1.1 Some examples of diatoms found in nature. (Scale bar = 10 micrometers)[1]

At the lower end of the size range, zeolites are microporous minerals assembled from SiO_4 tetrahedral building blocks linked together to form frameworks with channels and cavities of dimensions ≤ 10 Å. They are thermally stable and can have high surface areas. Over 150 structure types are known, 48 of which are naturally occurring (but often in small quantities and mixed with other minerals). They have a wide range of applications, for example in ion exchange, catalysis and adsorption, which can be seen in Table 1.1. Zeolites are commonly described as molecular sieves due to their ability to selectively sort molecules based on size exclusion, derived from their regular sub-nanometre pore structure. The maximum size of the molecular or ionic species that can enter the pores of a zeolite is controlled by the free diameters of the windows.

Table 1.1 Applications for zeolites

Area	Applications
Commercial and Domestic	Ion-exchange beds in domestic and commercial water purification Removal of H_2O, CO_2 and SO_2 from low-grade natural gas stream
Petrochemical industry	Fluid catalytic cracking and hydro-cracking
Agriculture	Clinoptilolite (a naturally occurring zeolite) is used as a soil treatment. It provides a source of slowly released potassium
Medical	Zeolite-based oxygen generation systems are widely used to produce medical grade oxygen
Heating and refrigeration	Zeolites can be used as solar thermal collectors and for adsorption refrigeration
Detergents	The largest outlet for synthetic zeolite is the global laundry detergent market. This amounted to 1.44 million metric tons per year of anhydrous zeolite A in 1992

In the last few decades, porous, silica-based materials have been used for an increasing variety of applications such as catalysis in the petrochemical industry **[2],** as sorbents in gas separation and in the synthesis of chemical and pharmaceutical products. So far the majority of these applications tend to use microporous materials which have pore sizes of approx 0.6-1.0 nm and possess the catalytically desirable properties of high surface area, adjustable pore size, hydrophilicity, acidity and high thermal and chemical stability. Problems arise when the molecules requiring separation/catalysis are larger, for example

bio-macromolecules such as proteins which are typically 3-30 nm in size. This limits the use of zeolites in biotechnology and presents a need for the development of material with larger pores, in the mesoporous region (20-500 Å).

1.2. History of mesoporous solids

Porous solids can be classified into three categories, according to the IUPAC **[3]** definition: microporous materials which have pore sizes less than 20 Å, mesoporous materials which have pore sizes between 20 – 500 Å, and macroporous materials with pore diameters greater than 500 Å, examples of which can be seen in Figure 1.2.

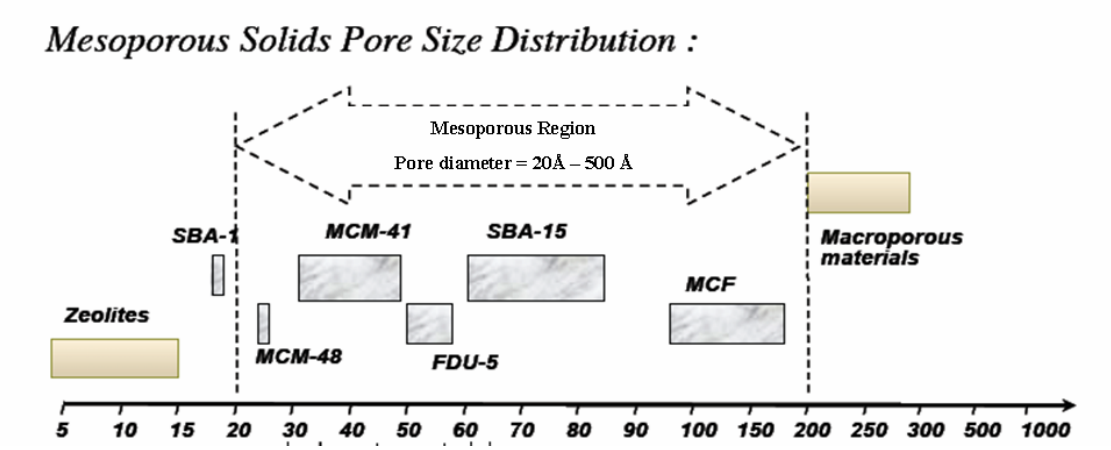

Figure 1.2 Schematic diagram of selected mesoporous solids and their pore diameters

The first group to synthesise and report ordered silica materials with porosity on the meso scale was the group of Beck *et al.* at Mobil in 1992 **[4,5]**. The material was subsequently patented as MCM-41**[6]**. Around the same time a group in Japan at Waseda University **[7]** detailed the synthesis of porous silica with a regular arrangement of pores between 2 and 4 nm. In fact the first patent in the area of mesoporous materials, before the Mobil patent **[6]**, was filed two decades earlier in 1971 by Chiola *et al.* **[8]**. TEOS (tetraethylorthosilicate) was hydrolysed and condensed in the presence of a cationic surfactant to form what they described as 'low bulk density silica'. However characterisation of that material was not reported and it was not until more than 25 years later that Di Renzo *et al.* **[9]** carried out the synthesis and found the product possessed many of the characteristic properties of well-

ordered mesoporous silica, such as the MCM-41 synthesised by Mobil. Not only was the work of Chiola *et al.* a forerunner to the synthesis of MCM-41 but it was also a very early example of using surfactants as 'templates' to synthesise well-ordered materials with larger pore sizes than zeolites.

Traditional zeolite synthesis commonly utilises structure directing agents or 'template' molecules and so the development of these larger pored mesoporous silica material is a continuation of this concept. Rather than a single small molecule, a group of molecules in the form of a micelle or a polymer acts as the template *via* 'Liquid Crystal Templating' (LCT) or related routes, described in section 1.3. Along with these routes there are many other approaches reported for the synthesis of mesoporous silicates. Yanagisawa *et al.* **[7]** demonstrated that such materials could be prepared *via* hydrothermal treatment of layered silicates, including the sodium silicate kanemite, in the presence of alkyltrimethylammonium surfactants. By adjusting the synthesis it is possible to improve the ordering within the material to produce a mesoporous material possessing a hexagonal arrangement of pores similar to MCM-41. Although both the LCT pathway and the use of layered silicates result in mesoporous silicates, the formation mechanisms differ, with MCM-41 formation involving surfactant-silicate liquid-crystalline arrays described in more detail in section 1.3. The 'layered silicate' route proceeds *via* intercalation of the surfactant cations and retention of the silicate layer. Materials prepared using this second route are less ordered, with broader pore size distribution and lower sorption uptakes than those prepared using the LCT method, such as MCM-41.

Synthesis of the silica-based mesoporous material, M41S **[4]**, opened the way for the synthesis of materials with differing structure and morphology. The first structures to be reported were MCM-41, a hexagonal structure, followed by a lamellar (MCM-50) and a cubic (MCM-48) structure: many others have followed.

The synthesis of mesoporous solids opened up many opportunities, with the initial materials possessing regular arrays of pores up to 4 nm in diameter. Some 6 years later, extra large pore mesoporous solids such as SBA-15 (pores up to 8-10 nm) and FDU-12 (with cages up to 16 nm in diameter) were prepared. Early work focused on using these materials for catalytic applications, such as supports for organometallic complexes, and it was not until recently that these materials became popular as supports for larger biomolecules, such as enzymes. They have many potential applications, some of which can

be seen in Table 1.2, including separation and adsorption, as catalyst supports, electrodes for fuel cells and in solar cells.

Table 1.2 Potential applications of mesoporous silica

Potential Applications of Mesoporous Silica	
Adsorbents	Remediation of heavy metal ions by thiol functionalisation **[10]**
Optics	Fibre lasers **[11-13]**
Catalysis	Silica-alumina-MCM-41 (Propene oligomerisation – gasoline and middle distillates production: C_9 and C_{12} hydrocarbon selectivity) **[14]**
	Ti-containing silica – selective oxidation **[15,16]**
	Chiral catalysis **[17,18]**
	Bimetallic hydrogenation **[19,20]**
Low dielectric constant insulators	Computer microchip **[21-24]**
Alternative to silica in above	Mesoporous carbon **[25,26]**

1.3 The surfactant templating route to mesoporous silica

The breakthrough discovery of well defined mesoporous solids (materials which have at least one pore dimension in the range 2-10 nm) achieved by Mobil **[7]** opened a new field of research in material science**.** Subsequently the synthetic route has been extended to give a range of different structure types of silica and also to non-siliceous mesoporous materials. The discovery of these materials possessing well defined arrays of pores with a narrow size distribution gave several scientific groups the motivation to work in this field and produce a range of materials with varying morphology and pore topology by understanding and refining the synthesis. Among the largest involved in this area is the group of Stucky from the University of California at Santa Barbara who have synthesised a range of materials denoted SBA-n **[27-29]** using different surfactants and reaction conditions, and the groups of Zhao at the University of Fudan, China and Ryoo at the Korea Advanced Institute of

Science and Technology who have synthesised series of solids designated FDU-n **[30-33]** and KIT-n **[34-36]** respectively.

Surfactants, which have the ability to self-assemble into well-defined meso structures or micelles, can be used as templates for the design and synthesis of inorganic materials with nanosized dimensions. A typical route is to hydrolyse a silica precursor such as tetraethylorthosilicate (TEOS) under controlled conditions of pH and temperature and in the presence of a surfactant, giving rise to a mesoporous (template-containing) silicate. Hydrolysis of the precursor molecule, which initiates polymerization, can be carried out in either basic or acidic conditions.

Figure 1.3 shows the liquid crystal templating (LCT) mechanism, proposed by Beck *et al.* **[5],** which is based on the interaction between ordered organic micellar phases and the inorganic precursor.

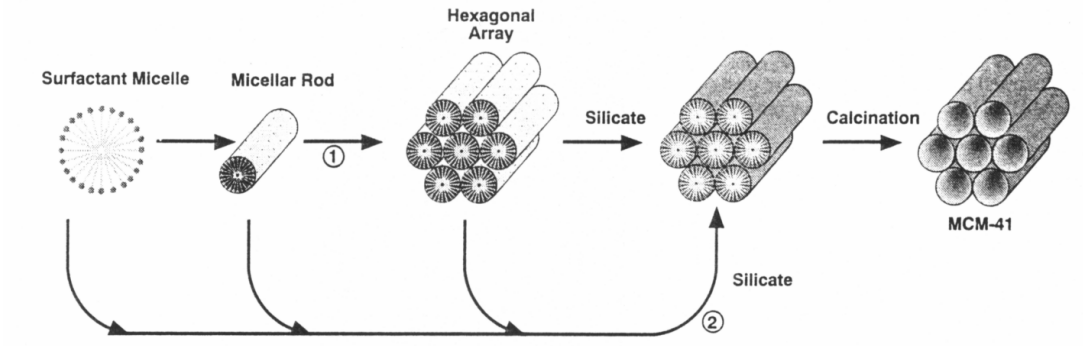

Figure 1.3 The LCT proposed mechanism for the synthesis of MCM-41 by Beck *et al.* [5] Pathway 1 shows the liquid crystal phase is present before the addition of the silicate species whereas pathway 2 shows that the addition of the silicate species itself is the driving force behind the subsequent silicate encased surfactant micelles

This mechanism was first proposed by Beck *et al.* in 1992 for the formation of the M41S materials. They propose that unlike the case of zeolite formation where silica condensation occurs around a template cation the formation of these M41S materials is due to the organisation of the surfactant molecules into micellar liquid crystals which in turn act as templates for silicate aggregation. The silica is in the form of a complex mixture of molecular and polymeric anionic species which exhibit control over the LC phase and they propose two possible pathways; that either the liquid crystal phase is present before the addition of the silicate species (shown as pathway 1 in Figure 1.3) or that the addition of

the silicate species itself is the driving force behind the aggregation of the subsequent silicate-encased surfactant micelles (pathway 2). The second mechanism is favoured and supported by the work of Davis *et al.* **[37]** who show *via* NMR studies that pathway 1 is absent in the formation of the molecular sieve throughout the sol-gel procedure. It is widely accepted that the second pathway is correct as the concentrations of surfactant used for the synthesis of MCM-41 are unlikely to form the necessary liquid crystal phase without the addition of a silicate anion.

An alternative model has been proposed by Stucky **[38]** in which the formation of the silica mesophase is divided into three steps; Multidentate binding of the silicate oligomers to the cationic surfactant; Preferential silicate polymerisation in the interface region; and charge density matching between the surfactant and the silicate.

1.4 Mechanisms

The synthesis used within this work is generally a 2-step synthesis consisting of a hydrolysis step followed by a condensation step. In the first step the silica source is hydrolysed with the alkoxy ligands attached to the atom Si being removed by hydrolysis under acidic or basic conditions.

$$Si(OR)_4 + H_2O \rightarrow HO\text{-}Si(OR)_3 + ROH$$

The synthesis described in this work is carried out under acidic conditions where the tetraalkoxysilane is hydrolysed with the alkoxy group being protonated which causes the electron density to move away from the Si atom. This then allows the oxygen of the water to attack *via* nucleophilic substitution and deprotonation follows *via* the removal of the alkoxide group, which leaves the silicon tetrahedral with three (-OR) ligands and a SiOH silanol group. The mechanism is shown in Figure 1.4 (a) below. It is also possible for the synthesis to be carried out in basic conditions whereby the hydroxyl (OH^-) ion acts as a nucleophile towards silicon (Figure 1.4 (b)) **[39]**

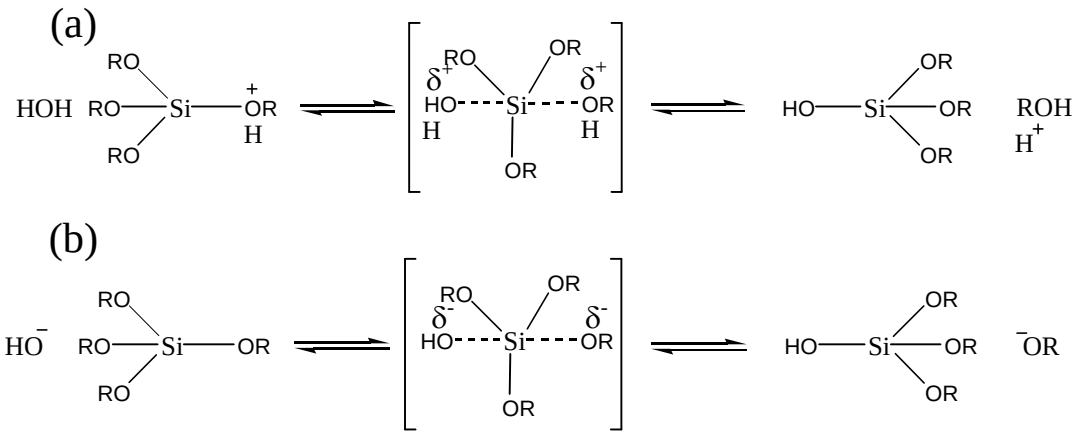

Figure 1.4 The hydrolysis step of a tetraalkoxysilane undertaken in either (a) acidic or (b) basic conditions

After the silicon has been hydrolysed it undergoes condensation **[40]**:

$$(RO)_3SiO^- + Si(OH)_4 \rightarrow (RO)_3Si\text{-}O\text{-}Si(OH)_3 + OH^-$$

Using acidic conditions a nucleophilic attack is also the pathway to forming Si-O-Si bonds. Silicon which is more electrophilic is formed *via* protonation and this is more vulnerable to nucleophilic attack, detailed in Figure 1.5(a). Under basic conditions the silanol groups are deprotonated forming negatively charged silica species (as shown in Figure 1.5 (b)).

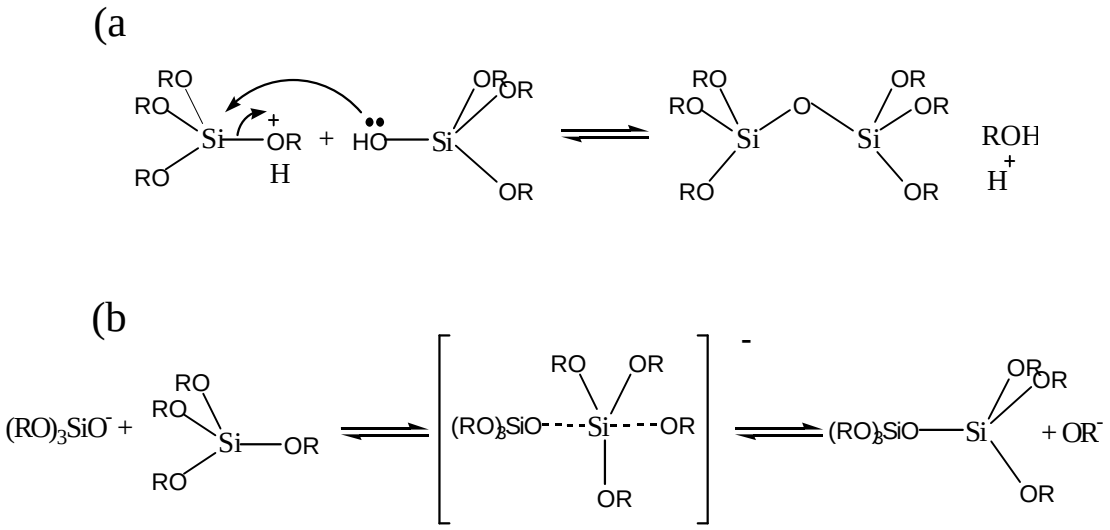

Figure 1.5 Condensation of the silanol group to form the Si-O-Si bond under acidic conditions (a) and basic conditions (b).

The various proposed mechanisms of the formation of mesoporous solids are given in Table 1.3, indicating the synthesis conditions including the surfactant type, pH and resulting structures. S^+ denotes cationic surfactant and I the condensed inorganic silica which can have a positive or negative charge. X^-, a counter-ion of appropriate charge balances the charges of the cationic surfactant and inorganic silicate species when working in acidic media below the isoelectric point of silica (pH < 2) where the silica species is protonated. Non-ionic surfactants, such as PEO_x-PPO_y-PEO_x ;PEO = polyethylene oxide; PPO = polypropylene oxide, where S^0 denotes the neutral surfactant can be protonated under acidic conditions.

Zhao *et al.* **[28]** proposed that the assembly of mesoporous silica under acidic conditions occurs through a (S^oH^+) (X^-I^+) pathway, where S is the neutral surfactant, X^- is the halide anion and I^+ is the protonated Si-OH moiety. They postulate that the alkoxysilane species is first hydrolysed

$$Si(OEt)_4 + nH_3O^+ \xrightarrow[pH<2]{hydrolysis} Si(OEt)_{4-n}(OH_2^+)_n + nEtOH$$

before partial oligomerisation at the silica

$$REO_m + yHX \xrightarrow{H_2O} REO_{m-y}[(EO)\cdot H_3O^+]_y \cdots yX^-$$

R=alkyl or poly (propylene oxide)

X^- = Cl^-, Br^-, I^-, NO_3^-, $H_ySO_4^{-2+y}$, $H_yPO_4^{-3+y}$

Table 1.3 Mechanisms for the synthesis of mesostructured solids

Mechanism	Surfactant type	Synthesis pH	Mesophase structures and symmetries
S^+I^-	Cationic	Basic	MCM-41 (p6mm), SBA-2 ($P6_3/mmc$,Fm3m)
$S^+X^-I^+$	Cationic	Acidic	SBA-1 (Pm3n), SBA-16 (Im3m)
S^-I^+	Anionic	5-10	AMS-n
$S^oH^+X^-I^+$	Neutral (block copolymers)	Acidic	SBA-15 (p6mm), FDU-5 (Ia-3d), FDU-12 (Fm3m), SBA-16 (Im3m)

1.5 Micelle formation

The **C**ritical **mi**celle **c**oncentration (**cmc**) is highly relevant to the formation of mesoporous solids synthesised using a surfactant templating method. It is defined as the concentration of surfactants in the bulk at which micelles start forming spontaneously. The hydrophobic parts of the surfactant pack together in a way which reduces their contact with water but the effects of electrostatic repulsion between the hydrophilic (polar) head-groups also have an effect on the way, and shape, in which the surfactants aggregate to form micelles **[41]**. The mesostructure formation occurs below the cmc and so addition of silicate species favours the formation and agglomeration of micellar structures.

The assembly of the surfactants gives rise to several possible geometries including lamellar (parallel stacks of bilayers), and cubic, as in Figure 1.6 **[42]**.

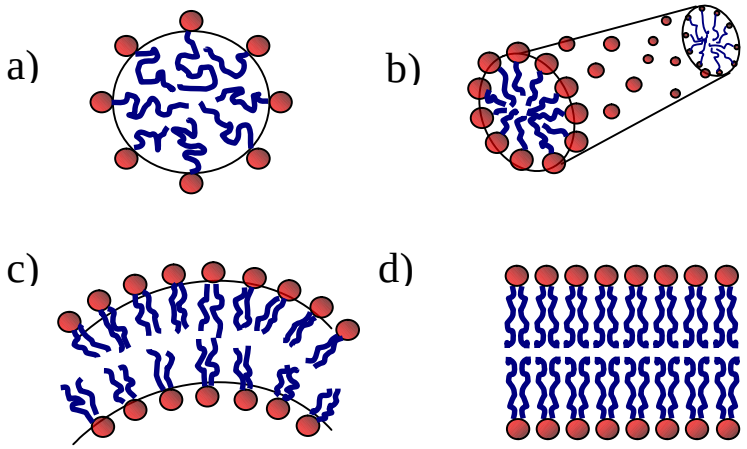

Fig 1.6 a) Spherical b) cylindrical c) flexible bilayers and d) planar bilayers (lamellar) [42]

The surfactant organization in amphiphilic liquid crystal arrays can be described in terms of the local effective packing parameter, $g = V/a_0l$, where V is the total volume occupied by the surfactant chains and any co-solvent organic molecules between the chains, a_0 is the head group area present at the micelle surface and l is the kinetic surfactant tail length or the curvature elastic energy. In micelle chemistry as the value of g is increased above critical values, mesophase transitions occur. When g increases it indicates the surface curvature decreases and the micelles have altered from spherical micelles to lamellar packing, which is shown in Table 1.4. $g < ⅓$ leads to the formation of spherical micelles, whereas $⅓ < g < ½$ favours cylindrical micelles and $g > ½$ forms parallel stacks of bilayers (lamellar).

Table 1.4 Surfactant arrangement depending on packing parameter

g	mesophase	Surfactant arrangement
1/3	Cubic (Pm3n)	Packed globular micelles
1/2	Hexagonal (p6m)	Hexagonally packed cylinders
1/2 - 2/3	Cubic (Ia3d)	Interpenetrating gyroid structure
1	lamellar	bilayers

1.6 Mesoporous structures available using templating method

A variety of mesoporous silica morphologies can be prepared by employing either a templating method or a phase transformation approach. Apart from typical particulate forms of materials such as MCM-41 it is possible to obtain mesoporous solids in the form of fibres and ropes, gyroids, hollow and solid spheres, films that are either supported or free standing and tubular or pillars within spheres. This array of possible morphologies is due to several factors:

(i) Silicate ions can act as counter ions to the cylindrical micelles which can organise into hexagonal liquid crystal arrangements.

(ii) Lyotropic surfactants can be exploited to form many differing meso-structures.

(iii) Fine tuning of the surface curvature is possible by changing compositions or reaction conditions which leads to the ability to control the hierarchical order of the material.
(iv)The self-organisation and siloxane bond formation process can be separately controlled.
A wide range of mesoporous silica structures are possible using a range of surfactants including cationic, anionic and block copolymers (discussed in section 1.7.2) and examples can be seen in Table 1.5 which details the surfactant, mechanism and the resulting mesophase.

Table 1.5 Mesoporous structures available using templating method

Mesoporous Material	Surfactant	Mesophase	Mechanism
SBA-1	Cationic (CTEABr) $CH_3(CH)_nNEt_3$	3D Cubic Pm-3n	$S^+X^-I^+$
SBA-2	Gemini C16-3-1	3D Hexagonal $P6_3/mmc$	S^+X^-
SBA-15	Non-ionic triblock copolymer (P123) $PEO_{20}PPO_{70}PEO_{20}$	Hexagonal planar p6mm	$N^0H^+X^-I^+$
SBA-16	Non-ionic triblock copolymer (F127) $PEO_{106}PPO_{70}PEO_{106}$	Cubic Im-3m	$N^0H^+X^-I^+$
FDU-12	Non-ionic triblock copolymer (F127) $PEO_{106}PPO_{70}PEO_{106}$	Cubic Fm-3m	$N^0H^+X^-I^+$
KIT-6	Non-ionic triblock copolymer (P123) $PEO_{20}PPO_{70}PEO_{20}$	Cubic Ia-3d	$N^0H^+X^-I^+$
MCM-41	Cationic (CTMABr)	Hexagonal planar	S^+I^-
MCM-48	Cationic (CTMABr)	Cubic Ia-3d	S^+I^-
MCM-50	Cationic (CTMABr)	Lamellar	S^+I^-
FSM-16	From Kanemite	Hexagonal planar	From Kanemite
HMS	Alkylamines	Hexagonal disordered	S^oI^o
MSU	Non-ionic ($C_{15}H_{33}E_{12}OH$)	Hexagonal disordered	N^oI^o

MCM-41 is synthesised using a cationic surfactant template such as cetyl trimethyl ammonium and proceeds *via* the S^+I^- mechanism in basic conditions where S^+ denotes the cationic surfactant and I^- the condensed silica. The synthesis results in a hexagonal, ordered mesophase which can be prepared with a variety of pore sizes as shown in Figure 1.7 **[5].**

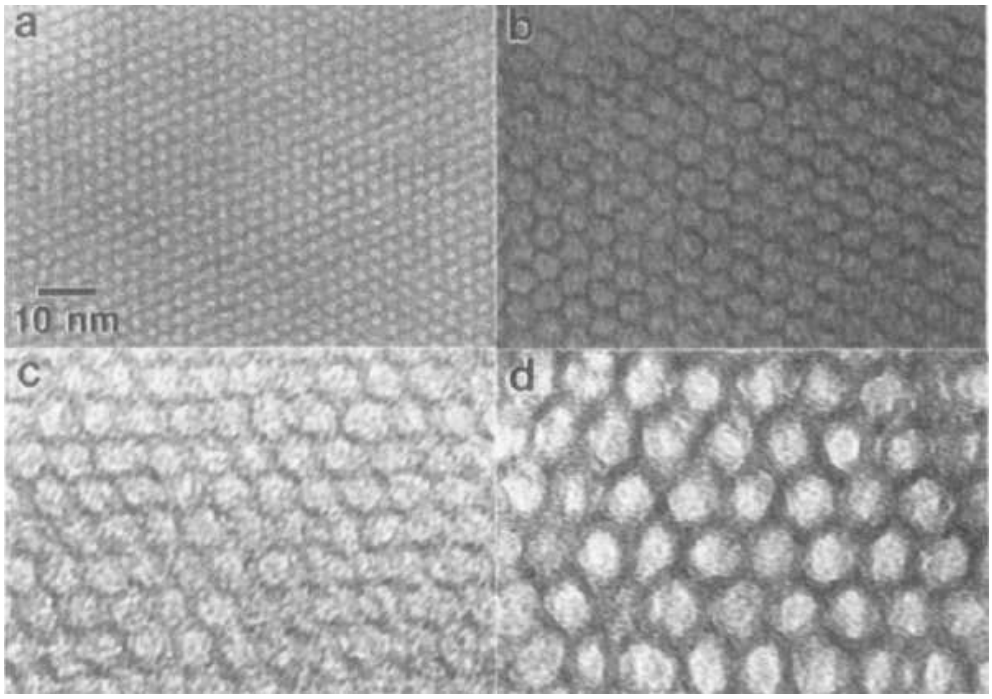

Figure 1.7 MCM-41, pore size 20, 40, 65 and 100 Å. Hexagonal array of uniform diameter channels, viewed down the channel axis. [5]

SBA-1, like MCM-41, uses a cationic surfactant but in this case the synthesis is carried out in acidic media and produces a 3D cubic structure which can be seen in Figure 1.8a.

Using the non-ionic triblock copolymer P123 ($PEO_{20}PPO_{70}PEO_{20}$) it is possible to synthesise a material analogous to MCM-41 with larger pores (between 60 and 260 Å) *via* the $S^0H^+X^-I^+$ mechanism, denoted SBA-15 **[27]**.

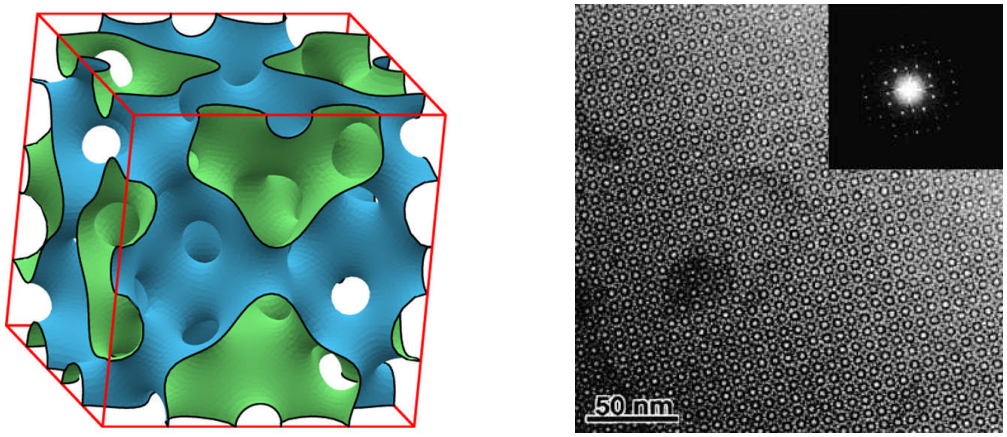

Figure 1.8a Minimal surface of SBA 1 as solved by Anderson *et al.* [43] and HRTEM of cubic structure [44]

By adding organic functional groups to the synthesis of SBA 15 it is possible to induce phase transformations to produce a cubic Ia-3d structure as seen in Figure 1.8b.

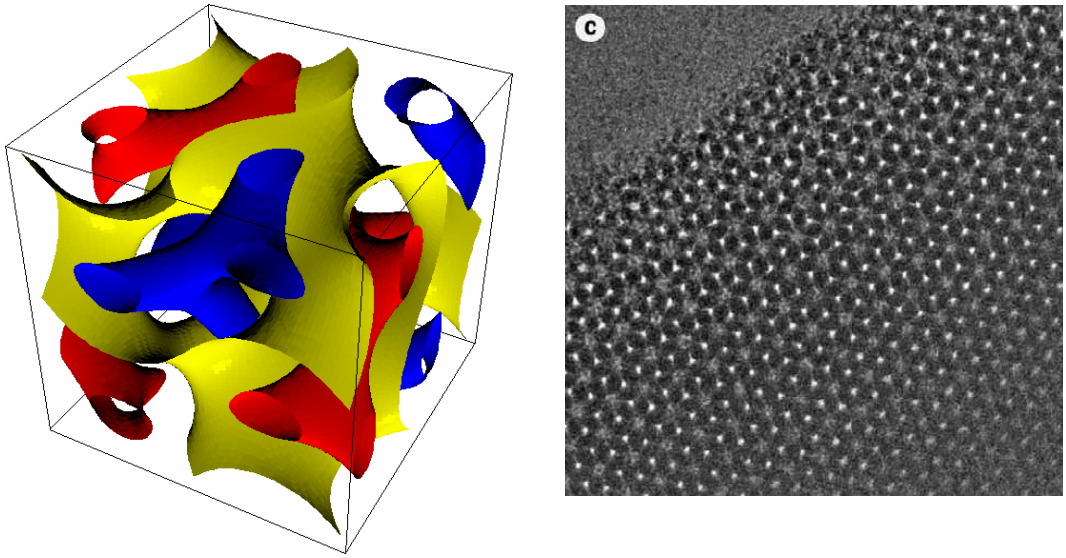

Figure 1.8b Simulated STA-11 [45] with bicontinuous cubic Ia-3d symmetry, large pore analogue to MCM-48. Gyroid silica surface shown in yellow and two separate pore networks shown in red and blue and HRTEM of STA-11 [46]

By changing the non-ionic block polymer to F127 it is possible, with the addition of salts and swelling agents, to produce a cubic mesocaged structure denoted FDU 12 with symmetry Fm3m which can be seen in Figure 1.8c **[47]**.

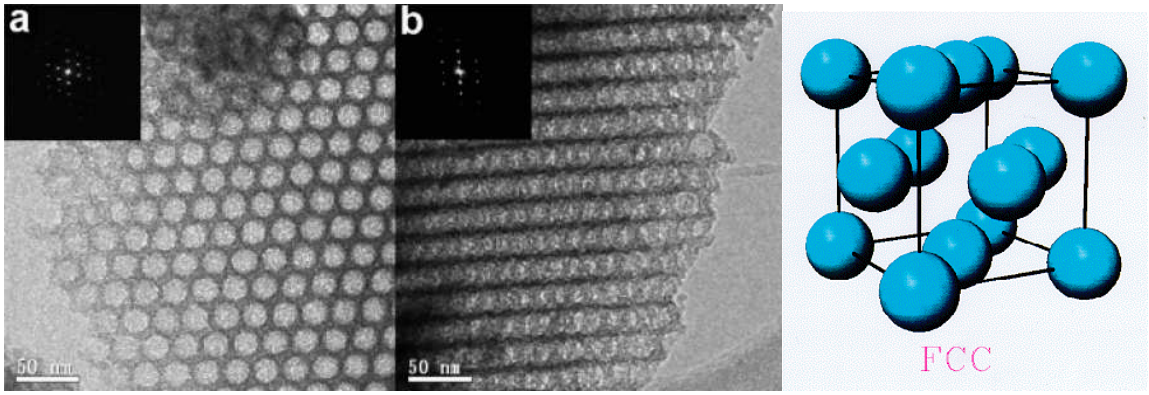

Figure 1.8c HRTEM showing a) [110] and b) [211] view [106] and FCC model of the position of spherical micelles in as-prepared FDU 12

Mathematical models of some of the possible mesostructured materials are shown in Figure 1.9 in which we can see the hexagonal SBA-15 structure (a), the bicontinuous minimal surface area representation of the cubic Ia-3d KIT-6 material (b), and two possible cubic cage structures; SBA-16 (c) – a body centred cubic Im3m phase and FDU-12 (d) – a face centred cubic Fm3m phase. SBA-15, KIT-6 and FDU-12 will be the subjects of this thesis and are described in greater detail in chapter 3.

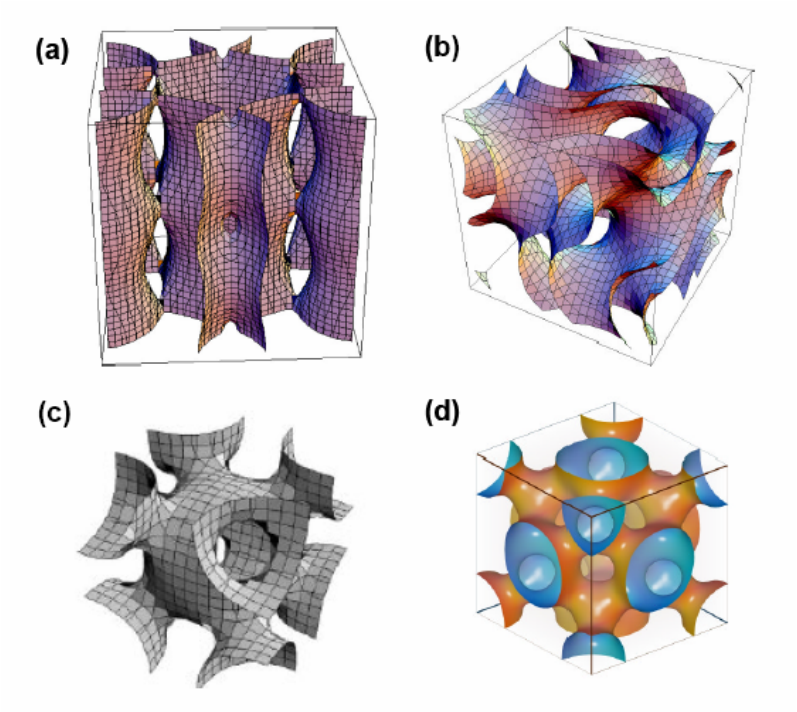

Figure 1.9 Mathematical models of mesoporous structures for (a) SBA 15 (b) KIT 6 (c) SBA 16 (d) FDU 12 [48-50]

1.7 Synthesis variables

There are several key variables in the synthesis of silicate mesophases. Mesoporous solids can be prepared under alkaline, acid or neutral conditions, with cationic, anionic or neutral surfactants of different types.

1.7.1 pH of the medium (acid or base)

The pH of the media in which mesoporous materials are prepared is crucial in determining the resulting mesophase. At acidic and basic pH the formation mechanism of mesostructured materials is different. The negatively charged silicate ions act as the counter ion at pH values above the isoelectric point (I.P) of silica (pH ≈2.0) whereas below pH 2 the positively-charged silica species acts as the counter ion. It is common for one surfactant template to produce 2 different mesophases solely by altering the synthesis pH.
The earlier mesoporous materials were synthesised at high pH but Stucky *et al.* subsequently used acidic media to prepare SBA-1, a mesoporous material with a cubic cage structure.
Silicon alkoxide is a typical silica source. Acid catalysis causes accelerates the hydrolysis versus the condensation rate and encourages mostly condensation at the ends of the silica polymers, giving linear silicate ions. These combine into mesostructures that subsequently condense. In contrast the synthesis carried out in basic conditions promotes both the hydrolysis and condensation step, which leads to rapid formation of a highly condensed structure where the two steps overlap.

A phase sequence can be determined by observing the synthesis behaviour using varying surfactants. Under acidic conditions the phase sequence is as follows:
Cubic (Pm3n, SBA-1), 3d hexagonal ($P6_3/mmc$, SBA-2) → 2d hexagonal (p6mm, SBA-3) → lamellar as the pH is decreased.
When conditions are basic the phase sequence changes to:
3D hexagonal ($P6_3/mmc$, SBA-2) → 2D hexagonal (p6mm, MCM-41) → cubic (Ia-3d, MCM-48) → lamellar (MCM-50)

The synthesis of both MCM-41 and MCM-48 proceeds *via* the S^+I^- mechanism using alkaline conditions under which the anionic silicates assemble around hexagonal p6mm and cubic Ia-3d micellar arrays of the surfactant, cetyltrimethylammonium ions.

1.7.2 Choice of surfactant (cationic, anionic, polymeric)

Surfactants play a vital role in the formation of the mesoporous solids by acting as a template for condensation of the silica source to form a uniform mesostructured material. In general surfactants can be seen to comprise of 2 components- hydrophobic and hydrophilic - and are therefore amphiphilic molecules. These molecules can then be divided into further categories depending on the groups that link together to form the various surfactants. They can be classified as cationic, anionic, non-ionic or zwitterionic and are shown in Figure 1.10.

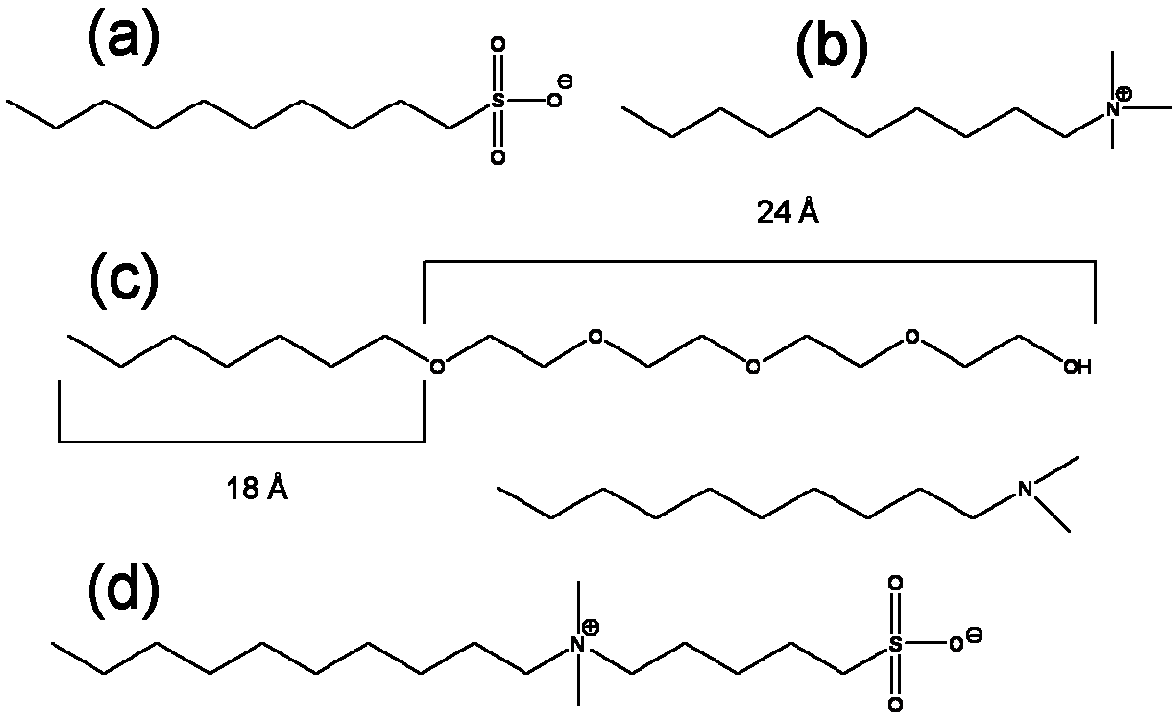

Figure 1.10 Surfactant types - a) anionic; b) cationic; c) non-ionic and d) zwitterionic.

Non-ionic organic-inorganic interactions have been investigated and used to develop additional approaches. Here, neutral surfactants, for example primary amines and poly (ethylene oxide), have been used to synthesise both HMS (hexagonal mesoporous silica) **[51,52]** and MSU **[53-55]** type materials (Michigan state university material). The surface

area of these materials is comparable to that of MCM 41 but they display a much broader pore size distribution.

1.7.2.1 Cationic Surfactants

Mesoporous materials can be synthesised under acidic as well as alkaline conditions. SBA-1 (shown in section 1.6), a cubic caged structure, was the first material to be prepared *via* this method using HTEABr surfactant and TEOS in acidic solution. It is possible to control the pore size of SBA-1 by altering the cationic surfactant chain length.

A mesoporous material with a hexagonal structure similar to MCM-41 denoted SBA-3 can be prepared in a similar way. By changing the condensation temperature or inorganic acid used it is possible to achieve SBA-1 by utilising H_2SO_4 and HCl or SBA-3 using HBr and HNO_3 **[56]**, as the head size of the surfactant is varied by inclusion of different anions.

1.7.2.2 Anionic Surfactants

One of the newest methods for synthesis of mesoporous materials has been developed by Che *et al.* **[57]**, who have devised a series of materials denoted AMS-n, Anionic surfactant-templated Mesoporous Silica. They observe the negatively charged head group of the anionic surfactant interacts with the amine/alkylammonium groups present on the functional siloxanes co-condensed with the silica source (TEOS). Altering the length of alkyl chain of the surfactant can be used in these materials to adjust the pore size, as can the addition of organic molecules such as aromatics or n-alkanes.

1.7.2.3 Non ionic Block Copolymer Surfactants

Currently, one of the most widely used series of surfactants used for the synthesis of mesoporous silica materials is that of the triblock copolymers, which consists of poly(ethylene oxide)$_x$-poly(propylene oxide)$_y$-poly(ethylene oxide)$_x$ -$(PEO)_x(PPO)_y(PEO)_x$ and is able to form liquid crystal structures in solution. A variety of structures can be formed from differing copolymers such as SBA-15 from Pluronic P123 and FDU-12 and SBA-16 from Pluronic F127 **[28]**. The formation mechanism for these materials is much less clear than that of MCM-41 synthesis but it is thought that the protonated ethylene oxide (EO) units and the cationic silicate species interact. It is these block copolymers that will be used as templates for the synthesis of well ordered large pore mesoporous silica in this work.

The surfactants used within this thesis can be classified as non-ionic and are triblock copolymers of ethylene oxide/ propylene oxide / ethylene oxide of various quantities and ratios (as shown in Figure 1.11). Pluronic P123 ($PEO_{20}PPO_{70}PEO_{20}$) is used as a template for materials including SBA-15 and KIT-6 and Pluronic F127 ($PEO_{106}PPO_{70}PEO_{106}$) for FDU-12 and SBA-16 type solids.

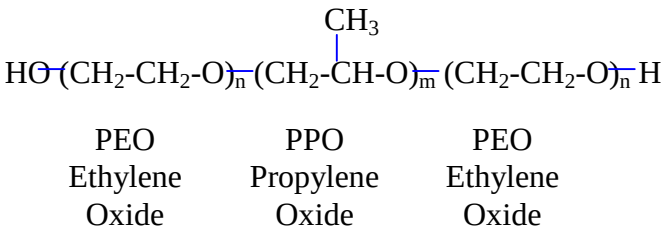

Figure 1.11 Block copolymer

1.7.3 Changing surfactants – modification of g

MCM-41 can be synthesised by using an alkyltrimethylammonium surfactant $C_nH_{2n+1}(CH_3)_3N^+$ where n = 10-18. There is no difference in the structure directing effects of surfactants with odd or even numbers of carbon atoms in the chains. Replacing the trimethyl alkyl ammonium surfactant by triethylalkylammonium surfactant ($C_nH_{2n+1}(C_2H_5)_3N^+$) with a larger head group favours the formation of SBA-1 under acidic conditions. With larger head-group surfactants it is possible to decrease the value of the surfactant packing parameter which in turn generates micelles with higher surface curvature.

Using surfactants with a hydroxyl head group favours the formation of mesophases which exhibit low surface curvature. A smaller effective a_0 is a result of the hydroxyl group decreasing the hydrophobicity of the head group. When $C_{16}H_{33}N^+(CH_3)_2(CH_2)_2OH$ is used a lamellar phase results. In comparison when a surfactant of similar structure is used, the only difference being a different head group, such as $C_{16}H_{33}N^+(CH_3)_2C_2H_5$, a high curvature mesophase MCM-41 results.

Gemini surfactants belong to a family of synthetic amphiphiles which are constructed of a long hydrophobic chain, an ionic group, a spacer, a second ionic group and an additional hydrophobic tail ($C_{m\text{-}s\text{-}m}$). A member of this series is the divalent quaternary ammonium surfactant, $C_{n\text{-}s\text{-}1}$, which can be thought of as an end member Gemini surfactant or a

doubly-charged head-group surfactant. These surfactants have a large scope in terms of modification with the opportunity to change the length and nature of both the side chains and the spacer group. The Gemini C_{m-s-m} surfactants can be described as dimers of the two-chain C_mH_{2m+1}-$(CH_2)_{s/2}N^+(CH_3)_2$ surfactants. Members of this surfactant family can be used to synthesise a variety of silica-based mesophase products. When s is small MCM-50 is the favoured product, whereas a larger s surfactant leads to the formation of MCM-41. For example, $C_{12-12-12}$ surfactant gives MCM-41 at room temperature and by increasing the value of m to $C_{16-12-16}$ produces MCM-48 at both room and high temperature.

SBA-2 is a regular caged mesoporous silica material synthesised using the divalent quaternary ammonium surfactant, C_{n-s-1} in both acidic and basic media. Under basic conditions it is possible to synthesise SBA-2 with varying unit cell and cage size by altering the chain length of the surfactant. When SBA-2 was first reported in 1995 it was proposed to be a 3d hexagonal cage derived from a hexagonal close packed arrangement with space group $P6_3/mmc$. After later work involving more extensive TEM studies was carried out it was reported to be a mixture of a cubic (Fm3m) and hexagonal phase.

In this thesis it can be seen that by changing the co-block polymer surfactant from P123 to F127 we observe a change in the morphology of the resulting materials with the F127 increasing the head group volume and thus giving more spherical micelles resulting in a cubic structure.

1.7.4 Co-solvents and salts

It has been reported that organic cosolvents can be added during the synthesis in order to control the morphology of the mesophase. These additives can dissolve in the surfactant phase. Non-polar additives, for example, can penetrate the hydrophobic part of the micelle thereby increasing the hydrophobic volume and radius. An example of this is the addition of trimethylbenzene (TMB) to SBA-15 which results in large unit cell changes **[28]**. SBA-15 can have its pore size dramatically increased up to 300 Å by the addition of TMB as can SBA-1 when prepared using the cationic surfactant HTEABr **[56]**. The addition of a co-solvent may have an adverse effect on the micelle formation and result in poorly ordered mesoporous silica and so the ratio of surfactant to co-solvent must be controlled carefully to avoid this. If additives of low polarity are added to the synthesis the favoured product will tend to be those which possess the lowest surface curvature.

MCM-41 has good thermal stability and hydrothermal stability in atmospheric water vapour but low hydrothermal stability in water and aqueous solutions. This results in loss of structure due to silicate hydrolysis which causes degradation of the framework. By adding salts such as sodium chloride, potassium chloride, sodium acetate or ethylenediaminetetraacetic acid tetrasodium salt during the hydrothermal process it is possible to improve the hydrothermal stability **[58]**.

Highly hydrophilic block copolymers such as F127 tend to produce less ordered mesostructured silica as the interaction of the silica species with the non-ionic block copolymers is weak. However, this can be overcome by the addition of inorganic additives including salts (KCl, NaCl) to the synthesis **[58].** This leads to a process called 'salting-out' which lowers the CMC value of the copolymers and gives rise to highly ordered mesoporous silica at lower block copolymer concentrations. Inorganic salts are also thought to improve the ordering as the 'salting-out' process dehydrates the PEO units and renders them more hydrophobic, increasing the silica-block copolymer interactions.

1.8 Functionalisation

One of the advantages of mesoporous silicas over their zeolitic counterparts is the ease with which their surfaces can be functionalised with organic groups. This arises because not all of the silicons are coordinated to other silicons through each of the oxygen's to which they are bound. Some (the so-called Q^3 or Q^2 silicons in NMR terminology) have dangling –OH groups that can be replaced by organic groups (of the form –RX) without disturbing the structure. Q^4, Q^3 (and Q^2) silicon atoms are represented in Figure 1.12 **[59]**. This additional functionality makes possible the binding and covalent linking of a wide range of other species.

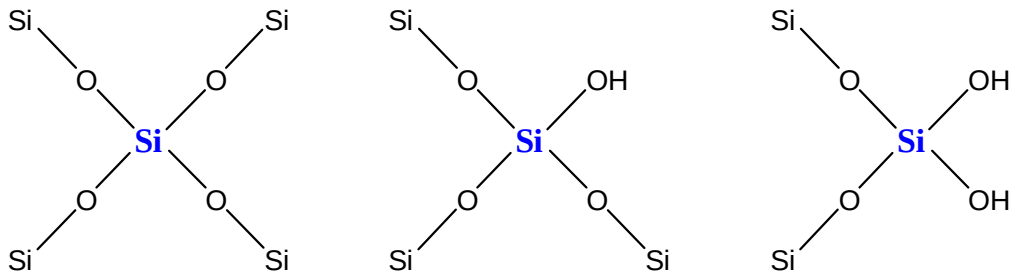

Figure 1.12 Q^4 silicon (left), Q^3 silicon (middle) and Q^2 silicon (right). Post-synthetic functionalisation on the highlighted silicon is only possible if silanol groups are present.

Since the discovery of highly ordered mesoporous silicas in the early 1990s a variety of materials with different structures and pore sizes have been reported. In order to widen the possible applications of these materials in the areas of catalysis, separation and adsorption, researchers have studied the possibilities of functionalising these materials with organic groups such as thiols, amines, and carboxylates. These materials have generated interest as they combine specific chemical reactivity due to the organofunctional groups and a hydrothermally stable material with high surface area and an ordered large pore structure within a single solid. In order to incorporate functional groups within a framework, organic groups can be added through *in situ* co-condensation or by post synthesis grafting onto the surface of the silica. Functional groups which have been used in the *in situ* functionalisation of mesoporous solids can be seen in Table 1.6.

Table 1.6 *In situ* functionalisation of mesoporous silica solids *via* the co-condensation of tetraalkoxysilane and organoalkoxysilanes.

Functionalised mesoporous solids *via* co-condensation			
Functional group	**Surfactant**	**Mesophase**	**Ref**
3-aminopropyl	CTAB	MCM-41	**[60]**
2-cyanoethyl	n-dodecylamine	HMS	**[61]**
Vinyl	CTAB	MCM-41	**[60, 62]**
Carboxylic acid	P123	SBA-15	**[63]**
3-mercaptopropyl	P123	STA-11 FDU-5	**[64]** **[32]**

1.8.1 *In situ* functionalisation

Co-condensation is in principle a simpler process as it minimises the number of preparative steps and a more uniform distribution of organic groups is achieved. A schematic representation of the co-condensation approach is shown in Figure 1.13. Also such *in situ* functionalisation often shows a higher loading of organic functionality, more importantly without closing or blocking the pore channels and entrances. A possible disadvantage of co-condensation is that adding an organoalkoxysilane during the synthesis can lead to a change in the resulting structure or disruption of the formation of the material. This has been shown by Hodgkins *et al.* who report that with 0-5 mol% MPTES added to typical

SBA-15 synthesis, the SBA-15 produced has space group p6mm, while the 7 mol% samples produced highly ordered silica with space group symmetry Ia-3d, while at >10 mol% the long range order is lost **[65]**.

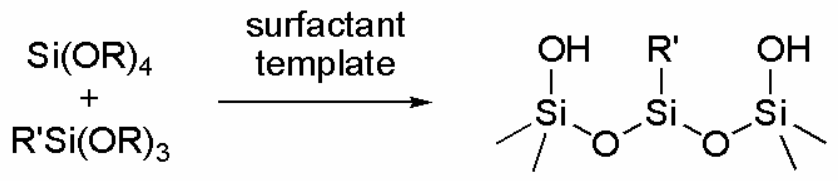

Figure 1.13 Co-condensation approach to organic functional group incorporation

1.8.2 Grafting

Grafting is carried out post-synthesis on calcined or extracted materials whose surface generally consists of partially condensed silica which possesses free silanol groups (as shown in Figure 1.14). These groups are able to react with many different groups including alkoxysilanes of structure $R'Si(OR)_3$. This allows the retention of the pore structure although the pore diameter may be reduced by the addition of functional groups to the pore walls. Although the structure remains intact there is a possibility that not all the organic groups will react and that they may only react with silanol groups at the pore entrances which could lead to blocking of the pores or poor dispersal of functional groups throughout the structure **[66]**.

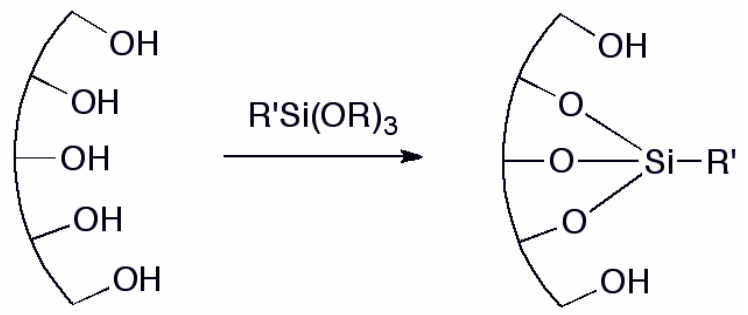

Figure 1.14 Grafting approach to organic functional group incorporation

In post-synthetic grafting of functional groups onto the internal silica surfaces the material is first calcined under flowing nitrogen (typically at 550 °C) followed by 4 hrs under flowing oxygen. This further condenses the inorganic silica framework and any remaining

silanol groups present are likely to form Si-O-Si bonds. In order for organic groups to be grafted onto the surface silanol groups are required to act as linkers for the groups so silanol groups must be created if a high coverage of functional groups is required. This is achieved by rehydrating the surface by refluxing the calcined material in water.

Benefits of this post grafting method include preservation of the mesostructure and also the final solids are free of residual surfactant. This may be important if the material is to be used *in vivo* as a drug delivery host as the surfactant may be harmful to cells.

The need for a high number of silanol groups leads to problems with achieving a high degree of functionalisation. Also, grafting onto these groups, which protrude into the pores, causes a reduction in the available pore volume and can have adverse effects if the pore size and volume is key to its use. In comparison to a one-pot synthesis, grafting is a more time consuming process with additional steps being required to ensure post synthesis addition of functional groups. With a one-step synthesis a more uniform distribution of organic groups can be achieved although if the loading of functional group is increased to a certain level then long-range order of the material and stability is compromised.

1.9 Surfactant removal

The materials prepared for this project were synthesised using surfactants as templates which results in materials in which the pore channels are filled.

Thermogravimetric and elemental analysis on the solids show that in a typical mesoporous material 40-50% of the sample weight is surfactant **[67]**.

1.9.1 Calcination

Typically in order to render the material porous, calcination is performed which removes the organic template leaving a network of channels/cavities. The material is heated at a controlled rate to a high temperature, typically 550 ^{o}C, under a continuous flow of gas, which can typically be air, or nitrogen followed by oxygen. A schematic of the calcination process is seen in Figure 1.15. (Direct calcination in oxygen is highly exothermic and can lead to explosion.)

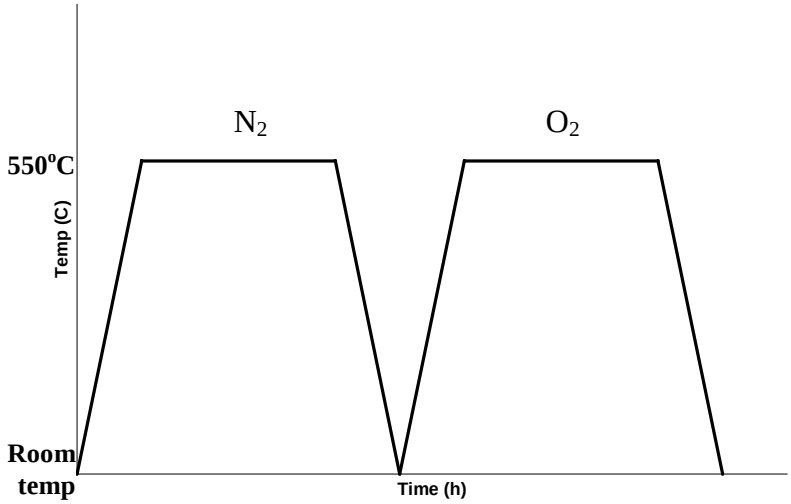

Figure 1.15 Furnace conditions for calcination of mesoporous material

The material is heated at a rate of 1.5 °C/min under a flow of nitrogen gas and held at the maximum temperature for 4 hours before being allowed to cool. The same process is repeated using a flow of oxygen. This method proves very effective with TGA results showing almost 100% surfactant removal. Calcination causes further condensation of the silica and can result in a reduction in pore size **[67]** or, with layered materials such as MCM-50, a collapse of the structure **[68]**.

1.9.2 Extraction

For materials functionalised *via* co-condensation, calcination would remove any organic functionality introduced and therefore an alternative method must be used. Solvent extraction can remove up to 80-90% of the surfactant using relatively mild conditions (using an alcohol if the surfactant is neutral) and although this is not as effective as calcination the functional groups remain intact. In this work materials which have been functionalised *in situ* had the template removed using sohxlet extraction with ethanol as the solvent. This method is preferred to refluxing the as-prepared material in ethanol as sohxlet extraction utilises a continual cycle of fresh solvent which is more effective.

1.9.3 Alternative template removal methods

In addition to calcination and solvent extraction other methods have been used to remove template from mesoporous materials. Microwave-assisted template decomposition has

been used to remove 95% of the surfactant from SBA-15 by using strong nitric acid and hydrogen peroxide **[69]** and ozone has been employed to remove the template through an oxidative mechanism using high concentrations over a short period of time **[70-72]**. Lower concentrations can be used by placing the sample under a UV lamp which can generate ozone from the oxygen in the atmosphere. It is thought that the formation of a radical species is responsible for the decomposition of ether linkages within the surfactant **[73**].

For some materials templated by neutral copolymers, such as SBA-15, there is microporosity present between the larger mesopores. It has been reported that a two step extraction process is often required to ensure complete removal of the template and leave the material with both meso and microporous channels **[74]**. The first step is removal of the surfactant from the mesopores with a strong acid followed by the removal of the surfactant from the micropores by calcination.

1.10 Mesoporous silicas prepared using non-ionic block copolymers

The study of amphiphilic block copolymer-templated mesostructure materials is an active research area offering great scientific and technological possibilities. Block copolymers are increasingly widely used as templates for mesoporous materials due to their diverse structural characteristics and low cost amongst others.

Ordered and disordered mesoporous solids can be prepared using block copolymers as templates. Typical ordered mesostructured silica materials synthesised using amphiphilic block copolymers are shown in Table 1.7. Non-ionic surfactants octaethylene glycol monododecyl ether ($C_{12}EO_8$ [$C_{12}H_{25}(CH_2CH_2O)_8OH$]) and octaethylene glycol monohexadecyl ($C_{16}EO_8$) have been shown to produce ordered silica in acidic media by Attard *et al.* **[54].** Stucky *et al.* have successfully synthesised a new family of mesoporous structures (including SBA-15) by employing non-ionic triblock copolymers in acidic aqueous media **[75,76]**. El-Safty *et al.* using Brij 56 ($C_{16}EO_{10}$) as the surfactant and alkanes of variable chain lengths as additives have produced a series of nanostructured silica monoliths (HOM-n) with 2-D and 3-D structures with controllable pore size in the region of 3 – 8 nm **[77,78]**, and Feng *et al.* **[79]** report the synthesis of large pore (up to 11 nm) mesoporous silica monoliths templated by non-ionic surfactants Pluronic F127 and

P123 (described in more detail in Chapter 3). Examples of ordered mesoporous silicas templated by non-ionic block copolymers can be seen below in Table 1.7.

Table 1.7 Ordered mesoporous silicas templated by non-ionic block copolymers

Space group	Researcher/Material	Block Copolymer	Remark	Ref.
$Fm\bar{3}m$	FDU-1	$EO_{39}PO_{47}EO_{39}$	Large cage	**[80]**
	FDU-12	$EO_{106}PO_{70}EO_{106}$	Ultra large cage	**[81]**
	HOM-10	$C_{16}EO_{10}$	Additive alkanes	**[78]**
$Im\bar{3}m$	HOM-1	$C_{16}EO_{10}$	Low [surfactant]	**[77,78]**
	SBA-16	$EO_{106}PO_{70}EO_{106}$	TMOS over TEOS	**[76]**
	ST-SBA-16	$C_{18}EO_{10}$	Small pore, thin wall	**[82]**
$Pm\bar{3}m$	SBA-11	$C_{16}EO_{10}$		**[76]**
	HOM-4	$C_{16}EO_{10}$	Additive alkanes	**[83]**
$Pn\bar{3}m$	HOM-7	$C_{16}EO_{10}$	High [surfactant] or additive alkanes	**[77,78,83]**
$P6_3/mmc$	SBA-12	$C_{18}EO_{10}$	Mixed hcp & ccp phases	**[76]**
	HOM-3	$C_{16}EO_{10}$	Medium [surfactant]	**[77,78]**
	Hodgkins *et al.*	$EO_{106}PO_{70}EO_{106}$	Large pore mixed hcp & ccp phases, additive propylthiol	**[46]**
p6mm	Attard *et al.*	$C_{12}EO_8$, $C_{16}EO_8$	Small pore	**[54]**
	SBA-15	$EO_{20}PO_{70}EO_{20}$	Large pore highly ordered	**[75,76]**
	Feng *et al.*	$EO_{106}PO_{70}EO_{106}$	Organic additives	**[79,84]**

	CMI-1	$C_{16}EO_{10}$		**[85]**
	HOM-2	$C_{16}EO_{10}$	Medium [surfactant]	**[77,78,83]**
	MSU-H	$EO_{20}PO_{70}EO_{20}$	Neutral pH	**[85a,86]**
$Ia\bar{3}d$	FDU-5	$EO_{20}PO_{70}EO_{20}$	MPTMS, ethanol evaporation	**[87]**
		$EO_{20}PO_{70}EO_{20}$	Post-solvothermal synthesis	**[88]**
	Hodgkins *et al.*	$EO_{20}PO_{70}EO_{20}$	Additive propylthiol (MPTES)	**[46]**
	Chan *et al.*	$EO_{17}MA_{23}$		**[89]**
	Flodstrom *et al.*	$EO_{20}PO_{70}EO_{20}$	Inorganic salts	**[90]**
	Wright *et al.*	$EO_{20}PO_{70}EO_{20}$	MPTES	**[91]**
	KIT-6 *et al.*	$EO_{20}PO_{70}EO_{20}$	Additive butanol	**[92]**
	Schüth *et al.*	$EO_{20}PO_{70}EO_{20}$	Vinyl, inorganic salts	**[93]**
	Che *et al.*	$EO_{20}PO_{70}EO_{20}$	MPTES	**[94]**
	HOM-5	$C_{16}EO_{10}$	Medium [surfactant]	**[77,78,83]**
Lamellar	HOM-6	$C_{16}EO_{10}$	Higher [surfactant]	**[83]**
	Wiesner *et al.*	PI-b-PEO	Organically modified aluminosilicate	**[95]**

1.10.1 History of block copolymers as templates

The first paper utilising block copolymers in the synthesis of mesoporous materials appeared in 1998 and showed materials with improved properties compared to the M41S

family, with larger pore diameters, thicker walls and higher stability **[28]**. Triblock copolymers are made up of a central polypropylene oxide group with a polyethylene oxide group on either side formed by varying the ratios of propylene oxide: ethylene oxide groups. These copolymers are known as Pluronics and exhibit anomalous behaviour with increasing temperature, i.e. an increase in hydrophobicity of the polymer as the temperature is raised. By increasing the temperature for certain Pluronics this can in turn alter the mesophase formation and result in a different structure. This can be seen with P123 and P103 ($(EO)_{17}(PO)_{60}(EO)_{17}$) which typically form 2D hexagonal structures but upon temperature increase direct the structure towards a multilamellar vesicle-like phase.

As mentioned previously an example of a mesoporous material synthesised using this method is SBA-15 (**S**anta **BA**rbara No. **15**), a 2D hexagonal (p6mm) silica-block copolymer mesophase. The pore system of SBA-15 comprises of a hexagonal arrangement of mesopores with interconnecting micropores, as shown by nitrogen adsorption and inverse platinum imaging by electron microscopy. These micropores are shown to be reduced by increasing the synthesis temperature which also causes an increase in the mesopore diameter. It is possible that the micropores are a result of the surfactant (P123) being incorporated into the mesopore walls which results in micropores being present after the surfactant is removed *via* calcination or extraction. TEM images of calcined hexagonal SBA-15 mesoporous silica with different average pore sizes, from BET and XRD results (**A**) 60 Å, (**B**) 89 Å, (**C**) 200 Å, and (**D**) 260 Å are shown in Figure 1.16 **[75].**

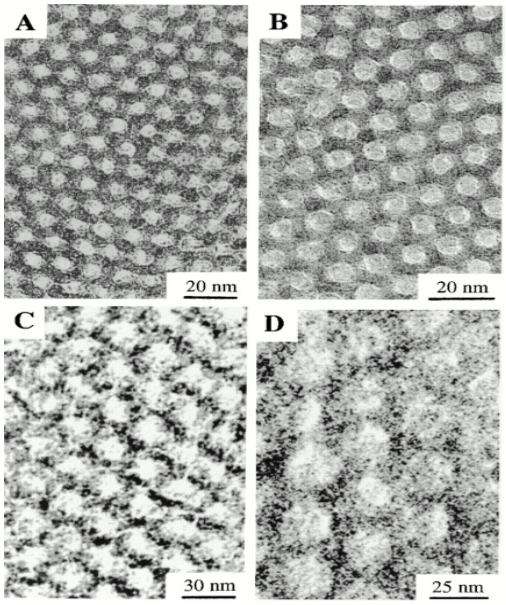

Figure 1.16 HRTEM images of calcined hexagonal SBA-15 with different average pore sizes, (A) 60 Å, (B) 89 Å, (C) 200 Å, and (D) 260 Å [75]

This thicker pore wall of SBA-15 when compared to that of MCM-41 increases the thermal and hydrothermal stability. The pore diameter can be adjusted by lengthening the treatment time and increasing the hydrothermal temperature.

Further investigations were carried out by Stucky *et al.* into morphological control of SBA-15 which resulted in the formation of micrometer-sized hard sphere-, fibre-, doughnut-, rope-, egg-sausage-, gyroid-, and discoid-like mesoporous silica SBA-15 **[96]** with the highly ordered hexagonal structure found in particulate SBA-15 (Table 1.8).

Table 1.8 Various SBA-15 morphology

Morphology	Silica source	Surfactant	Co-solvent/additive
Fibre-like	TMOS	P123	
Donut-like	TEOS	P123	DMF
Micrometer hard spheres	TEOS	CTAB and P123	
Gyroid/disc-like	Pre-hydrolysed TEOS in ethanol	P123	$MgSO_4$ or Na_2SO_4

1.10.2 Inversion of the pore system

It is possible to obtain an inverse image of a mesoporous material in which the pore system of a typical mesoporous material can be filled with carbon and the silica dissolved, known as nanocasting. Ryoo *et al.* have produced a series of carbon negative replicas using mesoporous solids as a template to provide both nano-rods and nano-tubes; these are termed CMK-n. CMK-1 is the negative replica of MCM-48 and is prepared by the polymerisation of sucrose within the pores of MCM-48 followed by the addition of sodium hydroxide in ethanol which removes the silica framework **[26**]. CMK-2 uses SBA-1 **[97]**, SBA 15 is used to form both CMK-3 –nano rods **[98]**, and CMK-5 nano-tubes **[99**] and CMK-8,-9 (KIT-6 template and analogous to CMK-3 and CMK-5 with regards to carbon filling respectively) **[100]** Representations of these inverse structures including the Negative replicas of SBA-15 and FDU-12 can be seen in Figure 1.17. Notably SBA-15 is found to have microporous (disordered) connections between the well ordered arrangement of large pores.

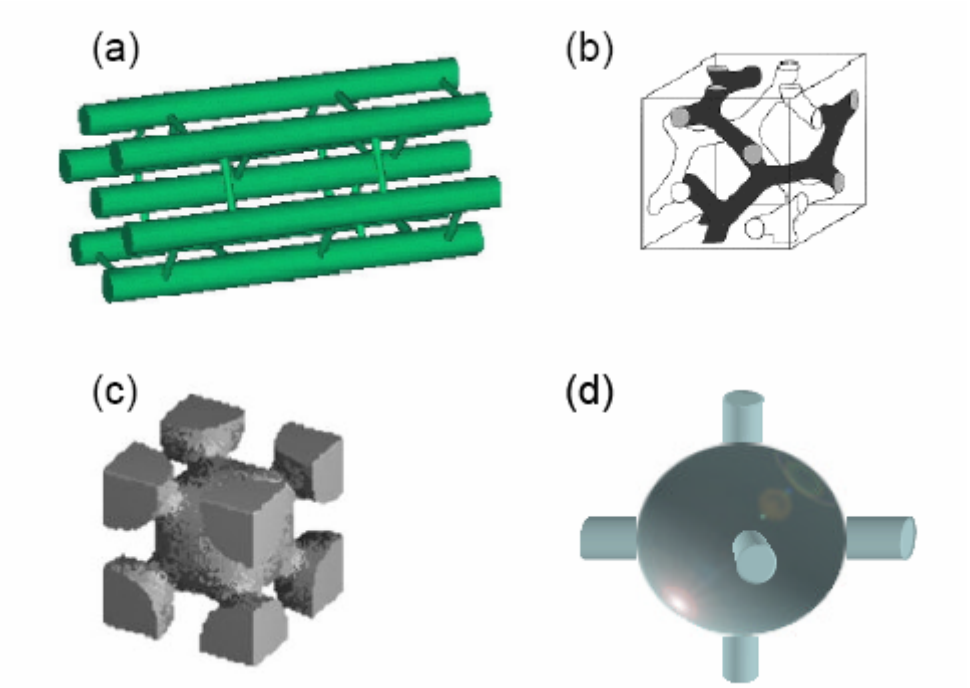

Figure 1.17 Negative replicas of (a) SBA-15 (b) KIT-6 (c) SBA-16 (d) FDU-12 [49, 101, 102]

1.10.3 Cubic structures

As well as the effects of mercaptopropyltriethoxysilane (MPTES) on SBA-15 synthesis, Hodgkins *et al.* **[65]** also studied the effects of adding MPTES to the synthesis of mesoporous silicas using Pluronic F127. Previously this synthesis has been reported independently by the two groups of Zhao and Ryoo, and this face centred (Fm3m) cubic structure has been designated FDU-12 **[33]** and KIT-5 **[35]**. These materials are formed with the condensation of silica around cubic close packed micelles and produce structures similar to previously reported smaller mesocages materials such as SBA-2, STAC-1 and STA-10 which employ a dicationic Gemini surfactant and the larger pore SBA-12, which is synthesised using a non-ionic surfactant, Brij 76. By adding MPTES to a synthesis which has been shown to form FDU-12 Hodgkins *et al.* **[65]** observed that the addition of thiol resulted in changes in the stacking sequence of the close packed micelles in the form of twinning and stacking faults.

Simultaneous to Hodgkin's publication of a large pore Ia-3d cubic structure another group reported the synthesis of a similar material, this time using the addition of an inorganic salt **[90]**. Previously Yu *et al.* **[81]** had demonstrated that adding alkali sulfates and/or chlorides enables the lowering of the synthesis temperature and additionally work has been published

which shows that the addition of a salt such as NaCl dehydrates the polyethylene oxide units and results in a more hydrophobic behaviour by the polymer. Typically the bicontinuous Ia-3d structure is only stable over a narrow range and in the synthesis utilised by Flodstrom *et al.* **[90]**, without the addition of NaI salt, a multilamellar vesicle phase results compared to the Ia-3d phase. They observe that the addition of sodium iodide opens up the crystallisation window situated between the lamellar and 2d hexagonal phases.

Although most of the interest in mesoporous materials has focused on hexagonal structures, MCM-41 in particular, cubic structures such as MCM-48 have a more appealing structure for many applications. It is based on the gyroid infinite periodic minimal surface (IPMS) and results in a very open network with two separate interconnecting sets of pores. MCM-48 has a unit cell of ca. 100 Å, compared to 260 Å which is the unit cell of as-synthesised material reported by Flodstrom *et al.*. This larger pored cubic structure is comparable to MCM-48 in the same way that SBA-15 is analogous to MCM-41.

1.11 Applications of mesoporous solids in adsorption and catalysis

Currently the commercial applications of microporous materials are much more prevalent than uses of mesoporous materials which leaves large scope and potential for mesoporous silica. Recent advances have led to interest in mesoporous silica for the purpose of catalysis **[103**], sensing and drug delivery **[104]**. These mesoporous molecular sieves have application potential in adsorption, molecular sieving, membrane separation and chemical sensing. If a faster mass and transfer is required then it is possible to use colloidal particles of mesoporous molecular sieves.

1.11.1 Adsorption

As mesoporous materials were developed many potential applications emerged including utilising the pores for their ability to adsorb a variety of molecules. One of the first studies involving mesoporous solids as adsorbates was investigating MCM-41 by introducing a variety of gases into the pores, including nitrogen, oxygen and argon. It was observed that oxygen and argon isotherms exhibited hysteresis loops whereas the nitrogen isotherm was seen to be reversible, attributed to capillary condensation within the narrow range or pores.

Various studies have been carried out investigating adsorption of argon, nitrogen, oxygen, water, and hydrocarbons such as cyclopentane and benzene **[105,106].**

1.11.2 Catalysis

With the synthesis of the first mesoporous silicas, possibilities were apparent in the area of catalysis. Zeolites and variations of these are typically used as catalysts **[2, 107]** due to their open structure and active sites but there were problems due to their limiting pore diameter, generally of approx 10 Å. Progress was limited to conversion of molecules which could fit within these pores but this changed with the development of larger pore materials, particularly silica frameworks. Silica has many attributes of an ideal catalyst support including well defined pore system, high surface area, stable in solvents at varying temperatures and pressures and high surface concentration of silanol groups.

Mesoporous solids can also be readily functionalised in such a way as to incorporate active sites within the walls of the silica or by coating the inner surface with a catalytically active species.

It has been reported that by incorporation of aluminium into MCM-41 it is possible to use this material for acid catalysis **[108]**. Alkylation of 2, 4-di-tert-butylphenol with cinnamyl alcohol is possible within the pores of aluminosilicate MCM-41 **[109,110]**, unlike in zeolite Y where pore size restricts the formation of the primary alkylation product 6,8-di-tert-2-phenyl-2-3-dihydro[4H]benzopyran. Friedel Crafts alkylation and acylation are possible using aluminosilicate MCM-41 **[110-116]**. In addition to alkylation it is possible to incorporate metals such as titanium **[117]**, vanadium **[118,119]**, and zirconia **[120]** into mesoporous solids and investigate their effect on catalysis.

As hydrothermal stability is important in the application of mesoporous materials in catalysis, several methods have been investigated to improve these properties. They include decreasing the silanol group content of the framework which makes the surface more hydrophobic and stable in water, thickening the walls of MCM-41 to improve the hydrothermal stability and generating microporous zeolite-mesostructure composite mixtures.

Thiol-functionalised materials have been used as solid acid catalysts once the thiols have been oxidised to sulfonic acid groups, as ion exchangers and as heavy metal adsorbers.

These have advantages over previous catalytic systems as they avoid problems such as corrosion, toxic waste and hazards during handling.

1.11.3 Adsorption of proteins; Immobilisation of enzymes

The wide range of mesoporous materials now available with differing pore sizes and morphology has opened up opportunities for the immobilisation of homogeneous and enzymatic catalysts **[121-124]**. Enzymes have been shown to give high turnovers at mild conditions in comparison to transition metal catalysts **[125]**.

Functionalisation can enhance the properties of mesoporous silica as a support for enzymes **[126,127]**. By functionalising the surface of mesoporous molecular sieves with enzymes this allows highly selective catalysis to be carried out using materials that are chemically and mechanically tough and which can be easily separated from reaction mixtures. Mesoporous molecular sieves such as MCM-48, MCM-41 and SBA-15 have been used in enzyme immobilisation **[128-131]**. Yiu *et al.* **[59]** showed that larger pore mesoporous molecular sieves such as SBA-15 have a greater potential in immobilising enzymes than the more traditional MCM-41. Methods of enzyme immobilisation and the use of mesoporous silica as a support are described in more detail in chapter 5.

Until recently the main focus of protein adsorption has been on controlled pore glass and sol-gel type materials. Controlled pore glass (CPG) can be synthesised with pores ranging from 2 – 20 nm and extensive work has been carried out using it as a support for biological molecules. Problems arise with this material as it is relatively expensive and the surface area decreases strongly as the pore size is increased. Sol-gels have also been investigated but their pore size distribution is usually broad and their stability in aqueous media can be poor. Soon after the publication of the first mesoporous materials **[4,5,7]** researchers began looking at these new materials and their possible applications. Due to their thick walls, high stability and well defined pore systems it was not long before groups started working on using these materials as supports for proteins and this is covered in detail in chapters 4 and 5.

1.11.4 Drug Delivery

The development of drug delivery systems (DDS) utilising mesoporous materials has expanded rapidly in the last few years since MCM-41 was first used as a delivery system

[132]. Since then a variety of materials have been employed as DDS, including MCM-41, SBA-15 and MCM-48 **[133, 134]**. These mesoporous materials can be described as potential drug carriers due to several key features; they possess homogenous, ordered pore structures which allow the control of drug loading and release kinetics. High pore volumes allow sufficient loading of the drug required and a high surface area gives a large potential for drug adsorption. The surface of the material usually possesses silanol groups which provide opportunities for surface functionalisation which can in some cases allow the modification and control of loading and release of drug molecules. This is discussed further in chapter 6.

1.12 References

[1] Bradbury J (2004) Nature's Nanotechnologists: Unveiling the Secrets of Diatoms. PLoS Biol 2(10): e306

[2] A. Corma, *Chem. Rev*., 1995, **95**, 559.

[3] *IUPAC Manual of Symbols and Terminology*, Pure. Appl. Chem., 1978, **31**, 578.

[4] C.T. Kresge, M.E. Leonowicz, W.J. Roth, J.C. Vartuli, J.S. Beck, *Nature*, 1992, **359**, 710

[5] J.S. Beck, J.C. Vartuli, W.J. Roth, M.E. Leonowicz, C.T. Kresge, K.D. Schmitt, C.T-W. Chu, D.H. Olson, E.W. Sheppard, S.B. McCullen, J.B. Higgins, J.L. Schlenker, *J. Am. Chem. Soc.*, 1992, **114**, 10834

[6] J.S. Beck, N.Y. Princeton, US Patent No. 5 057 296, 1991

[7] T. Yanagisawa, T. Shimizu, K. Kuroda, C. Kato, *Bull. Chem. Soc. Jpn.*, 1990, **63**, 988

[8] V. Chiola, J.E. Ritsko, C.D. Vanderpool, US Patent No. 3556725, 1971

[9] F. DiRenzo, H. Cambon, R. Dutartre, Micropor. *Mesopor. Mater.*, 1997, **10**, 283

[10] X. Feng, G.E. Fryxell, L.Q. Wang, A.Y. Kim, J. Lui, K.M. Kemmer, *Science*, 1997, **276**, 923

[11] Q. Huo, D. Zhao, J. Feng, K. Weston, S.K. Buratto, G.D. Stucky, S. Schacht, F. Schüth, *Adv. Mater.*, 1997, **9**, 974

[12] F. Marlow, M.D. McGehee, D. Zhao, B.F. Chmelka, G.D. Stucky, *Adv. Mater.*, 1999, **11**, 632

[13] J. Loerke, F. Marlow, *Adv. Mater.*, 2002, **14**, 1745

[14] G. Bellussi, C. Perego, A. Carati, S. Peratello, E.P. Massara, G. Perego, *Stud. Surf. Sci. Catal.*, 1994, **84**, 85

[15] J.M. Thomas, *Nature*, 1994, **368**, 289

[16] T. Maschmeyer, R. Rey, G. Sankar, J.M. Thomas, *Nature*, 1995, **378**, 159

[17] J.M. Thomas, *Angew. Chem. Int. Ed. Engl.*, 1999, **38**, 3588

[18] M.D. Jones, R. Raja, J.M. Thomas, B.F.G. Johnson, D.W. Lewis, J. Rouzard, K.D.M. Harris, *Angew. Chem. Int. Ed. Engl.*, 2003, **42**, 4326

[19] D.S. Shephard, T. Maschmeyer, J.M. Thomas, B.F.G. Johnson, G. Sankar, D. Ozkaya, W. Zhou, R.D. Oldroyd, R.G. Bell, *Angew. Chem. Int. Ed. Engl.*, 1997, **36**, 2242

[20] J.M. Thomas, R. Raja, B.F.G. Johnson, T.J. O'Connell, G. Sankar, T. Khimyak, *J. Chem. Soc. Chem. Commun.*, 2003, **10**, 1126. See also *Science*, 2003, **300**, 867

[21] M.A. Carreon, V.V. Guliants, *Eur. J. Inorg. Chem.*, 2005, **1**, 27

[22] D.A. Doshi, A. Gibaud, V. Goletto, M. Lu, H. Gerung, B. Ocko, S.M. Han, C.J. Brinker, *J. Am. Chem. Soc.*, 2003, **125**, 11646

[23] H. Fan, H.R. Bentley, K.R. Kathan, P. Clem, Y. Lu, C.J. Brinker, *J. Non-Cryst. Solids*, 2001, **285**, 79

[24] R.D. Miller, *Science*, 1999, **286**, 421

[25] S. Che, A.E. Garcia-Bennett, X. Liu, R.P. Hodgkins, P.A. Wright, D. Zhao, O. Terasaki, T. Tatsumi, *Angew. Chem. Int. Ed., 2003*, **42**, 3930

[26] R. Ryoo, S.H. Joo, S. Jun, *J. Phys. Chem. B*, 1999, **103**, 7743

[27] Q. Huo, R. Leon, P.M. Petroff, G.D. Stucky, *Science*, 1995, **268**, 1324

[28] D. Zhao, Q. Huo, J. Feng, B.F. Chmelka, G.D. Stucky, *J. Am. Chem. Soc.*, 1998, **120**, 6024

[29] D. Zhao, Q. Huo, J. Feng, J. Kim, Y. Han, G.D. Stucky, *Chem. Mater.*, 1999, **11**, 2668

[30] C. Yu, Y. Yu, D. Zhao, *Chem. Commun.*, 2000, **7**, 575

[31] S. Shen, Y. Li, Z. Zhang, J. Fan, B. Tu, W. Zhou, *Chem. Commun.*, 2002, **19**, 2212

[32] X. Liu, B. Tian, C. Yu, F. Gao, S. Xie, B. Tu, R. Che, L. Peng, D. Zhao, *Angew. Chem. Int. Ed.*, 2002, **41**, 3876

[33] J. Fan, C. Yu, F. Gao, J. Lei, B. Tian, C. Wang, Q. Luo, B. Tu, W. Zhou, D. Zhao, *Angew. Chem. Int. Ed.*, 2003, **115**, 3254

[34] R. Ryoo, J.M. Kim, C.H. Ko, C.H. Shin, *J. Phys. Chem.*, 1996, **100**, 17718

[35] F. Kleitz, D. Liu, G.M. Anilkumar, I.N. Park, L.A. Solovyov, R. Ryoo, *J. Phys. Chem. B*, 2003, **107**, 14296

[36] F. Kleitz, S. H. Choi, R. Ryoo, *Chem. Commun.*, 2003, **17**, 2136

[37] C. Y. Chen, S.L. Burkett, H.L. Li, M.E. Davis, *Microporous Mater.*, 1993, **2**, 27

[38] Q. Huo, D. Margolese, U. Ciesla, D. Demuth, P. Feng, T. Gier, P. Sieger, A. Firouzi, B. Chmelka, F. Schüth, G.D. Stucky, *Chem. Mater.*, 1994, **6**, 1176

[39] C.J. Brinker, G.W. Scherer, Sol-Gel Science, Academic Press, San Diego, 1990

[40] R.K. Iler, The chemistry of silica – Solubility, polymerisation, colloid and surface properties and biochemistry, John Wiley and sons, 1979

[41] Q. Huo, D.I. Margolese, G.D. Stucky, *Chem. Mater.*, 1996, **8**, 1147

[42] J.N. Israelachvili, Intermolecular and surface forces, 2nd ed., 1991, Academic press, New York

[43] M.W.Anderson, C.C.Egger, G.J.T.Tiddy, J.L.Casci, K.A.Brakke, *Angew. Chem. Int. Ed.*, 2005, **44**, 2-6

[44] S. Che, Y. Sakamoto, O. Terasaki, T. Tatsumi, *Chem. Mater*., 2001, **13**, 2237

[45] R.P.Hodgkins, University of St Andrews, April 2005

[46] R.P. Hodgkins, A.E. Garcia-Bennett, P.A. Wright, *Micro. Meso. Mater.*, 2005, **79**, 241

[47] T. Yu, H. Zhang, X. Yan, Z. Chen, X. Zou, P. Oleynikov, D.Zhao, *J. Phys. Chem. B*, 2006, **110**, 21467

[48] O. Terasaki, T.Ohsuna, Z. Liu, Y.Sakamoto and A.E. Garcia-Bennett, Stud. *Surf. Sci. Catal*., 2004, **148**, 261

[49] Y.Sakamoto, M.Kaneda, O.Terasaki, D.Y.Zhou, J.M.Kim, G.D. Stucky, H.J.Shin and R.Ryoo, *Nature*, 2000, **408**, 449

[50] R.P.Hodgkins, University of St Andrews, April 2005

[51] P.T. Tanev, T.J. Pinnavaia, *Science*, 1995, **267**, 865

[52] P.T. Tanev, M. Chibwe, T.J. Pinnavaia, *Nature*, 1994, **368**, 321

[53] S. A Bagshaw, E. Prouzet, T. J. Pinnavaia,. *Science* 1995, **269**, 1242.

[54] G. S Attard, J. C. Glyde, C. G. Göltner, *Nature* 1995, **378**, 366.

[55] A. C Voegtlin,. F. Ruch, J. L Guth,. J. Patarin, L. Huve, *Microporous Mater.* 1997, **9**, 97

[56] M. J. Kim, R. Ryoo, *Chem. Mater*., 1999, **11**, 487

[57] S.Che, A. E. Garcia-Bennett, T. Yokoi, K. Sakamoto, H. Kunieda, O. Terasaki, T. Tatsumi, *Nature Materials*, 2003, **2**, 801

[58] R. Ryoo, S. Jun, J. *Phys. Chem. B.*, 1997, **101**, 317

[59] H.H.P. Yiu, P.A. Wright, N.P. Botting, *J. Mol. Catal. B Enzym.*, 2001, **15**, 81

[60] C.E. Fowler, S.L. Burkett, S. Mann, *Chem. Commun.*, 1997, **18**, 1769

[61] D.J. Macquarrie, *Chem. Commun.*, 1996, **16**, 1961

[62] M.H. Lim, A. Stein, *Chem. Mater*., 1999, **11**, 3285

[63] C.M. Yang, B. Zibrowius, F. Schüth, *Chem. Commun.*, 2003, **14**, 1772

[64] STA-11 thiol p123

[65] R. P. Hodgkins, A. E. Garcia-Bennett and P. A. Wright, *Microporous Mesoporous Mater*., 2005, **79**, 241

[66] F. Hoffmann, M. Cornelius, J. Morell, M. Froeba, *Angew. Chem., Int. Ed*., 2006, **45**, 3216

[67] M. Kruk, M. Jaroniec, C.H. Ko, R. Ryoo, *Chem. Mater*., 2000, **12**, 1961

[68] U. Ciesla, F. Schuth, *Microporous Mesoporous Mater*., 1999, **27**, 131

[69] B. Z. Tian, X. Y. Liu, C. Z. Yu, F. Gao, Q. Luo, S.H. Xie, B. Tu, D.Y. Zhao, *Chem. Commun.*, 2002, **11**, 1186

[70] J. Patarin, *Angew. Chem., Int. Ed*., 2004, **43**, 3878

[71] T. Clark, J.D. Ruiz, H.Y.Fan, C.J.Brinker, B.I. Swanson, A.N. Parikh, *Chem. Mater.*, 2000, **12**, 3879

[72] M. T. J. Keene, R. Denoyel, P. L. Llewellyn, *Chem. Commun*., 1998, 2203

[73]G. Buchel, R. Denoyel, P. L. Llewellyn, J. Rouquerol, *J. Mater. Chem*., 2001, **11**, 589

[74]C. M. Yang, B. Zibrowius, W. Schmidt, F. Schuth, *Chem. Mater*., 2003, **15**, 3739

[75] D. Zhao, J. Feng, Q. Huo, N. Melosh, G.H. Fredrickson, B.F. Chmelka, G.D. Stucky, *Science*, 1998, **279**, 548

[76] D. Zhao, Q. Huo, J. Feng, B.F. Chmelka, G.D. Stucky, *J. Am. Chem. Soc.*, 1998, **120**, 6024

[77] S.A. El-Safty, T. Hanaoka, *Chem. Mater*., 2003, **15**, 2892

[78] S.A. El-Safty, T. Hanaoka, *Chem. Mater*., 2004, **16**, 384

[79] P. Feng, X. Bu, G.D. Stucky, D.J. Pine, *J. Am. Chem. Soc*., 2000, **122**, 994

[80] C.Z. Yu, Y.H. Yu, D.Y. Zhao, *Chem. Commun.*, 2000, **7**, 575

[81] J. Fan, C.Z. Yu, T. Gao, J. Lei, B.Z. Tian, L.M. Wang, Q. Luo, B. Tu, W.Z. Whou, D.Y. Zhao, *Angew. Chem. Int. Ed.*, 2003, **42**, 3146

[82] L.M. Wang, H. Fan, B.Z. Tian, H.F. Yang, C.Z. Yu, B. Tu, D.Y. Zhao, *Micro. Meso. Mater*., 2004, **67**, 135

[83] S.A. El-Safty, T. Hanaoka, Nanotechnology in mesostructured materials, 2003, **146**, 173

[84] P.Y. Feng, X.H. Bu, D.J. Pine, *Langmuir*, 2000, **16**, 5304

[85] J.L. Blin, A. Léonard, B.L. Su, *Chem. Mater.*, 2001, **13**, 3542

[85a] S.S. Kim, A. Karkamkar, T.J. Pinnavaia, M. Kruk, M. Jaroniec, *J. Phys. Chem. B.*, 2001, **105**, 7663

[86] S.S. Kim, T.R. Pauly, T.J. Pinnavaia, *Chem. Commun.*, 2000, **17**, 1661

[87] X. Liu, B. Tian, C. Yu, F. Gao, S. Xie, B. Tu, R. Che, L.M. Peng, D. Zhao, *Angew. Chem. Int. Ed.*, 2002, **41**, 3876

[88] B.Z. Tian, X.Y. Liu, L.A. Solovyov, Z. Liu, H.F. Yang, Z.D. Zhang, S.H. Xie, F.Q. Zhang, B. Tu, C.Z. Yu, O. Terasaki, D.Y. Zhao, *J. Am. Chem. Soc.*, 2004, **126**, 865

[89] Y.T. Chan, H.P. Lin, C.Y. Mou, S.T. Liu, *Chem. Commun.*, 2002, **23**, 2878

[90] K. Flodstrom, V. Alfredsson, N. Kallrot, *J. Am. Chem. Soc.*, 2003, **125**, 4402

[91] A.E. Garcia-Bennett, PhD thesis, University of St. Andrews, September 2002

[92] F. Kleitz, S.H. Choi, R. Ryoo, *Chem. Commun.*, 2003, **17**, 2136

[93] Y.Q. Wang, C.M. Yang, B. Zibrowius, B. Spliethoff, M. Lindén, F. Schüth, *Chem. Mater.*, 2003, **15**, 5029

[94] S. Che, A.E. Garcia-Bennett, X. Liu, R.P. Hodgkins, P.A. Wright, D. Zhao, O. Terasaki, T. Tatsumi, *Angew. Chem. Int. Ed.*, 2003, **42**, 3930

[95] M. Templin, A. Franck, A. DuChesne, H. Leist, Y.M. Zhang, R. Ulrich, V. Schadler, U. Wiesner, *Science*, 1997, **278**, 1795

[96] D. Zhao, J. Sun, Q. Li, G. Stucky, *Chem. Mater.*, 2000, **12**, 275

[97] R. Ryoo, S.H. Joo, S. Jun, T. Tsubakiyama, O. Terasaki, *Stud. Surf. Sci. Catal.*, 2001, **135**, 150

[98] S. Jun, S.H. Joo, R. Ryoo, M. Kruk, M. Jaroniec, Z. Liu, T. Ohsuna, O. Terasaki, *J. Am. Chem. Soc.*, 2000, **122**, 10712

[99] S.H. Joo, R. Ryoo, *J. Phys. Chem. B*, 2002, **106**, 1256

[100] F. Kleitz, S.H. Choi, R. Ryoo, *Chem. Commun.*, 2003, **17**, 2136

[101] W.Z.Zhou, K.K.Zhu, B.Yue, H.Y.He and C.Dickinson, *Stud. Surf. Sci. Catal.*, 2004, **154**, 924

[102] H.J.Shin, R.Ryoo, Z. Liu and O.Terasaki, *J. Am. Chem. Soc.*,2001, **123**, 1246

[103] A. Corma, *Chem. Rev.*, 1997, **97**, 2373

[104] M. Vallet-Regi, *Chem. Eur. J*, 2006, **12**, 1

[105] O. Franke, G. Schulz-Ekloff, J. Rathouský, J. Stárek, A. Zukal, *J. Chem. Soc., Chem. Commun.***,** 1993, 724

[106] P. J. Branton, P. G. Hall, K. S. W. Sing, ***J****. Chem. Soc., Chem. Commun.***,** 1993, 1257

[107] A. Corma, *Chem. Rev.*, 1997, **97** , 2373

[108] S. Jun, R. Ryoo, *J. Catal* , 2000, **195**, 237

[109] R. Tismaneanu, B. Ray, R. Khalfin, R.Semiat, M. S. Eisen, *J. Mol. Cat. A:Chem.*, 2001, **171**, 229

[110] E. Armengol, M.L. Cano, A. Corma, H. García, M.T. Navarro, *J. Chem. Soc., Chem. Commun.* 1995, 519.

[111] Armengol, E.; Corma, A.; García, H.; Primo, J. *Appl. Catal. A.*, 1995, **126**, 391

[112] Armengol, E.; Corma, A.; García, H.; Primo, J. *Appl. Catal. A.*, 1997, **149**, 411.

[113] Le, Q. N. U.S. Patent 5,191,134, 1993.

[114] Gunnewegh, E. A.; Gopie, S. S.; Van Bekkum, H. *J. Mol. Catal. A: Chem.*, 1996, **106**, 151.

[115] Van Bekkum, H.; Hoefnagel, A. J.; Van Koten, M. A.; Gunnewegh, E. A.; Vogt, A.H. G.; Kouwenhoven, H. W. *Stud. Surf. Sci. Catal.* 1994, **83**, 379.

[116] Kloestra, K. R.; Van Bekkum, H. *J. Chem. Res. (S)* 1995, **1**, 26.

[117] A. Corma, M. T. Navarro, J. Pérez-Pariente, *J. Chem. Soc., Chem. Commun.* 1994, 147

[118] W. Zhang , T.J. Pinnavaia, *Catal. Lett.* 1996, **38**, 261

[119] K. M. Reddy, I. Mondrakovski, A. Sayari, *J. Chem. Soc., Chem. Commun.* 1994, 1059

[120]P.E. Marti, M. Maciejewski, A. Baixer, *J. Catal.* 1993, **139**, 494

[121] A. Daehler, G. W. Stevens and A. J. O'Connor, in *Nanoporous Materials—Science and Engineering*, ed

[122] G. Q. Lu and X. S. Zhao, Imperial College Press, London, 2004, 812.

[123] H. H. P. Yiu and P. A. Wright, in *Nanoporous Materials—Science and Engineering*, ed.

[124] G. Q. Lu and X. S. Zhao, Imperial College Press, London, 2004, 849

[125] H. E. Schoemaker, D. Mink, M. G. Wubbolts, *Science*, 2003, **299**, 1694

[126] Y.-J. Han, G. D. Stucky and A. Butler, *J. Am. Chem. Soc.*, 1999, **121**, 9897

[127] H. H. Weetall, *Appl. Biochem. Biotechnol.*, 1993, **41**, 157

[128] J. W. Zhao, F. Gao, Y. L. Fu, W. Jin, P. Y. Yang and D. Y. Zhao, *Chem. Commun.*, 2002, 752

[129] J. F. Díaz and K. J. Balkus, Jr., *J. Mol. Catal B: Enzym.*, 1996, **2**, 115

[130] J. Lei, J. Fan, C. Yu, L. Zhang, S. Jiang, B. Tu and D. Zhao, *Microporous Mesoporous Mater*, 2004, **73**, 121

[131] A. Vinu, V. Murugesan and M. Hartmann, *J. Phys. Chem. B*, 2004, **108**, 7323

[132] M. Vallet-Regi, A. Ramilla, R. P. del Real, J. Perez-Pariente, *Chem. Mater*., 2001, **13**, 208

[133] F. Balas, M. Manzano, P. Horcajada, M. Vallet-Regi, *J. Am. Chem. Soc*., 2006, **128**, 8116

[134] J. C. Doadrio, E. M. B. Sousa, I. Izquierdo-Barba, A. L. Doadrio, J. Perez-Pariente, M. Vallet-Regi, *J. Mater. Chem*., 2006, **16**, 462

2. Characterisation methods

2.1 Introduction

It is important to establish the type and 'quality' of porous solids to rationalise their behaviour in applications. In this work the characterisation has mainly been performed using nitrogen adsorption and electron microscopy. Nitrogen adsorption establishes whether the solid is mesoporous and the nature of the porosity - how well defined the porous system is and also the pore size distribution and surface area. Electron microscopy gives details of the order of the mesophase structure and can indicate the presence of intergrowth and other defects. It is also possible to obtain information about the long range order of the bulk sample from XRD, but diffraction peaks are only present at very low angles and only in very well ordered structures. Silicas functionalised using propylthiol groups have been characterised by elemental analysis and thermogravimetric analysis.

2.2 Porosimetry *via* Nitrogen Adsorption

Nitrogen adsorption at 77 K is a convenient and widely used method to establish details of porosity. When a gas or vapour is brought into contact with a porous solid, it may be taken up by the solid or remain on the external surface. For porous solids, the internal volume is considered as an internal surface and adsorption is the general term used to describe the uptake. Two different methods were used to measure adsorption: gravimetric and volumetric. Gravimetric analysis measures the sample weight at known equilibrium pressures of gas within the system whereas volumetric analysis calculates the uptake by measuring pressure changes as known amounts of gas are admitted to the system. The results can be expressed as adsorbed masses or as a volume of gas (at standard temperature and pressure) adsorbed per gram.

The pore volume and pore size distribution can be measured by analysis of gas adsorption, which can therefore be used to determine whether a sample is microporous or mesoporous. It can also be used, where appropriate, to determine the surface area and for mesoporous solids, channel and window dimensions. It is based on the fact that gas condenses to liquid in narrow pores at pressures less than the saturated vapour pressure of the adsorbate.

Typically, adsorbate uptake is measured at constant temperature as a function of adsorbate pressure, typically expressed in relation to its saturated vapour pressure (P/P_o). For N_2 this is 1 bar at 77 K. Adsorption of monolayers onto surfaces or into micropores occurs at low P/Po values (< 0.1) whereas adsorption onto open surfaces as multilayers or into mesopores occurs gradually over the whole range of P/Po values.

The data gathered can be used to plot a graph of total number of moles of adsorbate per gram of adsorbent versus pressure. These graphs may be categorised as one of 5 different types of adsorption isotherm – known as the Brunauer classification **[1]**, shown in Figure 2.1.

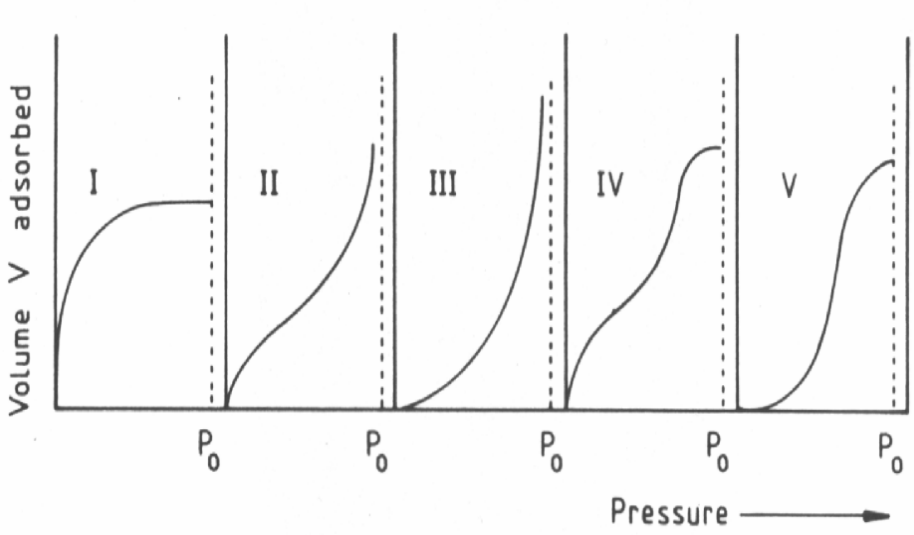

Figure 2.1 The Brunauer classification of the five types of adsorption isotherms. Po is the saturation vapour pressure [2]

Microporous solids, solids with pore widths < 2 nm, typically produce type I isotherms. They are characterised by a rapid rise in the volume adsorbed at low pressures followed by a plateau. This rapid rise is due to pore filling, whilst the plateau is determined by total pore volume. Any gradual increase in adsorption at high partial pressures, therefore, is attributable to multilayer coverage of the external surfaces.

Type II isotherms are characteristic of adsorption on an open surface, where the initial formation of a monolayer is followed by the formation of multilayers. Under these conditions the Brunauer-Emmett-Teller (BET) theory gives equation 2.1 **[3]** which is derived from the polarisation theory of De Boer and Zwicker **[4]**:

$$\frac{P}{V(P_0 - P)} = \frac{c-1}{V_m c} * \frac{P}{P_0} + \frac{1}{V_m c} \qquad \text{Equation 2.1}$$

where V is the volume of gas adsorbed (corrected to STP) at a specific value of P, an equilibrium pressure with the constant c. The BET equation assumes that a monolayer of gas adsorbed will possess a fixed heat of adsorption (H_1), subsequent layers having heats of adsorption equal to the latent heat of evaporation (H_L). However the equation does have limitations, as it can only be applied for the linear part of the isotherm, at pressures 0.05<P/Po<0.35 for open surfaces. This proves a problem in the case of some mesoporous materials where capillary condensation occurs in this region.

Adsorption on mesoporous solids typically exhibits type IV isotherms, where the initial monolayer coverage is built upon by multilayer adsorption at higher adsorbate pressures, in a similar way to that observed in type II. Capillary condensation within the mesopores, at higher relative pressures, results in a steeper upward slope, characteristic of type IV isotherms. The pore size distribution can be derived traditionally using the Barrett-Joyner and Halenda (BJH) **[5]** and the De Boer modifications **[6]** of the Kelvin equation and expressions for the multi-layer adsorbate film thickness as a function of adsorbate pressure, P.

Mesopores of different diameters exhibit capillary condensation at pressures given by the Kelvin equation (equation 2.2):

$$\ln \frac{P}{P_o} = \frac{-2\gamma V_L}{RT} \frac{1}{r_m} \qquad \text{Equation 2.2}$$

It is possible to use the Kelvin equation to estimate pore radii from a gas adsorption isotherm. At any equilibrium pressure P, pores of radii less than r_m will be filled with condensed vapour. P/P_o is the relative pressure of vapour in equilibrium with a meniscus having a radius of curvature r_m, and γ and V_L are the surface tension and molar volume respectively, of the liquid adsorbate.

Multilayer adsorption usually accompanies capillary condensation in the pores of solids and this means that the Kelvin equation will not give the correct radius as the radius of the silica channel at condensation will have been effectively reduced by the thickness of the adsorbed layer. This is accounted for by the factor t in equation 2.3 which represents the

thickness of the adsorbed monolayer. The thickness can be calculated from the BET equation, as mentioned previously.

$$r_p = \frac{2\gamma V}{RT \ln \frac{Po}{P}} + t \qquad \text{Equation 2.3}$$

For mesoporous solids with a narrow pore size distribution there is a significant increase in uptake over a narrow pressure region and the type IV isotherm – now distinguished from the type II isotherm – upon pore filling reaches a plateau with the upper limit of adsorption governed by the total pore volume.

For type IV solids demonstrating a capillary condensation step, over a narrow P/Po range, the pore size distribution can be derived by using the Barrett-Joyner and Halenda (BJH) or the De Boer modifications of the Kelvin method. In this work the pore size distribution curve is calculated on the adsorption branch of the isotherm in the high relative pressure region using the De Boer model in the case of the gravimetric analysis. When using a volumetric adsorption method the pore size distribution can be calculated on both the adsorption and desorption branch using BJH theory. Valuable information about the specific surface area, the size, shapes of pores, the setting in of reversible capillary condensation and complete filling of pores may therefore be obtained.

Porosity measurements were obtained gravimetrically using a Hiden Intelligent Gravimetric Analyser (IGA-II) automated gravimetric analyser (Figure 2.2) and also volumetrically using a Micromeritics ASAP 2020 (Figure 2.3). In the case of the IGA, typically between 10 – 25 mg of sample are used in each isotherm run. The sample is suspended in a weighing boat within a sealed metal jacket which is heated and the sample is outgassed at 393 K for 2 hours before being cooled, to typically 308 K, when the dry mass is set. The sample inside the metal jacket is submerged in a liquid nitrogen dewar and data collection started at typically 80 K. The isotherm run follows a program consisting of an adsorption branch followed by a desorption branch.

If volumetric analysis is being performed the solid (100-500 mg) is placed in a glass tube which is connected to the ASAP 2020 and outgassed as with the gravimetric method before undergoing a similar liquid nitrogen submersion.

Figure 2.2 A Hiden IGA (Intelligent Gravimetric Analyser) used to measure N_2 isotherms at 77K.

Figure 2.3 Micromeritics ASAP 2020 [7]

For mesoporous solids, the desorption isotherm shows hysteresis when compared to the adsorption isotherm. Two types of hysteresis behaviour are observed for mesoporous solids, depending on their internal structure and pore connectivity. Cylindrical pore or channel networks, such as SBA-15 and KIT-6, give a type H1 hysteresis loop whereas the large pore cage-like structures SBA-16 and FDU-12, which consist of a series of cavities connected by smaller windows, exhibit type H2 hysteresis. Type H1 hysteresis have parallel adsorption and desorption branches due to the uniform channel and entrance sizes and can be seen in Figure 2.4.

In the large pore cage silica materials the size of the large cavities determines the position of the adsorption branch of the isotherm, whereas the size of the smaller connecting windows controls the pressure at which the gas is desorbed and can be followed using the desorption branch **[8]**. The smaller these entrances the lower the relative pressure has to be for the gas to leave the solid. The desorption branch will always return to meet the adsorption branch at a partial pressure of 0.42, as this point is the thermodynamic limit for the stability of bulk nitrogen **[9]**.

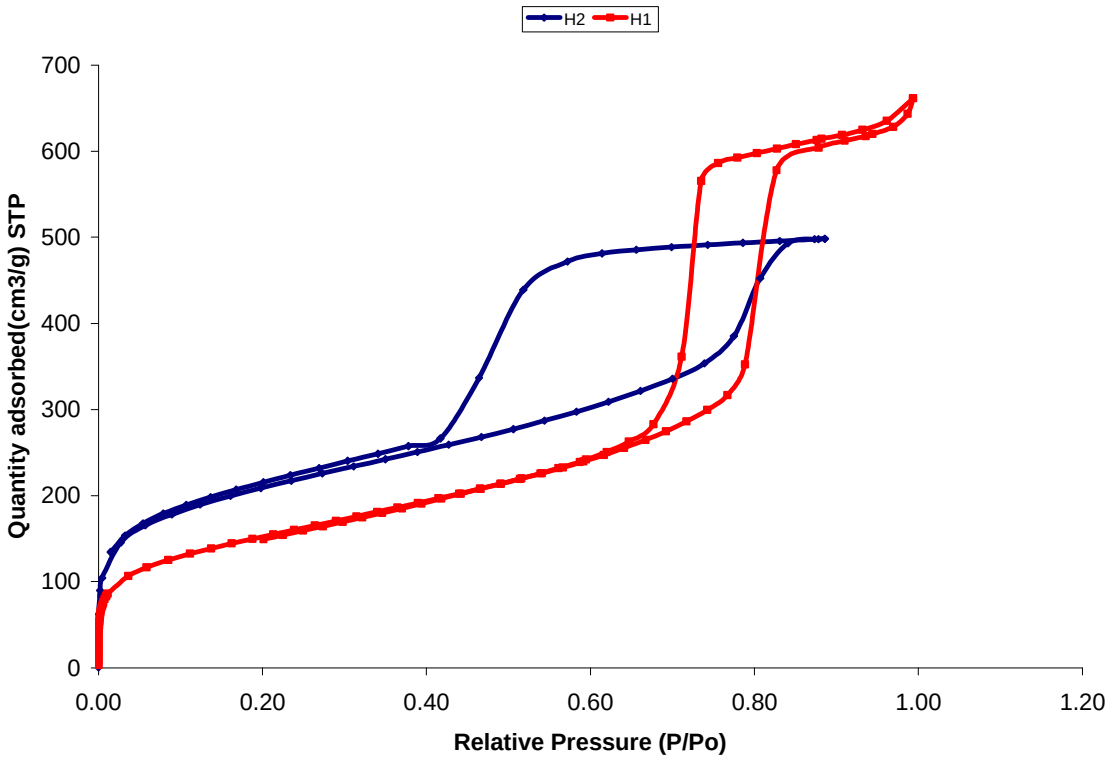

Figure 2.4 Two possible hysteresis types obtained from mesoporous silica - H1 and H2. H1 hysteresis is obtained from mesoporous materials possessing a cylindrical channel network whereas H2 results for cage structures where large cavities are connected by smaller windows

For adsorption on samples that exhibit type H2 hysteresis there is first an initial monolayer of adsorption, in which all the adsorbed molecules are in contact with the surface layer of the adsorbate. This is followed by multilayer adsorption as the adsorption space is able to accommodate more than one layer of molecules. Smaller entrances can become filled but the gas is able to diffuse to larger cavities until capillary condensation occurs. This is due to multilayer adsorption from the vapour proceeding to the point at which pore spaces are filled with liquid separated from the gas by a meniscus.

Desorption occurs through the smaller entrance windows with the gas from the larger cavities continually leaving the solid *via* these windows. The windows are filled by the adsorbate during the de-gassing process until finally all the adsorbate has been desorbed at low pressure, controlled by the pore diameter. This can be seen in Figure 2.5 with the desorption branch of the hysteresis being shifted to higher pressure when the pore size is increased.

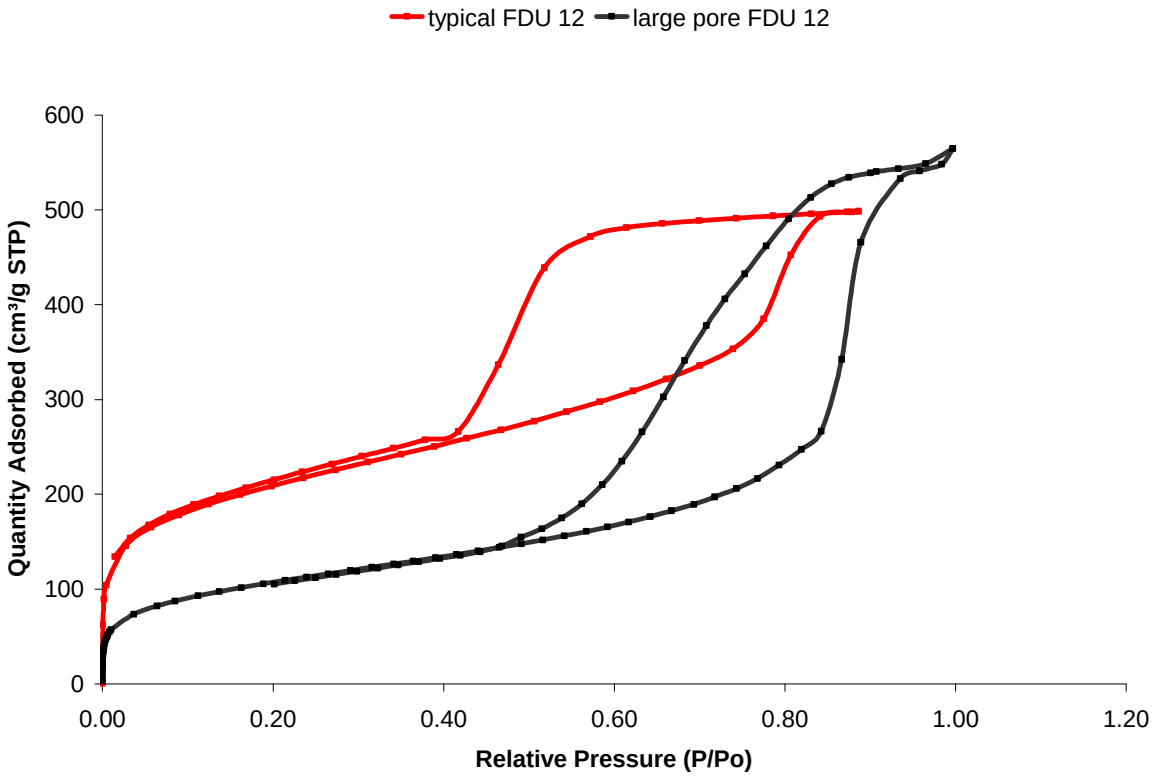

Figure 2.5 Effect of pore size on H2 type hysteresis loop. Typical FDU-12 isotherm shows characteristic drop in the desorption branch at 0.42 P/Po whereas as the cavity and entrance window size are increased the adsorption and desorption branches are shifted to higher relative pressure

As described, two gas adsorption porosimeters were used throughout this work; the IGA-II series automated gravimetric analyser (Figure 2.2) and the volumetric Micromeritics ASAP 2020. In order to ensure we can compare samples run on both porosimeters a sample of SBA-15 was analysed using both machines and the isotherms obtained can be seen below in Figure 2.5.1.

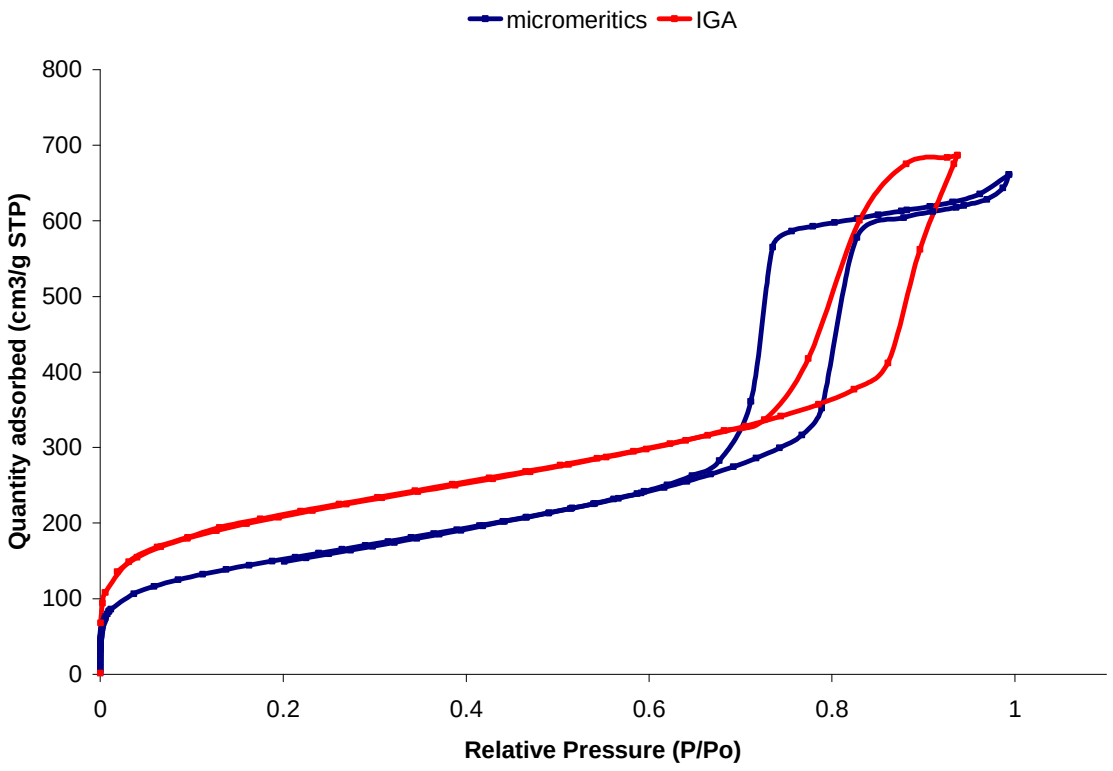

Figure 2.5.1 Nitrogen isotherm for SBA-15 on both IGA gravimetric and Micromeritics volumetric analyser.

The IGA gives a pore diameter of 8 nm whereas the Micromeritics gives a slightly lower value of 7.5 nm. The surface area is also slightly higher with a surface area of 631 and 540 m^2/g for the IGA and Micromeritics respectively. It is likely that the temperature of the sample is slightly higher during an isotherm run using the IGA as the sample is not in direct contact with the wall of the apparatus. As a result of this it is possible that the values of pore dimensions measured on the IGA will be overestimated. In this project when comparing a series of samples the materials were all run using the same machine and conditions, predominantly the Micromeritics ASAP 2020.

2.3 Transmission Electron Microscopy

High resolution transmission electron microscopy (HRTEM) is crucial in structural characterisation of ordered mesoporous materials. High resolution imaging provides structural details, but only of a small volume within a sample. It is most useful when combined with other techniques such as nitrogen adsorption and X-ray diffraction which give the pore structure and an indication of the long range order in the bulk. In comparison to microporous solids, images of mesoporous solids can be obtained at relatively low magnification as they possess a larger unit cell so there are fewer problems with loss of structure under the electron beam. Extensive and substantial work has been carried out on the use of HRTEM to solve the structures of mesoporous solids and as a result it is possible to identify different phases on the basis of characteristic electron micrographs taken down particular zones **[10,11]**.

2.3.1 Theory and Practice

The transmission electron microscope was first developed in the 1930s when it became apparent that atomic resolution would be possible using electrons of high energy**.**
Applying a potential drop of 100-1000 keV generates a high energy beam of kinetic energy (Equation 2.4)

$$eV = \frac{m_0 v^2}{2} \qquad \text{Equation 2.4}$$

Increasing the potential, i.e. the positive voltage, accelerates the electron. Increasing the velocity decreases the wavelength and leads to the relationship between the electron wavelength, λ and the accelerating voltage of the electron microscope, V (Equation 2.5)

$$\lambda = \frac{h}{(2m_0 eV)^{1/2}} \qquad \text{Equation 2.5}$$

Where m_0 and e are the mass and charge of the electron respectively and *h* is Planck's constant. De Broglie related the wavelength of the electrons to their energy, E. (Equation 2.6):

$$\lambda = \frac{1.22}{E^{1/2}} \qquad \text{Equation 2.6}$$

with E in electron volts (eV) and λ in nm.

Therefore for a 100 keV electron microscope the theoretical wavelength is about 4 pm (0.004 nm), much smaller than the diameter of the atom, although electron microscopes do not achieve such theoretical resolutions due to imperfections in the magnetic lenses. A series of lenses are required in order to focus and magnify the beam through the microscope. A schematic representation of an electron microscope from the electron source to the image is shown in Figure 2.6.

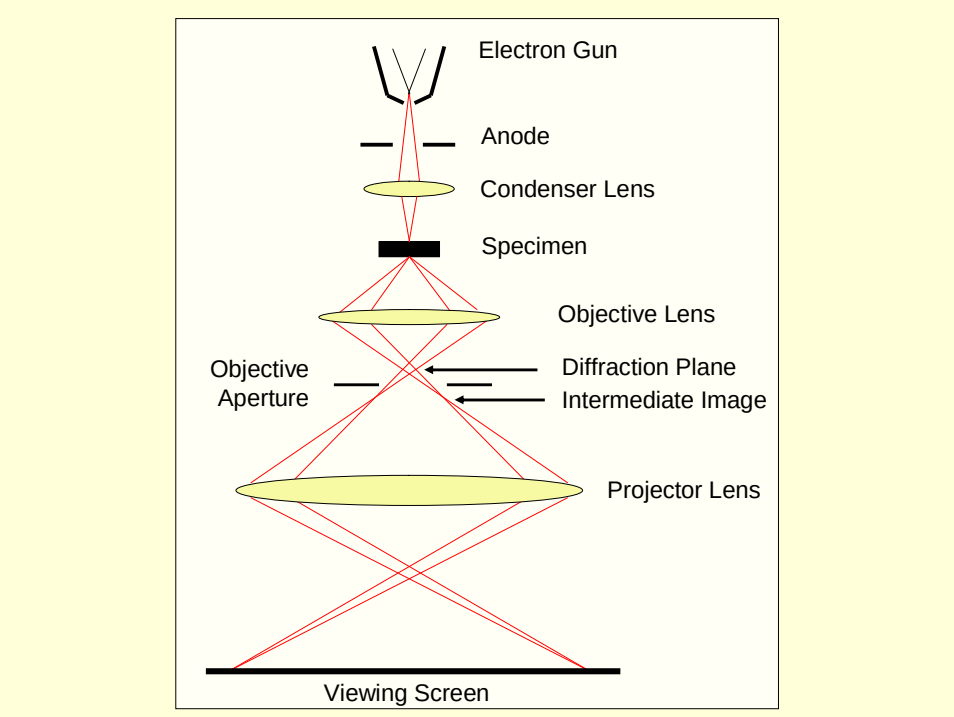

Figure 2.6 Schematic representation of electron microscope

In the JEOL 2011 instrument used in this work (Figure 2.7), electrons are generated by heating a lanthanum hexaboride (LaB_6) filament in a vacuum. When located at the filament the electrons have high potential energy and low kinetic energy. Due to the operating voltage (200 keV in the JEOL 2011) the electrons are accelerated to the anode and pass through it. As the electron beam moves down the electron microscope column it passes through a series of lenses. The first lens is the condenser lens; this focuses the beam on the specimen. As the electron beam passes through the specimen some electrons are scattered whilst the remainder are focused by the objective lens either onto a phosphorescent screen or a CCD detector to form an image. Unfocussed electrons are blocked out by the

objective aperture, resulting in an enhancement of the image contrast. The contrast of the image can be increased by reducing the size of this aperture. The remaining lenses on the TEM are the intermediate lens and the projector lens. The intermediate lens is used to control magnification. The projector lens corresponds to the ocular lens of the light microscope and forms a real image on the fluorescent screen at the base of the microscope column.

Figure 2.7 High resolution transmission electron microscope equipped with EDX operating at 200 keV at the University of St. Andrews

Image formation is through recombination of transmitted electron beams. The TEM can operate either in diffraction mode, where the diffracted beams are observed on the screen or (by changing lenses after the specimen) an image can be obtained by refocusing scattered beams. The quality of the image is dependent on the alignment of the electron beam. The condenser lens is the first lens that the beam passes through, which focuses the beam onto the specimen. Combined with the objective aperture it is now possible for the

contrast of the sample to be changed. Once the beam has passed through the specimen it then passes through the objective lens, whereby a diffraction pattern can be viewed. Finally the beam passes through the projector lens which then displays the resulting image on the viewing screen.

A parallel beam is needed since it is more coherent than a con- or divergent beam and this enhances phase contrast and makes interpretation of such images more straightforward.

If the beam is under focused it is focused beneath the plane of the specimen which means it is a more parallel beam than if were focused above (or at) the plane of the specimen since then the electrons would be diverging strongly. This is shown below in Figure 2.8.

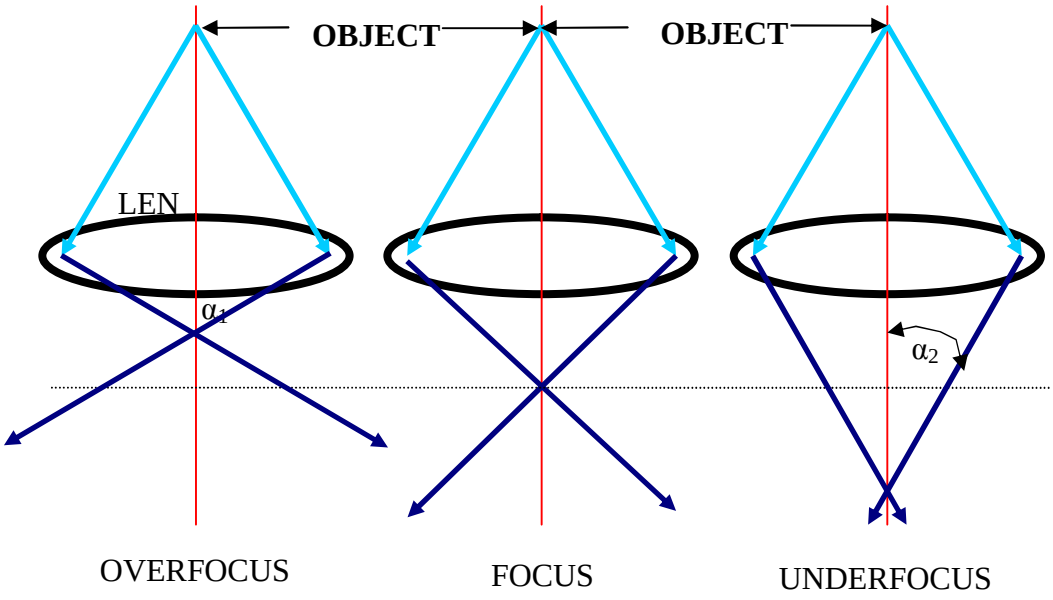

Figure 2.8 Under focusing gives a more parallel beam and thus enhances phase contrast of the image

There are several factors which can limit the resolution of the images produced. The objective lens does not have an infinite size and this results in difficulty in re-focusing wide angle diffracted beams and loss on resolution. Astigmatism can occur due to asymmetry of the magnetic field within a lens which can lead to a distortion of the observed image.

Alignment of the electron beam is crucial in obtaining a high quality image with high resolution. As it is near impossible to make a perfectly curved lens, defects can arise due to spherical aberration. The effect is a measure of the difference between where the beam

should be compared to where it is actually located combined with the magnification, spherical aberration and the solid angle.

The resolution of image is based on the focus conditions, of which electron microscope resolution is best at out-of-focus conditions (Figure 2.9-A). There are two such out-of-focus conditions, over (Figure 2.9-B) and under focus (Figure 2.9 C). Under focus gives the correct view of the sample where as over focus gives the reverse contrast. It can be seen that the pores are white for under focus and black for over focus.

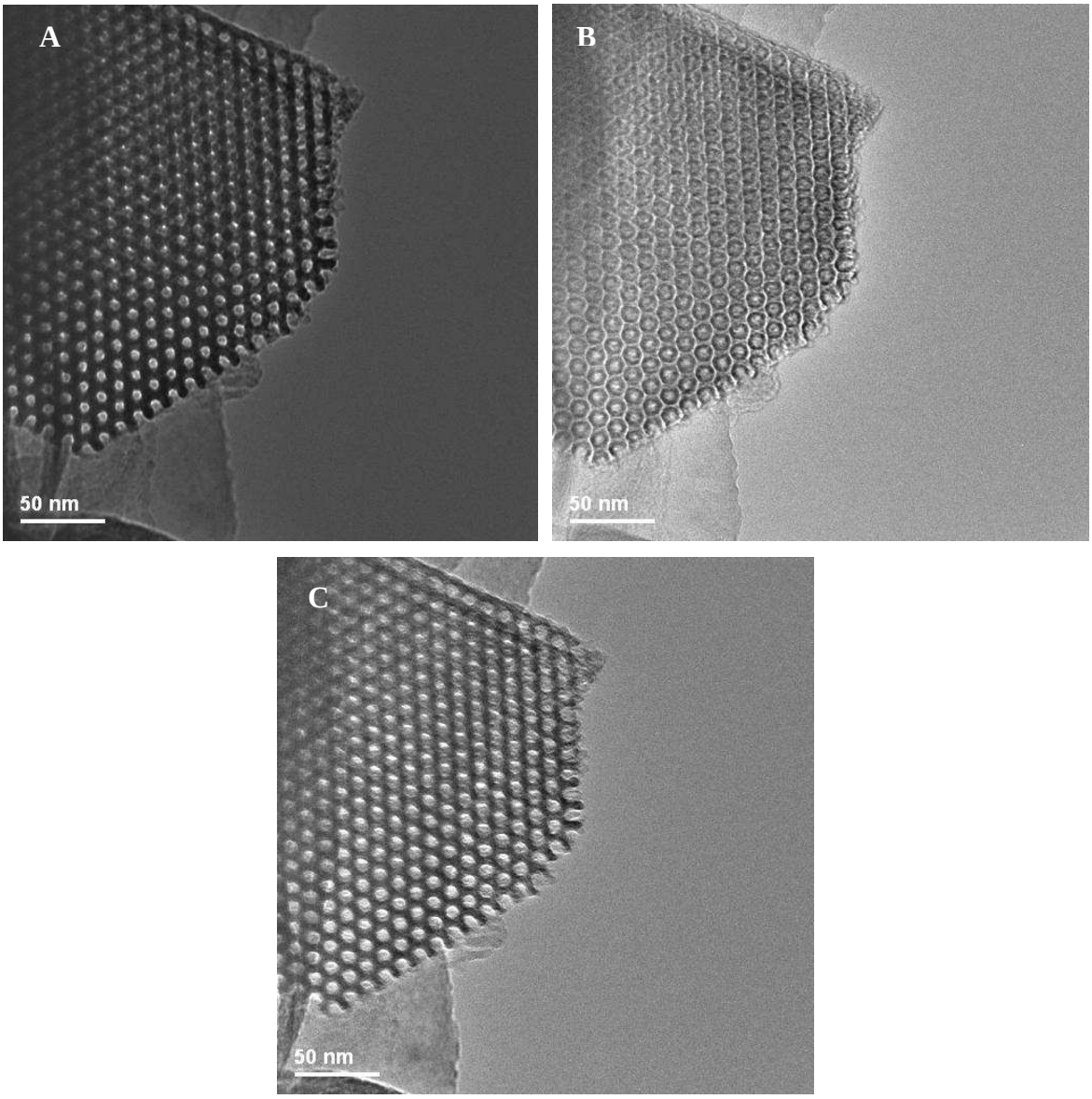

Figure 2.9 TEM focus conditions; A-at focus, B-over focus, C-under focus

As well as diffraction and imaging, which make use of electrons scattered elastically (diffraction) or transmitted through the thin specimen (imaging), additional processes occur within an electron microscope. The energetic electrons in the microscope strike the sample and various interactions can occur as shown below (Figure 2.10). The interactions noted on the top side of the diagram are most important when examining thick or bulk specimens (SEM) while those that give transmission are those examined in thin or foil specimens (TEM).

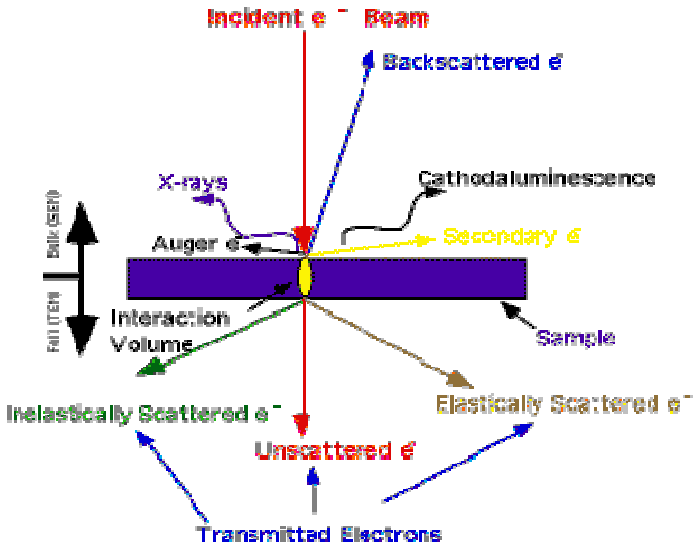

Figure 2.10 Schematic of the path taken by electrons as they strike the sample

The specimen grid used is typically 3 mm in diameter and it is possible to achieve magnification of up to 1 200 000x.

The JEOL 2011 TEM (shown in Figure 2.7) also has a GATAN CCD camera attached, which saves images straight to the computer. Analytical elemental analysis can be carried out on the specimen using the EDX system attached. The TEM has a resolution of 0.18 nm and can be operated at accelerating voltages between 80 and 200 kV.

2.3.2 Sample preparation

Sample preparation for HRTEM is dependent on the stability of the sample and can either be carried out as a dry preparation or solvent suspension (used in this thesis). The solvent most commonly used is acetone as it evaporates rapidly although ethanol can also be used. The sample is ground using a mortar and pestle before a few drops of acetone are added and the two are mixed together. A pipette can then be used to transfer a few drops of the suspension onto a carbon film covered in tiny holes which is supported on a copper grid (schematic shown in Figure 2.11). The solvent then evaporates leaving the sample on the carbon film ready for use.

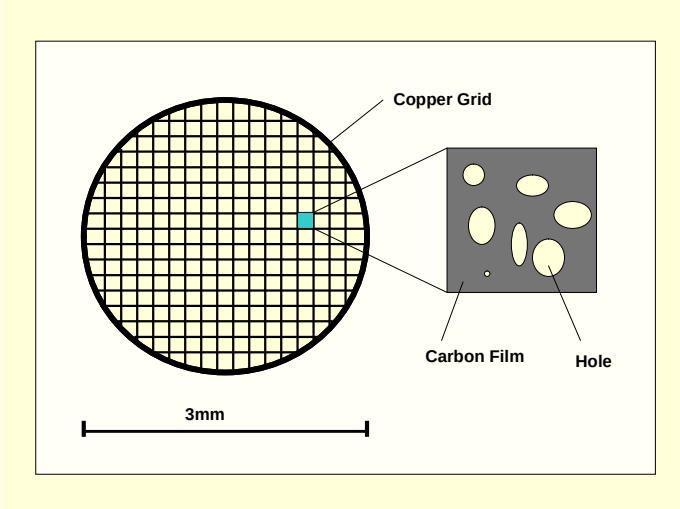

Figure 2.11 Schematic representation of copper grid used

Along with beam alignment and focusing conditions the location of the specimen on the copper grid is of importance. Within the grid there are many possible sites that a particle can be found in (shown in Figure 2.12, A-D). They can be situated overlapping the copper wall at the edge of the sample grid which can distort any images obtained and interfere with any elemental techniques such as EDX (A). If the particle is positioned on the carbon film rather than over a hole in the grid the amorphous carbon can cause problems for high resolution imaging (B). Problems can arise with achieving clear images if the particle is surrounded or overlapped by additional particles (C). The ideal locality for attaining a good

image is when the particle is found with an edge over a hole, providing a clear background so as to prevent any interference from the carbon film (D).

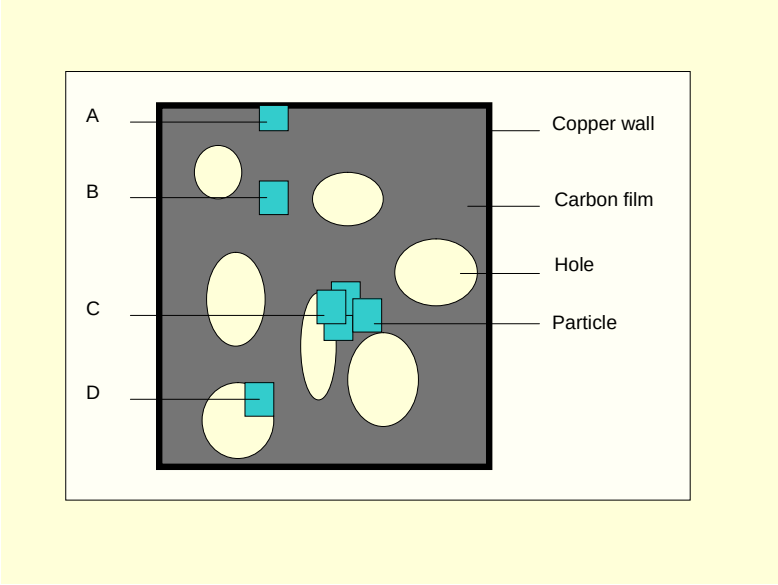

Figure 2.12 Possible positions of the material on the copper grid

TEM is used to understand the local structure of a sample and in the case of mesoporous solids it can be used to solve structures and therefore extensive research has been carried out utilising HRTEM to help solve their structures. **[10,11]** TEM can be used to identify various pore arrangements and symmetry including cubic systems such as FDU-12 (Fm3m) and KIT 6 (Ia3d) as seen in Figure 2.13. The GATAN software used to examine the images obtained can produce Fourier transform diffraction patterns (FTT) as shown in Figure 2.13.

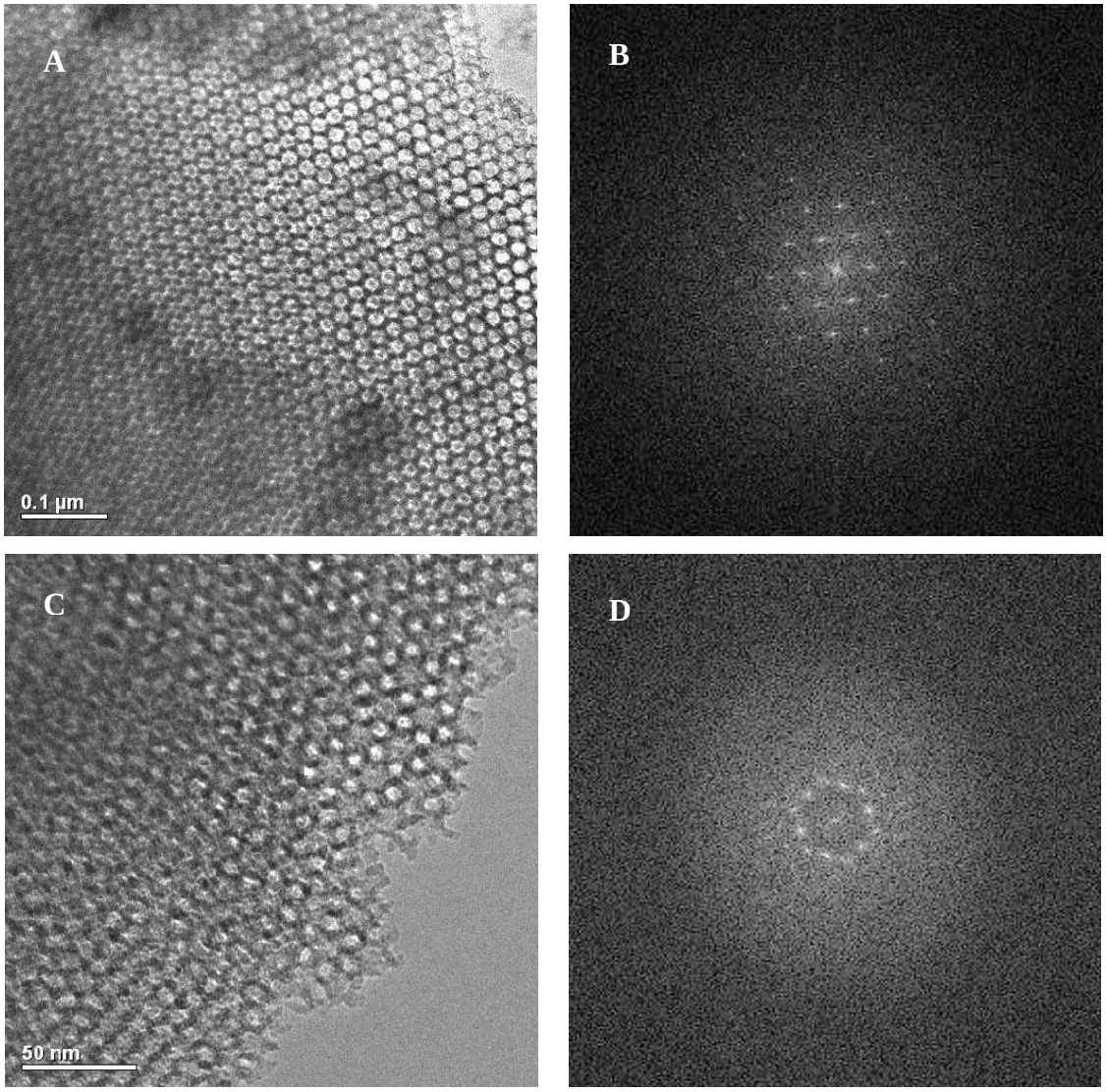

Figure 2.13 HRTEM of (A) FDU-12 [110] view and (C) KIT 6 [111] view and corresponding FFT (Fourier transform) images for FDU-12 (B) and KIT 6 (D)

SBA-15 is a 2D hexagonal mesoporous silica and there are two possible views obtained using an electron microscope and these are shown in Figure 2.14 with the channel axis parallel to the electron beam seen in A, showing the entrances to the pores and channels shown in C where the beam is perpendicular to the channels. B shows the Fourier transform 'diffraction pattern' (FFT) of image A, indicating all the area examined is a single crystal.

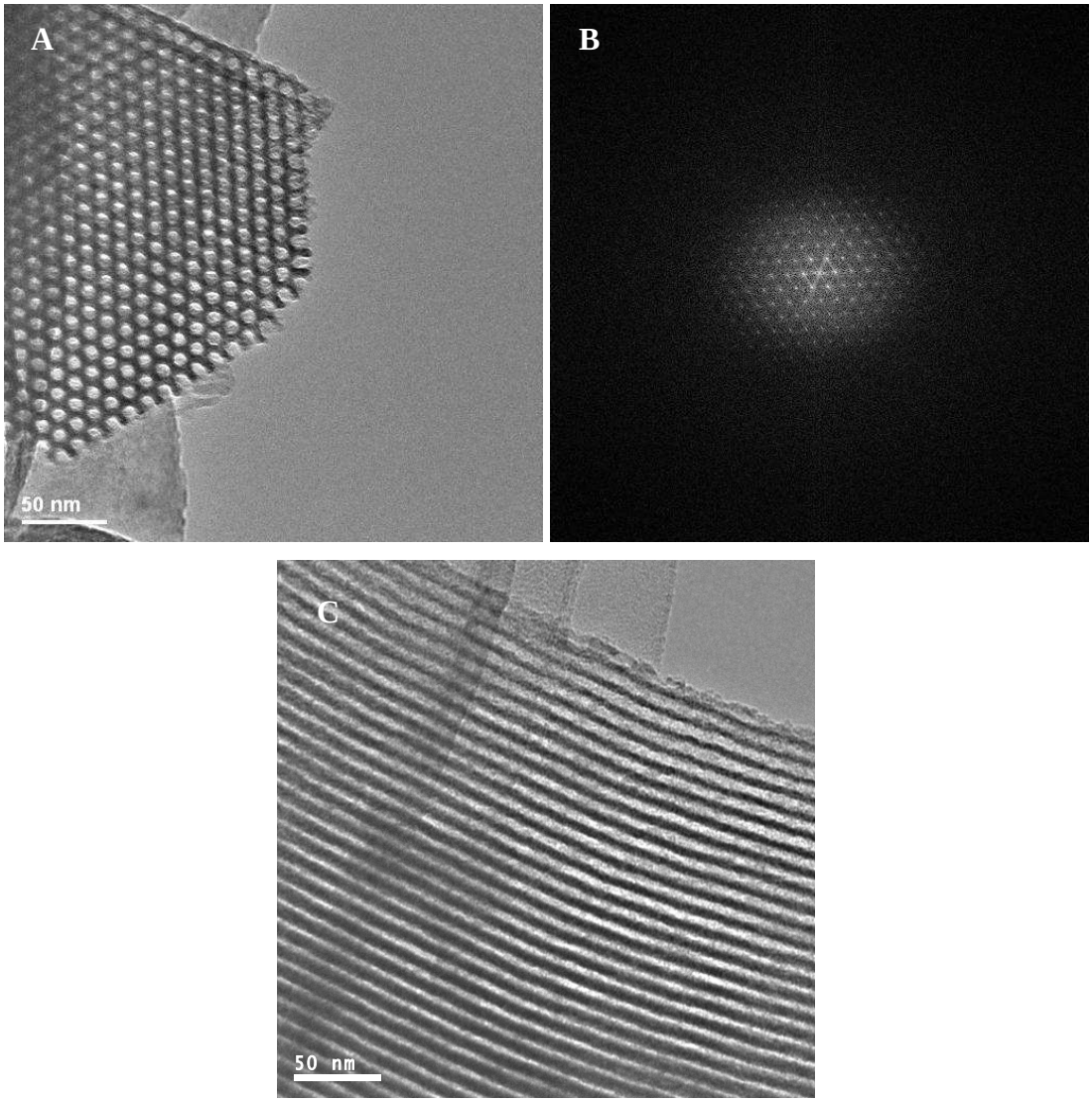

Figure 2.14 A-[0 1] zone axis of SBA-15 B-FFT image produced from image A, C- [1 1] view of SBA-15

TEM can also be used to determine particle morphology and microstructure (including defects). It is for example, possible to identify mesostructured foam like material as shown in Figure 2.15. This is formed by adding a swelling agent such as trimethylbenzene (TMB) to the synthesis of SBA-15.

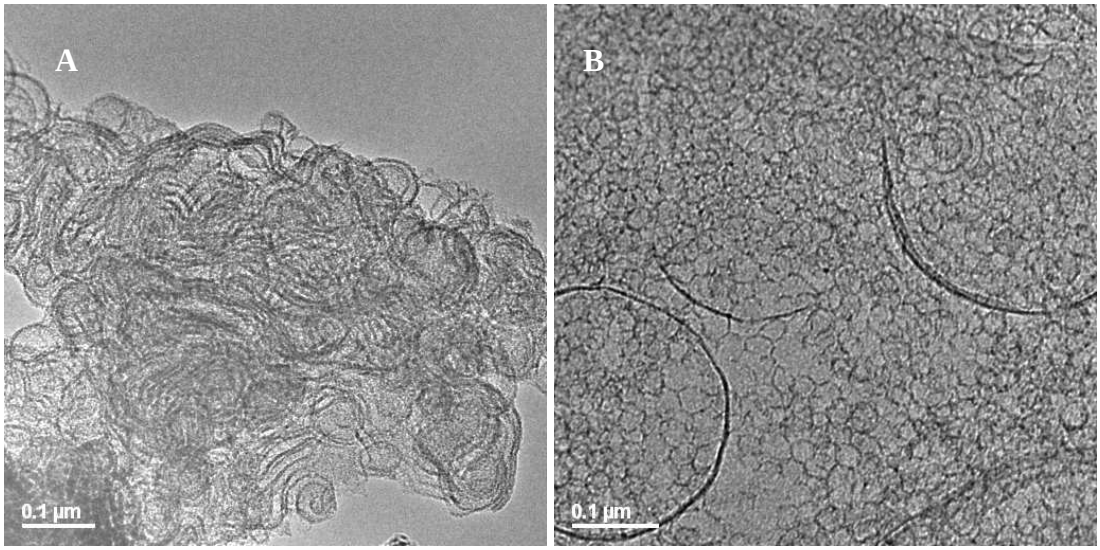

Figure 2.15 Foam type structure (synthesised by G.M.Smith, University of St Andrews) synthesised by adding TMB and MPTES (A) and TMB only (B)

2.4 X-Ray diffraction

Although we can use HRTEM to determine the medium to short-range structure and morphology of mesoporous materials it is helpful to use additional techniques to provide information on the long range order of a material and establish bulk properties. XRD can be used to look at the bulk sample and determine if any long range order is present. For samples of sufficient order it can be used to determine the symmetry and unit cell dimensions by comparison with diffraction patterns reported in the literature.

2.4.1 Theory

X-rays are a form of electromagnetic radiation with wavelengths in the range of 10 to 0.01 nm. **[12]** They are highly penetrating rays which are produced when high energy electrons strike a metal target, normally copper or tungsten, and the metal atom loses an electron. When the resulting vacancy is filled with a higher energy level electron characteristic X-rays are emitted.

Diffraction is caused by the interference in the path of the wave by regular objects and a diffraction pattern results indicating the pattern of varying intensity. It was first suggested by Max von Laue **[13]** that x-rays may be diffracted when interacting with a crystal. This is due to the wavelength of x-rays being in the same range as crystal lattice spacing. XRD has

become a vital and widely used technique and led to W.H Bragg and son, W.L Bragg designing spectrometer to measure diffraction patterns and also producing a law of diffraction, known as Bragg's law **[14]**.

Atoms within an X-ray beam scatter the X-rays coherently in all directions. These interfere constructively in certain directions if the sample is crystalline, giving Bragg peaks, or reflections which can be determined using the Bragg equation (equation 2.7). The Bragg diffraction by a crystal can be seen in Figure 2.16.

$$n\lambda = 2d\sin\theta \qquad \text{Equation 2.7}$$

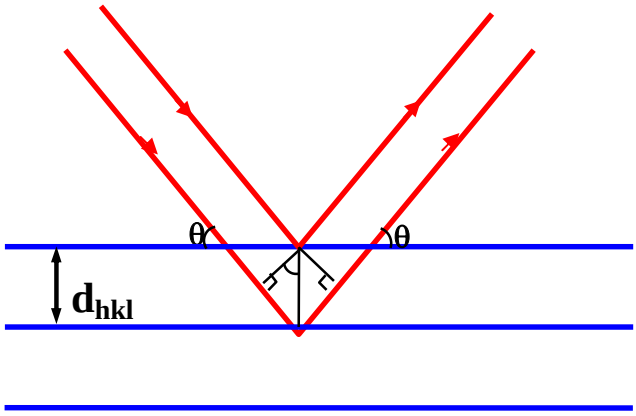

Figure 2.16 Bragg diffraction by a crystal.

Typically powder x-ray diffraction patterns are presented as diffracted intensity as a function of the diffraction angle, 2θ. The pattern results from the sum of diffraction from crystallites in all possible orientations and therefore all possible *hkl* planes. It is possible to use Miller indices (*hkl*) to index the lattice planes present. The d-spacings of observed reflections, as calculated from 2θ values, are characteristic of its unit cell parameters and the symmetry of the material. Unit cell dimensions are calculated from the interplanar spacings, d *via* appropriate equations.

With mesoporous materials very few peaks can be observed in a diffraction pattern and what few peaks that can be detected are present at very low 2θ, typically below 5^{o} 2θ. The low 2θ values derive from their very large unit cells **[15-19]**. The rapid fall-off of

diffracted intensity with scattering angles results from the lack of true crystalline order in the walls of the mesoporous silica.

An example of the typical XRD pattern for mesoporous SBA-15 can be seen in Figure 2.17 in which only a few reflections are detected at very low 2 theta values.

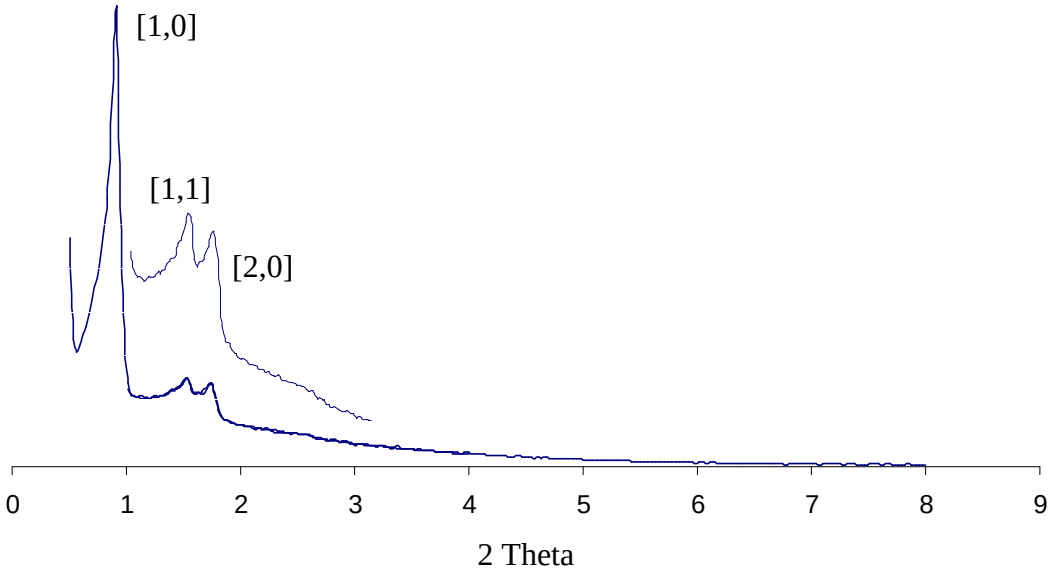

Figure 2.17 Typical XRD pattern of SBA-15 showing low angle reflections with the [1, 0] reflection below 1° 2θ due to large unit cells. Few reflections present as mesoporous solids are not crystalline solids

2.4.2 Sample preparation

In this thesis samples were measured using a Phillips X'Pert Multipurpose diffractometer in a 2theta range of 0.6-10^{o} with a step size of 0.02^{o}.

The mesoporous material is ground, using a mortar and pestle, until a fine powder is obtained. The sample is then placed between two glass slides within a metal mould to hold the sample in place.

2.5 Thermogravimetric Analysis

Thermogravimetric Analysis (TGA) is used to determine how the weight of a material changes as the temperature is increased under controlled conditions. Usually this is carried out under a flow of gas and can indicate how stable a material is under certain temperature

conditions and can show thermally induced changes such as decomposition, loss of water/solvent/organic. An example of a typical TGA trace for a mesoporous silica material can be seen in Figure 2.18.

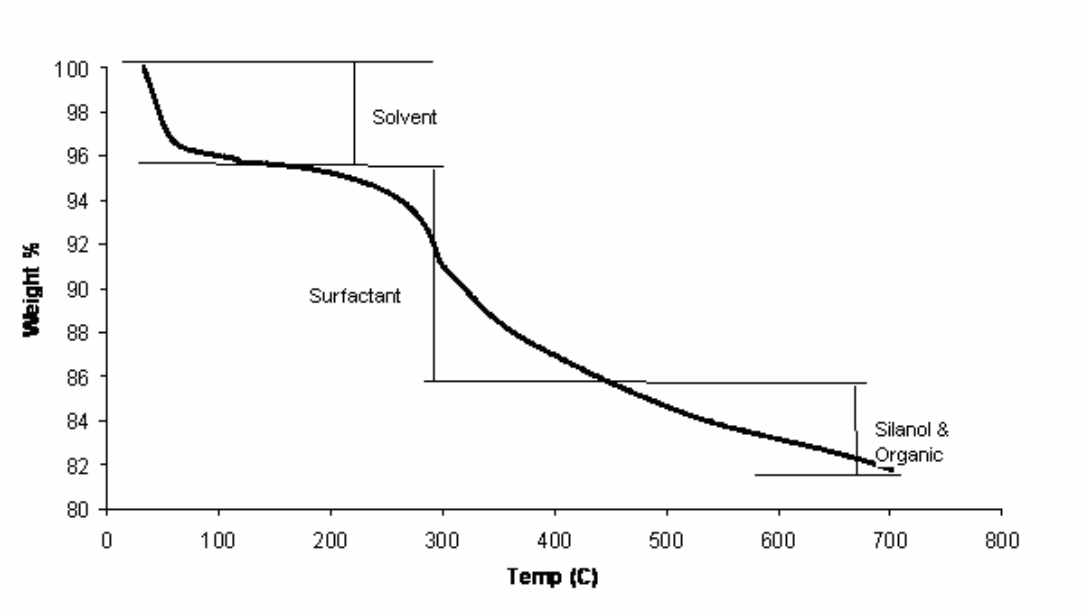

Figure 2.18 TGA trace for thiol functionalised FDU-12 (5%)

A TGA trace typically shows several weight loss sections beginning with a loss in weight due to evaporation of the solvent. This is followed by weight loss due to the burning out and decomposition of any remaining template within the sample. Above 350 ^{o}C weight loss can be attributed to silanol condensation which results in a loss of water and any organic functional groups decomposing.

Thermogravimetric (TG) analysis was performed between 30 and 700 ^{o}C at a heating rate of 5 ^{o}C/min (under gentle flow of air) using a Perkin-Elmer Pyris Diamond TG analyser.

2.6 Elemental analysis

Elemental analysis is a common method of determining the elemental composition of a material, particularly in organic chemistry. The ratio of elements present can be used to determine an empirical chemical formula for a compound or material. Elemental analysis can also be use to confirm the formula of an already known compound and determine any impurities.

To perform elemental analysis the sample undergoes complete combustion and the resulting products are separated *via* a chromatographic method and analysed for their composition. In terms of mesoporous materials problems can arise due to any residual surfactant not removed by calcination or extraction. If a material has been functionalised by any groups containing nitrogen or sulfur then it is possible to determine their presence and quantity. Elemental analysis was performed on a Macroanalyzer Leco CNS-2000-I.

2.7 References

[1] S. Brunauer, L. S. Deming, W.E. Deming and E. Teller, *J. Am. Chem. Soc.*, 1940, **62**, 1723

[2] S. Brunauer, Physical Adsorption of Gases and Vapours, OUP, 1944

[3] S. Brunauer, P.H. Emmett, E. Teller, *J. Am. Chem. Soc.*, 1938, **60**, 309

[4] J.H. DeBoer and C. Zwicker, *Z. Phys. Chem.*, 1929, **3**, 407

[5] E.P. Barret, L.G. Joyner, P.H. Halendar, *J. Am. Chem. Soc.*, 1951, **73**, 373

[6] B.C. Lippens, B.G. Linsen, J.H. De Boer, *J. Catal.*, 1965, **4**, 319

[7] Micromeritics ASAP 2020 Physisorption Brochure

[8] J. Fan, C. Yu, F. Gao, J. Lei, B. Tian, L. Wang, Q. Luo, B. Tu, W. Zhou, D. Zhao, *Angew. Chem. Int. Ed.*, 2003, **42**, 3146

[9] P.I. Ravikovitch, S.C. Odomhnaill, A.V.Neimark, F. Schuth and K.K. Unger, *Langmuir*, 1995, **11**, 4765

[10] W. Zhou, H.M.A. Hunter, P.A. Wright, Q. Ge, J.M. Thomas, *J. Phys. Chem. B.*, 1998, **102**, 6933

[11] Y. Sakamoto, I. Díaz, O. Terasaki, D. Zhao, J. Pérez-Pariente, J.M. Kim, G.D. Stucky, *J. Phys. Chem. B.*, 2002, **106**, 3118

[12] A.R West, Basic Solid State Chemistry, 1988, John Wiley and Sons, Chichester, UK

[13] P. P. Ewald, *Acta Cryst.* 1960, **13**, 513-515

[14] W.L. Bragg, "The Diffraction of Short Electromagnetic Waves by a Crystal", *Proceedings of the Cambridge Philosophical Society*, 17 (1913), 43–5

[15] M. Kaneda, T. Tsubakiyama, A. Carlsson, Y. Sakamoto, T. Ohsuna, O. Terasaki, *J. Phys. Chem. B*, 2002, **106**, 1256

[16] C. Yu, J. Fan, B. Tian, G.D. Stucky, D. Zhao, *J. Phys. Chem. B*, 2003, **107**, 13368

[17] M. Kruk, M. Jaroniec, C.H. Ko, R. Ryoo, *Chem. Mater.*, 2000, **12**, 1961

[18] D. Zhao, J. Feng, Q. Huo, N. Melosh, G.H. Fredrickson, B.F. Chmalka, G.D. Stucky, *Science*, 1998, **279**, 548

[19] S. Che, A.E. Garcia-Bennett, T. Yokoi, K. Sakamoto, H. Kunieda, O. Terasaki, T. Tatsumi, *Nat. Mater.*, 2003, **2**, 801

3. Synthesis and Characterisation of Mesoporous Silicas with different Structures and Morphologies

3.1 Introduction

This chapter details the synthesis of well ordered mesoporous silica supports with a variety of structures and morphologies. The main characterisation methods are nitrogen adsorption and transmission electron microscopy but additional techniques including small angle XRD, elemental analysis and thermal gravimetric analysis have also been used. The materials are based on SBA-15 **[1]**, KIT-6 **[2]** and FDU-12 **[3]** which are described in sections 3.2-3.4, 3.5 and 3.7 respectively. The aim of this section is to detail the modification of the morphology of SBA-15 by the use of additives, the preparation of the Ia-3d type material with larger pore size (KIT-6) and also with organic functionalisation and finally to describe the synthesis of FDU-12 with a range of cage diameters and window sizes and to understand the role of different steps in the published procedures. These large pore mesoporous silicas are then suitable for the uptake, support and release of proteins and enzymes.

3.1.1 SBA-15

SBA-15 is a highly ordered 2D hexagonal (p6mm) silica-block copolymer mesophase. It is synthesised in acidic media from a poly (alkylene oxide) triblock copolymer, Pluronic P123 with the source of silica being tetraethylorthosilicate (TEOS). It was first reported by Zhao *et al.* in 1998 **[1]** and was noted for its unusually large d_{100} spacings of 104-320 Å. It was seen to have a BET surface area ranging from 690 – 1040 m^2/g, and pore sizes of between 46 and 300 Å. The silica wall thickness was found to be 31-64 Å and its maximum pore volume was 2.5 cm^3/g. TEM images of calcined hexagonal SBA-15 mesoporous silica with different average pore sizes are shown in Figure 3.1 (from BJH and XRD) of (**A**) 60 Å, (**B**) 89 Å, (**C**) 200 Å, and (**D**) 260 Å.

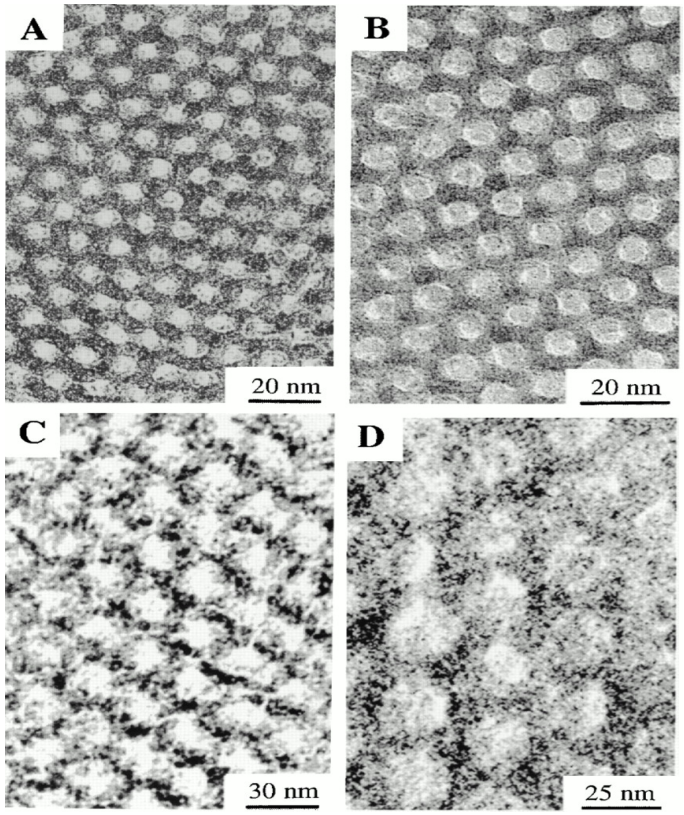

Figure 3.1 HRTEM images of calcined hexagonal SBA-15 with different average pore sizes, (A) 60 Å, (B) 89 Å, (C) 200 Å, and (D) 260 Å [1]

3.1.2 Modification of the morphology of SBA-15

Zhang *et al.* **[4]** reported a mesoporous silica SBA-15 with cuboidal morphology, prepared using an excess of decane as co-solvent and in the presence of NH_4F in solution. The preparation produced the first reported case of channels of the material running parallel to the short axis of the cuboidal SBA-15. Using SEM and TEM, they observed that without the addition of decane, fibrous particles were obtained under the same conditions. When decane was added in a ratio of 5.8:1 to the polymer P123, the morphology changed dramatically from fibrous to cuboidal particles. The channels, which typically run parallel to the long axis in SBA-15, run parallel to the short axis (Figure 3.2) but the material retains a hexagonal arrangement of channels.

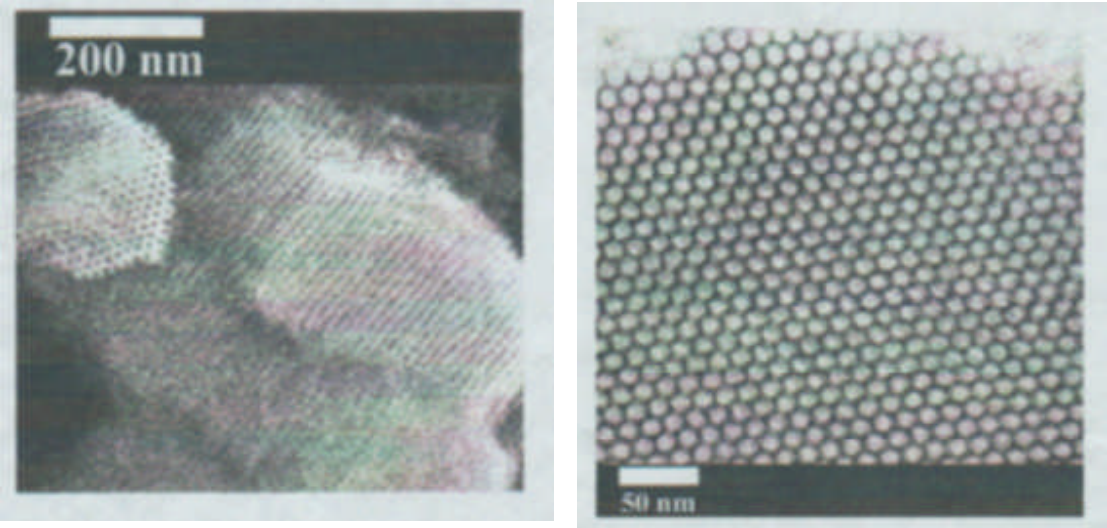

Figure 3.2 HRSEM and TEM image of SBA-15 synthesised at decane to P123 weight ratio of 5.8:1 [4]

The authors suggest that decane plays two roles in the procedure: as a swelling agent, expanding the pore size of the material, and also to confine the formation of silica-doped micelles, resulting in a decrease of particle size and a change of the channel orientation. A proposed mechanism of the role played by decane in the synthesis can be seen in Figure 3.3. Our interest in this synthesis derives from the change in direction of the channels from running parallel to the long axis to running parallel to the short axis of the particles, which could be beneficial in terms of molecular transport properties relevant to enzyme immobilisation or drug delivery.

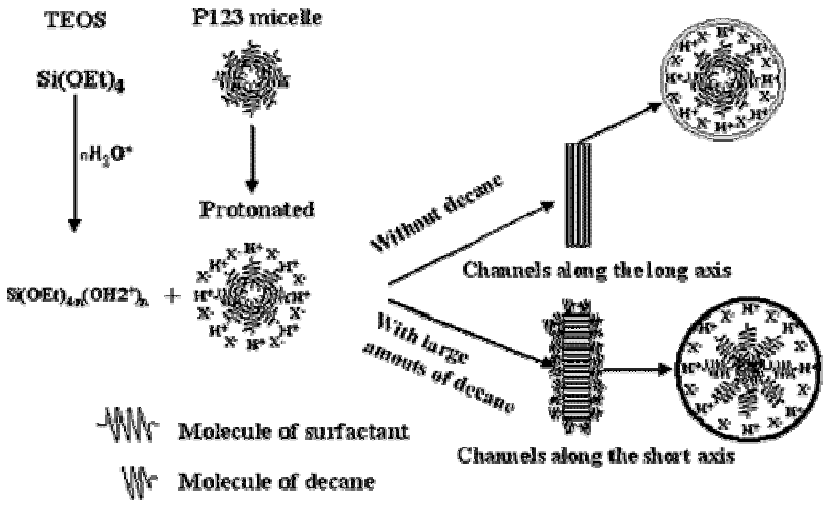

Figure 3.3 Schematic representation of the bifunctional role played by large amounts of decane – taken from Zhang *et al.* [4]

3.1.3 Ia-3d structure

MCM-48 was the first reported bicontinuous mesostructured silica (Ia-3d) and can be synthesised using a cationic alkylammonium surfactant, mixed cationic/anionic surfactants, or cationic/non ionic surfactants as the surfactant molecule. STA-11 is analogous to MCM-48 and was synthesised by Hodgkins *et al.* **[5]** at the University of St Andrews (HRTEM in Figure 3.4). STA-11 was prepared using a block copolymer and has larger pores than MCM-48 but these are still smaller than those of SBA-15 and therefore it remained a challenge to prepare a material with a pore size comparable to or larger than that of SBA-15 but with cubic Ia-3d morphology.

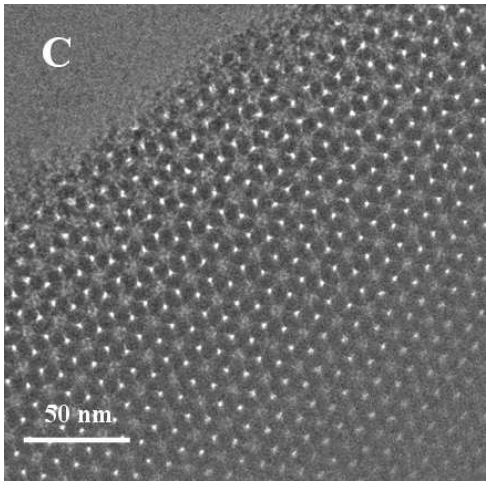

Figure 3.4 HRTEM of cubic Ia-3d STA-11 [5]

MCM-48 materials have relatively small pore size (1.5-4.5 nm) which can be limiting in terms of applications including adsorbents, separators and catalysts, particularly for proteins and enzymes. Liu *et al.* **[6]** have reported the synthesis of large pore 3D bicontinuous mesoporous silica *via* a room temperature, acidic media synthesis using a commercial non-ionic triblock copolymer as a template. The material was designated FDU-5 and is an Ia-3d structure with pores in the range of 4.5-9.5 nm. They achieved the larger pore sizes by employing a room temperature synthesis using an ethanol solution and a solvent evaporation method. Additives including MPTES and benzene derivatives were also used.

Following on from this publication further work has been reported by Che *et al.* **[7]** with the synthesis of a large pore Ia-3d cubic structure for the first time using a hydrothermal synthesis. Despite the publication of the FDU-5 synthesis the hydrothermal method for

synthesising highly ordered material had not been fully developed. The hydrothermal synthesis of Che *et al.* allows for a large pore cubic silica with greatly improved structural integrity and thermal and hydrothermal stability. The synthesis utilises P123 as a template surfactant but without the addition of MPTES it is not possible to obtain the cubic Ia-3d mesophase under these conditions. The change of phase of the hexagonal p6mm structure to the cubic Ia-3d phase with the addition of MPTES is illustrated schematically in Figure 3.5.

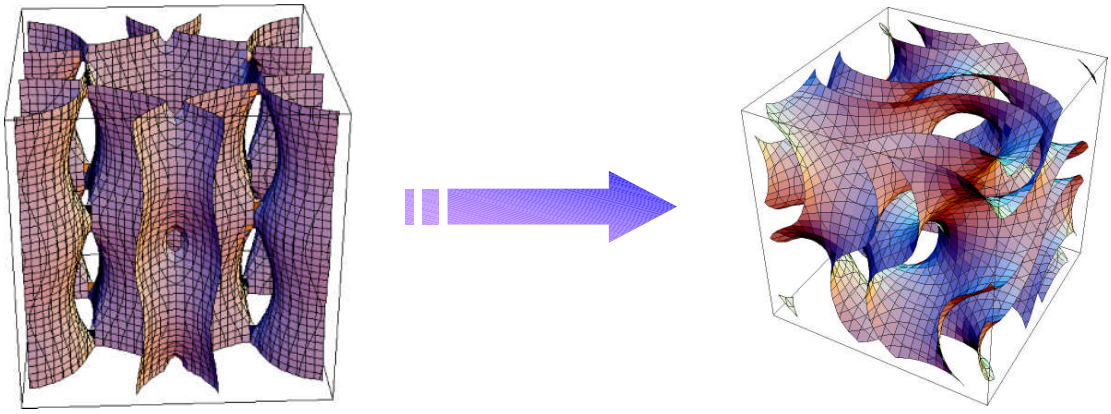

Figure 3.5 Phase from (left) SBA-15 – hexagonal p6mm to (right) large pore cubic Ia-3d upon organo-siloxane and/or additives to the direct synthesis. Solid region of model shows silica wall.

It was concluded that synthesis of the Ia-3d cubic mesostructure under these conditions could not be achieved without the use of additives. In the reported synthesis of FDU-5, Liu *et al.* **[6]** report that when MPTES was used as an additive, the Ia-3d structure was only achieved when the MPTES/TEOS molar ratio was between 0.046-0.058. Without additives a 2D hexagonal structure (p6mm) was obtained and if the MPTS/TEOS molar ratio was lower than 0.046 then a mixture of hexagonal and cubic mesophases was observed, indicating a possible phase transition. By adding an organic molecule the hydrophobic/hydrophilic ratio is increased and this can cause a transition from the high-curvature hexagonal p6mm structure to the lower curvature bicontinuous cubic Ia-3d structure. KIT-6 is a large pore Ia-3d mesoporous silica reported by Ryoo *et al.* **[2],** similar to those reported by Zhao **[3],** Flodstrom **[8]** Hodgkins **[5]** and Liu **[6]** but instead of the addition of salts or thiols, KIT-6 can be prepared by utilising the commercially available copolymer, P123 and butanol and has tuneable pores between 4 and 12 nm. Here the

addition of butanol causes the morphology of the material to change from hexagonal to cubic.

3.1.4 Cubic cage structures

FDU-12 is a mesoporous silica material synthesised using Pluronic F127 as a structure directing agent. It is a highly ordered three dimensional close packed cage structure which can be assigned as a face centred cubic structure with Fm3m symmetry (shown in Figure 3.6). A combination of HRTEM, XRD and N_2 adsorption indicates that it has large pores (up to 15 nm in diameter) separated by amorphous silica walls and connected, one to another, through windows some 4 nm in diameter. The super-cage structure of FDU-12 is similar to that reported previously for the cubic regions observed in SBA-2 but on a much larger scale **[3].**

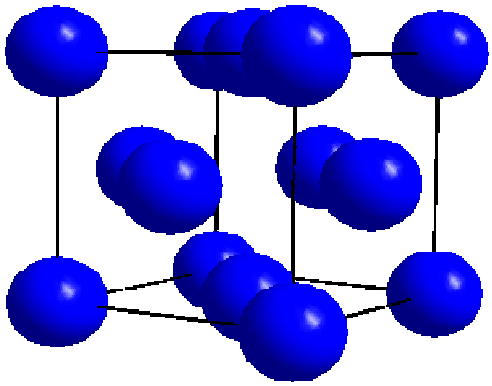

Figure 3.6 Face centred cubic arrangement of spherical micelles(FDU-12).

The first two research groups to have published the synthesis of cubic mesoporous silicas with Fm3m symmetry are the group of Ryoo in Korea **[9]** (who refer to the material as KIT-5) and the group of Zhao in Fudan, China who have named the material FDU-12 **[3]**. The synthesis methods differ slightly with the KIT-5 synthesis based on a low HCl concentration and FDU-12 being prepared using additives and salts, trimethylbenzene (TMB) and KCl. Both materials have been characterized using HRTEM, low angle XRD and N_2 adsorption and a combination of these can be used to give an accurate structure of the solid. FDU-12 is shown to contain large cages with diameters of 10-12 nm, depending on the hydrothermal temperature, connected by smaller windows of 4 nm diameter.

Pluronic F127 is a triblock copolymer ($EO_{106}PO_{70}EO_{106}$) with a higher EO/PO ratio than Pluronic P123 (which is used to synthesise the hexagonal mesoporous material SBA-15). This high hydrophilic to hydrophobic volume ratio implies a high curvature of the micelles and whereas P123 has been shown to template the synthesis of hexagonal and cubic channel structures, F127 is observed to produce a cubic cage structure. This high curvature of the micelle is as a result of the local effective packing parameter, g, as described in section 1.5 whereby as g increases the surface curvature decreases and the micelles alter from spherical micelles to lamellar packing. $g < ⅓$ leads to the formation of spherical micelles, whereas $⅓ < g < ½$ favours cylindrical micelles and $g > ½$ forms parallel stacks of bilayers (lamellar).

The ability to control and tailor the pore structure and framework is crucial to determining the possible applications of the material. The initial synthesis of FDU-12 produces a material with pore entrance size of 4 nm. Increasing this in a controlled way will allow the material to encapsulate and separate proteins where biomolecules with larger molecular weights are present. Previous methods of enlarging pore sizes have been reported, with the use of swelling agents such as 1, 3, 5-trimethylbenzene (TMB) employed in the increase of SBA-15 pore sizes **[10]**. It was observed that adding TMB in a weight ratio of less than 0.5 to the surfactant produced a material with pore size 12 nm and by increasing the ratio to 2, SBA-15 with pore size up to 30 nm can be achieved. Upon increasing the TMB the structure loses its hexagonal regularity and the material undergoes a transition to mesostructured cellular foam (MCF) with poorly defined connections between the large pores. Increasing the pore size was also carried out by increasing the synthesis temperature. This is possibly due to the ethylene and propylene oxide moieties present within the surfactant being more hydrophobic at higher temperatures. But there are limits to the extent to which the pores can be expanded using this method and this led to Zhao *et al.* **[11]** reporting a novel low temperature strategy to produce a highly ordered material with very large pores.

They have successfully managed to synthesise a face centred cubic structure with cavities of up to 27 nm and adjustable entrance dimensions of between 4 and 16.7 nm measured on the basis of the adsorption and desorption branches of the nitrogen isotherm. The synthesis is as reported previously but this time varying the hydrolysis temperature between 10-60 ^{o}C. After 24h at the hydrolysis temperature the mixture was transferred to an oven at 100 ^{o}C to undergo condensation for 24h before being filtered and dried. The as-made product

then underwent a high temperature acid erosion treatment with the material heated in a solution of 2M HCl at 100-140 ^{o}C. They observed very little change when the synthesis was conducted in the range 23-60 ^{o}C, producing a structure with a unit cell of 29.5-26 nm. This changed when the hydrolysis temperature decreases to 15 ^{o}C with the unit cell swelling to 44.5 nm. At temperatures below 14 ^{o}C a disordered material was formed and below 10 ^{o}C no solid was produced. Using nitrogen adsorption the pore cavities and entrance dimensions were determined and again the same trend was observed with decreasing the hydrolysis temp from 23 to 15 ^{o}C showing an increase in cavity size from 14 to 22 nm. As mentioned in previous studies, increasing the hydrothermal treatment temperature can increase the entrance size and this is seen here. By comparing samples synthesised at 15 ^{o}C followed by a 100 or 140 ^{o}C hydrothermal step, it can be seen that by increasing the acid erosion step the entrance is enlarged from 4 nm to 16.7 nm and the hysteresis observed in the nitrogen adsorption and desorption branches of the 77K isotherm changes from type H2 towards type H1.

3.2 SBA-15: Experimental

The preparation of 'standard' SBA-15 and modified preparations, with the aim of preparing 'nano' particles more suitable as enzyme supports, are reported here.

3.2.1 Synthesis

SBA-15

SBA-15 was prepared according to a literature procedure **[12]**. The surfactant, P123 (4 g, BASF) was dissolved in a mixture of water (138 g) and HCl (12.2 g, 37 %). TEOS (8.2 g) was added dropwise and stirred for 24 h at 40-60 ^{o}C before being transferred to a thick walled Teflon flask and heated at 100 ^{o}C for 48 h. The resulting product was washed using distilled water and filtered before being air dried. The surfactant was removed by calcination at 550 ^{o}C for 4 h under flowing nitrogen, followed by oxygen.

Preparation of modified SBA-15

It was hoped that by adding decane to the synthesis a change in the channel direction of the SBA-15 material would be observed. P123 (2.4 g) was dissolved in 84 mL of HCl solution (1.07 M) and stirred at room temperature until the solution became clear. Decane was added to the solution in various different weight ratios to P123 **[4]**. Four weight ratios were used to follow the resulting changes in morphology and channel direction – 0:1, 2:1, 5.8:1 and 7.6:1. The mixture was stirred for a further hour before 0.027 g of NH_4F followed by 5.1 g of TEOS was added. It was then stirred at 40 ^{o}C for 20 h, transferred to a Teflon bottle and heated at 100 ^{o}C for 48 h. The solid was collected by filtration, dried in air, and calcined at 550 ^{o}C in air for 5 h to ensure the removal of the templates.

3.2.2 Transmission Electron Microscopy

SBA-15 was prepared according to reported procedures and investigated by transmission electron microscopy (TEM). The resulting images showed particles on the nano scale with typical pore structure and particle morphology. Figure 3.7 (image A) shows a TEM micrograph of SBA-15 with pores running perpendicular to the incident beam whereas image B shows a view of the pores running parallel to the beam. Using the GATAN software we can estimate the pores to be approx 6 nm in diameter, which is slightly smaller than the values obtained by nitrogen adsorption shown in section 3.2.3. The HRTEM gives the expected typical micrographs associated with hexagonal p6mm symmetry.

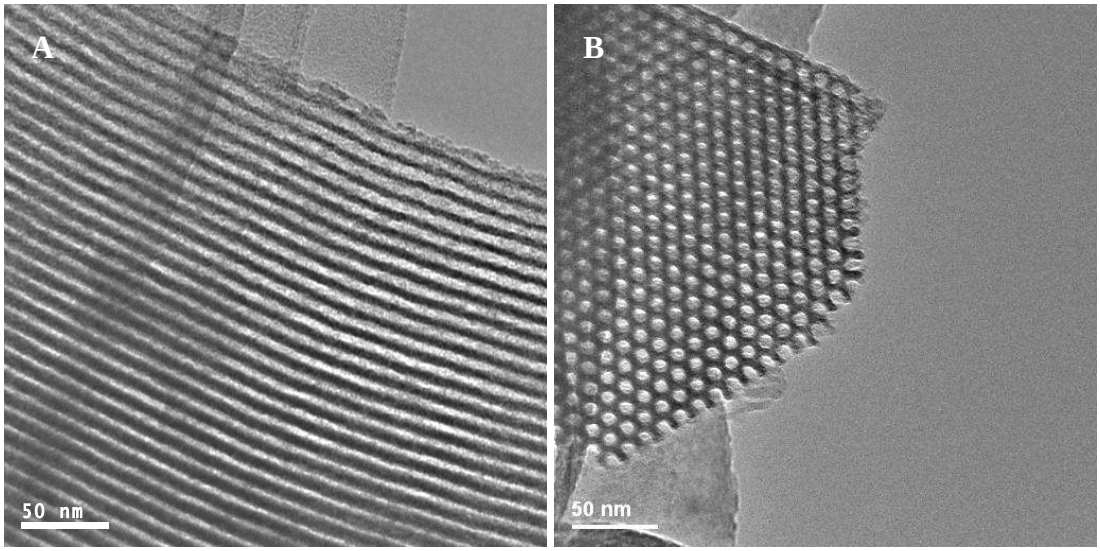

Figure 3.7 HRTEM of SBA-15 showing images of the pore channels (A) and pore entrances (B)

Attempts to reproduce the effects on particle size and aspect ratio of SBA-15 reported by Zhang *et al.* **[13]** and shown in section 3.1.2 were unsuccessful. Instead, using the reported ratios under the conditions described here, there is a tendency to form assemblages of a few mesoporous channels, with these showing branching, see Figure 3.8.

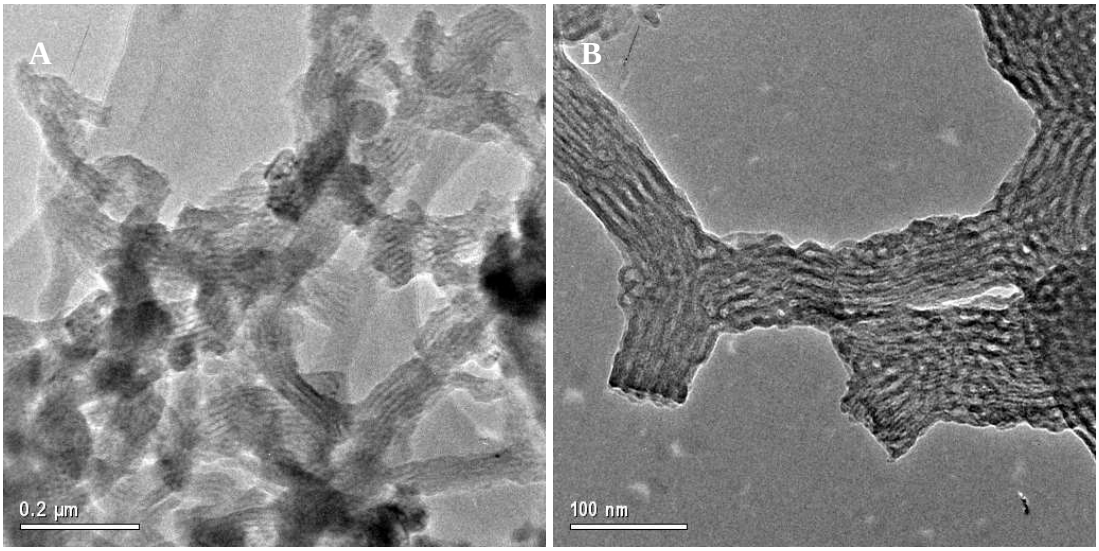

Figure 3.8 SBA-15 synthesised with addition of decane:surfactant in ratio (A) 2:1 and (B) 5.8:1

The importance of the presence of decane in the synthesis in causing this change in particle morphology is illustrated by the results of varying its concentration in the synthesis gel. Whereas decreasing the concentration produced larger particles, more like typical SBA-15 (Figure 3.8 A) by increasing the concentration we observe branching to a much greater extent (Figure 3.8 B).

3.2.3 Nitrogen Adsorption

SBA-15 gives a type IV isotherm, shown in Figure 3.9, with a sharp capillary condensation step at P/P_o of around 0.85. It has a well defined adsorption with a high uptake of over 600 cm^3/g. The BET is calculated within the range of 0.05 to 0.4 P/Po and is found to be 631 m^2/g. The pore size distribution is calculated on the adsorption branch of the isotherm using the De Boer approximation and for this material is seen to be 8 nm, which is slightly higher than the value obtained using the TEM image. This agrees with the value published by Zhao *et al.* **[1]**.

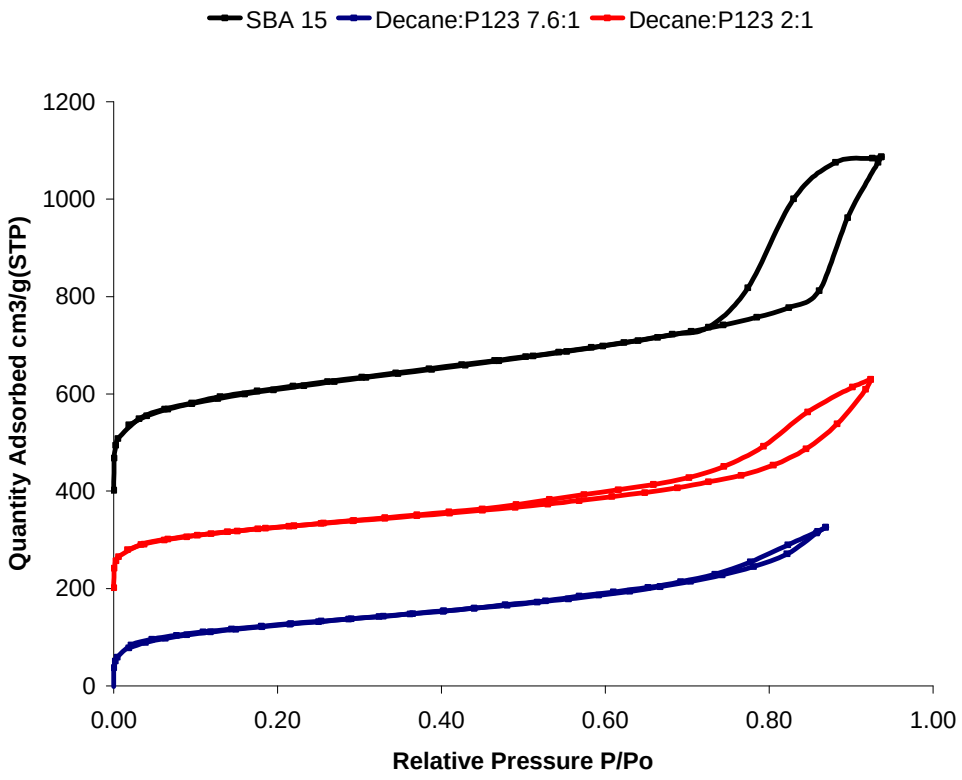

Figure 3.9 Isotherm comparison for addition of decane in weight ratio to surfactant, each isotherm successively offset by 200 cm^3/g obtained using Hiden IGA

The isotherm produced by SBA-15 is a type IV isotherm with well defined hysteresis. The sharp uptake over a narrow P/Po region indicates the high degree of order within the material and a narrower pore size distribution. The two samples shown here with additional decane all show a much lower uptake of N_2 in comparison to pure SBA-15 both in the mesoporous region and at very low P/P_o values (< 0.1). This combined with the broader pore size distribution and HRTEM indicate less order within the materials. The low uptake in the pressure range where capillary condensation is expected suggests that the amount of mesoporosity in the 6-10 nm region (as indicated by TEM) is reduced. Zhang *et al.* published BET surface areas of 560 and 610 m^2/g for samples containing 5.8:1 and 7.6:1 of decane: P123 respectively compared to 431 and 411 m^2/g for samples shown here.

The BET surface areas for the 3 samples were all seen to be less than standard SBA-15 and results are shown in Table 3.1.

Table 3.1 BET surface area values of SBA-15 type material

Decane:surfactant weight ratio	BET surface area m^2/g and error (+/-)
0	631 (11)
2	394.4 (7)
5.8	431 (8)
7.6	411 (5)

Pore size distribution can be obtained from data gathered during nitrogen adsorption and an example can be seen below in Figure 3.10. It shows the distribution seen in a standard SBA-15 sample with a singular sharp peak seen at 8 nm indicating a narrow pore size distribution and good order within the sample. (If the peak was seen to be much broader or multiple peaks were observed this would be an indication of a range of varying pore sizes present within a sample).

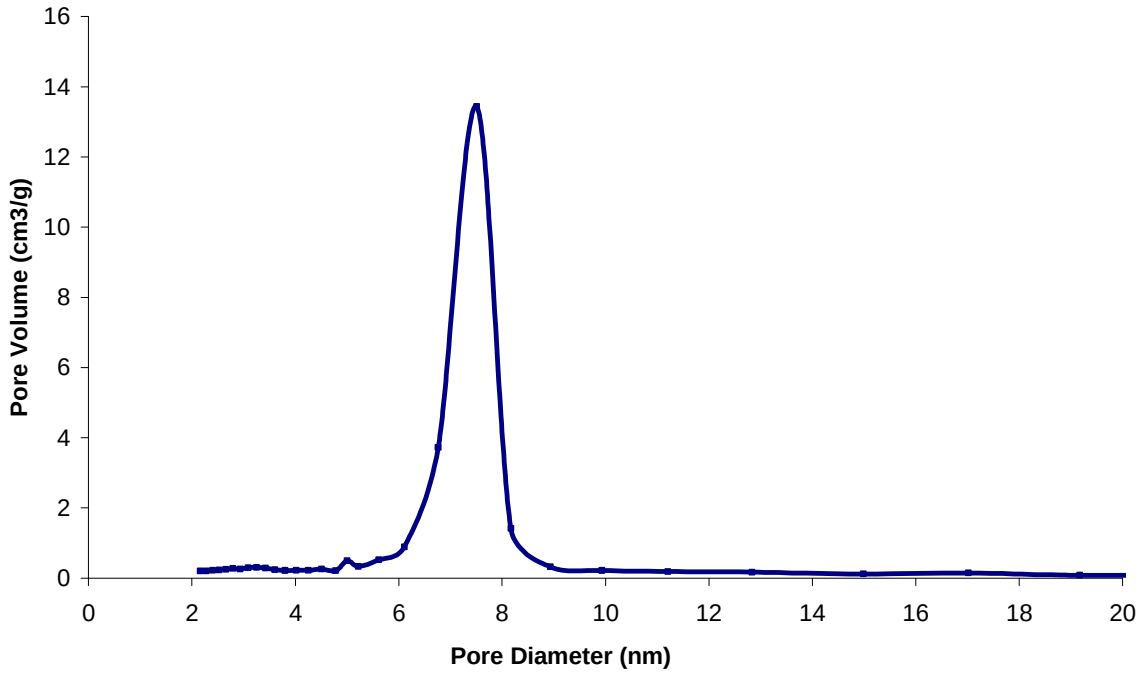

Figure 3.10 Pore size distribution for SBA-15 obtained using Hiden IGA

3.3 Modified synthesis of mercaptopropyl-functionalised silicas

Given that the addition of decane to the SBA-15 synthesis changed the morphology, the effect of adding decane to thiol-functionalised silica under the same conditions was examined, since thiol groups were of interest as giving additional binding to enzymes/proteins and it was also known that adding mercaptopropylsiloxanes had a structure-controlling effect.

3.3.1 Thiol functionalised SBA-15

Sol-gels were prepared with molar compositions

(1-x) $Si(OEt)_4$: x $(EtO)_3Si(CH_2)_3SH$: 0.017 P123 : 2.9 HCl: 200 H_2O (x = 0-0.1)

Decane was added in a weight ratio to P123. The surfactant was added to an acidic solution and stirred at 323 K until it had completely dissolved. TEOS, decane and mercaptopropyltriethoxysilane (MPTES) were added simultaneously and stirred for a further 24 h. This was to allow hydrolysis to begin and the mesostructure to form. The mixture was then placed in a Teflon bottle and heated at 100 ^oC for 48 h, enabling condensation of the framework. The solid produced was filtered, dried and calcined in nitrogen for 4 h at 550 ^oC, followed by oxygen at 550 ^oC for 4 h, to remove all of the surfactant

A series of samples were prepared with a 7 mol% content of MPTES, to which were added various amounts of decane in a weight ratio to P123. This was also repeated for samples with a 2 mol% content of MPTES. Samples were prepared with weight ratios of decane to P123 of 0.4:1, 2:1 and 5.8:1. Due to the promising results it was decided to look at samples with decane: P123 ratio between from 2:1 to 6:1.

For comparison, similar syntheses were attempted replacing decane with dodecane and octane. This was carried out using the method described previously for a series of samples containing 7 mol % thiol and dodecane or octane in a weight ratio to P123 of 1:1, 2:1, 4:1 and 5.8:1.

3.3.2 Transmission Electron Microscopy

Material synthesised with 2 % thiol with the addition of decane in a weight ratio of 5.8:1 to P123 causes morphological change as the TEM micrographs show features (see Figure 3.11) that differ from typical SBA-15. In one case a bundle of 7 channels can be observed, forming a hexagonal structure (shown by an arrow on Figure 3.11 B). This could show the early stages of SBA-15 formation, interrupted by the presence of decane.

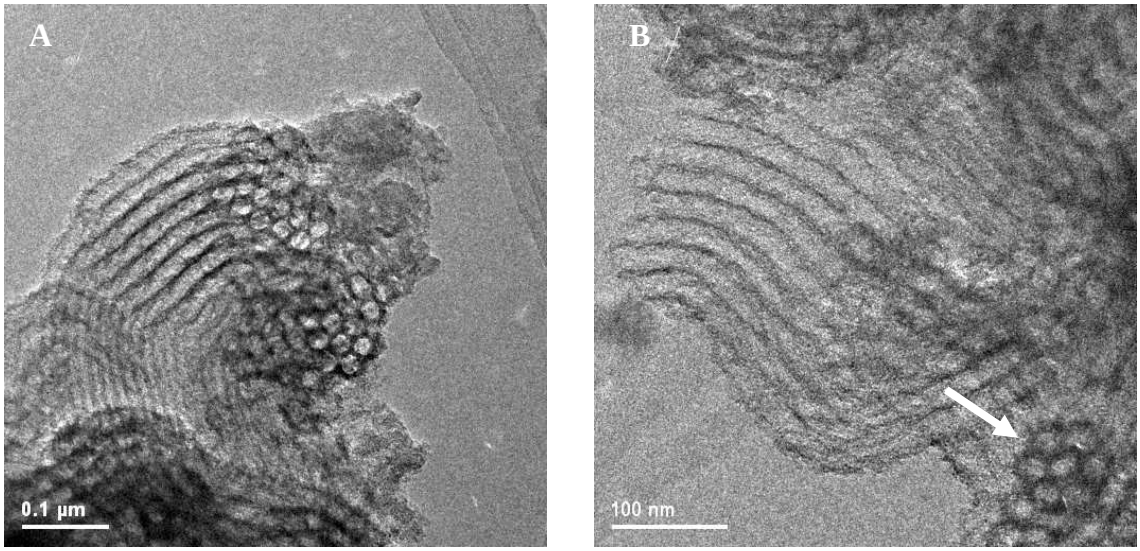

Figure 3.11 HRTEM of 2%SH-SBA-15 with 5.8:1 Decane: surfactant

Two samples were prepared with 7 % thiol added and with decane in a weight ratio to the surfactant of 2:1 and 5.8:1, respectively. TEM reveals interesting structural features quite different from the Ia-3d structure observed by Hodgkins *et al.* for a material synthesised with 7 % thiol. Figure 3.12 shows an unusual ‘onion ring’ morphology produced by adding decane in a 2:1 ratio and Figure 3.13 shows the change caused by adding more decane. By adding more decane the ‘onion ring’ structure has become better defined, comparing Figure 3.13 with 3.12.

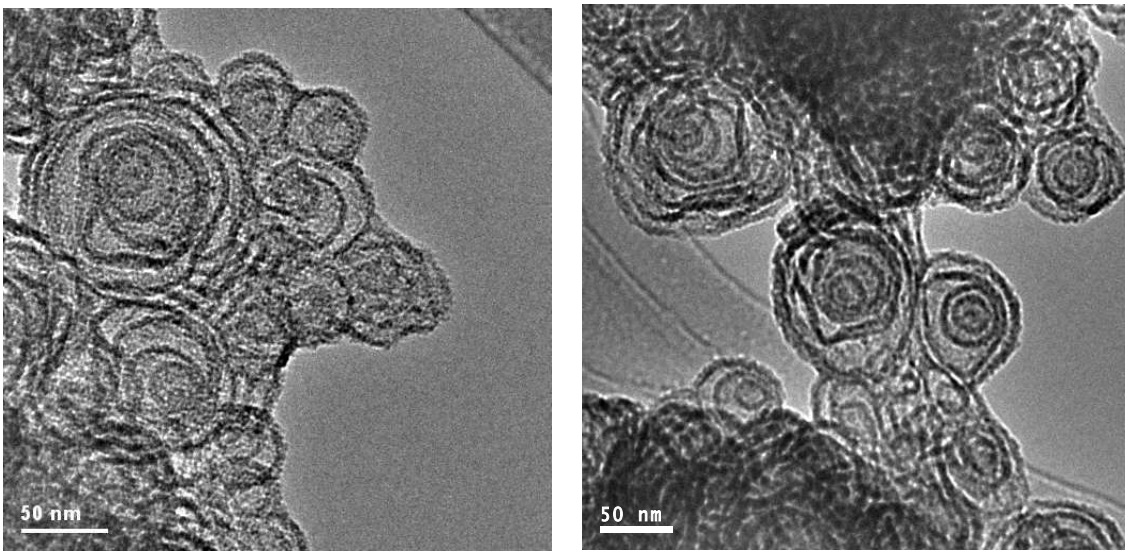

Figure 3.12 HRTEM of 7%SH-SBA-15 and 2:1 Decane: Surfactant

Figure 3.12 is highly representative of the structures present within the sample. (The onion rings shown in Figure 3.13 were not the predominant feature seen in that sample).

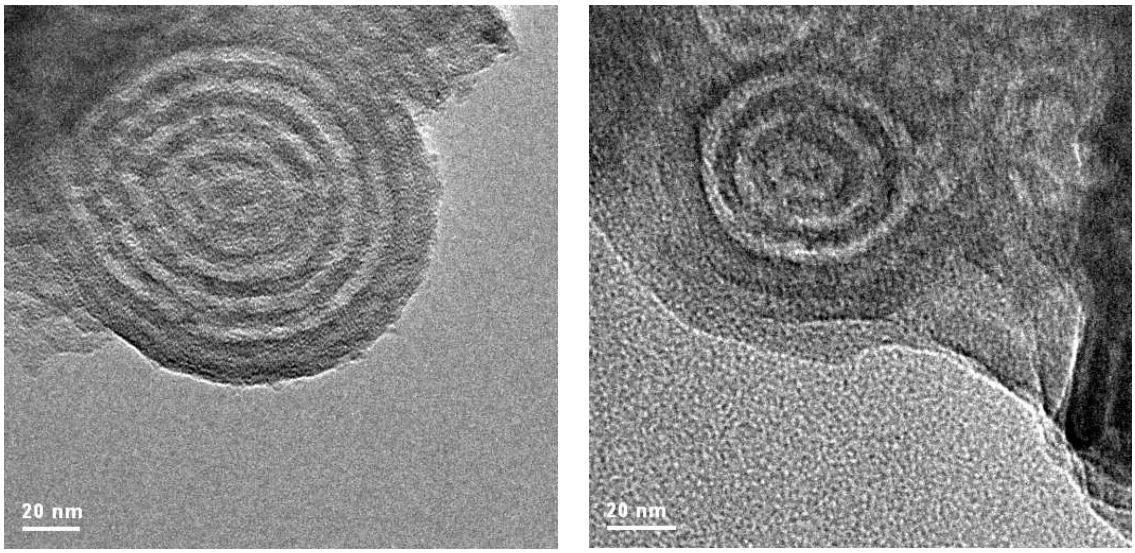

Figure 3.13 HRTEM of 7%SH-SBA-15 and 5.8:1 decane: surfactant

As adding decane to mercaptopropyl-functionalised silica produced these unusual 'onion ring' morphologies it was decided to investigate the effect of other alkanes. Dodecane and octane were chosen as they differ only in 2 carbons either side of decane. A series of samples were prepared with 7mol % thiol which produces, without alkane addition, highly

ordered Ia-3d silica. Using octane in place of decane produces less well defined onion ring structures, as seen in Figure 3.14.

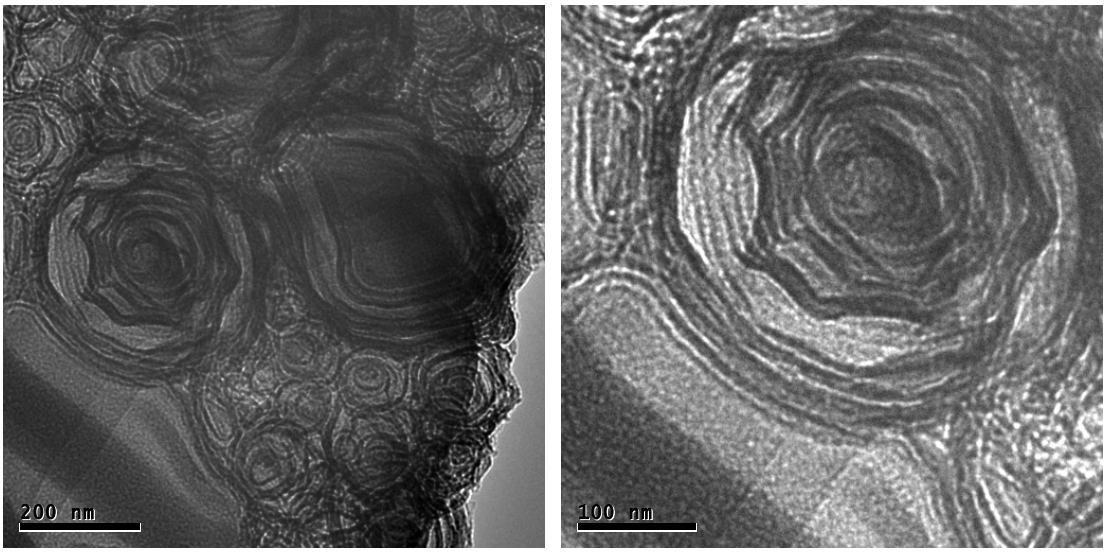

Figure 3.14 HRTEM of 7%SH-SBA-15, octane: surfactant 2:1

Increasing the octane ratio distorts the structure from the cubic structure expected without the addition of an alkane, to a more ribbon like structure and produces disordered material without distinguishable onion ring particles, as seen in Figure 3.15.

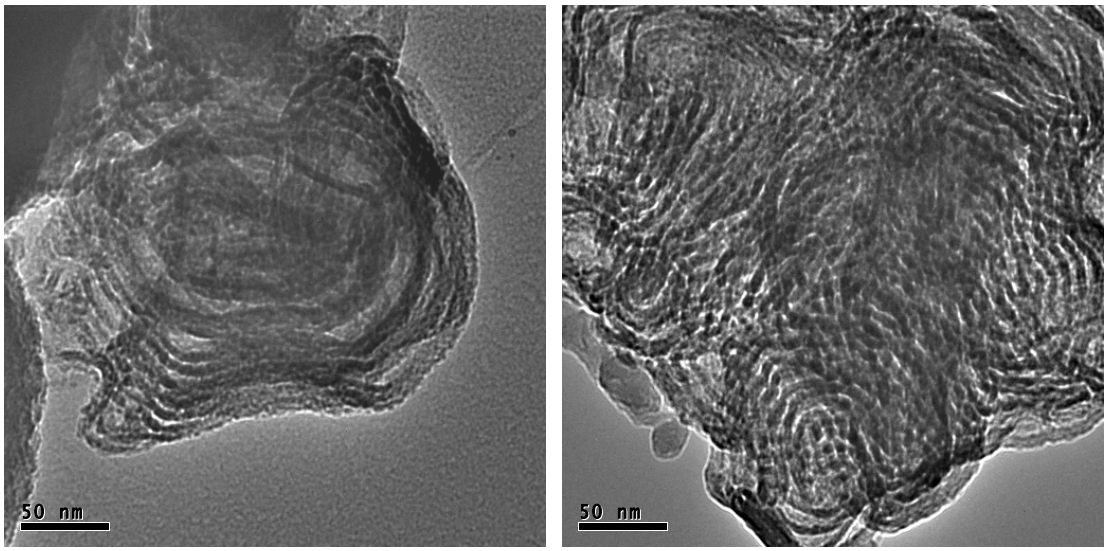

Figure 3.15 HRTEM of 7%SH-SBA-15, octane:surfactant 6:1

3.3.3 Porosity of Thiol-functionalised materials prepared in the presence of decane

The addition of decane to thiol-bearing syntheses that otherwise give well ordered channel structures has been shown to disrupt and modify the phase formation giving onion ring structures at higher thiol inclusion. Adsorption isotherms confirm the change in pore structure, where all materials show less well defined capillary condensation (Fig. 3.16 and 3.17). The BET surface areas remain quite high and in some cases comparable to those of well ordered silicas prepared in the absence of thiol (i.e. up to 743 m^2/g compared to 812 m^2/g quoted by Hodgkins *et al.* **[5]**), but the mesoporous structure required for applications of the types envisaged in this thesis was not obtained. Notably the high surface areas measured for the onion ring structures prepared by addition of 7 mol % MPTES in the synthesis (Figure 3.13 and Table 3.2) indicate that these structures are porous to nitrogen, but do not possess channels or cages of mesoporous dimensions that are accessible to nitrogen. It is likely that these onion rings form as a result of bilayers folding back on themselves changing from a lamellar phase to form spherical vesicles. Further preparations concentrated on approaches to modify pore structure rather than external morphology or particle size.

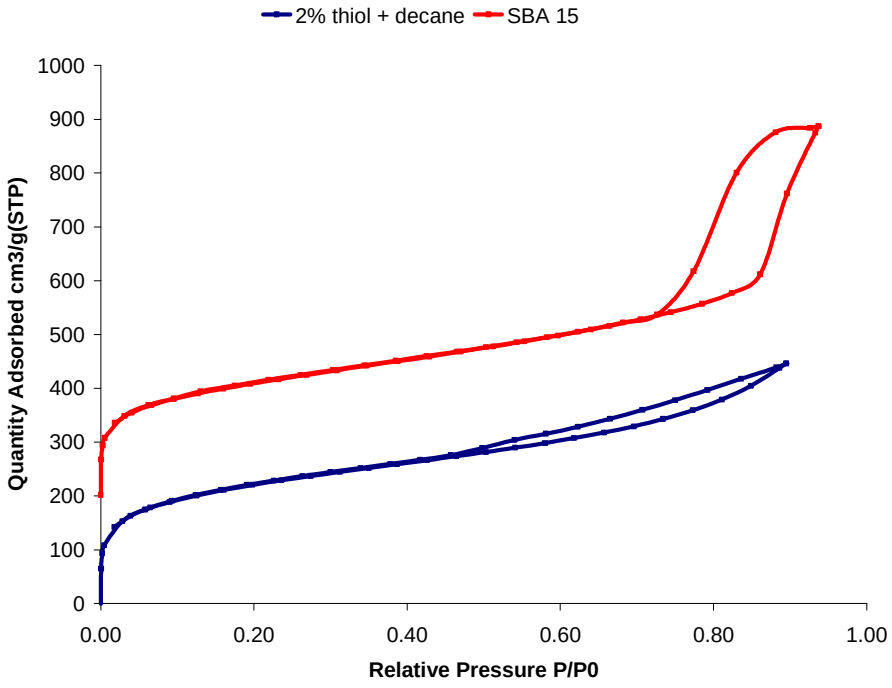

Figure 3.16 Isotherm showing effects of adding both 2 mol % MPTES and decane on SBA-15 – isotherms offset by 200 cm^3/g

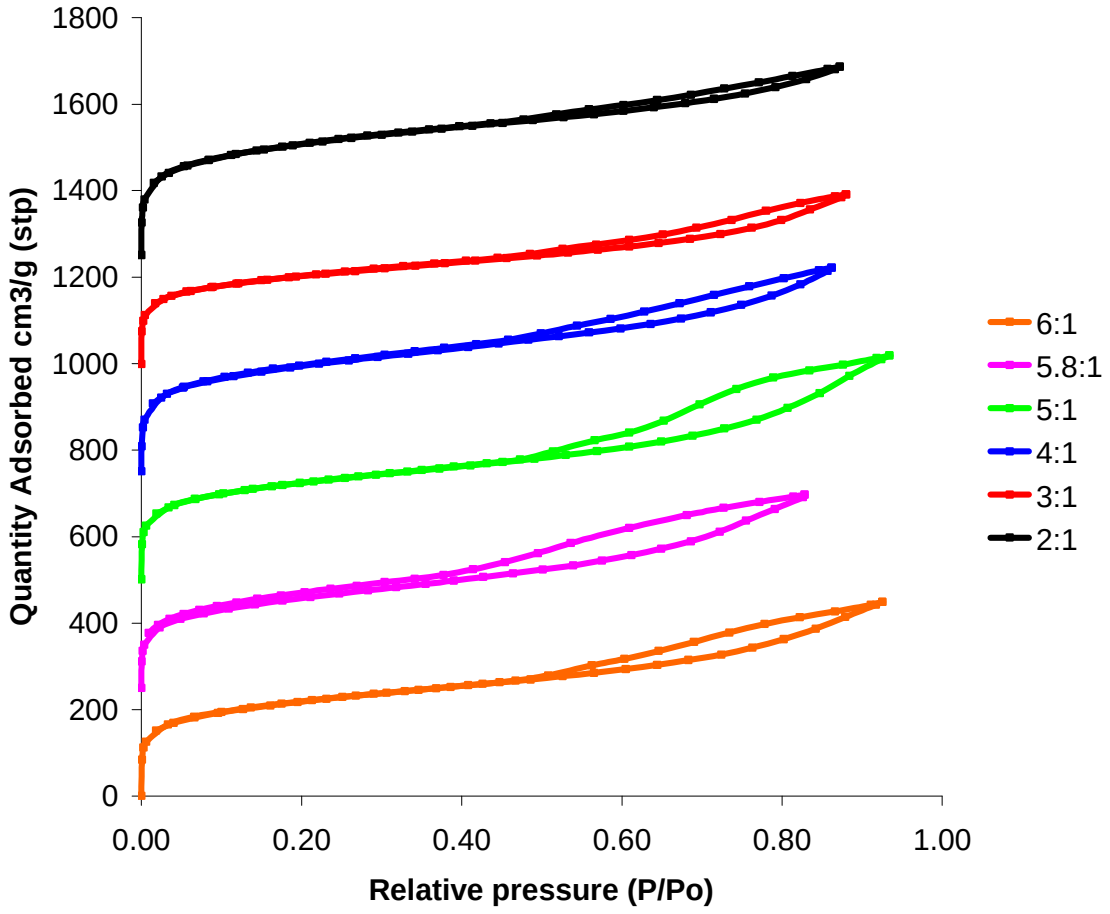

Figure 3.17 Isotherms showing effect of increasing decane ratio on7% MPTES functionalised SBA-15 material, (Each material offset by 250 cm^3/g)

Table 3.2 BET surface area values of samples with 7 mol % MPTES and increasing weight ratio of decane to surfactant

Decane: P123	BET surface area m^2/g and error(+/-)
2:1	619 (13)
3:1	693 (12)
4:1	657 (12)
5:1	830 (10)
5.8:1	670 (8)
6:1	848 (12)

3.4 Modifying synthesis temperature of SBA-15

It has been reported that by employing a low temperature hydrolysis step and subsequent acid erosion step it is possible to increase the cage and window size of cubic FDU-12 material significantly, *via* a three step synthesis: a low temperature hydrolysis step at 15^{o} C; a 100^{o} C condensation step; and an additional acid erosion step at 100-140 ^{o}C **[11]**. This method has been used to prepare materials for this thesis, as described in section 3.7. It was also decided to use this 3 step approach in the synthesis of SBA-15 to see what effect, if any, a change in temperature would have on the sample morphology and pore size. Therefore the aims were to study the combined effects of addition of thiol and decane while using 15 ^{o}C (rather than 40 ^{o}C) as the hydrolysis temperature, and including an acid erosion step.

3.4.1 Synthesis

P123 (2 g, BASF) was dissolved in a mixture of H_2O (69 mL) and HCl (6.1 g, 37 %) at 15 ^{o}C and stirred for 2 h. TEOS, thiol and decane (in a weight ratio to P123 of 5.8:1) were added simultaneously and stirred at 15 ^{o}C for a further 24 h before being transferred to a thick walled Teflon bottle at 100 ^{o}C for 24 h. The samples were then filtered and dried at room temperature and 0.5 g per 30 mL 2M HCl was placed back in the Teflon bottle at 100 or 140 ^{o}C for 48h. The resulting product was washed using distilled water and filtered before being air dried and calcined at 823 K for 4 h under nitrogen, followed by oxygen, or sohxlet extracted using ethanol in the case of organically-functionalised materials. Samples synthesised using this low hydrolysis temperature pathway are shown in Table 3.3.

Table 3.3 Samples prepared using 3-step, low hydrolysis temperature synthesis pathway

Additives	TEOS (g)	MPTES (g)	Decane (g)	Acid step temp (^{o}C)	Comment (Phase)
P123	4.1			100	Typical SBA-15, slightly larger pores
P123, 2%MPTES	4.0	0.1		100	Hexagonal SBA-15
P123, 2% MPTES+decane	4.0	0.1	11.6	100	Parallel channels SBA-15
P123, 7% MPTES	3.9	0.34		100	Channel material SBA-15
P123, 7% MPTES+ decane	3.9	0.34	11.6	140	STA-11 (Ia-3d material)

3.4.2 Transmission Electron Microscopy

Using this low temperature pathway a regular, well ordered material is obtained as seen in Figure 3.18(A) when the SBA-15 synthesis is repeated using this method. The image shows the entrances to the pore system and measurement of the pore diameter from the TEM indicates the average pore size is 6.5 nm.

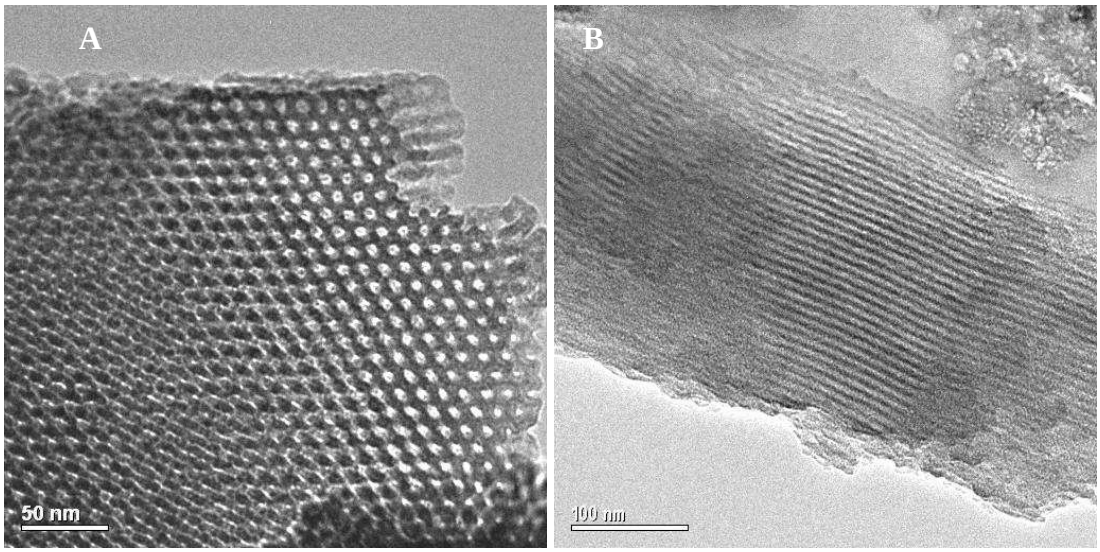

Figure 3.18 HRTEM of SBA-15 (A) and 7%SH SBA-15 (B) synthesised with 3 step synthesis route

Adding 7% thiol to the synthesis of SBA-15 under typical conditions has previously been shown to produce a cubic Ia-3d material. At low hydrolysis temperature SBA-15 with large particle size is formed, shown in Figure 3.18-B (above) but if the synthesis is modified by adding both thiol and decane to the prep and the higher acid erosion temperature of 140 ^{o}C is used then a material which has Ia-3d symmetry and a pore size of 7-8 nm is obtained, shown in Figure 3.19. This has the pore structure of STA-11 (itself prepared by adding 7 mol % thiol to an 'SBA-15' preparation): The sample shown in Figure 3.19 is therefore denoted 'STA-11 + decane' in this text.

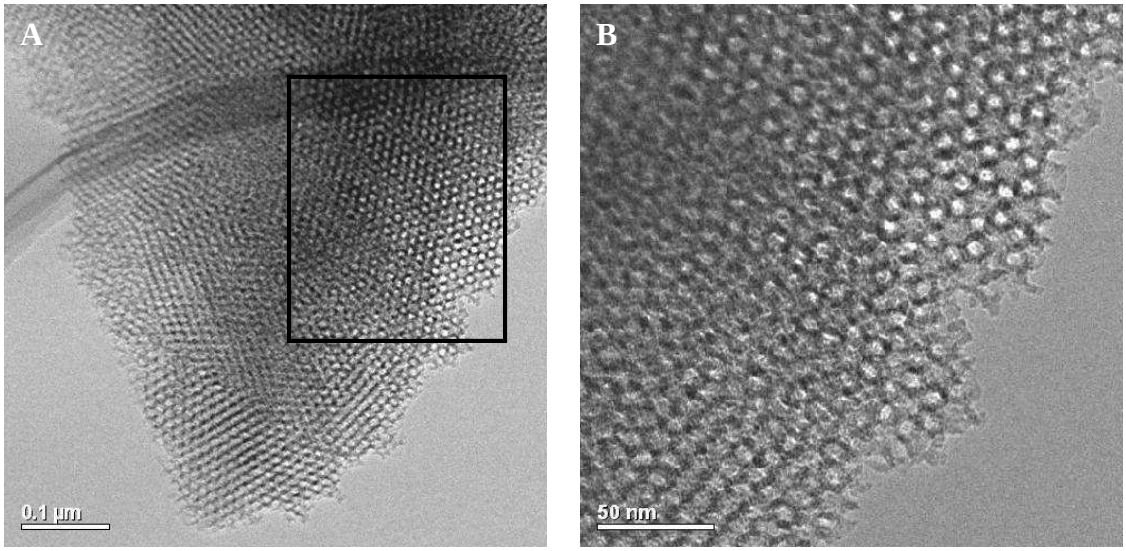

Figure 3.19 HRTEM image of 7%SH-SBA-15+decane (STA-11) synthesised with low hydrolysis temperature with a hydrothermal step at 140^{o}C - showing large particle showing both cubic and hexagonal pore arrangement(A) and focusing on Ia-3d morphology with view down [111] axis (B)

By only adding a small amount of thiol (2 mol %) the typically hexagonal arrangement of pores seen for SBA-15 is observed, shown in Figure 3.20-A and even when decane is added large particles are observed with the porous channels aligned (Figure 3.20-B) as for typical SBA-15 material.

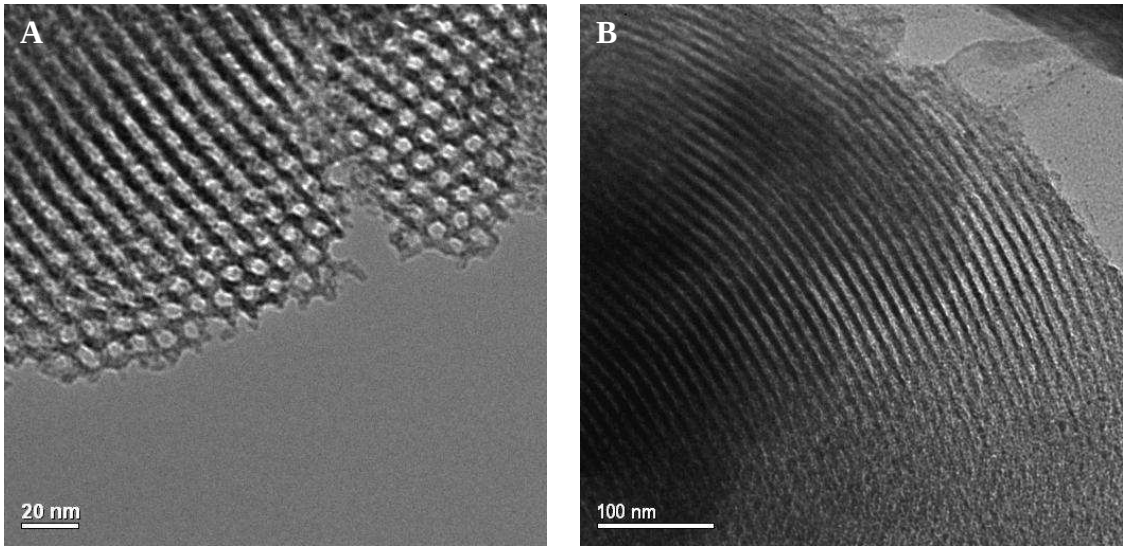

Figure 3.20 HRTEM of 2%SH-SBA-15(A) and 2%SH-SBA-15+decane (B) synthesised at low temperature with hydrothermal step at 100°C.

3.4.3 Nitrogen adsorption

Figure 3.21 shows the isotherms obtained for samples synthesised at low temperature with the addition of thiol and decane. Typical SBA-15 gives an isotherm with a sharp capillary condensation between 0.6-0.8 P/Po and has an uptake of over 600 cm^3/g. By adding 2% thiol the desorption branch is more gradual (P/P_o = 0.4-0.7) and the hysteresis is closer to type II, indicating the presence of constrictions in the channels. When decane is added the resulting solid appears to have a mixture of type I and II hysteresis and could indicate a physical mix of normal SBA-15 and a part of the solid that has constrictions within the channels. If 7% MPTES is added to the synthesis an isotherm typical of SBA-15 is produced : by adding decane to this synthesis an increase in uptake to 650 cm^3/g and a capillary condensation at a higher P/P_o value ~0.8 are observed.

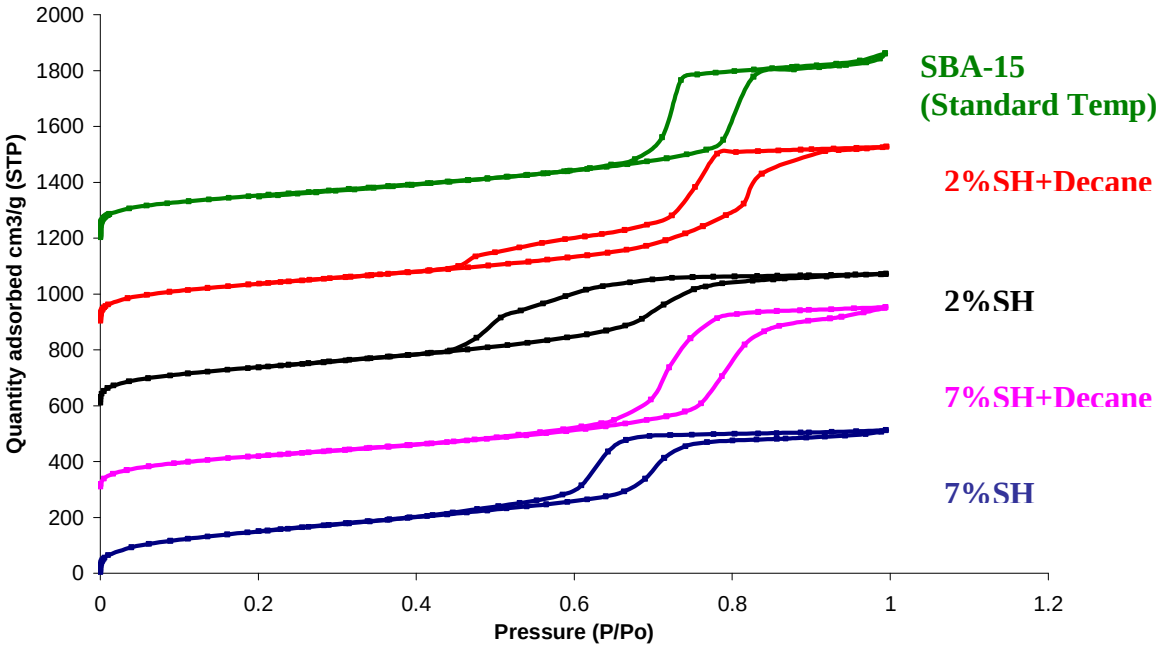

Figure 3.21 Isotherms showing effects of low temperature pathway on SBA-15 synthesis offset by 300 cm^3/g obtained using Micromeritics ASAP 2020

Pore size distributions determined from the adsorption and desorption branches of the isotherms via BJH theory are shown in figures 3.22 and 3.23, and the pore sizes and surface areas (calculated via the BET equation) are summarised in table 3.4. The most significant result for this thesis is the preparation via this three step route of a cubic Ia-3d structure with 7 % thiol and decane as additives, with a pore size of 8-10 nm, larger than previous 'STA-11' type materials. In this synthesis the thiol additive changes the phase from p6mm to Ia-3d, whereas the addition of decane acts to expand the channel dimensions.

Table 3.4 BET surface area and pore diameter of materials prepared via 3 step procedure compared to SBA-15 prepared at 40°C ('standard conditions')

Synthesis	BET surface area m^2/g	Average pore diameter (BJH ads)
SBA-15 (standard temp)	631	10.0
2%SH-SBA-15	512	6.5
2%SH-SBA-15+decane	505	11.5
7%SH-SBA-15	563	6.5
7%SH +decane 'STA-11'	454	9.0

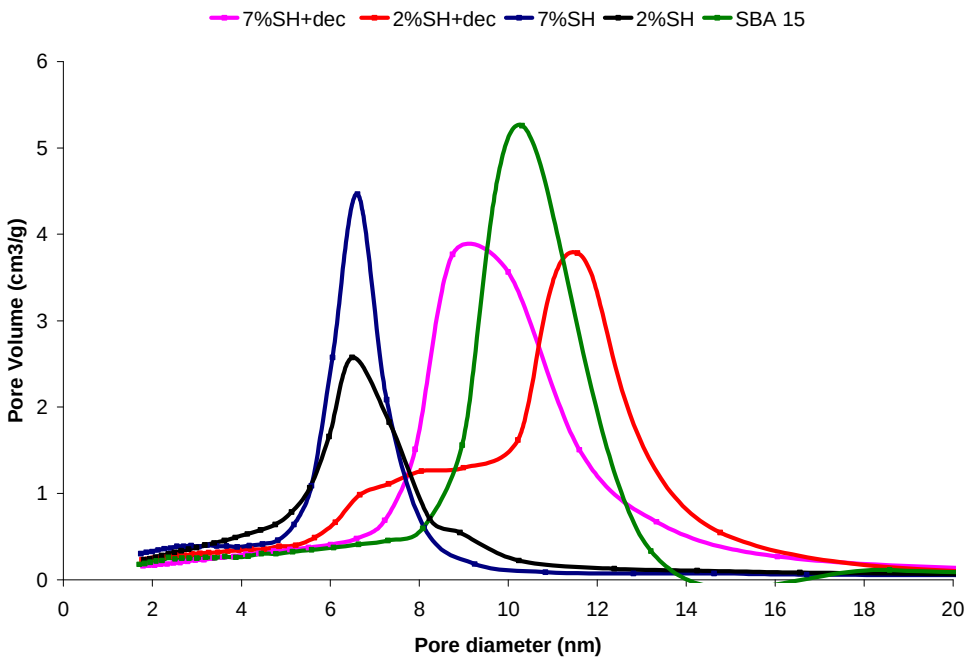

Figure 3.22 Pore size distribution curve calculated from adsorption branch of isotherm for modified SBA-15 type and STA-11 materials synthesised at low temperature.

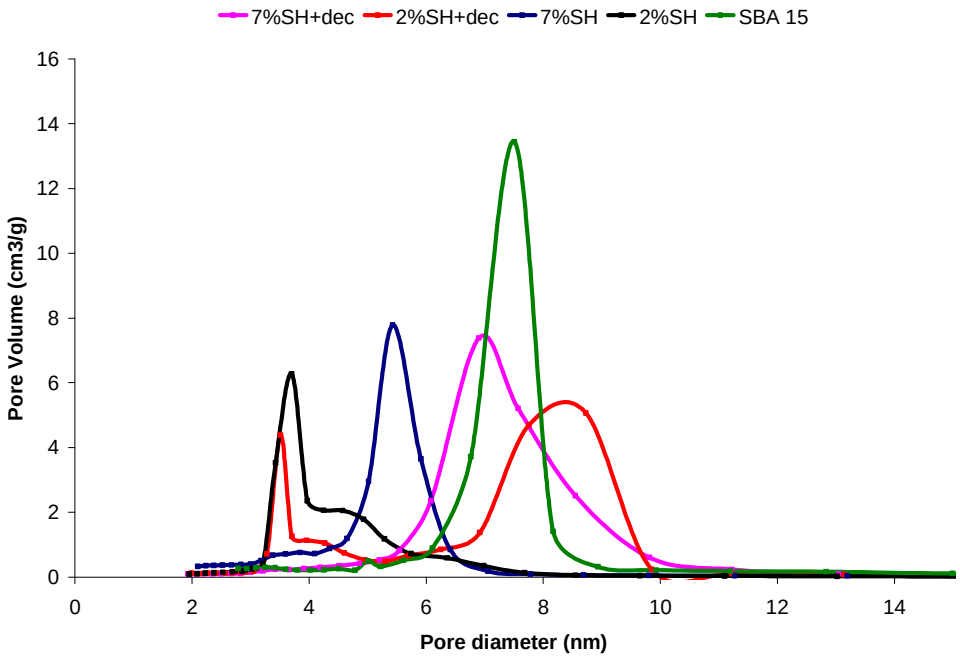

Figure 3.23 Pore size distribution curve calculated from desorption branch of isotherm for modified SBA-15 type and STA-11 materials synthesised at low temp

3.4.4 Summary

SBA-15 was successfully prepared according to literature procedure as a standard for comparison of modified materials. Materials possessing branched particles, onion ring structures and showing interrupted stages of formation were all obtained by using additives including MPTES and decane in the synthesis. In order to try and obtain materials with larger pores the syntheses were repeated using a low temperature pathway which resulted in a cubic Ia-3d material being produced similar to STA-11, but with a larger pore size of 7-8 nm.

3.5 KIT-6: Experimental

As described in section 3.4 a material has been prepared with cubic Ia-3d symmetry using a low temperature SBA-15 synthesis with the addition of decane and thiol. The first reported bicontinuous mesostructured silica was MCM-48 but the pore size was relatively small (1.5-4.5 nm). Much work has been carried out looking at these bicontinuous Ia-3d structures with the aim of increasing the pore size to that of SBA-15. Alternative routes to larger pore Ia-3d material include synthesis of KIT-6 by Ryoo *et al.* **[2],** and this was followed with the aim of preparing materials with pores from 4-12 nm by tuning the synthesis. This was chosen as a starting point for the preparation of 'standard' KIT-6 and preparations were modified using functional groups, with the aim of increasing the pore size to allow larger biomolecules to enter.

3.5.1 Synthesis of KIT-6

Mesoporous KIT-6 silica with a cubic Ia-3d bicontinuous pore structure was synthesised according to the method reported by Ryoo *et al.* **[2]**. P123 (6 g, BASF) was dissolved in distilled water (217 g) and conc. HCl (11.8 g, 35 wt %). To this butanol (6 g, Aldrich) was added under stirring at 35 ^{o}C. After stirring for 1 hour, tetraethyl orthosilicate (TEOS, 12.9 g, 98% Aldrich) was added under stirring at 35 ^{o}C. The resultant gel, which had molar composition

1 TEOS: 0.017 P123: 1.83 HCl: 195 H_20: 1.31 BuOH

was left stirring for 24 h at 35 ^{o}C in a Teflon bottle, and subsequently heated at 100 or 130 ^{o}C for 24 h. Varying the hydrothermal treatment temperature from 100 to 130 ^{o}C was expected to result in an increased pore size. The resulting solid was filtered, dried and calcined at 550 ^{o}C, under nitrogen for 4 h, followed by oxygen for 4 h.

3.5.1.2 Functionalisation of KIT-6 samples

Thiol-functionalised KIT-6 samples were prepared by *in situ* functionalisation with the addition of 5 mol % mercaptopropyltriethoxysilane (MPTES, 99% Fluka). Synthesis as above with 12.9 g TEOS being replaced by 12.0g TEOS and 0.72g MPTES with the molar composition being

0.95 TEOS: 0.05 MPTES: 0.017 P123: 1.83 HCl: 195 H_20: 1.31 BuOH

Functionalised samples were extracted with ethanol using sohxlet extraction for 24 h.

3.5.2 Characterisation

Materials were characterized using transmission electron microscopy (TEM), X-ray diffraction (XRD), thermogravimetric analysis (TGA), N_2 adsorption and elemental analysis. TEM images from KIT-6 samples were obtained using a JEOL 2011 transmission electron microscope operating at 200kV. Low angle XRD patterns were collected using a Phillips X'Pert Multipurpose diffractometer in a two theta range of 0.6-10^o with a step size of 0.02^o. Thermogravimetric analysis was performed between 30 and 700^o C at a heating rate of 5^o C/min (under gentle flow of air) using a Perkin-Elmer Pyris Diamond TG analyzer. Surface area and pore size was determined by N_2 adsorption isotherm obtained at -196 ^{o}C on a Micromeritics ASAP2010. For all samples 100-150 mg of material was degassed at 120 ^{o}C for 2 hours under a vacuum before undergoing nitrogen adsorption. Elemental analysis was performed on a Macroanalyzer Leco CNS-2000-I.

3.5.3 Transmission Electron Microscopy

By utilising a hydrothermal treatment temperature of 100 ^{o}C the synthesis of a KIT-6 material was successful with TEM showing a material with an ordered pore structure as shown in Figure 3.24. By increasing the hydrothermal treatment temperature to 130 ^{o}C it is possible to produce a material which possesses an Ia-3d cubic symmetry as shown in Figure 3.25. Image A shows a view of the Ia-3d morphology which can be seen more closely in image B.

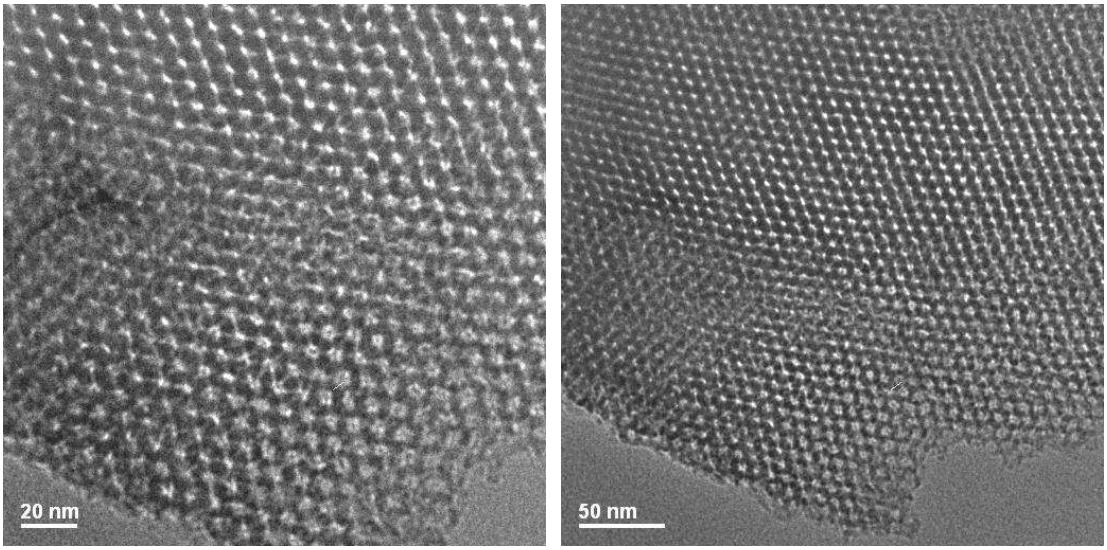

Figure 3.24 HRTEM of KIT-6 synthesised using hydrothermal treatment temperature of 100° C (medium pore material, pore diameter 6 nm) viewed down the [110] axis

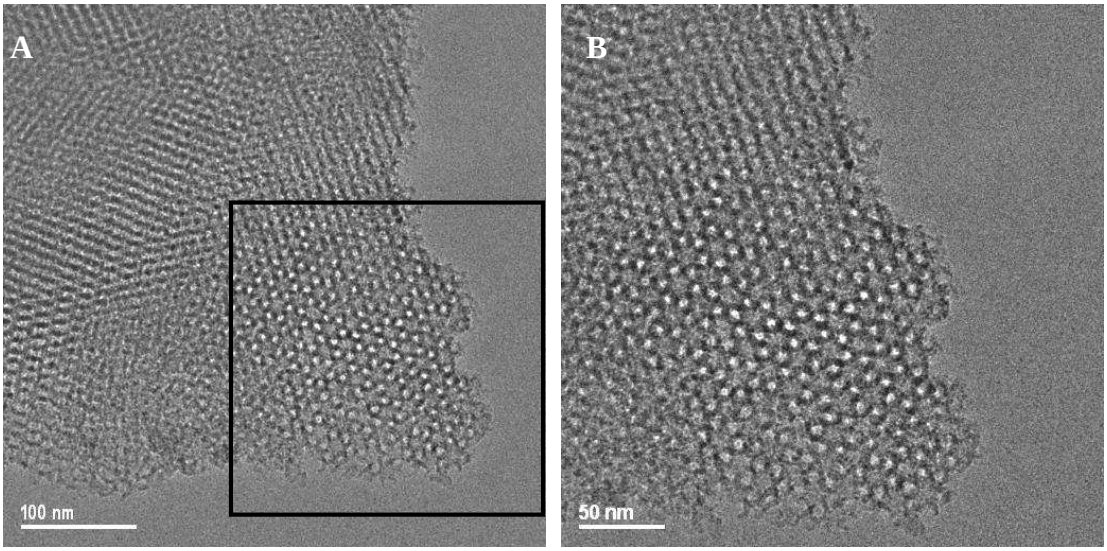

Figure 3.25 HRTEM of KIT-6 synthesised using hydrothermal treatment temperature of 130° C (larger pore material, pore diameter 8 nm) viewed down the [111] axis.

3.5.4 Low angle X-Ray Diffraction

Small angle XRD of KIT-6-130 (Figure 3.26) shows a well-resolved diffraction pattern with reflections characteristic of the cubic structure of silica KIT-6 and in good agreement with reported patterns (Figure 3.27)

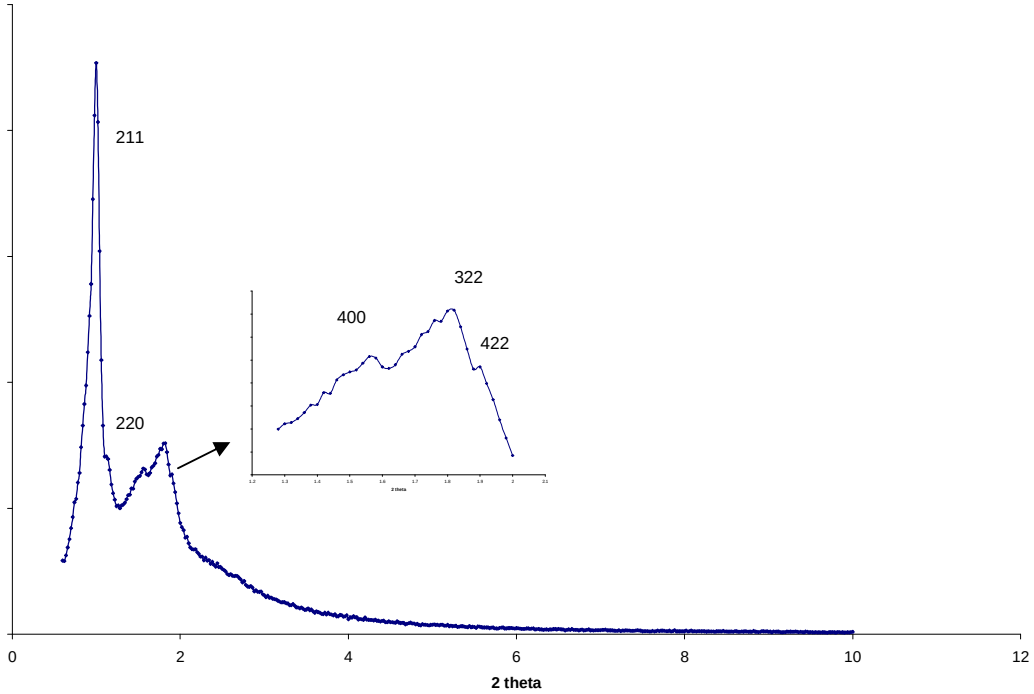

Figure 3.26 X-ray Diffraction of calcined KIT-6-130 material

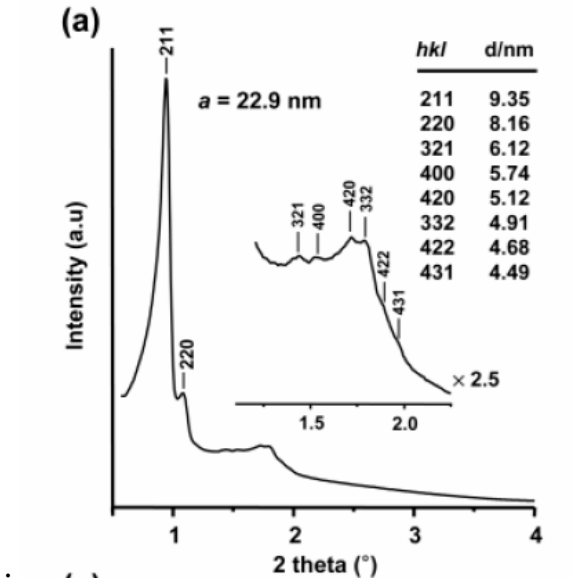

Figure 3.27 Literature diffraction pattern of KIT-6 XRD [2]

The XRD pattern of the functionalised KIT-6 (Figure 3.28) indicates that functionalising the pore reduces the degree of long range order.

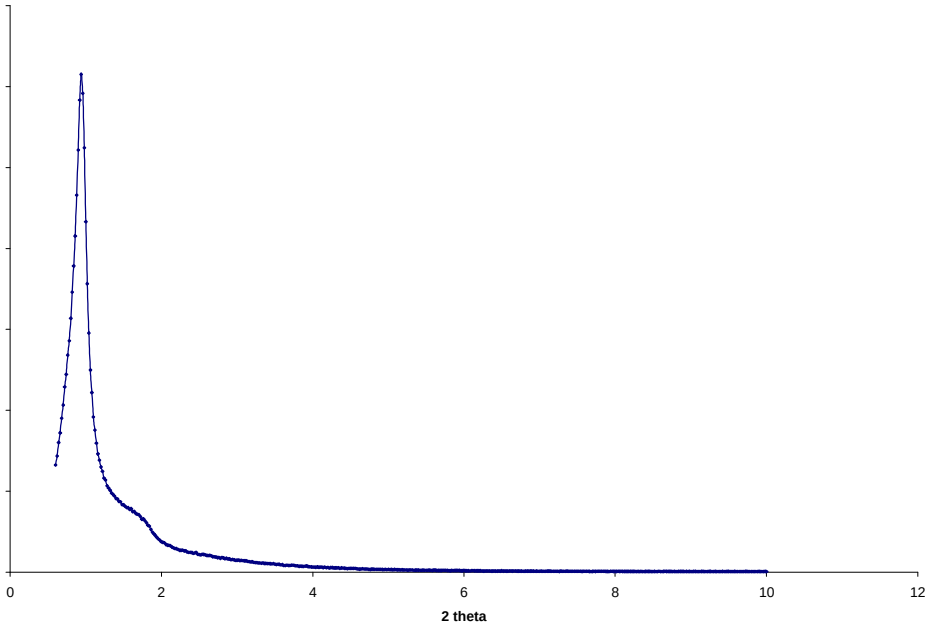

Figure 3.28 X-Ray Diffraction of thiol functionalised KIT-6 material (extracted)

3.5.5 Nitrogen adsorption

Nitrogen adsorption isotherms of all KIT-6 materials are given in Figure 3.29, along with STA-11 material reported in section 3.4 for comparison, and the pore size distributions calculated from the adsorption and desorption branches are give in Figures 3.30 and 3.31. All KIT-6 solids display well defined capillary condensation, type H I hysteresis and narrow pore size distributions. The surface areas, pore volumes and pore diameters calculated from the adsorption branch are shown in Table 3.5. KIT-6 100 denotes samples synthesised at 100 ^{o}C and KIT 6 130 those at 130 ^{o}C. Increasing the hydrothermal treatment temperature from 100 ^{o}C to 130 ^{o}C gives a material which, when calcined, has larger pores (9 nm vs. 6.5 nm). If the surfactant is removed by extraction rather than calcination the pore size is larger still (at 9.5 nm) because there is no shrinkage due to thermally induced Si-O-Si bond formation, but the adsorbed volume is lower because no microporosity is produced in the walls by removal of included surfactant. Functionalising the KIT-6 by inclusion of thiol groups also gives a well defined channel structure, with a slightly reduced diameter. By comparison with the 'STA-11' type material; all of the KIT-6 samples have a narrower distribution of pore sizes.

Table 3.5 KIT-6 samples prepared

Sample	Pore size (nm)	BET Surface area (m^2/g)	Pore Volume (cm^3/g)
STA-11 +decane	9.0	454	1.06
KIT-6 130 calcined	9.0	646	1.32
KIT-6 130 extracted	9.5	451	1.07
KIT-6 130 + 5%SH (ex)	7.5	507	1.03
KIT-6 100 calcined	6.5	638	0.95

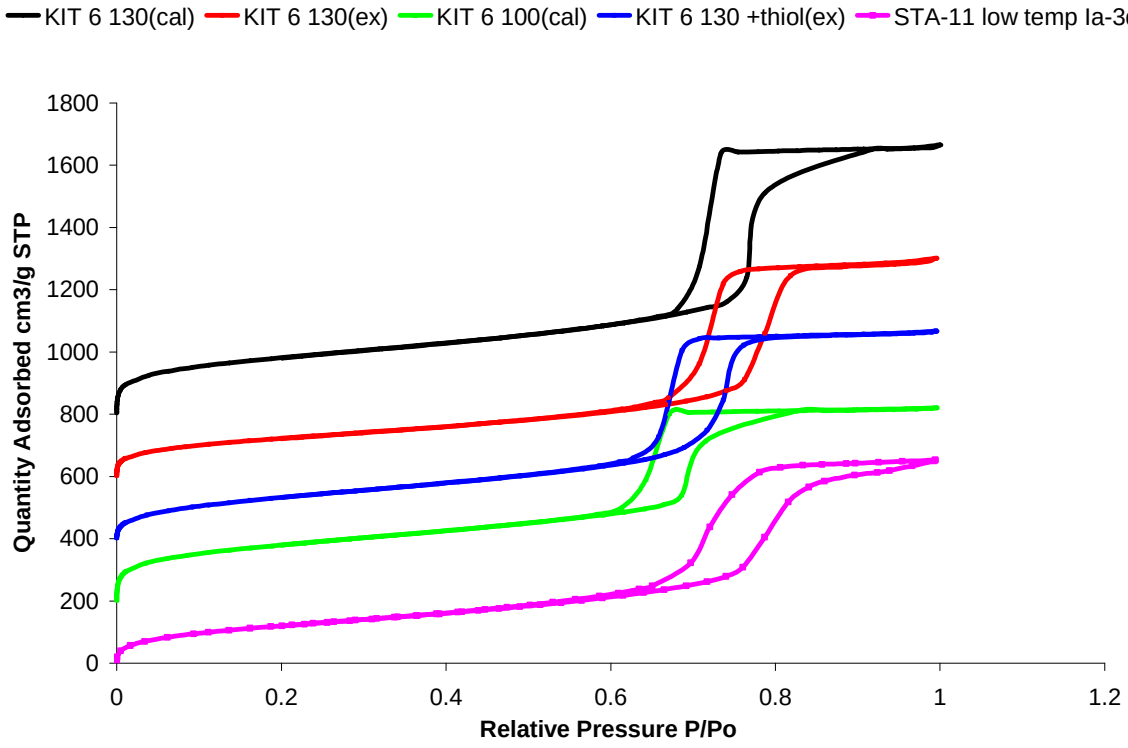

Figure 3.29 Nitrogen adsorption isotherms obtained for KIT-6 materials, offset by 200 cm^3/g

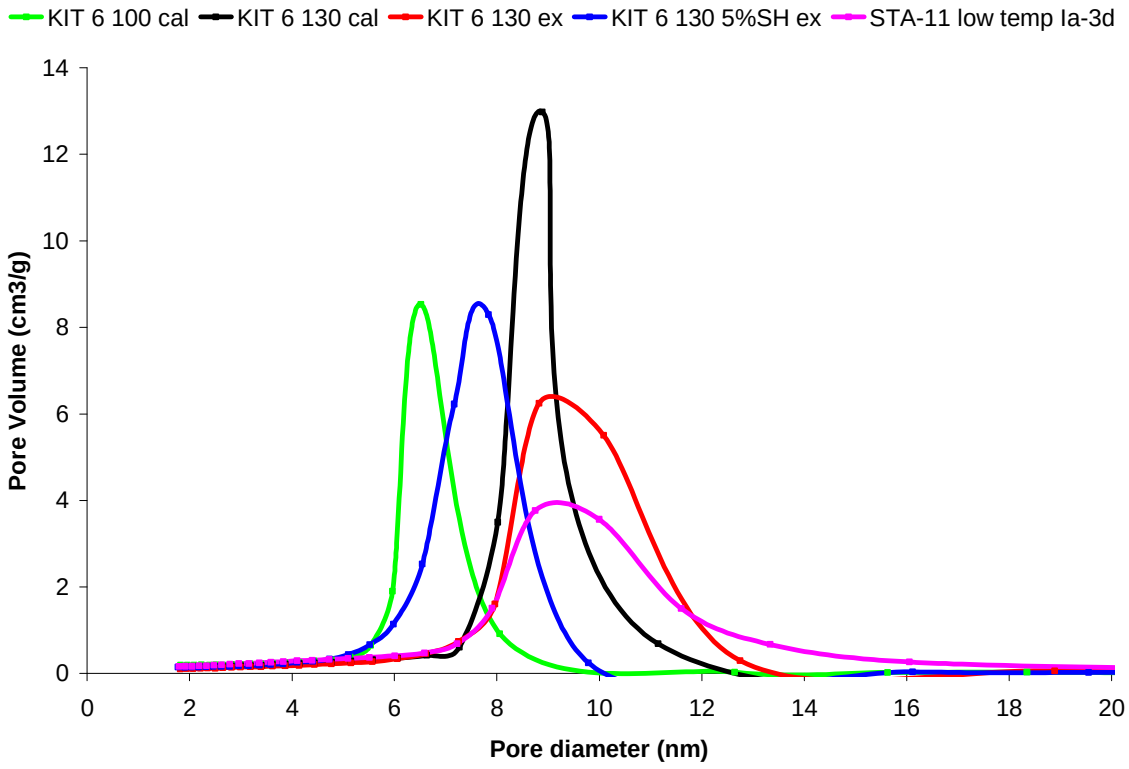

Figure 3.30 PSD curves for KIT-6 type material obtained from adsorption branch of isotherm

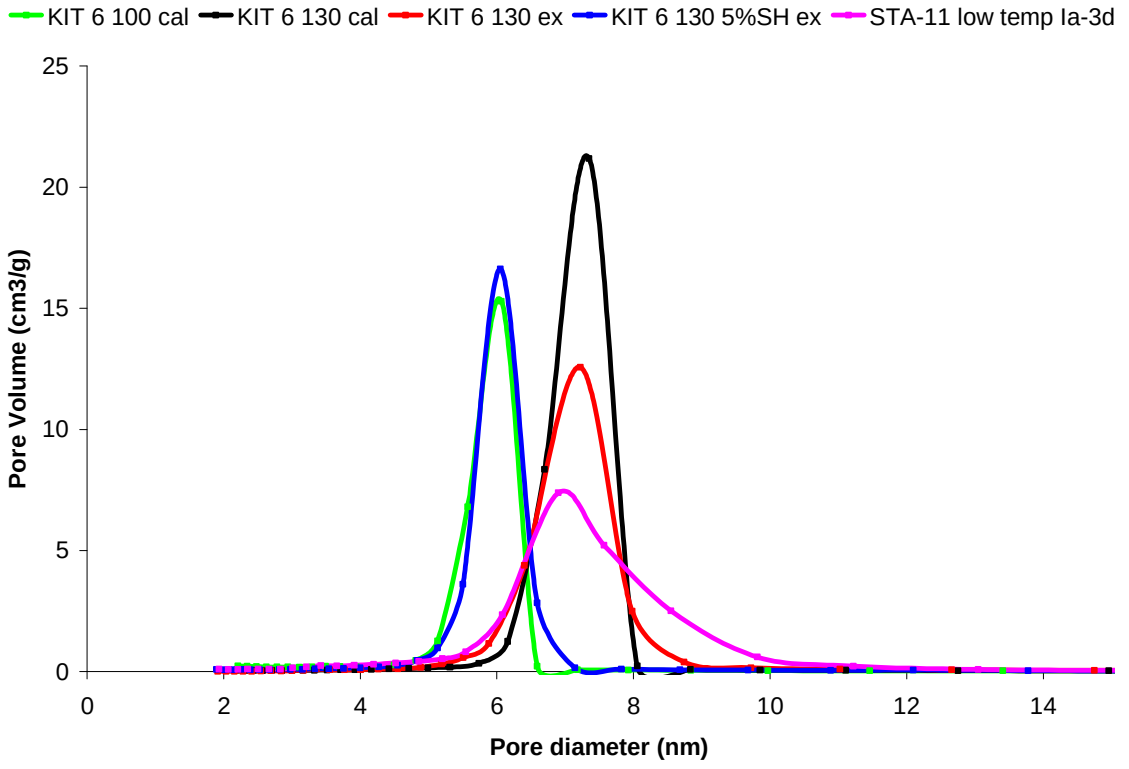

Figure 3.31 PSD curves for KIT-6 type material obtained from desorption branch of isotherm

3.5.6 Thermogravimetric analysis

Surfactant template can be removed from KIT-6 by calcining the as-prepared material or by extraction using a suitable solvent. Calcination is expected to completely remove the surfactant due to the high temperature employed whereas solvent extraction is carried out at relatively mild conditions. TGA was performed on an as-prepared material, where the surfactant remains within the material, an extracted sample and a calcined material (Figure 3.32).

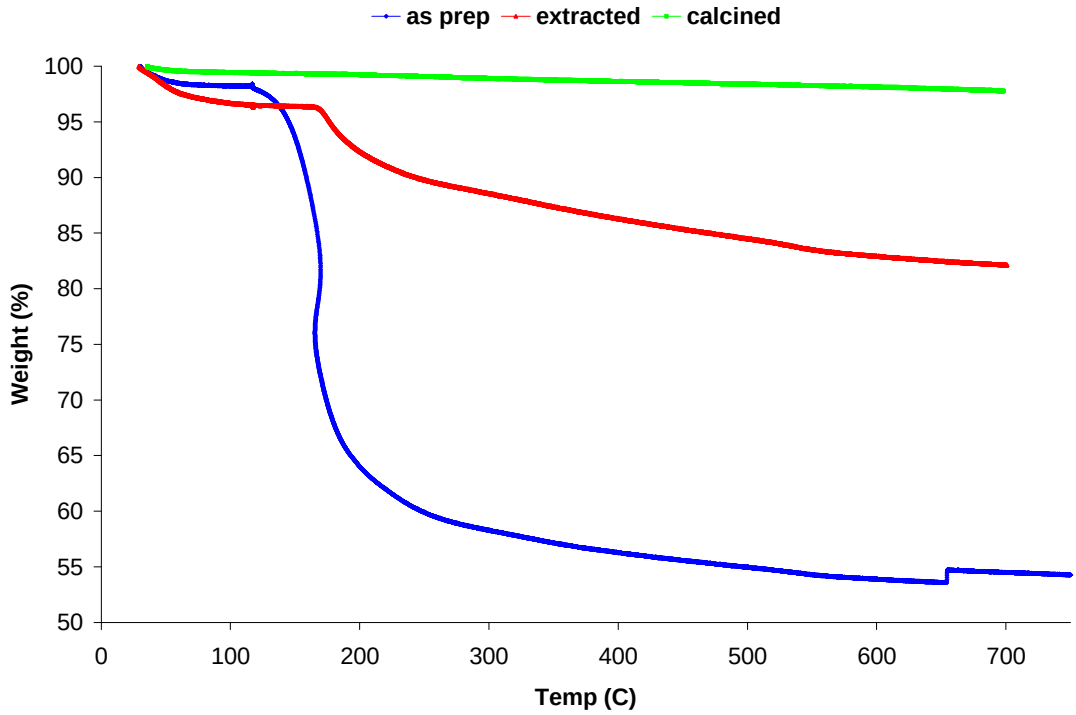

Figure 3.32 TGA trace of KIT-6 (large pore) materials, as prepared, extracted and calcined

As expected the calcined material shows very little weight loss as the material is heated from 40 to 700 ^{o}C (< 2 %). For the extracted sample a 3-4 % weight loss is observed as the sample is heated to 150 ^{o}C, due to residual solvent from the extraction process. As the temperature is increased above 200 ^{o}C we see a loss of an additional 10 wt % which can be attributed to surfactant which has not been removed by extraction. TG analysis on an as-prepared sample shows a small loss in weight as the sample is heated to 150 ^{o}C as

physically adsorbed water is removed. Between 150 and 300 ^{o}C there is a loss of almost 50% of the weight of the sample as the template is removed.

For KIT-6 which has been functionalised with thiol groups and extracted there is a small loss in weight as the temperature is increased to 200 ^{o}C (shown in Figure 3.33), due to residual solvent, followed by a loss of 25% of the total weight as the sample is heated from 200 to 500 ^{o}C as a result of the removal of organic functional groups and surfactant not removed during extraction. TGA on the as-prepared functionalised material gives a similar trace to the unfunctionalised as-prepared material, with a slightly greater total weight loss (>50 %) as the template and functional groups are removed.

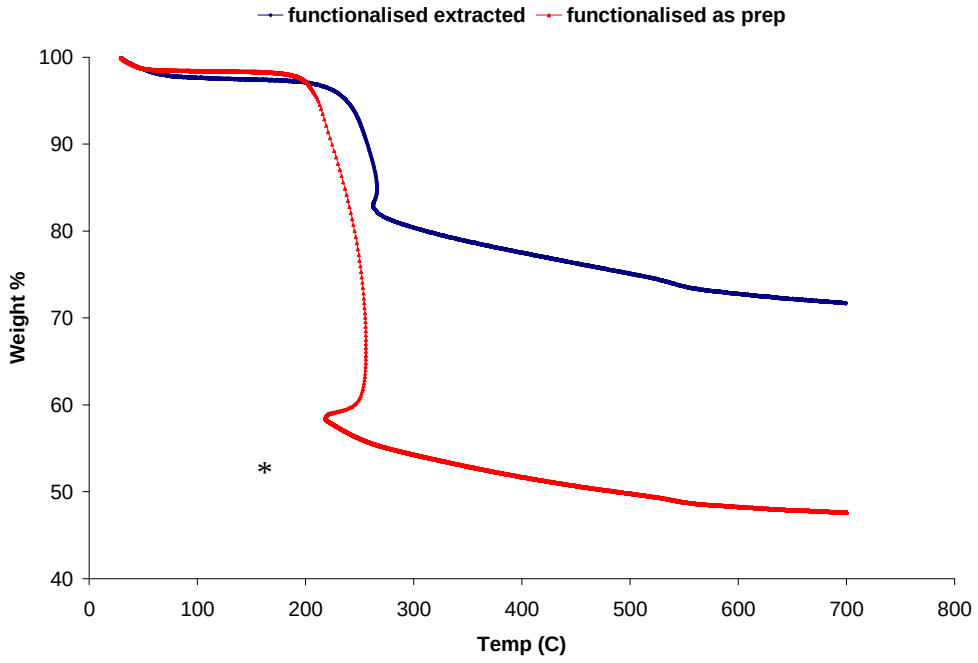

Figure 3.33 TGA trace of functionalised large pore KIT-6 both as prepared and extracted. The reason for the section of the TGA indicated by '*' results from the heating rate being too fast to permit complete combustion of all the surfactant.

3.5.7 Elemental Analysis

Elemental analysis for sulfur indicates the amount of thiol that has been incorporated and the carbon content indicates the extent of surfactant removal after calcination or extraction. Table 3.6 shows the wt% of C, H and S in each sample for the KIT-6 materials synthesised. For both the 'thiol' extracted and 'thiol' as-prepared samples we can see that sulfur is present indicating that the in situ functionalisation has been successful. In the case of the as-prepared materials we see a high carbon content (over 20 wt %) due to the surfactant.

After extraction carbon analysis indicates that not all the surfactant has been removed, and agrees with the TGA traces shown in section 3.5.6. After calcination there is no carbon present in the sample which shows that complete template removal occurs during calcination.

Table 3.6 Elemental analysis of KIT-6 materials

Samples	%C	%H	%S
KIT-6 130 (Large pore) as prepared	23.95	4.57	
KIT-6 130 (Large pore) extracted	5.73	1.94	
KIT-6 130 (Large pore), calcined		0.38	
5%SH-KIT-6 130 (Large pore) as prepared	28.33	5.13	1.06
5%SH-KIT-6 130 (Large pore) extracted	12.45	2.98	1.34

3.6 Mesoporous cage structures

The successful synthesis of 1D and 3D connected channel structures prompted the further synthesis of large pore cage structures consisting of cavities connected by smaller windows for comparison in applications. Several reported methods were followed and assessed in order to find the most successful:

3.6.1 Copolymer blends

Teresaki *et al.* **[13]** demonstrated that it was possible to use copolymer blends to synthesise a range of cubic cage structures with different cavity and pore dimensions. Using 2 different surfactants (P123 and F127) and by varying the synthesis conditions it was possible to prepare a range of materials with entrance dimensions from 1 to 6 nm and cavity mesopores of 4.5 to 9 nm **[13]**. A series of samples were therefore prepared using different gel compositions and synthesis temperatures ranging from 60 to 130 ^{o}C. The nitrogen adsorption and TEM images indicated that the materials were not suitable as supports for proteins, however.

3.6.2 KIT-5

KIT-5, like FDU-12, is a large pore, face centred (Fm3m) cubic structure synthesised using the triblock copolymer F127. Unlike the synthesis reported for FDU-12, Ryoo *et al.* **[14]** use a low HCl concentration method without salts or organic additives. A series of samples were prepared at 60, 100 and 130 ^{o}C (hydrothermal temperature) in order to try and increase the pore size. Increasing the pore size was successful as indicated by the larger hysteresis and higher uptake of nitrogen during the adsorption of nitrogen but the pore windows were smaller than required for adsorption of large proteins.

The TEM images and N_2 77K isotherms of samples prepared using these two methods can be seen below in Figure 3.34 and 3.35. The micrographs confirm the Fm3m mesocage structure. The N_2 isotherms are compared with FDU-12 material synthesised with 4 nm pore entrances. Neither the KIT 5 material synthesised at 160 ^{o}C nor the material synthesised using a copolymer blend at 130 ^{o}C shows any improvement on the nitrogen

uptake or in shifting the desorption branch of the isotherm to higher P/P_o, which would be observed for larger pore windows.

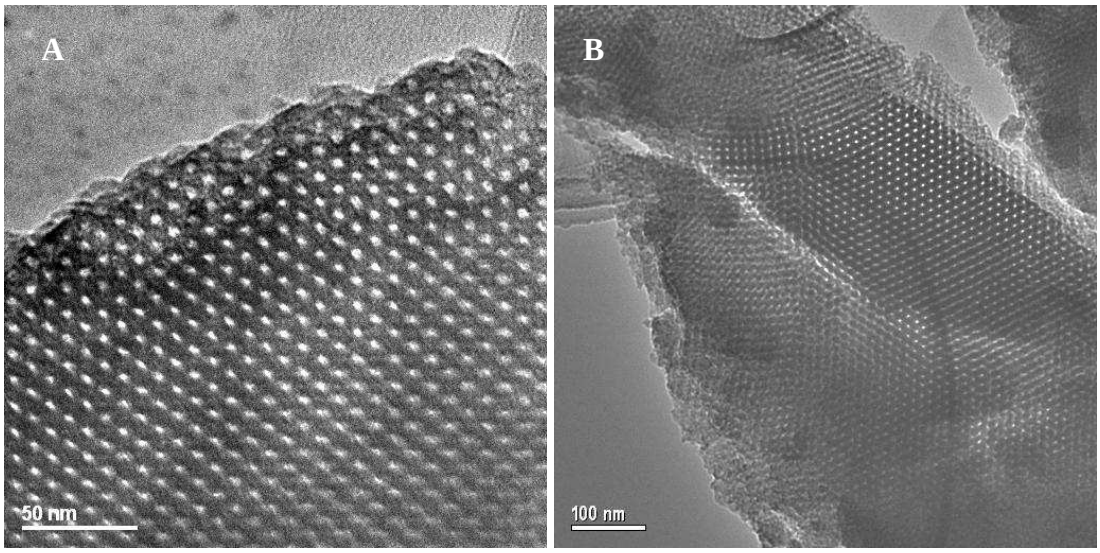

Figure 3.34 HRTEM of copolymer blend material (A) and KIT 5 (B)

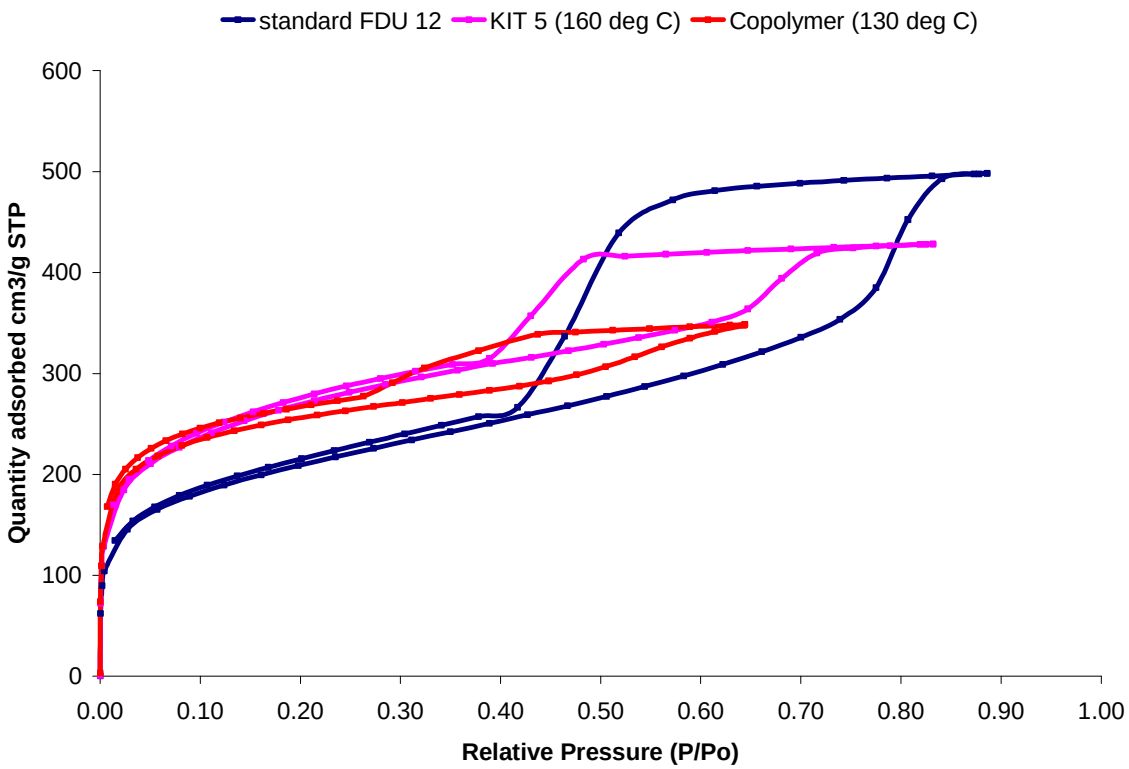

Figure 3.35 Nitrogen isotherms for range of cubic cage materials.

3.6.3 FDU-12 *via* the low temperature pathway

During the course of this work Zhao *et al.* **[11]** described the synthesis of a range of FDU-12 materials with tuneable entrance windows of 4 to 16 nm and cavities of up to 27 nm. Mesoporous FDU-12 was therefore synthesised according to the method of Zhao *et al.* **[11]**. The aim was to produce a range of cubic cage materials with varying cavity and entrance sizes and with and without thiol groups to act as protein supports.

The synthesis route has three steps; a hydrolysis step, a condensation step, and a final acid treatment step. These first two steps are typical for the synthesis of mesoporous silicas with the third being a novel treatment step introduced by Zhao *et al.*. This section investigates the effects of varying the conditions of these three steps on the resulting material.

3.7 Low temperature synthesis of FDU-12

F127 (0.5 g, BASF), trimethylbenzene (0.6g, TMB, Aldrich) and potassium chloride (2.5g, KCl) were dissolved in 2M HCl (30 mL) at 15 or 50 ^{o}C and stirred for 2 h. Tetraethyl orthosilicate (2.08 g, TEOS, 98% Aldrich) was added and stirred at 15 or 50 ^{o}C for a further 24 h before being transferred to a Teflon bottle at 100 ^{o}C for 24 h. The samples were then filtered and dried at room temperature. Finally the as-prepared material (0.5 g per 30 mL 2M HCl) was placed in a Teflon bottle at 100 or 140 ^{o}C for 48 h to undergo the acid treatment step. The resulting product was washed using distilled water and filtered before being air dried and calcined at 550 ^{o}C for 4 h under flowing nitrogen, followed by flowing oxygen for 4 h.

A variety of materials with differing pore sizes were synthesised by varying the hydrolysis and acid treatment temperature. Samples are denoted FDU-12 (X-Y), where X is the hydrolysis temperature and Y is the additional acid treatment temperature. (In all cases the condensation step temperature was 100 ^{o}C).

3.7.1 *In situ* functionalisation of FDU-12

Thiol-functionalised FDU-12 samples were prepared by *in situ* functionalisation with the addition of mercaptopropyltriethoxysilane (MPTES, 99% Fluka). Synthesis was carried out

as above with 1.97 g TEOS and 0.12 g MPTES replacing the 2.08 g TEOS. Functionalised samples were extracted with ethanol using sohxlet extraction for 24 h.

3.7.2 Investigating the role of the acid erosion step

Initially, the role of the third step was investigated by taking an FDU-12 sample prepared using this low temperature synthesis, 15 ^{o}C for 24 h followed by 24h at 100 ^{o}C and then acid treating the material under different conditions by varying both time and temperature. The aim of this was to examine the effect of the additional acid erosion step and to see how it increases the entrance window and cavity size of the resulting material.

Transmission Electron Microscopy

After 3 days in a weak acid solution at both 100 and 140 ^{o}C an ordered porous material was obtained (Figure 3.36). At the higher temperature the TEM shows an unusual feature where the complete erosion of some of the pores is visible (Figure 3.36 B).

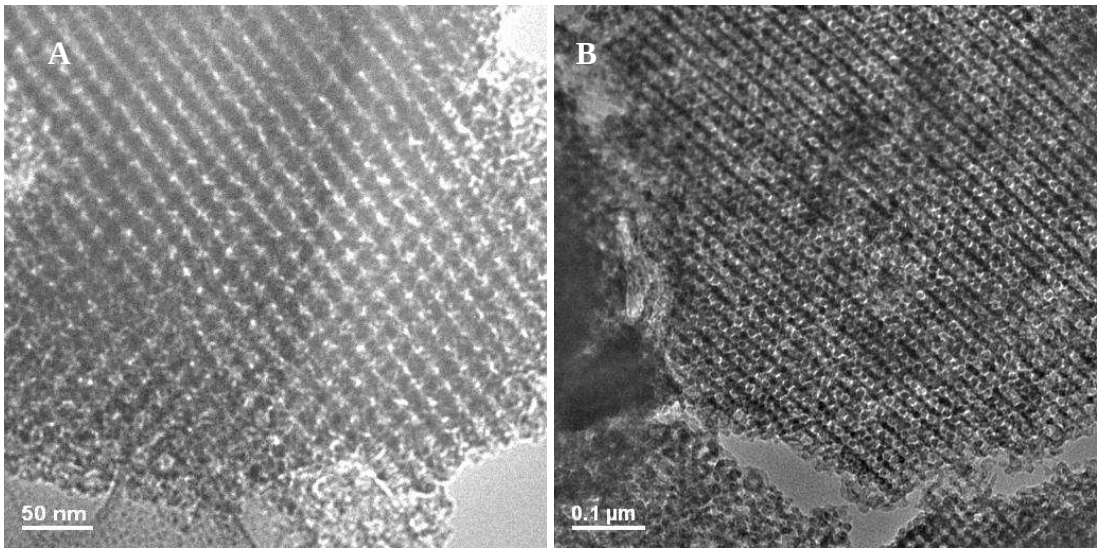

Figure 3.36 HRTEM of resulting material after 3 days hydrothermal treatment in weak acid solution; effect of increasing temperature – 100 ^{o}C(A) and 140 ^{o}C(B)

As the time the as-prepared material spends in the weak acid is increased the effect of increasing the temperature becomes clearer (Figure 3.37). At 100 ^{o}C after 6 days an

ordered porous material is observed (Figure 3.37-A) but at 140 ^{o}C the material is eroded, giving large pore windows and resulting in merging of cavities (Figure 3.37-B).

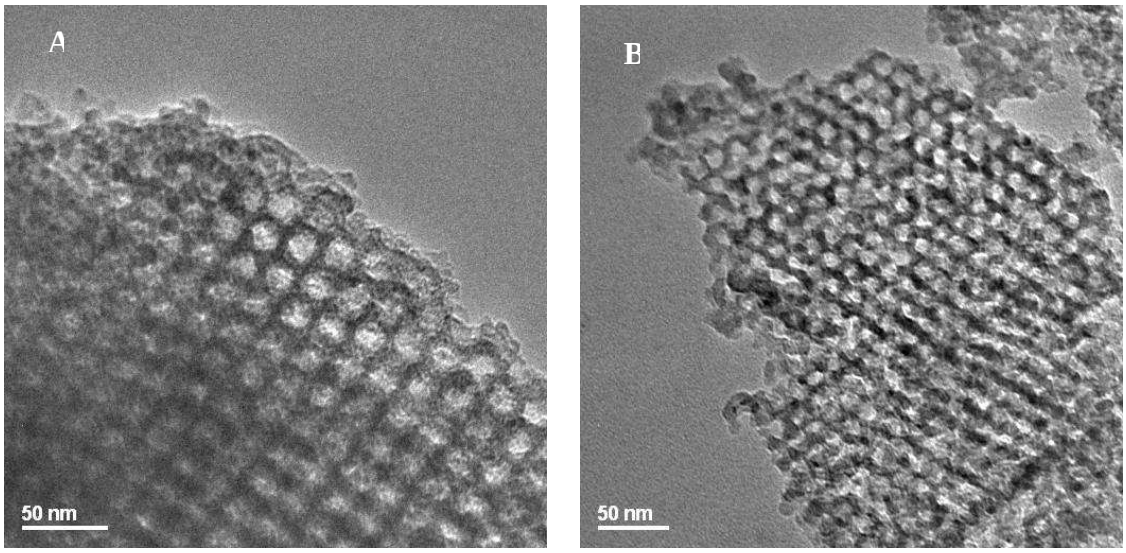

Figure 3.37 HRTEM of FDU-12 material showing effect of increasing the temperature of the acid erosion step carried out for 6 days; A-100 ^{o}C, B-140 ^{o}C

Nitrogen adsorption

This additional acid erosion step has a strong effect on the mesostructure of the material and also the nitrogen isotherm even for the lower acid erosion temperature (Figure 3.38). Rather than the 2 stepped adsorption branch seen for the FDU-12 material prior to the acid step (shown in black) this effect disappears after suspending the material in weak HCl at 100^{o}C for 72 hours (shown in red). A larger hysteresis loop is observed and the uptake increases to 550 from 400 cm^{3}/g.

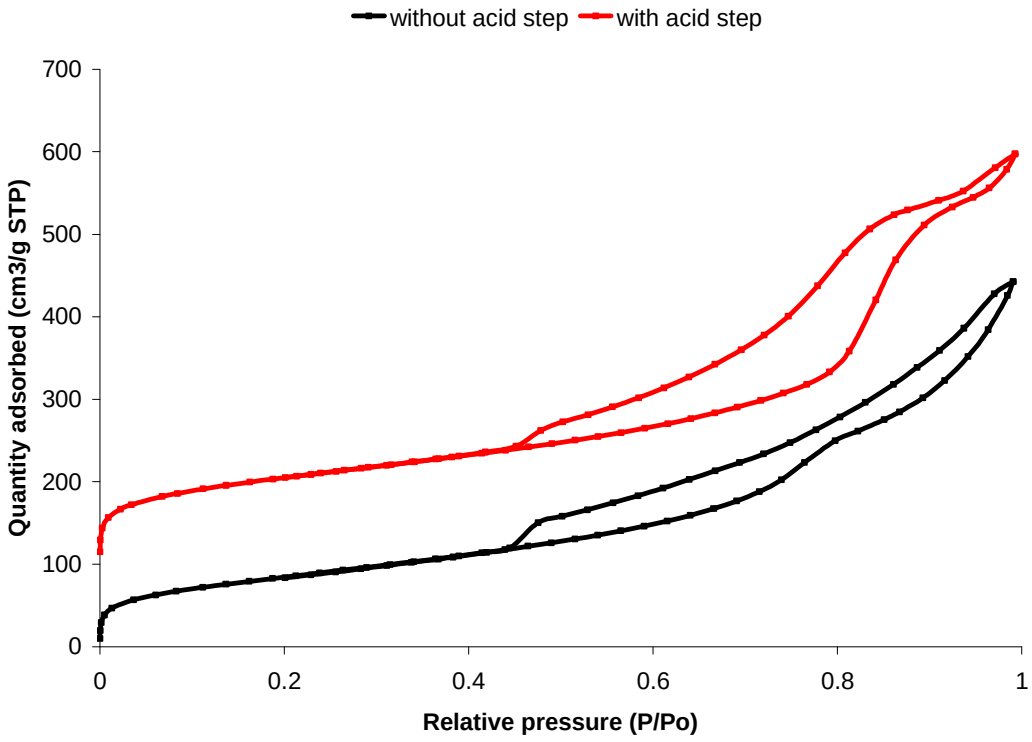

Figure 3.38 Effect of additional condensation/acid erosion step performed by placing the as prepared material in dilute HCl at 100 °C for 72 hours. Isotherms offset by 100 cm^3/g.

By using this additional step the surface area, cavity and entrance window and pore volume are increased (Table 3.7).

Table 3.7 Effect of acid erosion step on surface area, psd and pore volume

Material	BET surface area m^2/g	Cavity size (nm)	Entrance window (nm)	Pore volume (cm^3/g)
No acid erosion step	308	8.5	<4	0.65
With acid erosion step	371	12.0	Distribution around 10	0.74

Prior to the acid erosion step the solid has cages of 8 nm diameter, with entrance windows of *ca*. 4 nm: after 72 hours in a weak acid solution at 100 °C gives an increase in cavity size from 8 to 12 nm whilst the desorption branch indicates a broad distribution in the diameter of entrance windows from 10 nm to below 4 nm. We observe sharp lines at 4 nm as the desorption branch has to collapse to the adsorption branch at $P/P_o \sim 0.42$.

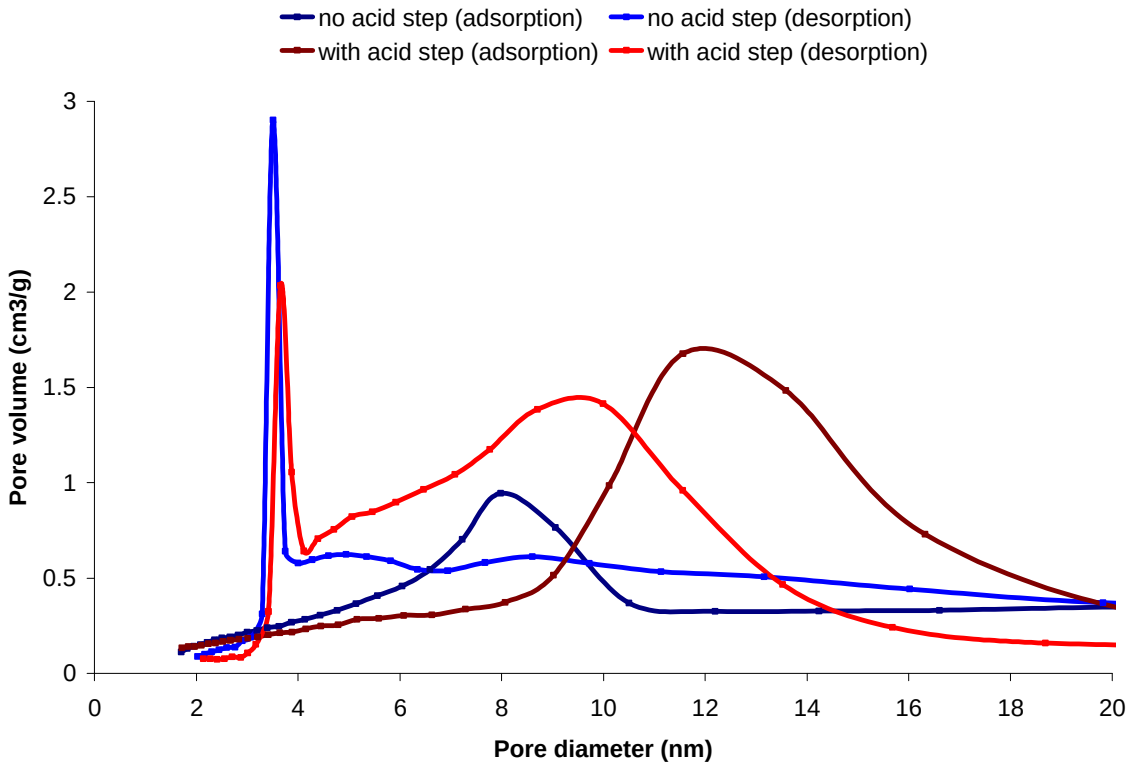

Figure 3.39 Pore size distribution curves from adsorption and desorption branches of nitrogen isotherms for materials before and after acid erosion step

By employing a 50 ^{o}C hydrolysis step and by increasing the hydrothermal temperature used for the additional acid step to 140 ^{o}C we also obtain an ordered material with an increase in pore/cage size, as shown in Figure 3.40. (50-140).

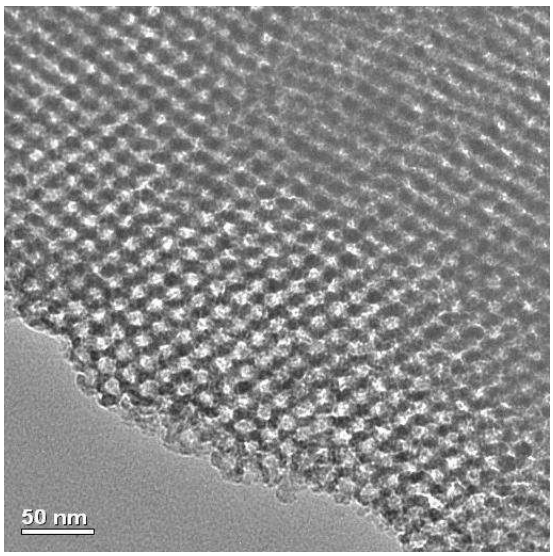

Figure 3.40 FDU-12 (50-140) HRTEM view along [110] axis

Increasing the acid erosion temperature to 140 ^{o}C shows a lower uptake of gas with 300 cm^{3}(stp)/g adsorbed up to a relative pressure of 0.9 due primarily to reduced uptake in the microporous regime (Figure 3.41). The desorption branch has been shifted to a higher relative pressure indicating that the window size has been increased from 4 to 8 nm.

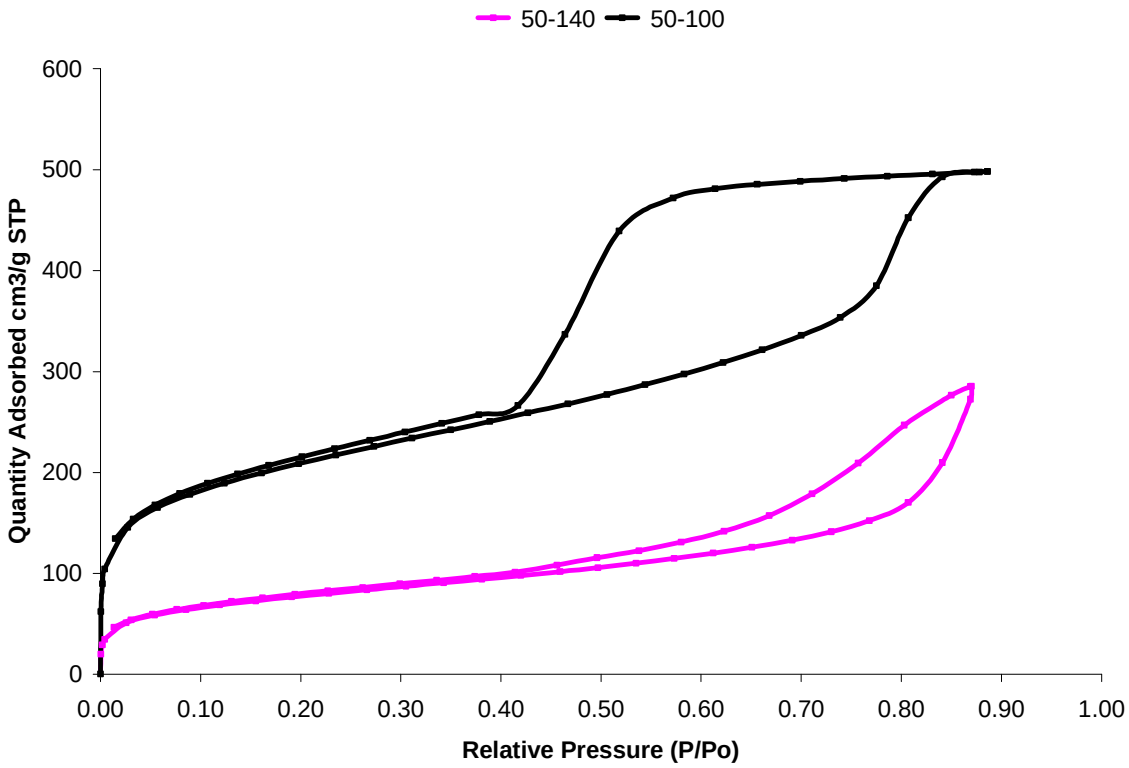

Figure 3.41 Nitrogen isotherm showing effect of increasing acid step temperature

This shows us that the acid treatment results in erosion of silica, initially at the windows and in the generation of larger mesopores. The conditions reported by Zhao, of a hydrolysis step at 15 ^{o}C and an acid erosion step at 140 ^{o}C, are optimum for improving the window size without too much erosion of the whole structure.

In many of the isotherms for the FDU-12 cage materials we do not see a typical H1 or H2 type hysteresis as discussed in chapter 2. Instead of the sharp drop at P/P_o 0.42 characteristic of pore windows less than 4 nm in cage materials we see a gradual decrease of the adsorption branch, indicating a range of window sizes typically between 4 and 16 nm. This can be explained by the cavities of the material being connected by channels with various diameters as shown in Figure 3.42. Here, all the cavities are of a similar size but

cages denoted type A are linked to the outside and nearby cages by larger windows and cages of type B are linked to the outside by smaller windows and will empty on the desorption branch at lower P/P_o values.

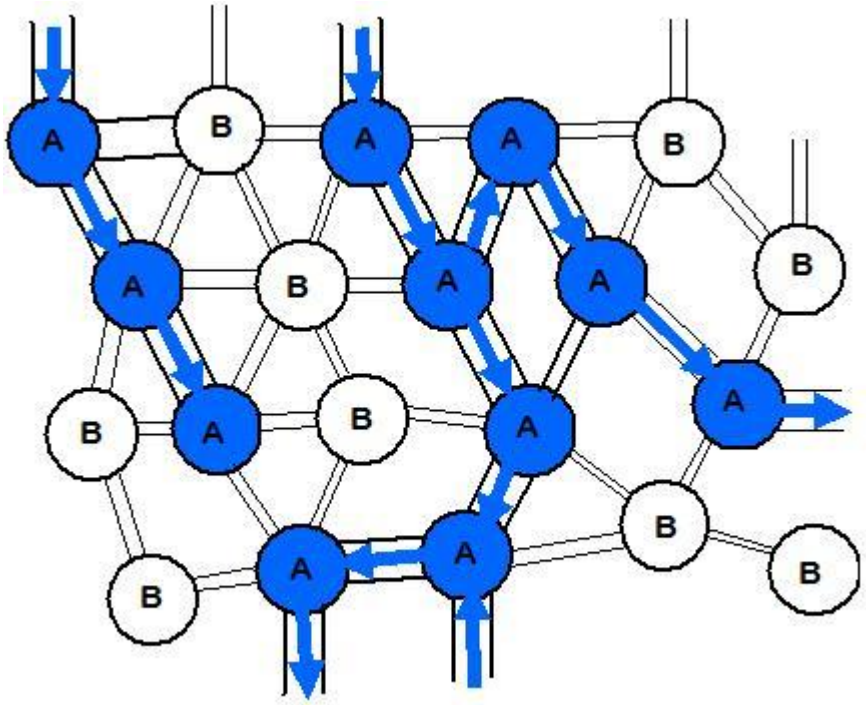

Figure 3.42 Schematic of adsorption within cage materials with differing connecting window diameters

3.7.3 Varying step 2 - hydrothermal treatment time

Samples were synthesised using the same initial low temperature step as described earlier, this time varying the second step synthesis time to establish optimum duration. Materials are prepared at a hydrolysis step at 15 ^{o}C followed by a condensation step at 100 ^{o}C for 2-8 days. No additional erosion step is included in these experiments.

3.7.3.1 Synthesis

F127 (0.5 g), TMB (0.6 g) and KCl (2.5 g) are dissolved in 2M HCl (30 mL) at 15 ^{o}C and stirred for 2 h. TEOS (2.08 g) was added and stirred at 15 ^{o}C for a further 24 h before being transferred to a thick walled Teflon bottle at 100 ^{o}C for 2-8 days. Samples are calcined in nitrogen for 4 hours followed by oxygen for 4 hours or are sohxlet extracted for 8h in ethanol extraction to remove the template.

3.7.3.2 Transmission Electron Microscopy

It can be seen from the TEM images that an ordered, porous material can be observed in all samples when the hydrothermal treatment time is varied between 2 and 8 days (Figure 3.43) but there are see slight differences in the nitrogen isotherms of the calcined products. Higher hydrothermal treatment times give, after calcination, products with higher uptakes and larger cavity sizes (Figure 3.44). At all hydrothermal treatment times employed a 2 step isotherm is observed.

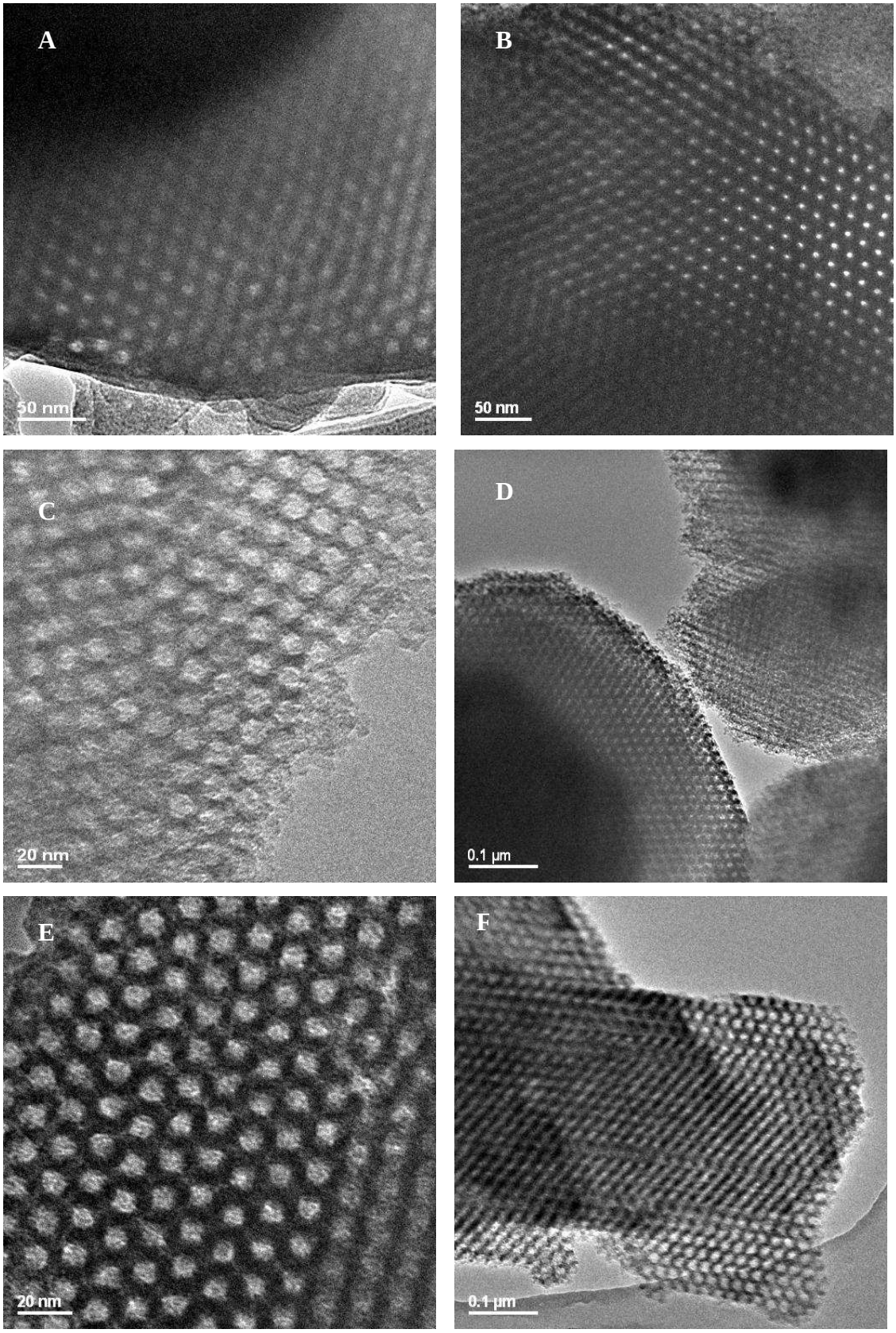

Figure 3.43 HRTEM of FDU-12 materials synthesised by varying the hydrothermal treatment time; 2 days(A), 3 days (B), 4 days (C), 6 days (D), 7 days (E), 8 days (F).

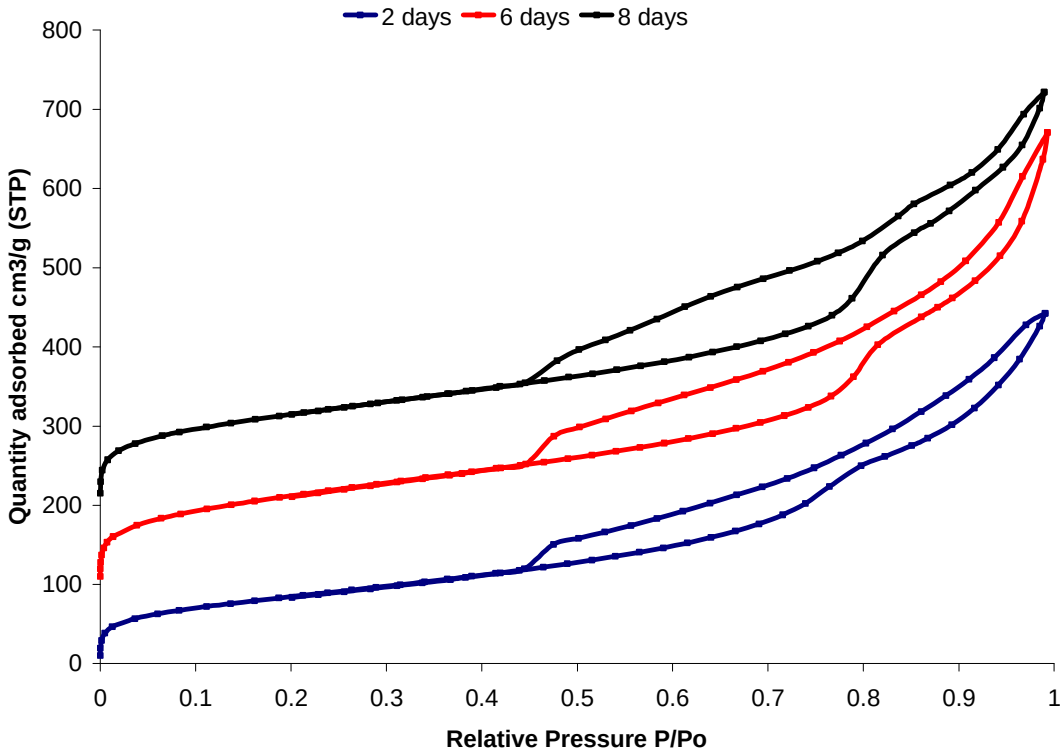

Figure 3.44 Effect of increasing hydrothermal time on FDU-12 isotherms, isotherms offset by 100 cm^3/g

The data obtained from the isotherms shown in Figure 3.44, including pore size distribution, pore volume and surface area can be seen in Table 3.8.

Table 3.8 Surface area and PSD for FDU-12 materials

Hydrothermal treatment time	Surfactant removal method	BET surface area m^2/g	Cavity size (nm)	Entrance window (nm)	Pore Volume (cm^3/g)
2 days	Calcination	308	8.5	<4 to >10	0.65
6 days	Calcination	188	8.7	<4 to >10	0.62
8 days	Calcination	411	10.7	<4 to >10	0.78

The cavity size of the material increases from 8 to 11 nm as the hydrothermal treatment time increases from 2 to 8 days (also seen in Figure 3.45 which shows the pore size

distribution of the cavities). The pore size distribution values obtained from the desorption branch show that all the materials have a range of entrance windows of down to < 4 nm.

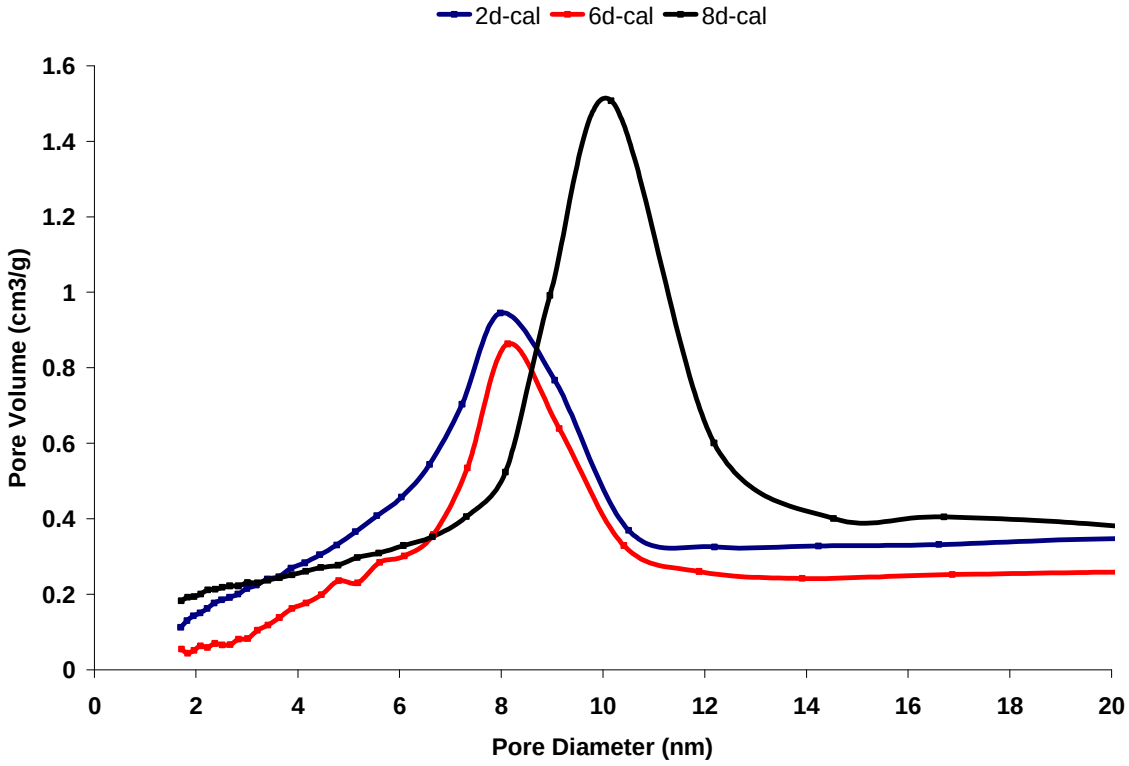

Figure 3.45 PSD curve from adsorption branch showing cavity size

These results show that by increasing the length of the hydrothermal step the pore size is increased although we have seen previously that by using an additional acid erosion step there is also an increase in pore size. So if the samples synthesised undergo this additional acid erosion step then an increase in hydrothermal treatment time will not affect the final pore size.

3.7.4 Varying step 1- temperature of hydrolysis step

After looking at the role of the acid step in the synthesis and the effect of changing the hydrothermal step time, here the effect of changing the hydrolysis step temperature is examined, changing from the typical 50 ^{o}C (commonly used in the literature) to 15 ^{o}C as used by Zhao *et al.* in their low temperature route to mesoporous FDU-12.

Using the literature synthesis for FDU-12 (50-100) a porous, ordered material is observed (Figure 3.46). It also shows intergrowths which result from stacking defects in the cubic close packed sequence (ABCABC).

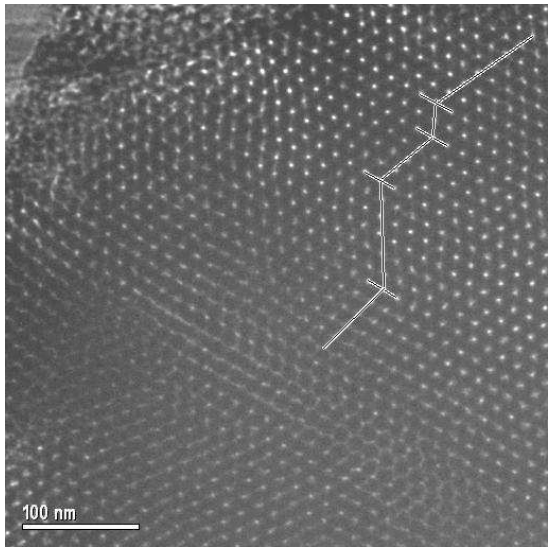

Figure 3.46 FDU-12 material synthesised using 50^{o}C hydrolysis step and 100^{o}C acid step. HRTEM view along the [110] axis

Lowering the hydrolysis step from 50 to 15 ^{o}C, the ordered, porous nature of the material is maintained (Figure 3.47) and the cavity size is markedly increased, confirming the strong effect of the temperature on the original micelle size. Nitrogen adsorption confirms the change in cavity size (Figure 3.48) as the adsorption branch is shifted significantly to higher pressure. The isotherm for sample 50-100 has characteristic H2 hysteresis, indicating a window size close to 4-5 nm, whereas lowering the hydrolysis temperature from 50 to 15 ^{o}C, the desorption branch follows the adsorption branch very closely and hysteresis is closer to type H1. This difference in the isotherm type results from an increase in average window diameter from *ca*. 4 to greater than 8 nm.

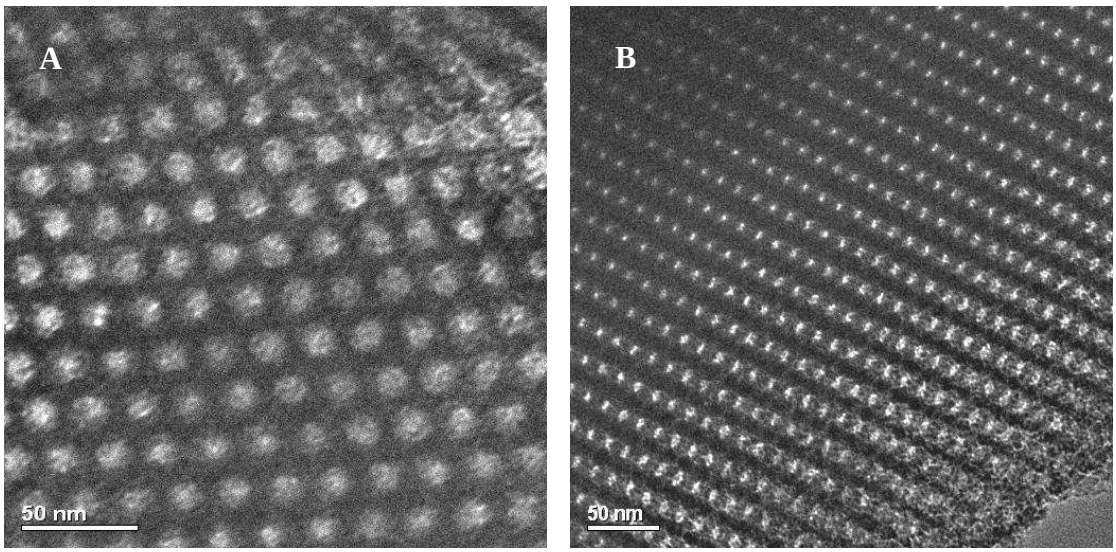

Figure 3.47 HRTEM of FDU-12 (15-100) along [110] axis (A) and [112] axis [B]

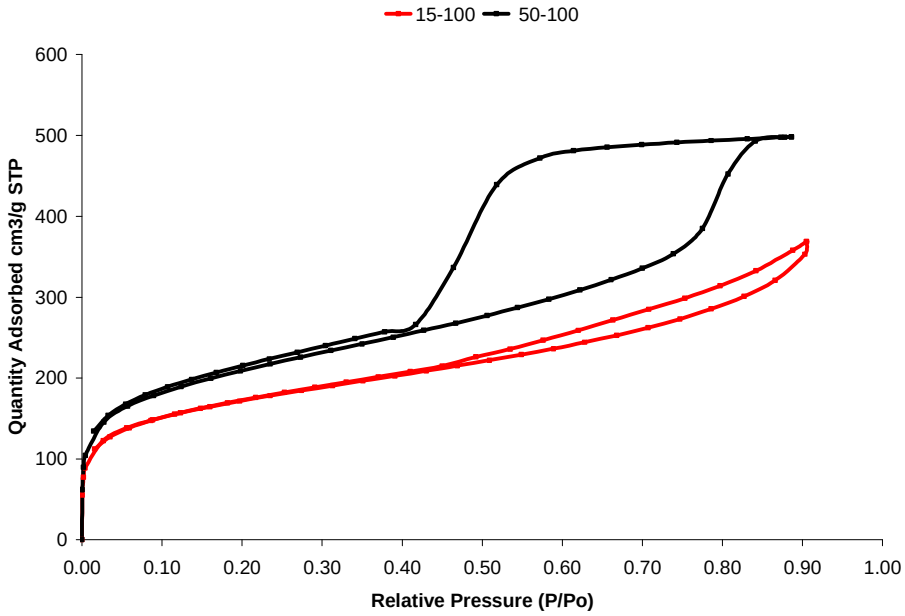

Figure 3.48 Nitrogen isotherm showing effect of reducing hydrolysis temperature.

The data obtained from the TEM images and isotherms can be seen in Table 3.9.

Table 3.9 FDU-12 material prepared by changing hydrolysis temperature

Sample	Window size (nm) (mean)	Cage diameter (nm) (from TEM)	BET Surface area (m^2/g)	Unit cell – *a* (nm) (from TEM)
50-100	4.1	10	622	22
15-100	10.1	15	565	34

3.7.5 Preparation of a series of FDU-12 materials

Having established the effects of varying the conditions of hydrolysis and acid erosion, it was possible to prepare a series of FDU-12 materials with different pore structures, and combinations of cavity and entrance window size. Table 3.10 lists the materials prepared, along with details of the pore structure determined from electron microscopy and nitrogen adsorption.

Table 3.10 FDU-12 material prepared

Sample	Window size (nm) (mean)	Cage diameter (nm) (from TEM)	BET Surface area (m^2/g)	Unit cell – *a* (nm) (from TEM)
50-100	4.1	10	622	22
15-100	10.1	15	565	34
50-140	8.4	12	192	25
5%SH-50-140	12.1	20	348	/
15-140	10.2	18	380	31
5%SH-15-140	12.0	15	420	31

The electron microscopy of these solids clearly shows the Fm3m pore structure and the increase in cavity size as the hydrolysis temperature is reduced.

It is possible to use the electron micrographs to calculate the unit cell parameters shown in Table 3.10. The typical FDU-12 material synthesised using (50-100) conditions results in a material which gives a unit cell *a* value of 22 nm, which is close to the value of 26 nm reported by Zhao. By increasing the acid erosion temperature to 140 ^{o}C we see an increase

to 25 nm (similar to the 27 nm reported). Decreasing the hydrolysis step temperature to 15 ^{o}C has been shown to increase the cavity size: for FDU-12 (15-100) and FDU-12 (15-140) there is an increase in the unit cell to 31-34 nm. This is lower than the reported 44 nm unit cell size indicating that we have not increased the cavity size as greatly as in the materials reported by Zhao.

The electron micrograph image of FDU-12 (15-140) (Figure 3.49), for example, indicates a cavity size greater than 15 nm.

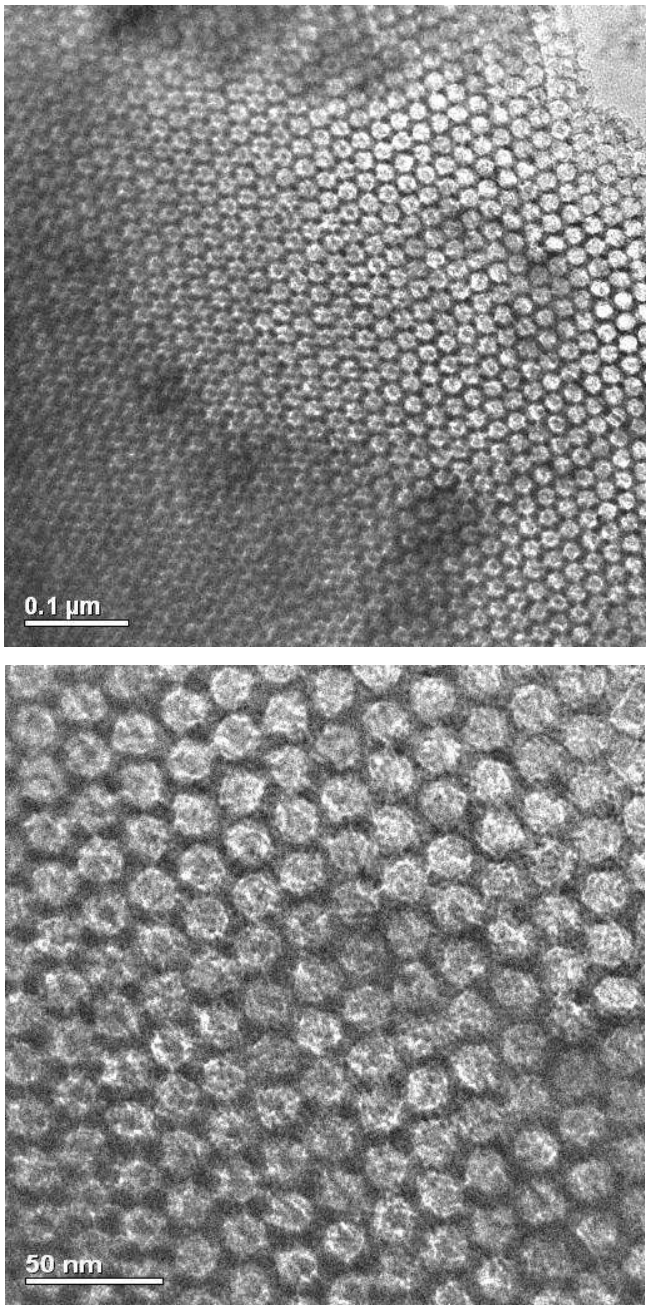

Figure 3.49 Large pore FDU-12 (15-140) HRTEM view along [110] axis

The nitrogen isotherms for typical FDU-12 and material synthesised using a low hydrolysis and high acid erosion step can be seen in Figure 3.50. It shows a large shift to higher pressure of both the adsorption and desorption branches of the isotherm indicating that both the cavity and entrance window dimension have been increased. This in confirmed by the decrease in surface area and pore size (Table 3.10). The surface area decreases from 622 to 380 m^2/g whilst we see an increase in window and cage size to 10 and 18 nm from 4 and 10 nm respectively.

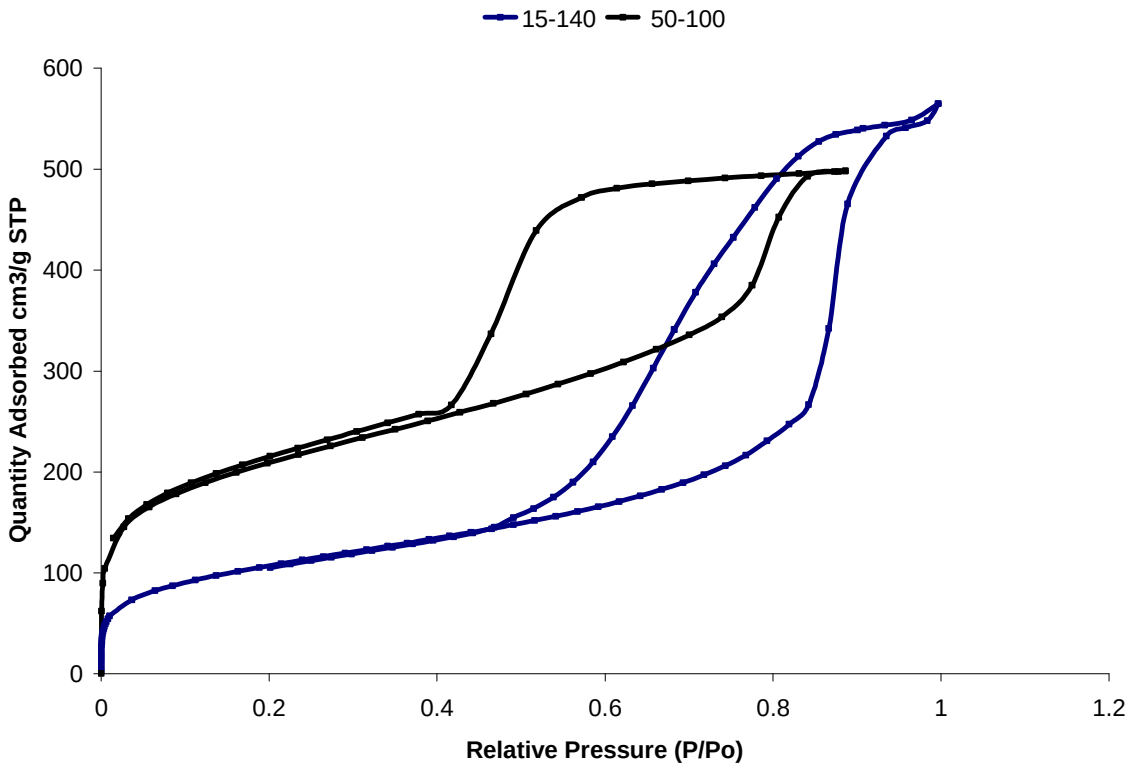

Figure 3.50 Nitrogen isotherm showing effect of decreasing hydrolysis and increasing acid erosion temperature

3.7.6 Functionalising with thiol

FDU-12 materials can be functionalised with between 2 and 7 mol % thiol to obtain materials with a regular arrangement of pores as seen in Figure 3.51.

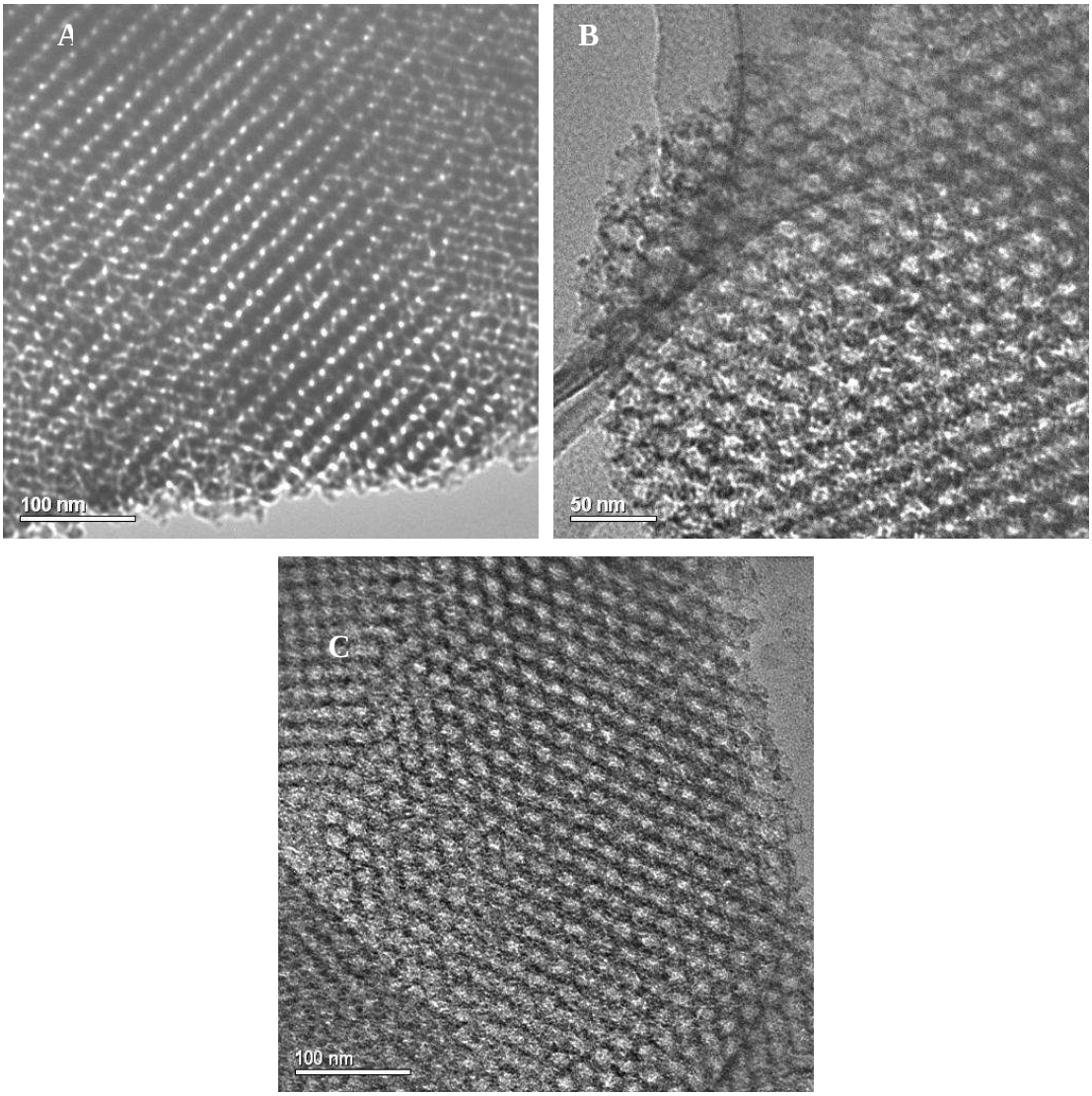

Figure 3.51 FDU-12 (15-140) with 2(A), 5(B) and 7(C) mol % thiol

Nitrogen adsorption isotherms of the 5% thiol functionalised FDU-12 (50-140) and (15-140) are shown in figures 3.52 and 3.53, where they are compared with unfunctionalised samples. Whereas the pore structure looks similar for the (15-140) materials, the functionalised (50-140) material has a larger cage size and a hysteresis close to type H1. Details are given in Table 3.10. The desorption branch of (50-140-5%SH) FDU-12 follows the adsorption branch closely until P/Po 0.45, where there is sudden closure indicating some entrance windows are smaller than 4 nm restricting the escape of nitrogen from some of the pores.

Like the unfunctionalised equivalent, the (15-140-5%SH) FDU-12 shows a gradual closure of the hysteresis loop, indicating a broad distribution of pore entrance sizes, between 5 and 12 nm.

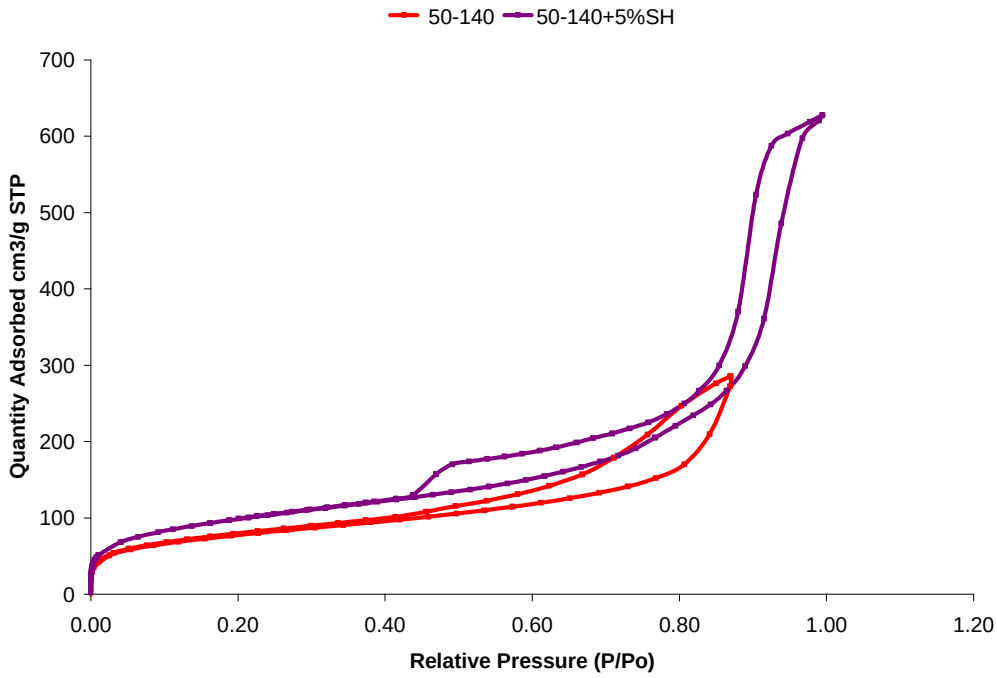

Figure 3.52 Nitrogen isotherms for (50-140) FDU-12 with and without thiol

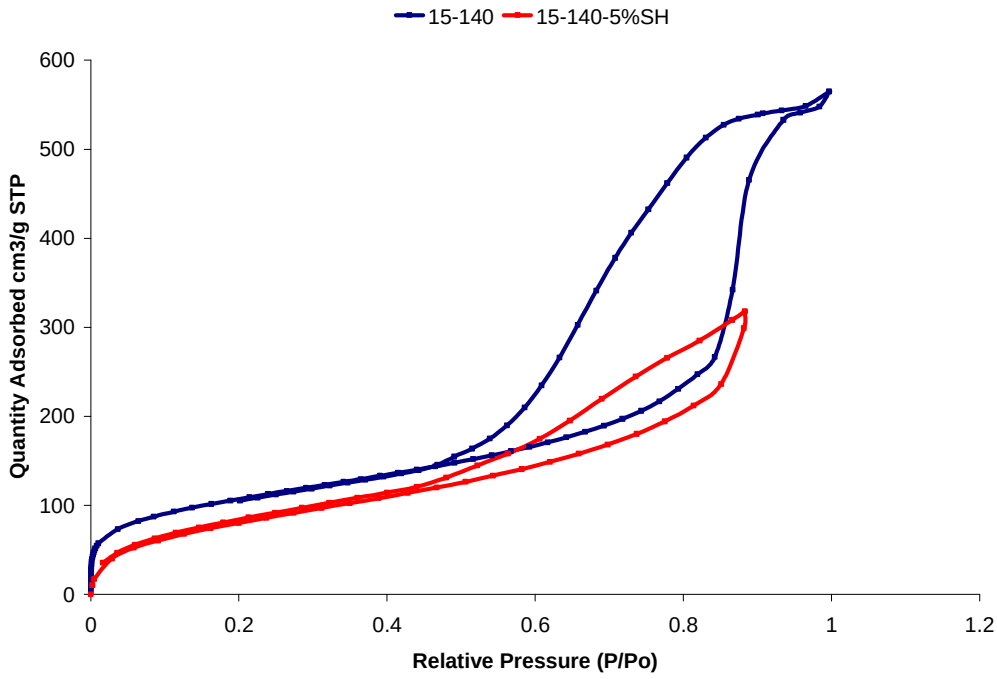

Figure 3.53 Nitrogen isotherms for (15-140) FDU-12 with and without thiol

The pore size distributions for the adsorption and desorption branches of nitrogen isotherm of (15-140) FDU-12 material with and without thiol can be seen in Figure 3.54, along with functionalised 50-140 FDU-12 material. The cavity size of the 15-140 FDU-12 material from the pore size distribution (PSD) agrees with TEM shown and is seen to be approx 16 nm, with a distribution of cavity sizes between 12 and 20 nm. The desorption branch shows a peak at 6 nm with a broad entrance window distribution from 5 to 12 nm. The functionalised 15-140 FDU-12 material is seen to have cavities of 10-15 nm, as shown by the adsorption branch and windows of 5 nm. Functionalising the 50-140 material results in much larger pores, with a broad distribution of cavity sizes from 20 to 30 nm showing a maximum at 25 nm. The desorption branch shows windows of both 4 nm and a broad distribution from 15 to 25 nm in size.

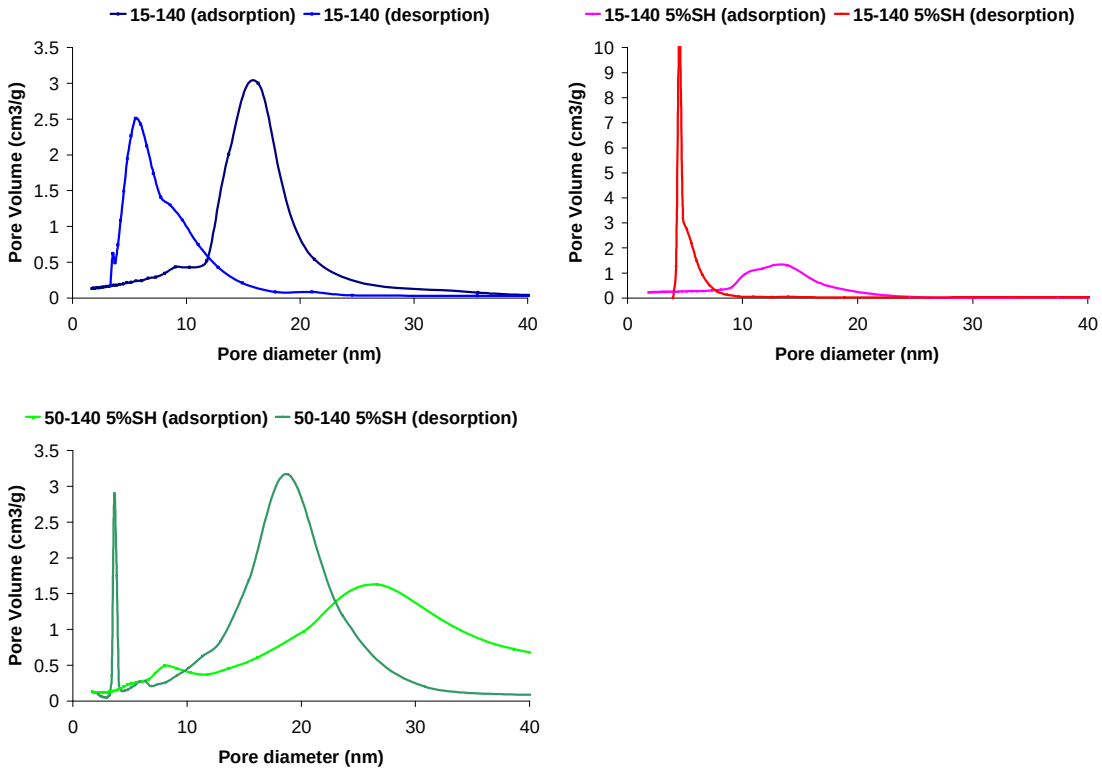

Figure 3.54 Pore size distribution curves for adsorption and desorption branches of nitrogen isotherm of FDU-12 materials

3.7.7 Thermogravimetric Analysis (TGA)

Calcined FDU-12 with large cages (FDU-12 15-140) (*ca*. 16 nm) loses very little weight as the solid is heated from 40 to 700 ^{o}C (Figure 3.55). A functionalised and subsequently extracted 15-140-5%SH material a minor weight loss of 2% as the residual solvent is removed up to 150 ^{o}C, followed by a larger loss in weight of 16% as the remaining surfactant decomposes at higher temperatures. FDU-12 50-140 shows a similar trend with 10% of the sample weight lost as the calcined material is heated to 700 whilst 18% of the functionalised, extracted sample weight is lost on heating.

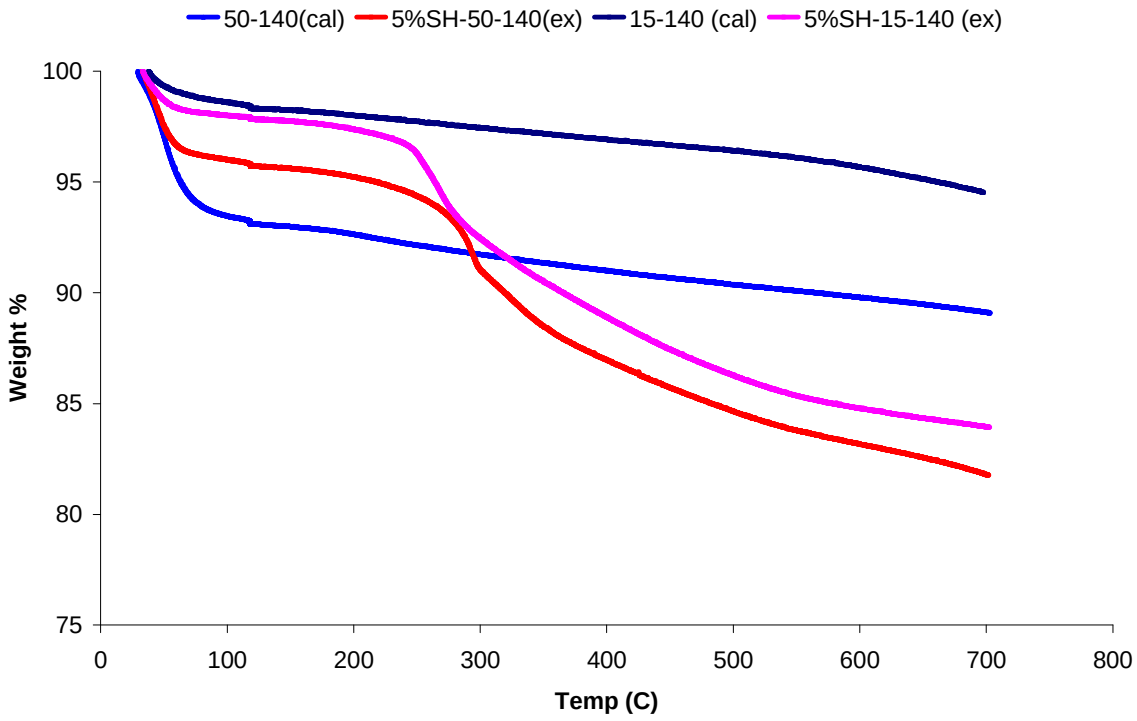

Figure 3.55 TGA trace for FDU-12 materials with and without thiol

3.7.8 XRD

As the cavity size of the FDU-12 (15-140) material is approx 16 nm the unit cell is very large, as shown in Table 3.10 with *a* parameters of up to 34 nm and so as a result obtaining low angle XRD is difficult. Figure 3.56 shows the low angle XRD obtained for the 15-140 material whilst Figure 3.57 shows the XRD obtained for the 50-140 FDU-12.

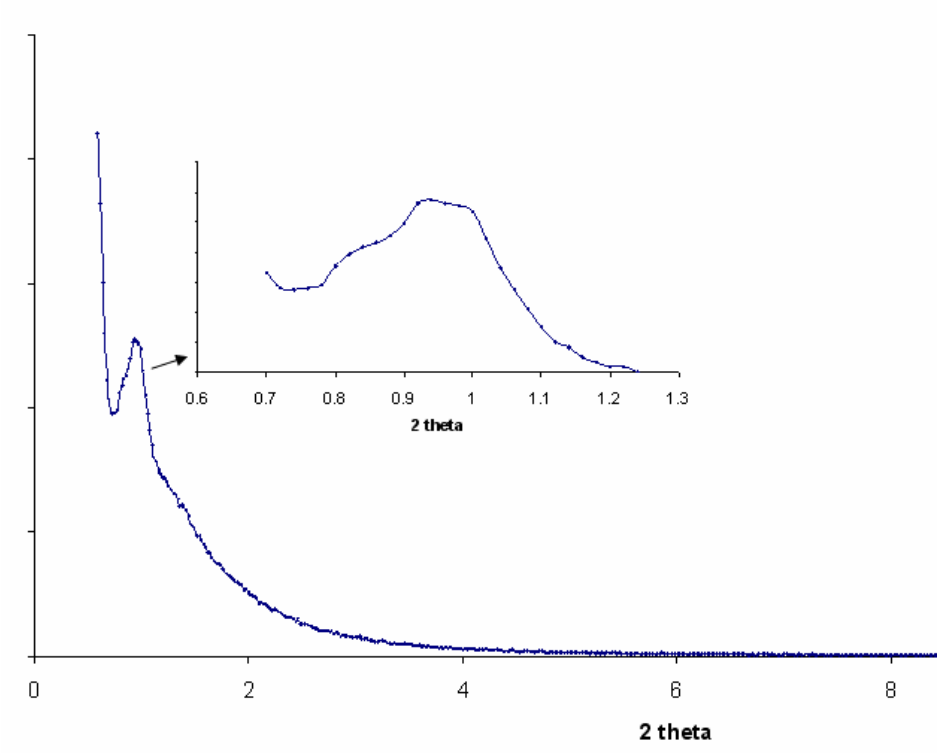

Figure 3.56 15-140 FDU-12

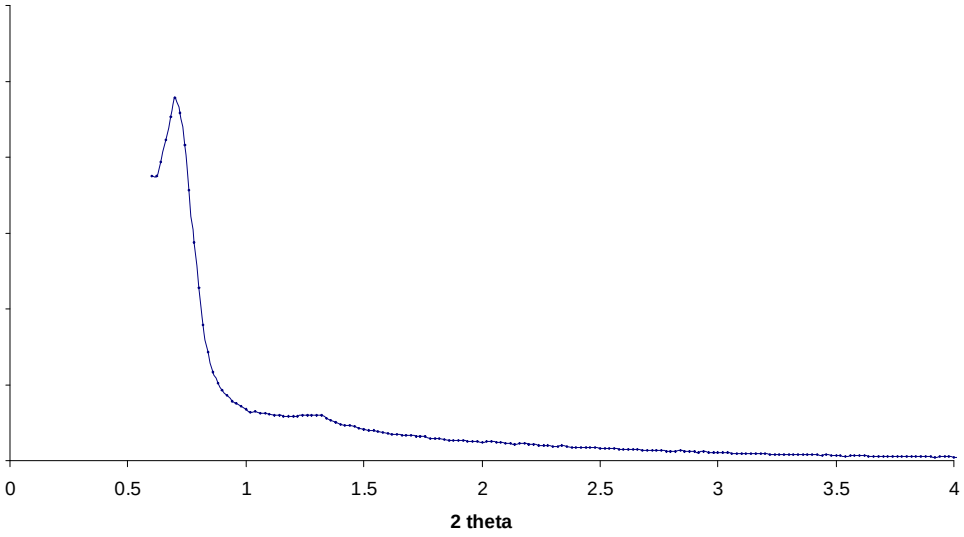

Figure 3.57 50-140 FDU-12

3.7.9 Elemental analysis

As shown in Table 3.11 we can see that the calcined materials have no or virtually no carbon content, indicating that all surfactant is being removed by calcination. Those materials which have been functionalised *in situ* indicate that sulfur is present and so functionalisation has been successful. The 5-6% carbon is as a result of both carbon from the organic functional group and also any remaining surfactant within the pores not removed during extraction.

Table 3.11 Elemental analysis of FDU-12 materials

Samples	%C	%H	%S
15-140, calcined		0.46	
15-140- 5%SH, ex	5.11	1.62	0.98
50-140, calcined	0.18	1.27	
50-140-5%SH, ex	6.18	1.88	1.53

3.8 Materials selected for enzyme immobilisation, protein adsorption and drug delivery

From the materials synthesised and characterised in chapter 3 a series of samples with varying morphology, pore diameter and functionality were chosen for use in the immobilisation of enzymes, proteins and in drug release studies. These materials are shown in Table 3.12.

Table 3.12 Materials selected for further work

Material	Comment
SBA-15	Hexagonal pore arrangement, p6mm symmetry, channel diameter 8 nm
SBA-15 (2:1)	decane:surfactant weight ratio 2:1 (branched particles)
SBA-15 (5.8:1)	decane:surfactant weight ratio 5.8:1 (branched particles)
SBA-15 (7.6:1)	decane:surfactant weight ratio 7.6:1

2%SH-SBA-15 (5.8:1)	2 mol % thiol functionalised SBA-15 with decane:surfactant weight ratio 5.8:1 (early formation – groups of pores in hexagonal arrangement)
7%SH-SBA-15 (2:1)	7 mol % thiol functionalised SBA-15 with decane:surfactant weight ratio 2:1 (onion ring type structure)
7%SH-SBA-15 (5.8:1)	7 mol % thiol functionalised SBA-15 with decane:surfactant weight ratio 5.8:1 (better defined onion ring structure)
LT-7%SH-STA-11 (5.8:1)	7 mol % thiol functionalised STA-11 with decane:surfactant weight ratio 5.8:1 synthesised using low temperature hydrolysis step – produces Ia-3d morphology
KIT-6-MP	KIT-6 with pore size 6 nm, hydrothermal temperature of 100 ^{o}C (MP-medium pore)
KIT-6-LP	KIT-6 with pore size 8 nm, hydrothermal temperature of 130 ^{o}C ; Ia-3d morphology (LP-large pore)
5%SH-KIT-6-LP	5 mol % thiol functionalised KIT-6 with pore size 6.5 nm, hydrothermal temperature of 130 ^{o}C
FDU-12(50-100)	Typical FDU-12 windows < 4 nm
FDU-12(15-100)	Low temperature hydrolysis step, windows < 4nm
FDU-12(50-140)	High temperature condensation step (140 ^{o}C), window size ~ 8 nm
FDU-12(15-140)	Large pore FDU-12 (cavity ~15 nm) synthesised using low temperature hydrolysis step (15 ^{o} C) and high temperature acid erosion step (140 ^{o}C) windows (~10 nm):
2%SH-FDU-12(15-140)	2 mol % thiol functionalised FDU-12
5%SH-FDU-12(15-140)	5 mol % thiol functionalised FDU-12
7%SH-FDU-12(15-140)	7 mol % thiol functionalised FDU-12
5%SH-FDU-12(50-140)	5 mol % thiol functionalised FDU-12 using high temperature acid step (140 ^{o}C) window size ~ 12 nm, cavity size 20 nm

3.9 Conclusions

The synthesis of a range of mesoporous silicas has been achieved and the materials characterised via microscopy, adsorption measurements, diffraction, TGA and elemental analysis.

The effects of the inclusion of organo-siloxanes and alkanes have been investigated in Pluronic P123-templated syntheses of mesoporous silicas in acidic media. Under specific levels of loading of propylthiol groups and alkanes we obtain materials of unusual morphology including branched and 'onion ring' particles. It has also been shown that we can obtain a material with cubic Ia-3d symmetry (similar to MCM-48, STA-11) by employing a low temperature synthesis method with the addition of decane and MPTES. The surfactant can be removed by calcination or extraction, although extraction does not fully remove the surfactant template. In the case of organo-functionalised materials extraction must be used in order to leave the functionality on the pore walls although sohxlet extraction has been shown to remove the majority of surfactant.

A series of materials with cubic Ia-3d symmetry, denoted KIT-6, were synthesised (with pores greater than those of MCM-48) with channel diameters from 6 to 8 nm both with and without propylthiol groups. By increasing the hydrothermal treatment temperature of the synthesis a larger pore material resulted which could be functionalised with propylthiol resulting in a decrease of the pore diameter.

Using the surfactant Pluronic F127 materials possessing the cubic Fm3m symmetry were synthesised using a novel low temperature method both with and without the *in situ* co condensation of propylthiol. These mesocage FDU-12 structures contain cavities connected by smaller entrance windows. The role of the three steps involved in the synthesis has been studied and the effects of varying temperatures and times in the preparation have been established. By decreasing the hydrolysis temperature the cavity size of the material is strongly increased and by using an additional acid erosion step the size of the entrance windows is increased.

3.10 References

[1] D. Zhao, J. Feng, Q. Huo, N. Melosh, G.H. Fredrickson, B.F. Chmelka, G.D. Stucky, *Science*, 1998, **279**, 548

[2] F. Kleitz, S.H. Choi, R. Ryoo, *Chem. Commun.*, 2003, **17**, 2136

[3] J. Fan, C.Z. Yu, T. Gao, J. Lei, B.Z. Tian, L.M. Wang, Q. Luo, B. Tu, W.Z. Whou, D.Y. Zhao, *Angew. Chem. Int. Ed.*, 2003, **42**, 3146

[4] H. Zhang, J. Sun, D. Ma, X. Bao, A. Klein-Hoffmann, G. Weinberg, D. Su, R. Schlogl, *J. Am. Chem. Soc.*, 2004, **126**, 7440

[5] R. P. Hodgkins, A. E. Garcia-Bennett and P. A. Wright, *Microporous Mesoporous Mater.*, 2005, **79**, 241

[6] X. Liu, B. Tian, C. Yu, F. Gao, S. Xie, B. Tu, R. Che, L. Peng, D. Zhao, *Angew. Chem. Int. Ed.*, 2002, **41**, 3876

[7] S. Che, A.E. Garcia-Bennett, X. Liu, R.P. Hodgkins, P.A. Wright, D. Zhao, O. Terasaki, T. Tatsumi, *Angew. Chem. Int. Ed., 2003*, **42**, 3930

[8] K. Flodstrom, V. Alfredsson, N. Kallrot, *J. Am. Chem. Soc.*, 2003, **125**, 4402

[9] F. Kleitz, D. Liu, G.M. Anilkumar, I.N. Park, L.A. Solovyov, R. Ryoo, *J. Phys. Chem. B*, 2003, **107**, 14296

[10] D. Zhao, Q. Huo, J. Feng, B.F. Chmelka, G.D. Stucky, *J. Am. Chem. Soc.*, 1998, **120**, 6024

[11] J. Fan, C. Yu, J. Lei, Q. Zhang, T. Li, B. Tu, W. Zhou, D. Zhao, *J. Am. Chem. Soc.*, 2005, **127**, 10794

[12] R.P. Hodgkins, University of St Andrews

[13] T. Kim, R. Ryoo, M. Kruk, K. P. Gierszal, M. Jaroniec, S. Kamiya, O. Terasaki, *J. Phys. Chem. B*, 2004, **108**, 11480

[14] F. Kleitz, D. Liu, G.M. Anilkumar, I.N. Park, L.A. Solovyov, R. Ryoo, *J. Phys. Chem. B*, 2003, **107**, 14296

4. Protein adsorption on mesoporous silica

4.1 Introduction

The discovery of ordered, high surface area mesoporous silicas with pores greater than 5 nm has opened the way to the study of mesoporous silicas as supports for biological molecules. Diaz *et al.* **[1]** were among the first groups to publish the use of mesoporous silica as a protein support and focused on the adsorption of four small proteins; cytochrome c, papain, trypsin and horseradish peroxidase, using MCM-41 as a support. A size effect was observed with the smallest protein, cytochrome c, showing complete uptake into the pores and exclusion of the peroxidase being observed

As cytochrome c is a relatively small and spherical protein with dimensions 26 x 30 x 32 Å it is an ideal candidate for studies in adsorption using mesoporous materials such as SBA-15 as the dimensions are much smaller than the average pore diameter **[2-4]**. Jing *et al.* **[5]** have shown that the enzyme penicillin acylase (PA) can be immobilised using MCM-41 as a support whilst Yiu *et al.* **[6]** have studied the adsorption of trypsin in a variety of supports including MCM-41, MCM-48 and SBA-15. The surface charges of the protein and the surface of the mesoporous support should be complementary in order to achieve significant adsorption, as seen by Deere *et al.* **[2,3]** when they studied the adsorption of cytochrome c using a mesoporous support. Hodnett *et al.* **[2, 3]** studied the adsorption of trypsin on MCM-41 and then went on to examine its use as a catalyst for the transesterification of N-acetyl-L-tyrosine ethyl ester. It has also been shown that catalytic activity in organic solvents and the stability of the immobilised enzymes depend greatly on the pore size and surface of the mesoporous support **[9]**. Horseradish peroxidase (HRP) has been adsorbed onto mesoporous supports including FSM-16, MCM-41 and SBA-15 with pore diameters ranging from 27 to 92 Å and their activity and stability in organic solvents studied. The type of surfactant used to synthesise the material can have an effect on the loading efficiency, with those materials prepared using cationic surfactants such as MCM-41 and FSM-16 showing much higher enzyme loading than SBA-15 which utilises a non-ionic surfactant. Also the pore size has an effect on the activity where the highest activity and best stability in an organic solvent occurred when the molecular diameter of the enzyme matched the pore diameter closely.

Proteins physisorb on the mesoporous materials due to electrostatic interactions or weak van der Waals forces between the surface and the protein **[7]**. By increasing the strength of these interactions it is possible to favour the adsorption: one way of achieving this is by functionalising the surface of the support. Organic functional groups can have favourable interactions with the amino acids of the proteins and the support can be tailored with specific functional groups depending on the enzyme. An example of this is the functionalisation of SBA-15 in order to immobilise trypsin **[8]**. Functional groups including thiol, amine, phenyl, alkyl chlorides and carboxylic acids were incorporated and their effects on trypsin immobilisation and leaching investigated. The greater immobilisation was observed when thiol groups were included.

Previous studies using mesoporous silica for protein adsorption includes the work by Wright *el al* **[13]** who have used thiol-functionalised SBA-15 to show a strong size selective adsorption of proteins. They showed that SBA-15 (6 nm pore size) exhibits size exclusion of those proteins with a molecular weight of 40 kDa and above and that the reversibility of the adsorption suggests that such materials possess potential for protein separation. Following on from this work it was decided to study the adsorption of a range of proteins using mesoporous silica with 3D cubic (Fm3m) cage morphology. SBA-15, like KIT-6 and STA-11 possesses cylindrical channels and the proteins are seen to adsorb according to channel diameter. As cage-type structures have large cavities connected by smaller windows it is harder to determine the pore size accurately. Therefore six readily available proteins were selected with molecular weights ranging from 17 to 160 kDa (shown in Table 4.1 below) and used to study the pore size of two FDU-12 materials.

Table 4.1 Proteins selected for adsorption on mesoporous supports

Protein	EC number	Source	Molecular weight/ kDa	Molecular dimensions/ Å
Myoglobin			17	21, 35, 44
CALB	3.1.1.3	Candida Antarctica	33	30, 40, 50
BSA		Bovine	66	50, 70, 70
β-Galactosidase*	3.2.1.23	Aspergillus oryzae	105	97, 97, 129
β-Glucosidase	3.2.1.21	From almonds	130	116, 122, 129
Glucose oxidase	1.1.3.4	Aspergillus niger	160	66, 66, 215

*homotrimeric structure

The protein information and structures were obtained using the RCSB Protein Data Bank and the enzyme database BRENDA **[16,17]** which provide molecular dimensions and weights. It is expected that proteins up to a certain molecular weight will be taken up within the pores of the two materials and that proteins that are larger than the pore dimension will be excluded. Due to the materials selected having quite different entrance windows (ca. 4 and 6-12 nm) different exclusion of certain proteins for each material will be observed. Some of the proteins selected are shown below in Figure 4.1.

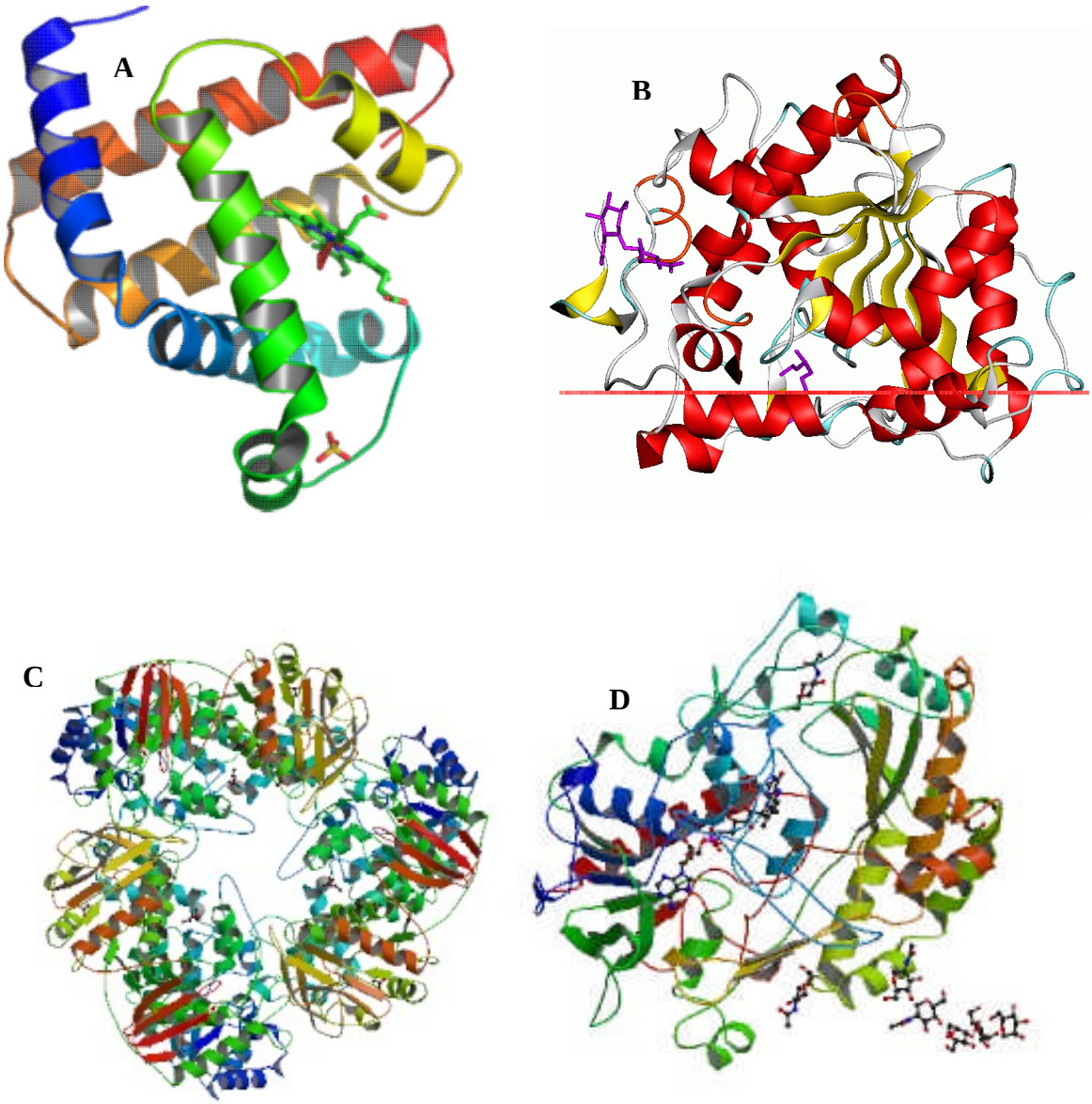

Figure 4.2 Protein secondary structure in; (A) myoglobin [14] (B) Triacylglycerol lipase Candida Antarctica [15] (C) B-Galactosidase and (D) Glucose oxidase [16]

4.2 FDU-12 materials

FDU-12 materials with differing pore sizes were selected in order to determine the maximum size of protein which could be taken up by each solid. Using the low temperature pathway method and additional acid erosion step, as described in section 3.7, two materials were synthesised, a large pore material with cavities ca. 16 nm in diameter and entrance dimensions of between 6 and 12 nm (FDU-12 15-140), and a smaller pore material with ca. 4 nm entrance windows and 6-8 nm cavities (FDU-12 50-100) (Figure 4.2). By adsorbing proteins with different molecular dimensions it was possible to determine the maximum size of the protein adsorbed and therefore the window size of the 2 solids and to see if they are comparable with the window dimensions from the desorption branches of nitrogen adsorption/desorption isotherms.

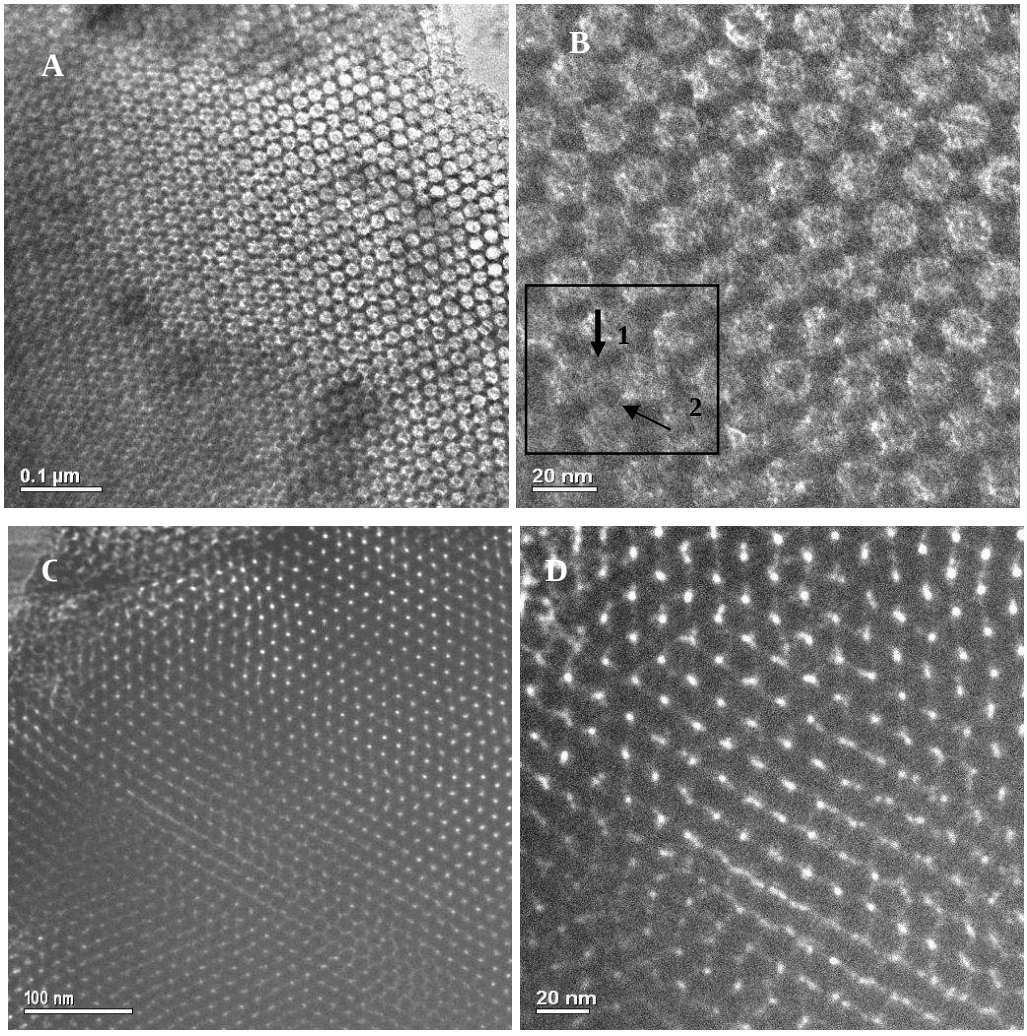

Figure 4.2 HRTEM images of large pore FDU-12 (15-140) showing well ordered material with cavity size of ~16 nm and window dimensions estimated at 6-12 nm (A+B) and FDU-12 (50-100) showing well ordered material with cavity and window size of <4 nm (C+D)

Image B in Figure 4.2 shows us the large cavities present in the material and as indicated by the arrows channels connecting the cavities can be seen. These connecting channels appear to be of different sizes, with a larger channel indicated by '1' and a smaller by '2'. From the nitrogen adsorption isotherms obtained for the small and the larger pore FDU-12 material a change in isotherm shape is observed as the pore diameter is increased *via* a change in the synthesis and acid erosion temperatures (Figure 4.3).

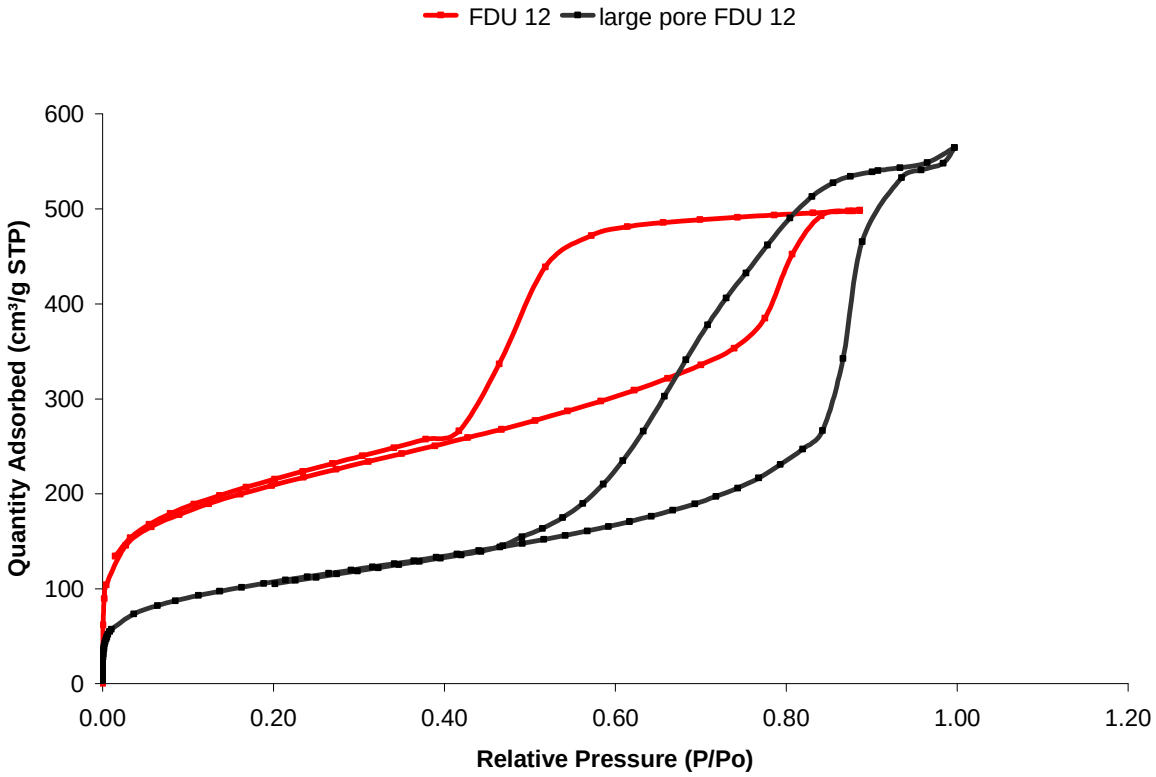

Figure 4.3 Isotherm of small and large pore FDU-12

The information obtained from the isotherms is shown in Table 4.2 where the effect of increasing the pore size on the BET surface area and pore volume can be seen. From the adsorption branch the size of the cavities can be determined and the entrance windows are calculated from the desorption branch. In the case of the large pore material the adsorption branch is at a higher relative pressure, indicating larger cavities. The desorption branch decreases over a large range, from 0.9 to 0.5 P/Po, which suggests that the entrance window diameters range from 6 up to 14 nm. The small pore material has a desorption branch which decreases over a narrow range of pressures (0.45-0.5) indicating a correspondingly narrow range of entrance sizes.

Table 4.2 Surface area and pore size of selected FDU-12 material

Sample	Entrance size (nm)	Cavity Size (nm)	BET Surface area (m^2/g)	Pore Volume (cm^3/g)
FDU-12 (15-140)	6-16	16	380	0.87
FDU-12 (50-100)	4-6	8-10	625	0.79

4.3 Protein adsorption

A stock solution of known concentration was prepared for each of the proteins shown in Table 4.1 which then could be diluted with buffer solution (at pH 6) to concentrations of 0.4, 0.8, 1.2, 1.6 and 2.0 mg of protein / mL. In each experiment, 20 mg of the mesoporous solid was suspended in 1.0 mL of protein solution made up to concentrations between 0.4 and 2 mg/mL (0.02-0.10 g protein/g support) and shaken for 240 hours at 37 ^{o}C in a micro centrifuge tube. After 36, 60, 120 and 240 hours samples were centrifuged and the supernatant was measured for protein. The protein content of the supernatant liquid was measured using the Bradford assay **[10]** and the amount adsorbed on the solid calculated by difference. The Bradford assay is used as it can measure both active and denatured protein and is a well established easy and reliable method **[11, 12]**.

4.3.1 Bradford Assay

The Bradford Assay is a simple method which utilises a dye molecule; Coomassie Brilliant Blue G-250 (shown in Figure 4.4) whose adsorption can be followed by UV.

The dye in its unbound form adsorbs at 465 nm which changes to 595 nm when in the presence of protein due to the dye molecule binding to it and changing from an unbound cationic form to an anionic form.

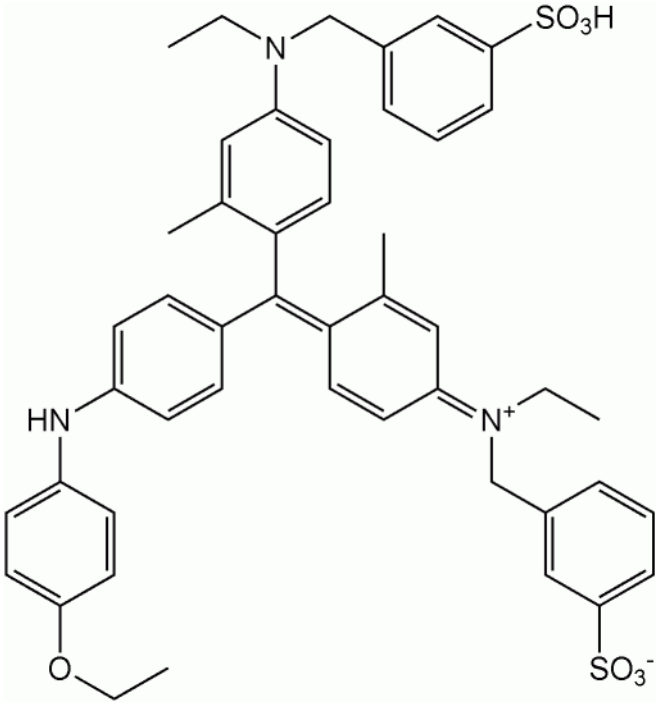

Figure 4.4 Coomassie Brilliant Blue G-250 dye used in Bradfords assay to determine protein concentration

When the Bradford solution is added to a solution containing protein the blue colour appears within minutes and remains for approx one hour. In order to ensure all results could be comparable the samples were left at room temperature for 30 minutes after the dye had been added and samples shaken for 10 seconds. Measurements were then carried out using a UVIKON 930 spectrophotometer to determine the protein concentration within each sample. To calculate the concentrations a calibration curve is plotted using a 1mg/mL solution of BSA as a standard of known concentration, as shown in Figure 4.5.

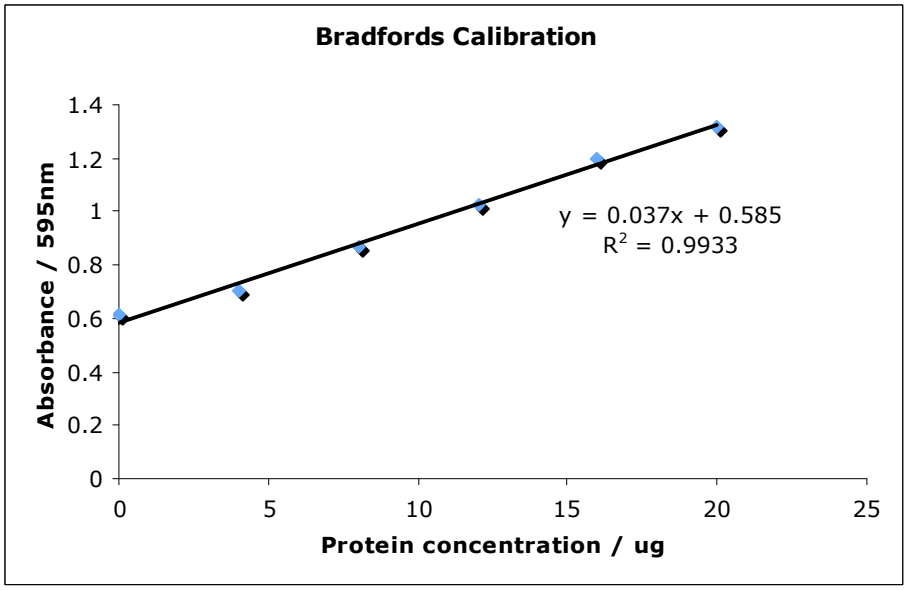

Figure 4.5 Bradford's Protein Assay BSA calibration

4.4 Rate of Protein uptake on different materials

For each protein used a graph can be plotted to show the uptake at varying protein concentrations on both the small and large pore material. Depending on the material and protein used, measurements were carried out after 36, 60, 120 and 240 hours using the Bradford assay to determine the remaining protein in solution and therefore how much of the protein has been adsorbed onto the mesoporous support. Three measurements were carried out on each sample to minimise error. Results are shown for protein loading in terms of grams of protein per gram of mesoporous support offered.

4.4.1 Myoglobin

From the data shown in Figure 4.6 and 4.7 the Myoglobin enters the larger pore (FDU-12 15-140) material faster and 100% uptake is observed for all loadings indicating that the pores of the material are large enough to adsorb a protein with dimensions approx 2 x 3 x 4 nm For the smaller pore material (FDU-12 50-100) the adsorption is much slower and incomplete adsorption occurs when the amount of protein offered is increased. This indicates that the protein is of a similar size to the pore diameter, resulting in pore blocking which prevents complete adsorption.

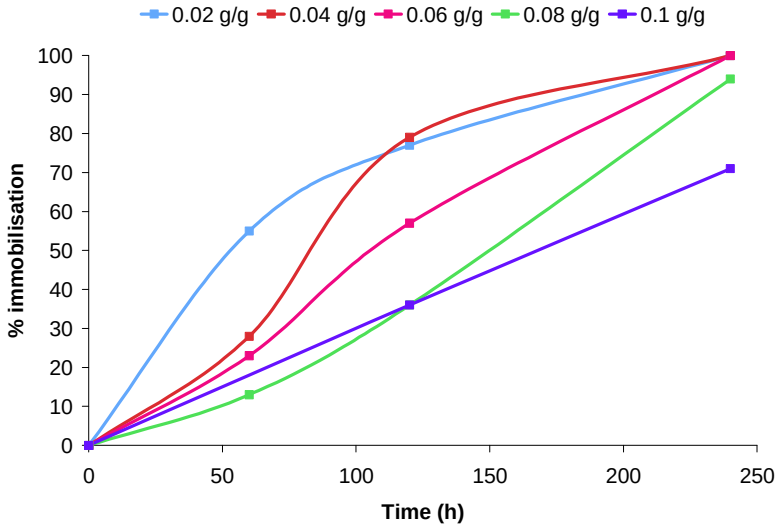

Figure 4.6 Myoglobin uptake on small pore material at varying concentrations

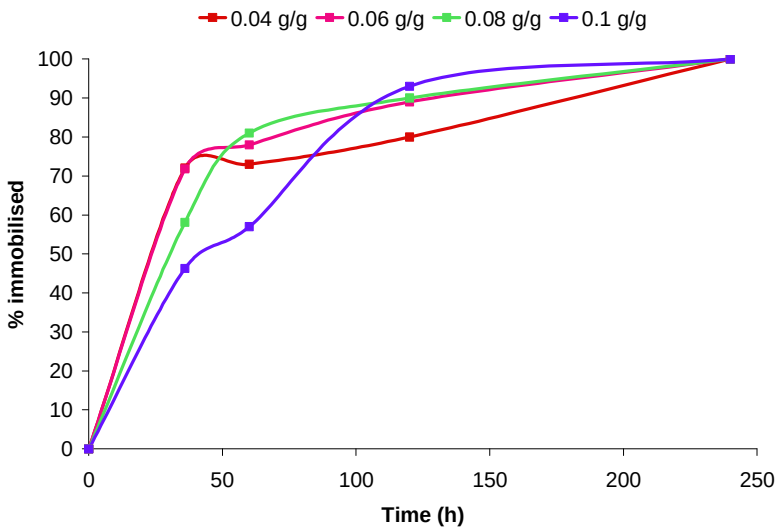

Figure 4.7 Myoglobin uptake on large pore material at varying concentrations

4.4.2 CALB

Although 100% of CALB offered to both the small and large pore material was adsorbed (shown in Figure 4.8 and 4.9) the time in which this occurs differs significantly. After 120 hours similar results were seen for the adsorption of CALB in the large pore material compared to the adsorption after 240 hours on the smaller pore material. This would indicate that some of the pores in the small pore material prevent the migration of CALB whereas others allow it and in the case of the larger pore material many more of the windows allow CALB to pass, so there will be high 3D connectivity.

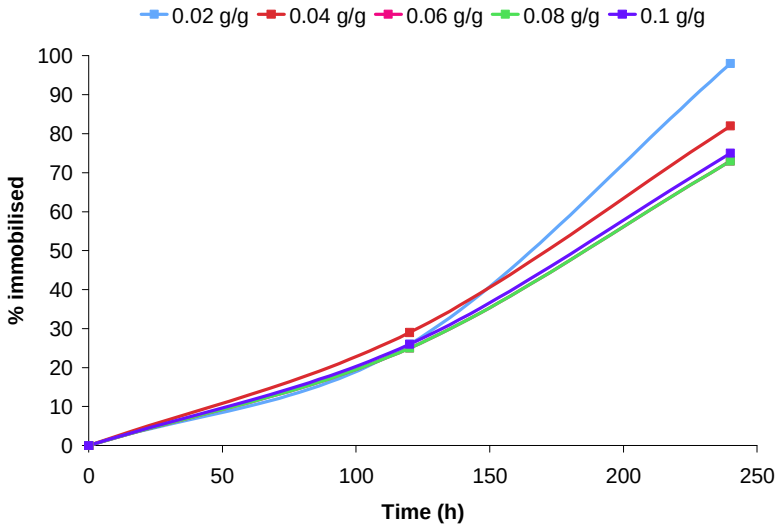

Figure 4.8 CALB uptake on small pore material at varying concentrations

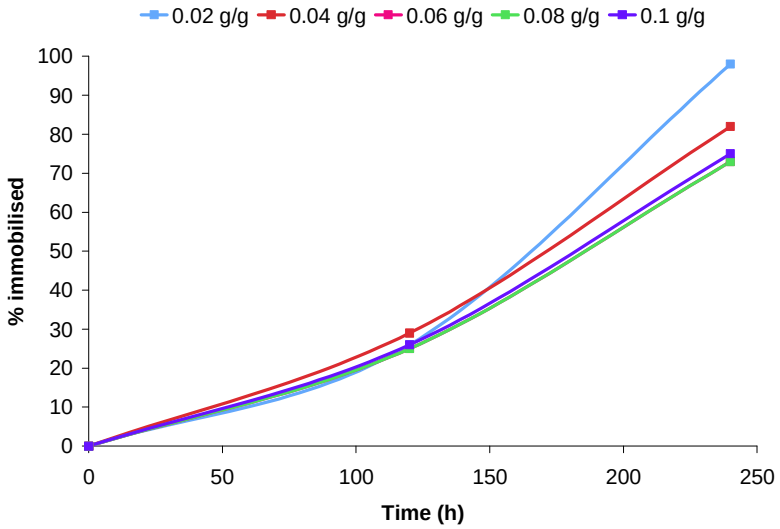

Figure 4.9 CALB uptake on large pore material at varying concentrations

4.4.3 BSA

With BSA uptake in the smaller pore material, seen in Figure 4.10, there is much lower uptake than with Myoglobin or CALB. This can indicate that the pores are too small for the BSA to enter and adsorption can be attributed to surface adsorption or adsorption round the pore entrances, resulting in pore blocking and limiting any further adsorption.

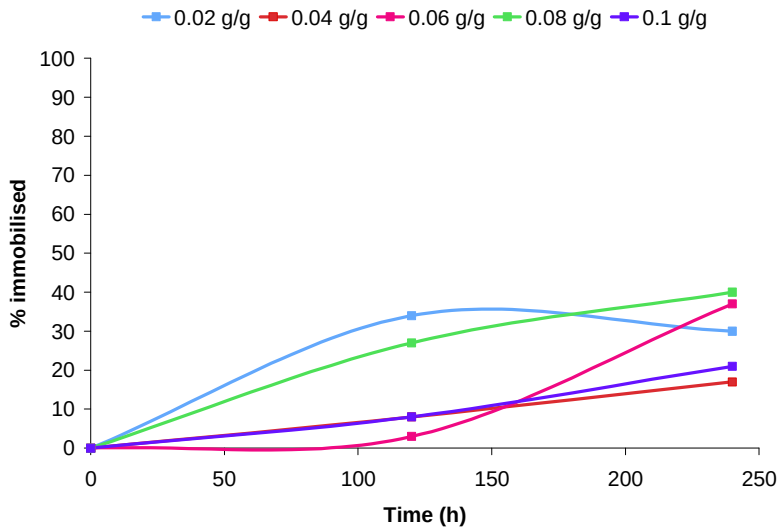

Figure 4.10 BSA uptake on small pore material at varying concentrations

For the adsorption of BSA into the larger pore material (Figure 4.11) there is a sharp initial adsorption, followed by a slow uptake at various loadings at 120 hours. Unlike the smaller pore material where there is no significant increase in adsorption as time is increased, the larger pore material is seen to show relatively high uptake of BSA after 240 hours

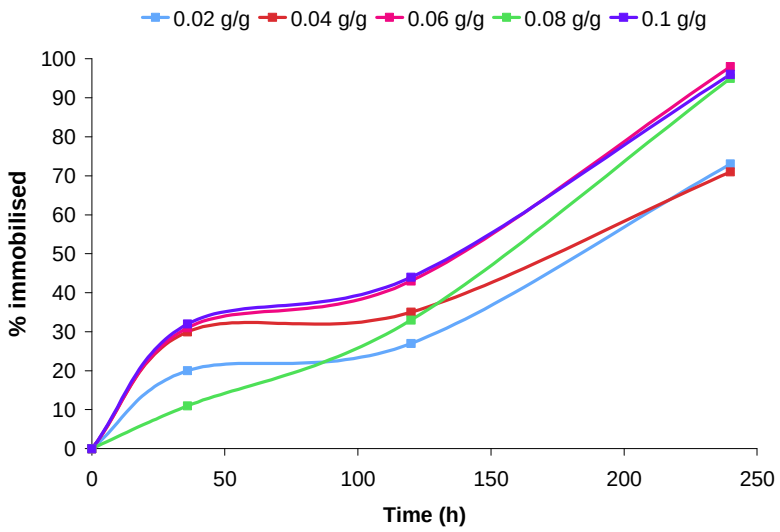

Figure 4.11 BSA uptake on larger pore material at varying concentrations

These results indicate that the adsorption of BSA is dependent on the entrance window size. The small pore material at 4 nm is unable to adsorb all the BSA offered (5 x 7 x 7 nm) and the adsorption observed in Figure 4.9 can be attributed to outer surface adsorption. Increasing the pore diameter gives a much greater uptake of BSA, with close to 100% adsorption, even at higher concentrations. This indicates that some of the entrance windows of the large pore material are at least 5-7 nm in diameter. Compared to CALB, BSA adsorption on the large pore material is much slower as a result of part of the pore network being inaccessible to all the BSA. Some of the connecting windows in the material are of a similar size to BSA meaning that if one BSA molecule becomes trapped in the entrance it will prevent further BSA from entering or leaving the cavity, slowing down complete uptake.

4.4.4 β -Galactosidase

β -Galactosidase adsorption within small pore FDU-12 is slow and incomplete (Figure 4.12).

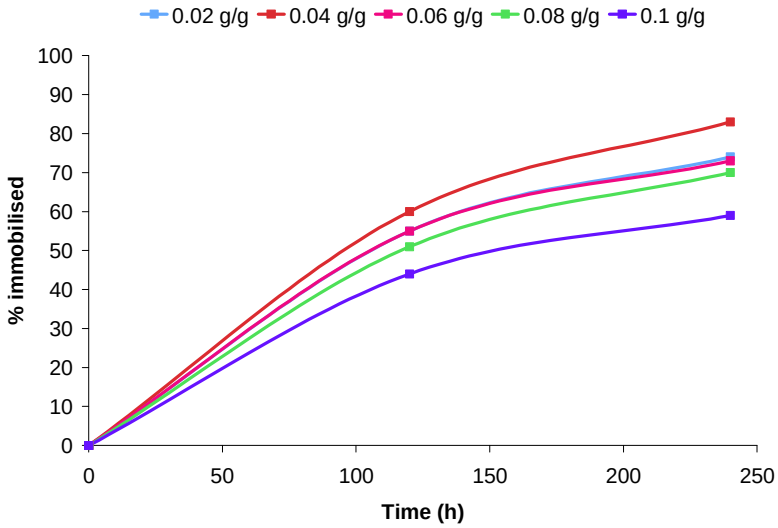

Figure 4.12 β -Galactosidase uptake in small pore material at varying concentrations

With the exception of the lowest protein loading, adsorption of β-Galactosidase in the large pore material at differing concentrations follows the same trace, as shown in Figure 4.13. In the large pore material adsorption is therefore much more rapid than in the smaller pore material. Again this shows us that although the β -Galactosidase is able to be adsorbed into the smaller pore material to some extent, this occurs in the larger pore material more rapidly and with higher % uptake at various concentrations.

From the molecular dimensions shown in Table 4.1 the β –Galactosidase is larger than the entrance window to the small pore material and so should not be adsorbed. This adsorption might be explained by the protein being a homotrimeric structure which if it breaks down into monomers will have smaller dimensions and be able to be adsorbed by the small pore material.

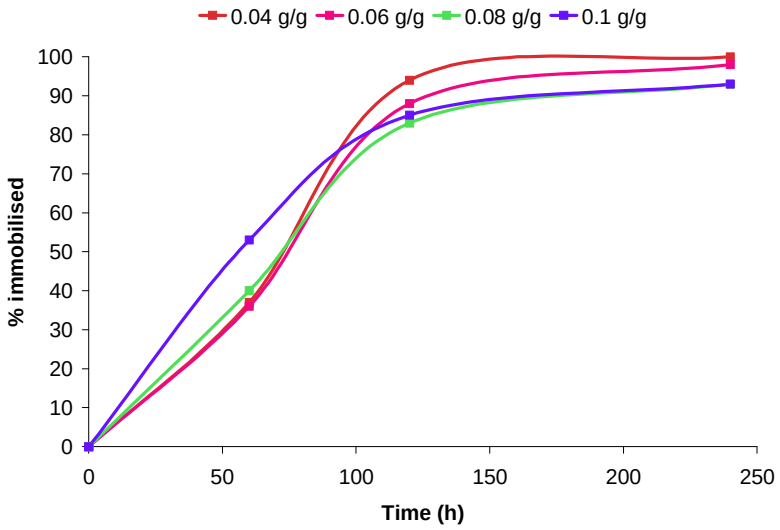

Figure 4.13 β -Galactosidase uptake in large pore material at varying concentrations

4.4.5 β -Glucosidase

With small pore FDU-12 the uptake of β -Glucosidase, as shown in Figure 4.14, appears to reach its maximum after 120 hours. As the pore size of the mesoporous material is increased no obvious change in adsorption of β -Glucosidase is observed (Figure 4.15). A very similar uptake after 120 and 240 hours is seen indicating that even by increasing the pore size the protein is not adsorbed within the pores. The protein which has dimensions greater than 10 nm should not be able to enter the small entrance windows of the small pore material (4 nm) and by increasing the pore window the adsorption of the protein is still incomplete as shown by the almost identical uptake of β -Glucosidase by both materials. The 50-60% uptake can possibly be attributed to adsorption of the β -Glucosidase on the outer surface and possibly pore windows, resulting in pore blocking.

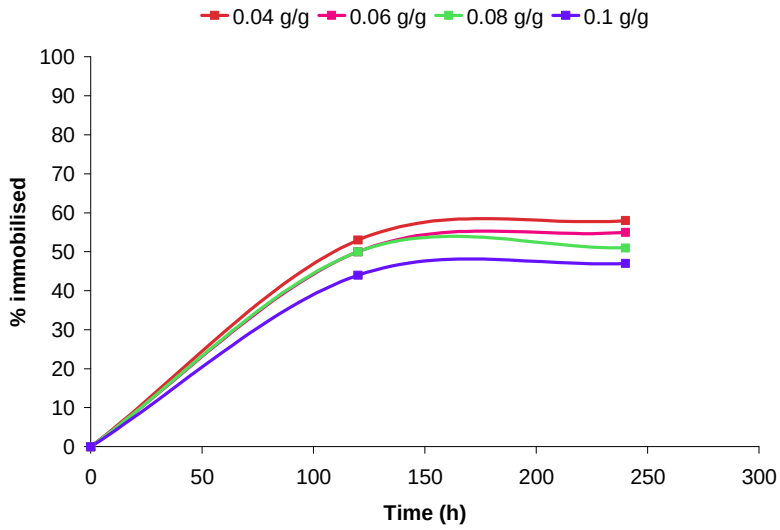

Figure 4.14 β -Glucosidase uptake on small pore material at varying concentrations

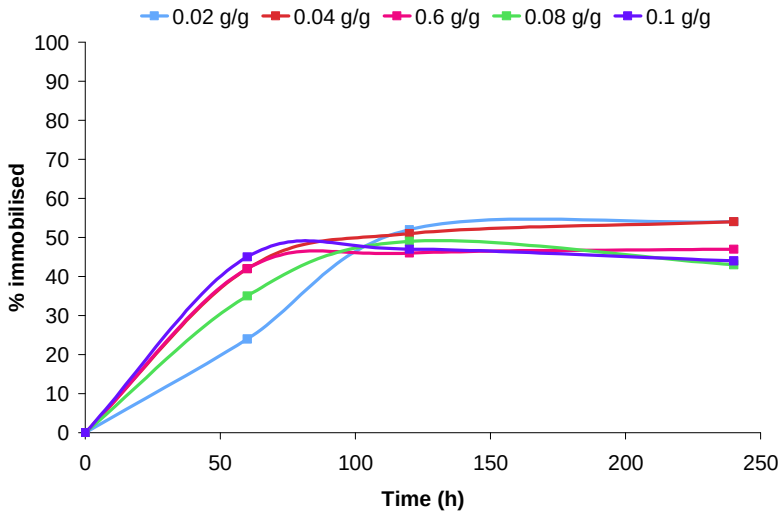

Figure 4.15 β -Glucosidase uptake on large pore material at varying concentrations

So in the case of β -Glucosidase no preferential adsorption into the larger pore material is seen over the smaller pore material indicating that the protein is larger than the entrance windows of both the materials.

4.4.6 Glucose Oxidase

Adsorption of Glucose oxidase (G.Ox) into small pore material is much slower than previous proteins (Figure 4.16).

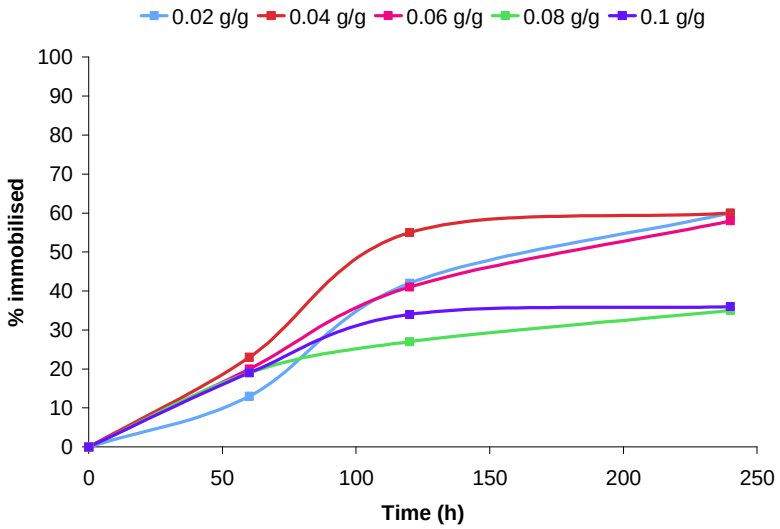

Figure 4.16 Glucose oxidase uptake on small pore material at varying concentrations

With the large pore material, protein uptake exhibits a more linear adsorption with a steady increase in Glucose oxidase adsorption over time, seen in Figure 4.17. Unlike the small pore material which only shows a small increase between 120 and 240 hours, there is a significant increase in uptake over this period with the larger pore material indicating that further adsorption may take place after 240 hours.

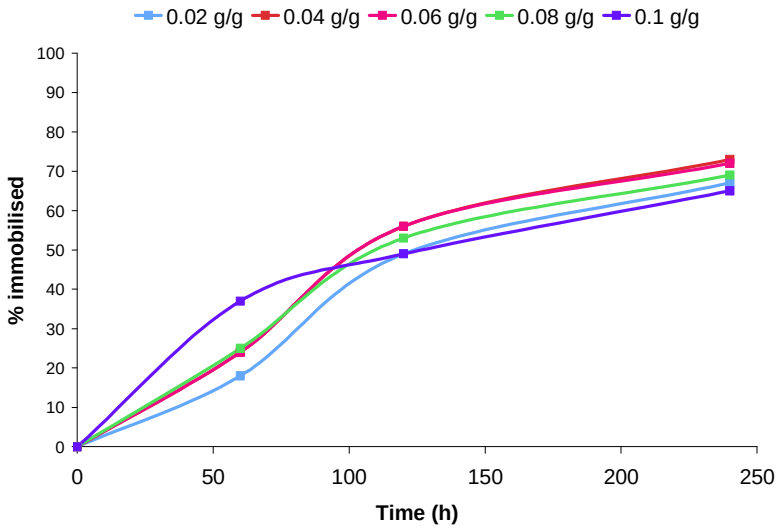

Figure 4.17 Glucose oxidase uptake on large pore material at varying concentrations

A difference in protein adsorption is observed between the two different materials. The maximum uptake of the protein occurs after 120 hours after which we see no further adsorption. The large pore material exhibits a continual adsorption of the protein up to 240 hours. With the small pore material we can attribute this to surface adsorption and as there is a noticeable difference with the larger pore material we can determine that this additional adsorption must be as a result of the protein being adsorbed into the pores as well as the surface of the material.

4.5 Protein adsorption results

Plotting the results of the adsorption of the six proteins at varying concentrations displays trends as a result of the protein, concentration, and time or support. Figure 4.18 shows the adsorption of the varying proteins onto the small pore material after 120 hours at concentrations 0.02-0.1 g/g. The adsorption of CALB is consistent at 75-85% for all protein concentrations. For the nominally slightly smaller protein, Myoglobin, up to 80% is adsorbed at low concentrations, falling to 35% as the Myoglobin concentration is increased. A similar trend is observed for the three largest proteins, β -Galactosidase, β -Glucosidase and Glucose oxidase, with the uptake falling from 40-60% at low concentration to 30-40% at higher concentrations. The exception to this trend of smaller proteins demonstrating higher adsorption is BSA which shows no obvious trend as the protein concentration is increased and relatively low uptake is seen at all loadings varying between 10 and 30%.

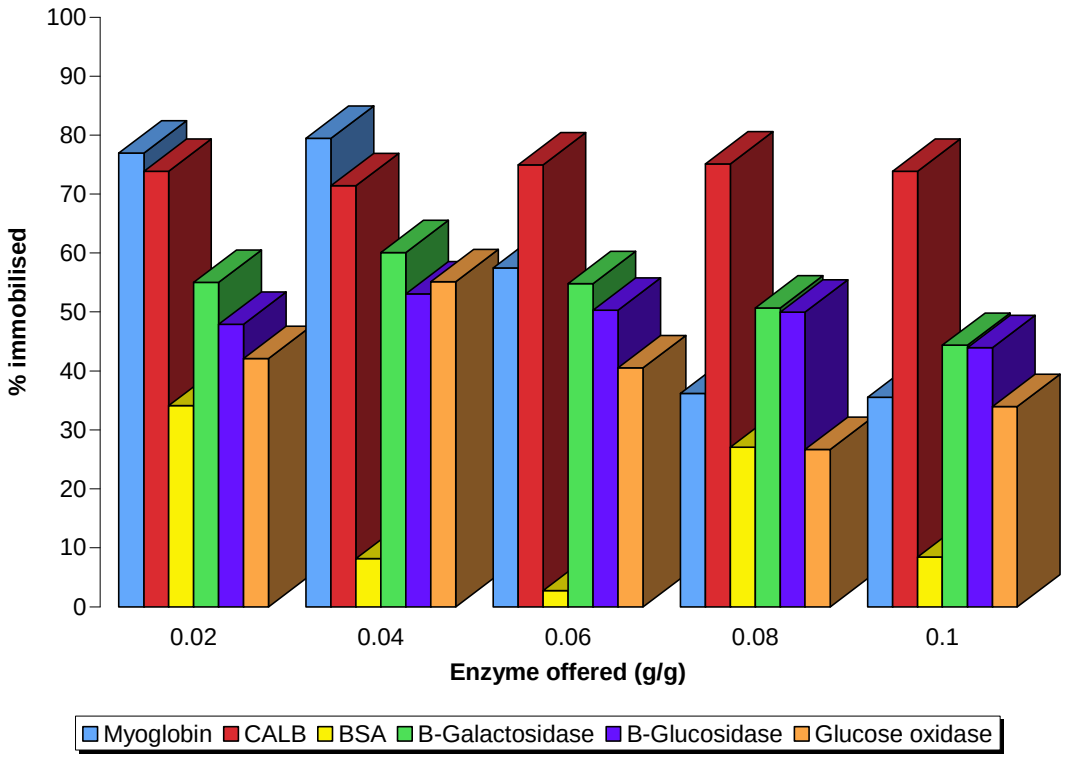

Figure 4.18 Uptake of various proteins on small pore FDU-12 after 120 hours

As the time is increased from 120 to 240 hours an increase in Myoglobin uptake is observed with 100% adsorption at low and 70% at higher concentrations as shown in Figure 4.19. In the case of CALB there is no significant additional adsorption with the exception of an increase at the lowest concentration. There has been an increase of between 10 and 20% adsorption of β-Galactosidase at all protein concentrations as the time has been increased. The same can be seen for the two largest proteins, β-Glucosidase and Glucose oxidase which show only a minimal increase in uptake after 240 hours. The adsorption of BSA into the small pore material still remains the lowest after 240 hours.

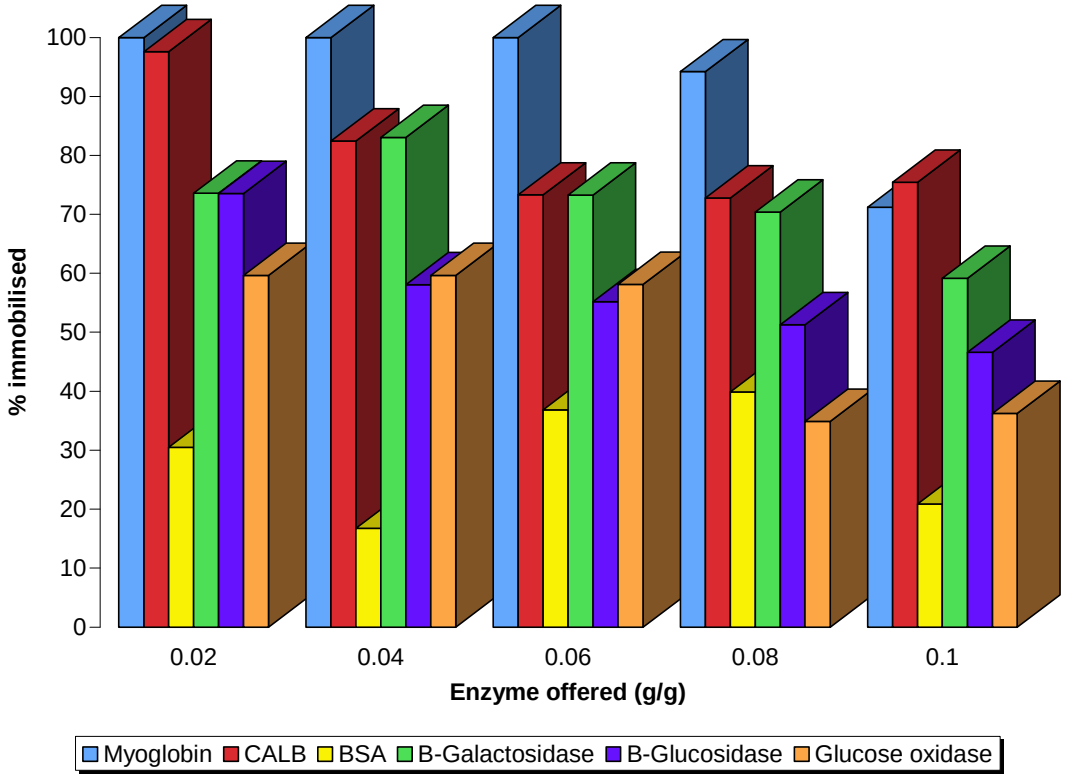

Figure 4.19 Uptake of various proteins on small pore FDU-12 after 240 hours

There is no obvious exclusion of proteins too large to be adsorbed within the support material as there seems to be adsorption of all the proteins to a certain extent. In the case where 100% of the protein is adsorbed is it likely that this is taking place within the pores and the outer surface where as when adsorption is lower (<60%) it is likely that this is due mainly to surface adsorption or agglomeration proceeding at or near the surface at longer times.

Adsorbing the proteins onto the larger pore support material shows significant differences in adsorption compared to those with the small pore material (Figure 4.20). In the case of the 4 smallest proteins there is 95-100% uptake of the proteins at even the highest protein concentrations indicating that the pore diameter of the support material is large enough for the proteins to be adsorbed into the pores. With β -Glucosidase there is an uptake of between 45 and 55%, with the higher uptake occurring at lower concentrations. This is comparable with the uptake of β -Glucosidase on the small pore material. In the case of the largest protein (Glucose oxidase) there is an apparant 70% uptake at all concentrations with the large pore material. This is a significant increase from the results obtained at 60 hours suggesting that the adsorption of this protein is much slower than the smaller proteins, CALB for example. The molecular dimensions of this protein could be one of the major factors in its slow adsorption, with its reported size being approx 7 x 7 x 22 nm. If the protein approaches the pore entrance in the correct conformation (7 x 7 nm) then it is possible for the protein to enter the pore where as if the 22 nm length of the protein is perpendicular to the pore then this will prevent the protein from entering the pore.

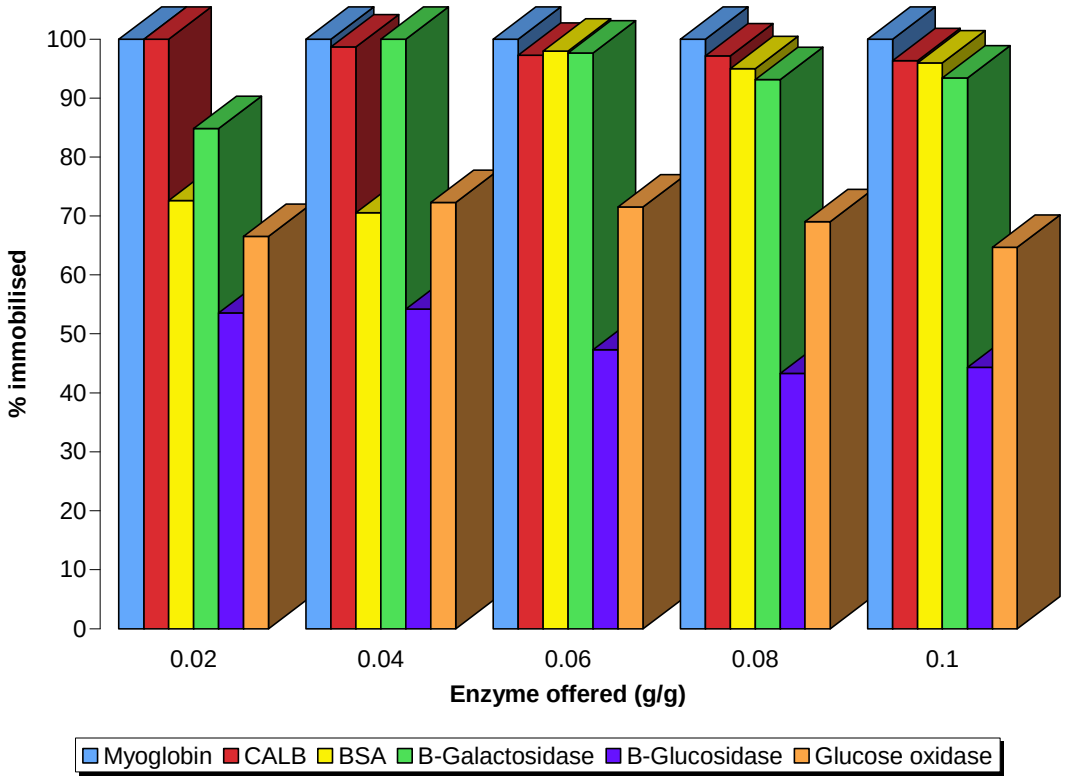

Figure 4.20 Uptake of various proteins on large pore FDU-12 after 240 hours

4.6 Conclusions

Protein adsorption depends on the size of the protein and the pore diameter of the support material. Within 240 hours the large pore material is able to adsorb the smaller 4 proteins completely, even at higher concentrations, whereas the small pore material is only able to adsorb 100% of the smallest proteins offered and only at the lower protein concentrations. Myoglobin and CALB both show a relatively fast initial adsorption with the large pore material with maximum uptake occurring after 120 hours. As the size of the protein is increased there is a slower, linear adsorption of BSA with the uptake continuing for 240 hours. Although β-Galactosidase has a greater molecular weight than BSA it is a trimeric structure and it is adsorbed by the large pore material faster than BSA. β-Glucosidase has dimensions of greater than 11 nm and as seen from the nitrogen adsorption isotherm for the large pore material the entrance windows have dimensions ranging form 6 to 12 nm. This results in the protein being able to pass through only some of the entrance windows whilst it will become trapped in the pores of others stopping any further adsorption and so we only see an uptake of 40-50% of the offered protein. The largest protein by molecular weight, Glucose oxidase (dimensions 7 x 7 x 22 nm) is seen to be taken up only slowly by the large pore material. This may be explained by the dimensions of the protein and so can pass through the pores (of diameter 8-12 nm) only if the protein is aligned correctly. If the protein approaches the entrance window with the largest dimension perpendicular to the entrance then there will be no adsorption and possible blocking of the pore which stops uptake of the protein.

With the small pore material we see a complete uptake of the two smallest proteins, with the CALB exhibiting a slightly slower uptake than myoglobin. The β-Galactosidase uptake is 50-80% as the concentration is increased and although the molecular weight is greater than BSA (which exhibits a low uptake of 30%, attributed to surface adsorption) it is a trimer and the monomers have a smaller molecular dimensions than BSA. β-Glucosidase and Glucose oxidase exhibit similar adsorption with the maximum uptake of 50% reached after a shorter time. These two proteins have much larger dimensions than the entrance window to the small pore material and so it was expected that they would not be adsorbed into the pore network and instead remain on the outer surface.

More generally it is likely that proteins are flexible, with the structure derived from single crystal being only a rough guide to its dimensions and therefore the dimensions of the

pores. In addition, there is appreciable uptake on the surface on the support materials and also the possibility of agglomeration over a longer period of time. Nevertheless there is still a strong difference going from small to large window materials, approximately consistent with protein size which indicates that FDU-12 materials exhibit molecular sieving to some extent. CALB is seen to be readily taken up by both FDU-12 materials, consistent with a ~4 nm pore size, but rates are seen to depend on the window size of the material with a much faster rate observed with the larger window material.

From the nitrogen isotherm obtained for the large cavity FDU-12 15-140 material (chapter 3) there is a range of window sizes present which can be estimated to be between 4 and ~12 nm. Approximately 50% of the material is thought to have windows greater than 7 nm allowing much more significant uptake of BSA than the small pore material, but slowly. From these results it is clear that the enzyme CALB can readily be adsorbed within the FDU-12 materials prepared in this study, and that the larger protein BSA is adsorbed both on the surface and within the pores of the larger pore FDU-12 material. Both conclusions are important when discussing the results of Chapters 5 and 6.

4.7 References

[1] J.F.Diaz, K. J. Balkus, *J. Mol. Catal. B: Enzym*., 1996, **2**, 115

[2] J. Deere, E. Magner, J. G. Wall, B. K. Hodnett, *Chem. Commun*., 2001, 465

[3] J. Deere, E. Magner, J. G. Wall, B. K. Hodnett, *J. Phys. Chem. B*, 2002, **106**, 7340

[4] M. E. Gimon-Kinsel, V. L. Jimenez, L. Washmon, K. J. Balkus, *Stud. Surf. Sci. Catal.*, 1998, **117**, 373

[5] H. Jing, X. F. Li, D. G. Evans, X. Duan, C. Y. Li, *J. Mol. Catal. B: Enzym*., 2000, **11**, 45

[6] H. H. P. Yiu, P. A. Wright, N. P. Botting, *Microporous Mesoporous Mater*., 2001, **44**, 763

[7] M. Matsui, Y. Kiyozumi, T. Yamamoto, Y. Mizushina, F. Mizukami, K. Sakaguchi, Chem. Eur. J., 2001, 7, 1555

[8] H. H. P. Yiu, P. A. Wright, N. P. Botting, *J. Mol. Catal. B: Enzym*., 2001, **15**, 81

[9] H. Takahashi, B. Li, T. Sasaki, C. Miyazaki, T. Kajino, S. Inagaki, *Microporous Mesoporous Mater*., 2001, **44-45**, 755

[10] M. M. Bradford, *Anal. Biochem*., 1976, **72**, 248

[11] C. V. Sapan, R. L. Lundblad, N. C. Price, *Biotechnol. Appl. Biochem*., 1999, **29**, 99

[12] C. G. Jones, J. D. Hare, S. J. Compton, *J. Chem. Ecol*., 1989, **15**, 979

[13] H. H. P. Yiu, C. H. Botting, N. P. Botting, P. A. Wright, Phys. Chem. Chem. Phys., 2001, **3**, 2983

[14] T. Takano, *J. Mol. Biol*., 1977, **110**, 569

[15] http://opm.phar.umich.edu/images/proteins/1lbs.gif

[16] http://www.rcsb.org/pdb/home/home.do - RCSB Protein Data Bank

[17] http://www.brenda-enzymes.info/

5. Enzyme Immobilisation on mesoporous solids

5.1 Introduction

The specific nature of enzyme catalysts provides potential applications in many fields including biosensors, pharmaceuticals, biofuel cells and fine chemical synthesis. A current limiting factor is enzyme stability which shortens their lifetime and hence effectiveness. By improving their stability we can increase the lifetime and re-usability of the enzyme and decrease the amount required **[1]**. In unbound form enzymes can often aggregate which in turn causes deactivation, and this is a major problem when they are used in organic solvents. Binding the enzyme to a solid stabilises the enzyme, reducing mobility and aggregation. Enzyme immobilisation is therefore desirable and has become widespread due to the resultant benefits of enhanced stability, reusability **[2]** and ready separation from reaction mixtures **[3]**. Compared to more traditional catalysts such as transition metals, immobilised enzymes have many benefits for industrial applications including high selectivity and low cost. An example of an immobilised enzyme widely used in industry for catalysis is glucose isomerase (GI). It can be used to catalyse the conversion of D-glucose to D-fructose and is typically used in the food industry to produce high fructose corn syrup **[4]**. On its own a high concentration of GI is required to achieve a reasonable rate of conversion and so without immobilising the enzyme in some way it becomes costly as GI is relatively expensive. There are many ways in which to immobilise GI including more recently using mesoporous silica **[5].**

5.1.1 Methods of immobilisation

It is possible to immobilise enzymes in several ways: the enzyme can be chemically bonded where covalent bonds bind the enzyme to the material, it can be physically adsorbed into/onto a material and held in place by hydrogen bonding, electrostatic and/ or hydrophobic interactions or it can be physically encapsulated **[6]**. These methods can be seen below in Figure 5.1.

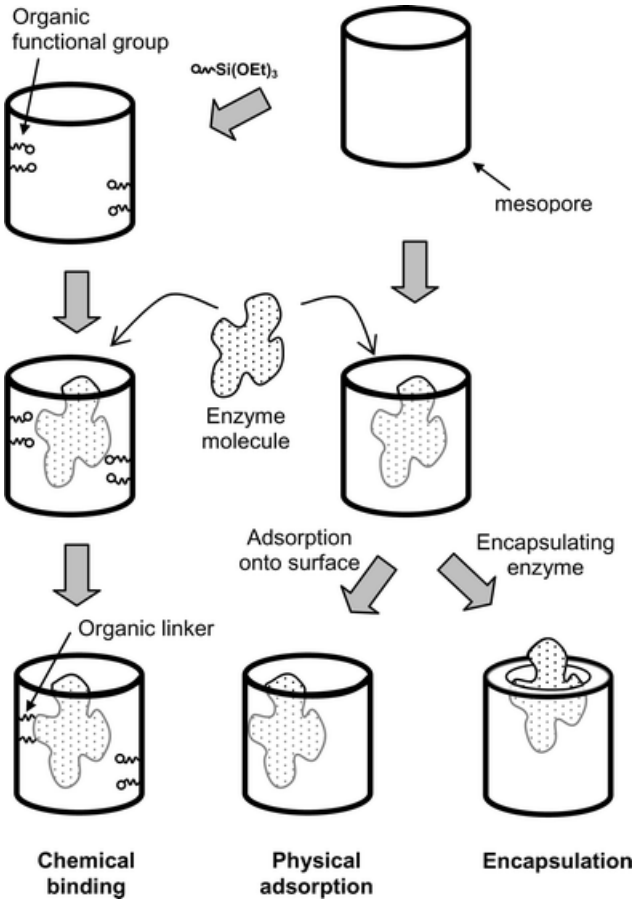

Figure 5.1 Strategies of three commonly used methods for enzyme immobilisation [7]

It is possible to use covalent bonding to attach the enzyme to the support material which forms a stable biocatalyst which shows very little leaching of enzyme. To covalently bind an enzyme/catalyst to a mesoporous support the chances of success are greatly increased if the surface is functionalised. Mesoporous materials present good prospects for immobilisation as they possess well defined silanol groups which can be readily functionalised with groups such as amines and carboxylates. Problems arise if the binding results in a conformational or orientation change which results in deactivation or reduced accessibility and activity

Cross-linked enzymes can become immobilised without the use of a support by intermolecular covalent bonding **[8, 9]**. Problems can arise with low stability and reduced activity and also a lack of support for the enzyme causes the material to be unsuitable for many applications.

The enzyme can also be physically adsorbed onto the surface and this method can be used for a wide variety of proteins without any loss in activity because the bonds formed are

weaker than covalent ones and are less likely to result in changes in the enzyme's configuration.

Polymers or gels can be used to entrap an enzyme and there has been substantial work in the area of silica sol-gel materials which show good stability and high retention of the enzyme **[10-12]**. The drying method of these support materials has a great affect on the stability: evaporation produces much denser xerogels whereas using carbon dioxide to dry the materials gives very low density aerogels **[13]**.

After the enzyme has been adsorbed onto a support material it can be encapsulated by trapping it within the pores/material. This prevents the enzyme from aggregating as it remains isolated and also slows down leaching. However, as the enzyme is trapped, difficulties may arise in the substrate accessing the enzyme and so catalytic activity may be reduced **[14, 15]**.

5.1.2 Covalent bonding of proteins to Mesoporous Supports

Glucose oxidase and Bovine serum albumin are two types of proteins which have been shown to be covalently attached to mesostructured cellular foam which has been functionalised with amino groups **[16]**. The support material is seen to be activated by the addition of glutaraldehyde which is then followed by mixing with the protein in solution.

In some cases it is seen that by covalently binding the enzyme rather than just adsorbing it within the pores we can observe a reduction in the reusability and activity of the enzyme. An example of this can be seen whereby glutaraldehyde is used to attach penicillin acylase to MCM-41 **[17]**. The solid support is first modified with APS, then with glutaraldehyde which binds to the enzyme. The activity of the bound enzyme can be measured as penicillin acylase acts as a catalyst in the hydrolysis of penicillin G to 6-aminopenicillic acid. The sample in which the protein was bound to the support exhibited only 25% of the activity seen in a sample in which the protein was adsorbed into the pores. The reason for this could be due to the modification of the support with glutaraldehyde and APS causing a reduction in the pore size and therefore lower uptake of protein which in turn results in lower activity.

5.1.3 Physisorption and encapsulation of protein within mesoporous solids

In general, for example in catalysis, it is not desirable for proteins which have been immobilised within a support to be released. To ensure that the proteins remain within the pores retention can be improved via many methods. The environment in which the protein is situated can be controlled using buffers to ensure binding is retained *via* electrostatic interactions or the surface of the support can be modified to increase favourable interactions. It is also possible to prevent the leaching of the protein from the pores using encapsulation.

Mesoporous materials can be tailored to many possible morphologies and pore systems and sizes. This is an advantage when it comes to studying encapsulation or adsorption of proteins as the pore size can be matched to the size of the protein which aids in the protein retention. Studies have been carried out on MCM-41 with trypsin immobilised within the pores in which 3-aminopropyltriethioxysilane is used to encapsulate the protein within the pores **[18]**. The solvent in which the APS is added to the support is crucial with toluene producing an immobilised enzyme with activity of less than 1% residual activity. When this solvent is changed from toluene to dichloromethane and slightly less APS is used the activity increases to 13%.

As well as aminopropyl groups, vinyl groups can be used to entrap enzymes or proteins within MCM-41. Porcine pancreatic lipase has been encapsulated within MCM-41 using vinyltrimethoxysilane and shows high residual activity of ~40% and excellent reusability with 94% of activity retained after 5 cycles **[19]**.

These examples use functional groups to encapsulate the proteins within the pores but it can also be achieved by immobilising the enzyme within mesoporous spheres which can then be coated with layers of polyelectrolytes and nanoparticles.

5.1.4 Using mesoporous materials for enzyme/protein adsorption

Immobilisation of enzymes using mesoporous materials was first carried out using MCM-41 by Diaz and Balkus in 1996 **[18]**, who observed that the efficiency of immobilisation was dependent on the molecular size of the enzyme. The development of larger pore materials such as SBA-15 and MCF increased the range and size of molecules which could be taken up. Much work has been carried out on the modification of these mesoporous

materials with the greatest interest being in enlarging the pore entrance and tailoring the pore structure and particle morphology.

The stability of the enzyme adsorbed within the mesoporous material depends on the size of the enzyme in comparison to the pore. Larger enzymes than the mesopore size cannot be adsorbed into the materials and so matching the size of the enzyme with the pore becomes a crucial part of immobilisation. If an unfunctionalised material has pore sizes significantly larger than the enzyme problems arise as the enzyme is able to leach out quickly from the pores. **[7]**

Charge interaction plays a key role between the enzyme and the mesoporous solids. If the net surface charge of the mesoporous material is opposite to that of the enzyme then the main effect will be to increase the strength of interaction and the position of equilibrium. It is possible that the adsorption in some cases could be slower as if adsorption is very strong this could lead to a blocking of the pores. If the enzyme and mesoporous surface have the same charge then this causes poor stability and repulsion between the enzyme and surface and reduced uptake. This problem can be overcome by using a buffer solution to change the pH which changes the charge of an enzyme and also functionalising the surface of the mesoporous material by the addition of an amino or carboxyl group. Functionalising the solid can impart a positive (NH_3^+) or negative (CO_2^-) charge. By varying the surface by changing the pH it is possible to match the charges on an enzyme to a mesoporous solid.

To be able to develop more suitable materials for biocatalysis/protein separation it is necessary to understand the reasons behind the immobilisation behaviour of proteins within mesoporous materials. A major factor is the relative size of the mesopore to the protein and it has been shown **[18]** that during a limited time period the amount of protein adsorbed on MCM-41 decreased with increasing protein molecular weight. Therefore the pore size within the material should be large enough to allow the desired protein access to the channels. Surface characteristics of the materials and proteins such as surface charges and electrostatic interactions between the two must be complementary and the interactions between enzyme and support depends strongly on the nature of the functional groups present at the surface of the support material.

Han *et al.* **[20]** have shown that amine-functionalised SBA-15 can selectively adsorb anionic proteins over a suitable pH range and then this can be reversed by changing the ionic strength of the solution and releasing the protein. Here the anionic proteins are

electrostatically attracted to the amine groups which had a positive charge under the experimental conditions.

Wright *et al.* **[21]** have carried out studies using SBA-15 and a thiol functionalised SBA-15 using a variety of proteins of differing sizes in order to determine whether size exclusion occurs when the proteins became too large for the pores. They observed that in general more adsorption occurs on the functionalised material, with the exception of the largest proteins which cannot fit in the functionalised material due to the reduced pore size caused by the addition of functional groups. A schematic showing the protein dimensions (estimated using the protein structure data base) in comparison to a functionalised pore wall of SBA-15 can be seen in Figure 5.2.

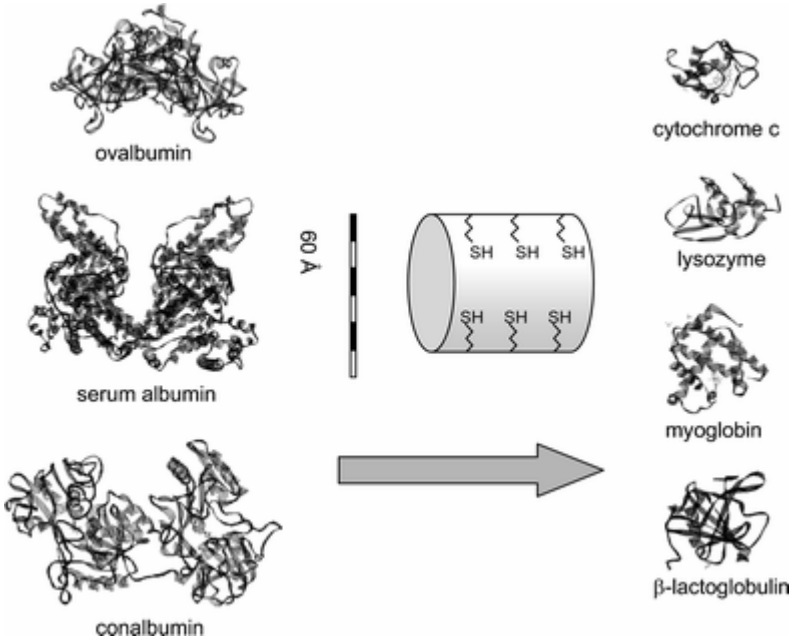

Figure 5.2. Protein size compared to pore size [7]

In summary, immobilising enzymes onto supports should allow them to maintain or improve their specific catalytic activity whilst allowing high enzyme-substrate contact and reducing deactivation.

5.1.5 Catalysis with immobilised enzymes on mesoporous materials

The aim of immobilising an enzyme within a mesoporous material is to prepare a material that can be used for catalysis with the added advantages of a heterogeneous system. A balance must be achieved in attaining a material with a very high enzyme loading but also taking into consideration the cost of the enzyme and whether a significant increase in activity is achieved.

Pore size can be crucial in the use of mesoporous materials for catalysis and studies have been carried out looking at the effects of varying the pore diameter in the assaying of immobilised trypsin by the hydrolysis of BAPNA **[22]**. Three materials with differing pore size and morphology were compared and it was observed that the larger pore material, SBA-15, gave the highest activity whilst the smaller pore materials showed reduced activity. MCM-41 and MCM-48 are of similar pore size but possess different pore structures with MCM-48 having a three dimensionally accessible system and MCM-41 a 1-D system. The results were taken to indicate that the difference in pore structure is not as crucial in reaction rate as the pore size, suggesting that the smaller pores result in reduced substrate diffusion.

An important application in the chemical industry is to carry out catalysis on immobilised enzymes within non-aqueous media. Takahashi et al **[23]** have shown that horseradish peroxidase, HRP (which has been extensively used as an environmentally friendly catalyst for oxidation reactions), can be immobilised onto FSM-16, MCM-41 and SBA-15 with differing pore sizes. The activity for these materials tested in an organic medium using toluene as the solvent. The activity of the immobilised HRP using FSM-16 was 10 times greater than the activity of the free (unsupported) enzyme and also the thermal stability was enhanced with the reduced loss in activity when exposed to a buffer solution at 70 ^{o}C for 120 min.

5.1.6 CALB

The enzyme chosen for immobilisation within a series of mesoporous silica materials was Candida Antarctica Lipase B (CALB) **[24],** shown in Figure 5.3, which is a small protein with approx dimensions of 3 x 4 x 5 nm **[25]**. It has been shown that CALB can be used as a catalyst for the hydrolysis of triacylglycerols under aqueous conditions and also in the

transesterification of secondary alcohols **[26, 27]**. Candida Antarctica Lipase B has many possible applications in industrial processes including the synthesis of triglycerides and the esterification of terpenic alcohols. It has also been shown that by varying the support used to immobilise the CALB, it can be very regioselective in the esterification of sugars, nucleosides, and steroids, and fully enantioselective in the resolution of secondary alcohols via hydrolysis or esterification in organic solvents **[28, 29].** Within CALB there is an active site which can be accessed by solvent which consists of a hydrophobic channel of aliphatic amino acid residues.

Before the development of mesoporous solids lipases had been immobilised using controlled pore glass (CPG) systems **[30]**. Clayton and Bosley showed that hydrophobic CPG could be used as a support and that a pore size of 35 nm was required to use the internal volume of the support particles in the immobilisation process.

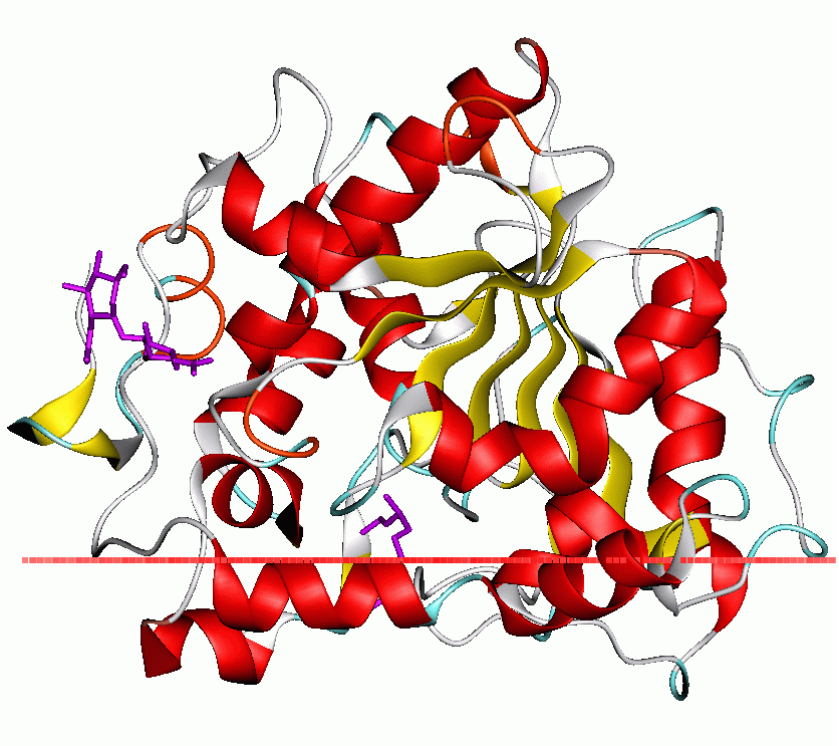

Figure 5.3 Schematic representation of CALB, scale bar = 5 nm

5.2 Immobilisation of CALB on mesoporous materials

To immobilise the enzyme on the support, the mesoporous solid is suspended in a solution of enzyme of known concentration and enzyme is allowed to adsorb within the pores. The solid is then separated by centrifugation and using p-NPB hydrolysis as an assay the enzyme concentration remaining in the buffer solution, and by difference the uptake on the solid, can be calculated. This technique assumes that there is no deactivation of the enzyme and any enzyme not present in the supernatant must be bound to the solid. The enzyme concentration of the supernatant can also be calculated *via* the Bradford assay, which gives the total protein content and this method was utilised on a selection of materials to confirm the protein was not denatured.

5.2.1 Method

Typically 100 mg of mesoporous material was placed in a 10 mL centrifuge tube and, for a 10 mg g^{-1} loading of enzyme, 3.9 mL of phosphate buffer (pH 6, 50 mM) and 0.1 mL *Candida Antarctica B.* (Novozym) were added to the solid. The tube was placed in a cold room (4 ^{o}C) on a Spiramix 5 Tube Roller for the desired time before being centrifuged at 9000 rpm for 5 minutes (Beckman fixed-angle JA-25.50 rotor)

In order to measure the activity of the solution, 10 μL of a 0.025M p-NPB solution was added to 10 μL of the supernatant in 1 mL of phosphate buffer solution (pH 8, 50 mM) and the activity of this enzyme solution was measured by hydrolysis of *para*-nitrophenyl butyrate (p-NPB) (UV, 400nm). The formation of *p*-nitrophenol (shown in Figure 5.4) is observed at 400 nm and so absorption measurements can be used to measure the activity of free enzyme after immobilisation, to observe the extent of uptake by the support. For every sample the activity was averaged over 3 assays.

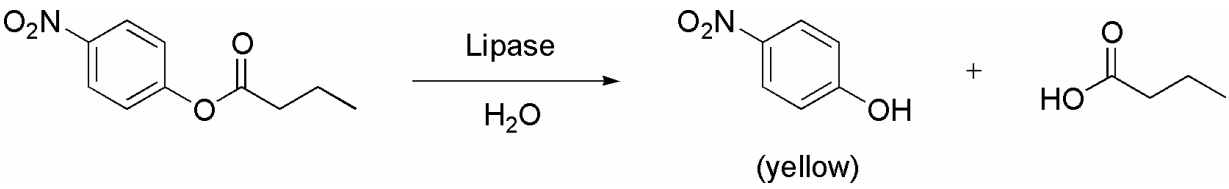

Figure 5.4 Hydrolysis of *para*-nitrophenyl butyrate (p-NPB)

The amount of enzyme adsorbed is determined from the difference between the activities of the free enzyme in buffer solution and immobilised enzyme samples. Measurements were carried out over hourly/daily intervals until the amount of enzyme immobilised reached a constant value.

5.3 Transesterification

It is possible to use an enzyme immobilised on mesoporous material as a catalyst in the selective transesterification of 1-phenylethanol and isopropenyl acetate to (*R*)-1-phenylethyl acetate, as shown in Figure 5.5. The reaction goes to completion because acetone is a product.

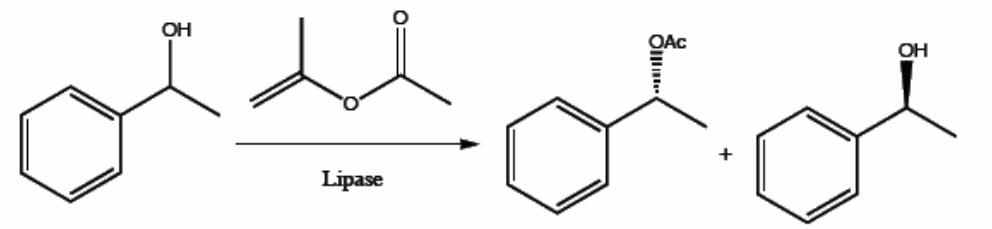

Figure 5.5 Transesterification of (*R*)-1-Phenylethanol

After the enzyme had been immobilised on the solid, the material underwent a series of washes and was then centrifuged to remove the solvents. Firstly the solids were washed with 1-propanol (2 x 5 mL) followed by methyl *tert*-butyl ether (MTBE, 2 x 5 mL). To each sample a substrate solution (5 mL) was added, containing racemic 1-phenylethanol (0.305 g, 2.5 mmol) and isopropenyl acetate (0.50 g, 5.0 mmol) and MTBE. The substrate was prepared by adding 1-phenylethanol (15.25 g, 0.125 mol) and isopropenyl acetate (25.00 g, 0.250 mol) in methyl tert-butyl ester (MTBE, HPLC grade). To ensure the substrate contained no water, oven-dried molecular sieves (4 Å) were added and left overnight before the substrate was used. After addition of the substrate samples were mixed using a Spiramix 5 Tube Roller at room temperature. Samples were then centrifuged and at specified times 1µL of the solution was injected into a CE Instruments GC Top8000 (Figure 5.6) to measure and follow the rate of transesterification using a Chirasil ChiraDEX CB WCOT fused silica chiral column, and detecting with an FID detector.

Figure 5.6 GC Top 8000

The reaction can be followed by the appearance and disappearance of peaks at certain retention times corresponding to the starting materials and product (Figure 5.7). The reactant mixture of (*R*)- and (*S*)-1-phenylethanol elutes at 6.93 and 7.39 minutes respectively. Upon reaction the peak due to the R-enantiomer decreases, to be replaced by *R*-1-phenylacetate, which elutes after *ca*. 5.40 min in the GC under these conditions. The DP700 integrator is connected to the GC and produces both a plot of the peaks (as shown in Figure 5.7) and a Table of peak integral values which can be normalised against the standards and used to calculate the concentration of starting material and product at various time intervals which can in turn be used to calculate the initial rate of reaction.

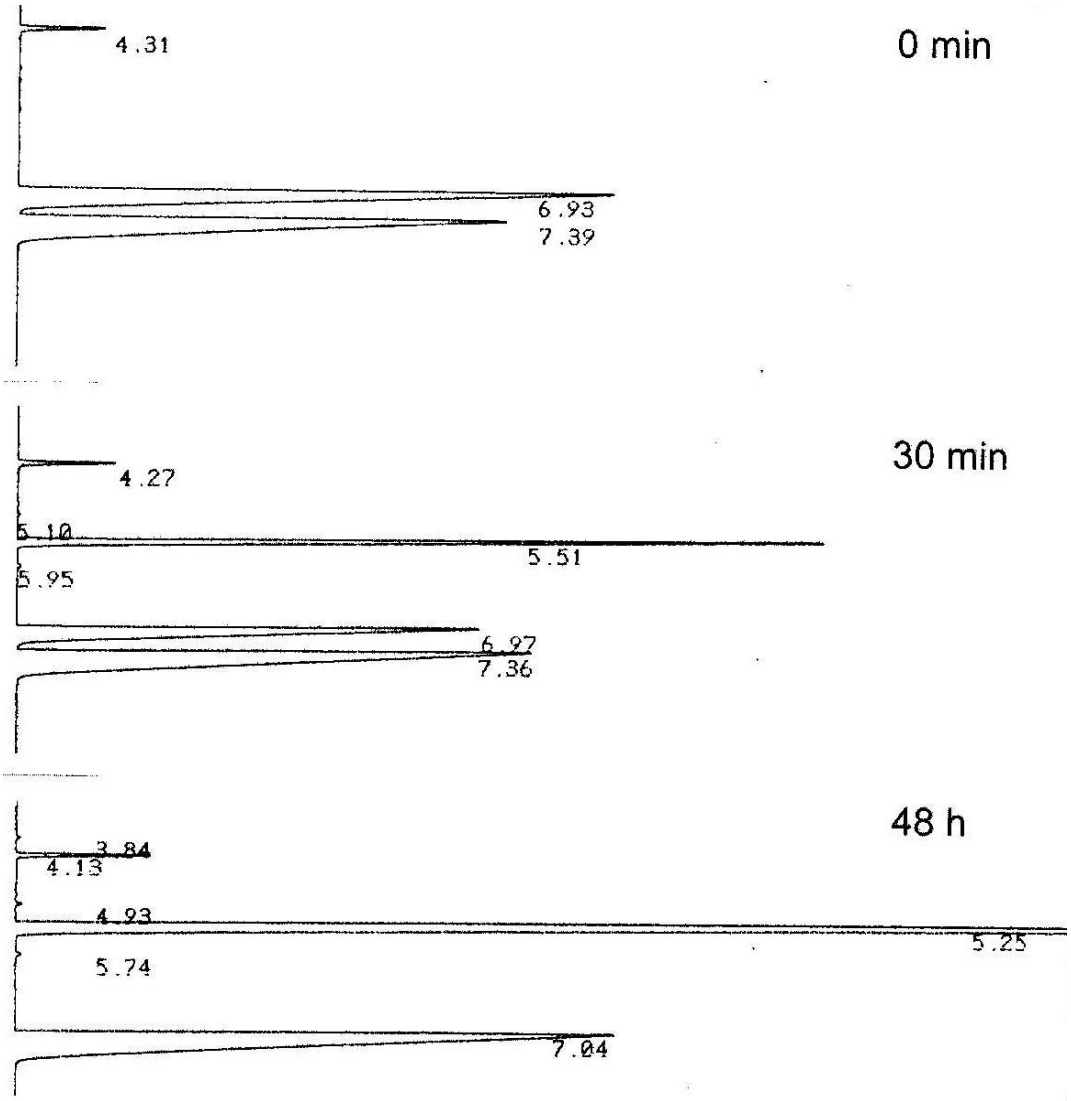

Figure 5.7 Acylation of 1-Phenylethanol with immobilised CALB

The decrease in *R*-1-phenylethanol and conversion to *R*-1-phenylethyl acetate can be plotted, as seen in Figure 5.8, which allows us to follow the reaction and observe when it reaches completion.

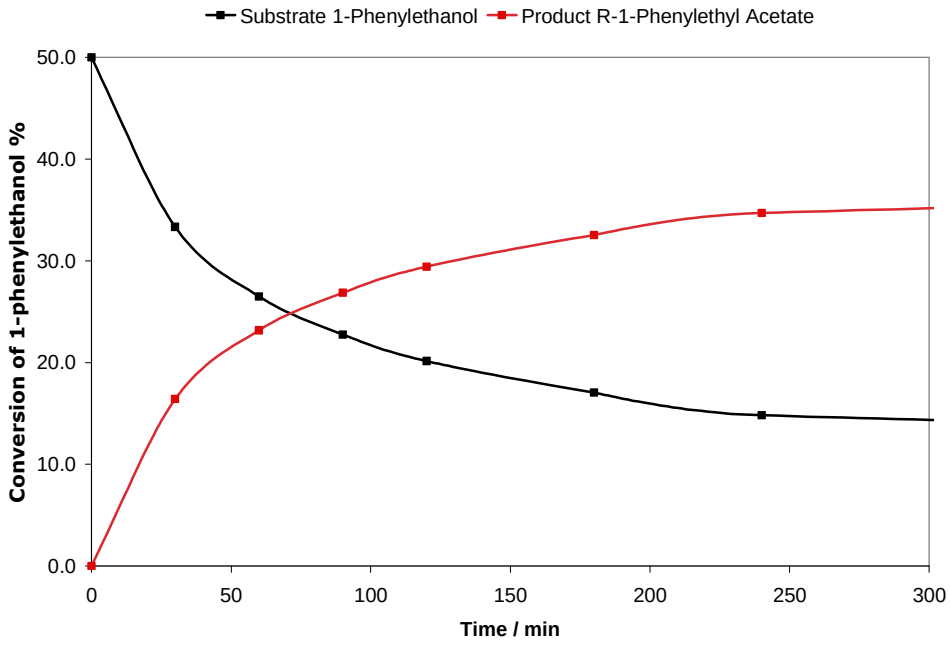

Figure 5.8 Conversion of a racemic mixture of 1-phenylethanol (substrate) to *R*-1-phenylethyl acetate (product) using 10 mg/g CALB immobilised on SBA-15 (red). Note that the maximum possible conversion of the mixture is 50%, because *S*-1-phenylethanol is not converted.

5.3.1 Reusability

After a sample has been used to measure the rate of transesterification it is possible to centrifuge the sample, remove the solvent and wash the remaining solid with 1-propanol and MBTE. The method described in section 5.4 can then be repeated with the addition of 5 mL of fresh substrate and repeated as required.

5.4 CALB immobilisation on SBA-15 material

The immobilisation of CALB was carried out as described in section 5.2.1 using SBA-15 as the mesoporous support material. As described previously p-NPB hydrolysis can be used to determine the enzyme activity of the supernatant and the free enzyme, the difference showing the amount of enzyme adsorbed into the material. If we leave the mesoporous support suspended in the enzyme solution for up to 24 hours we can see a significant change in activity between the supernatant and free enzyme (Figure 5.9). The activity of the supernatant is zero indicating that in this case the enzyme has been completely immobilised by the mesoporous support material and none remains in the supernatant. The Bradford assay can also be used to confirm there is no protein in the supernatant as it can detect protein even if it has become denatured and is inactive, unlike the p-NPB hydrolysis which only detects active enzyme.

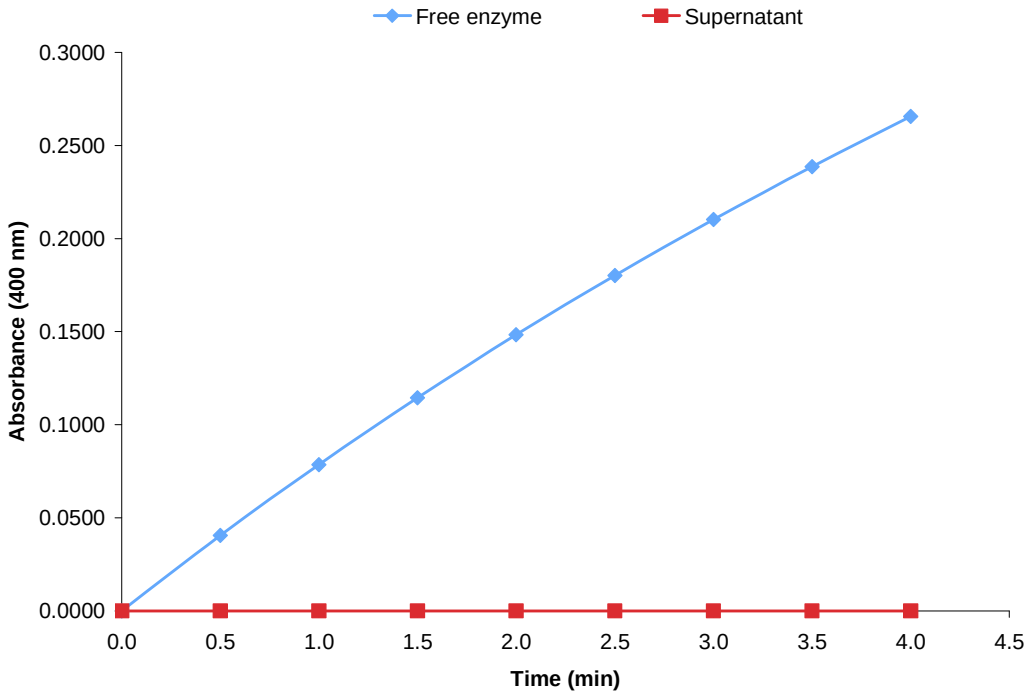

Figure 5.9 Supernatant and free CALB activity after adsorption by SBA-15

The uptake of CALB in calcined SBA-15 is tabulated below in terms of time and loading (Table 5.1). With loadings of 10 and 20 mg/g, almost all the enzyme is immobilised by the material after 24 h. As the loading is increased to 50 mg/g we see a reduction in the %

immobilised with 90% of the offered CALB immobilised. The results are broadly in agreement with those of Smith (Ph.D thesis, University of St Andrews, 2007).

Table 5.1 CALB immobilisation on calcined SBA-15 at increasing loading

Support	Time(h)	Enzyme offered (mg/g)	Immobilised (%)	Loading
SBA-15 (cal)	0	10	0	0
SBA-15 (cal)	24	10	99	9.9
SBA-15 (cal)	48	10	100	10
SBA-15 (cal)	24	20	97	19.4
SBA-15 (cal)	48	20	97	19.4
SBA-15 (cal)	24	50	90	45
SBA-15 (cal)	48	50	90	45

5.4.1 Effect of extraction/functionalisation on SBA-15 enzyme immobilisation

Organo-functionalised silicas must be rendered porous by extraction to remove the template. The control reaction is to measure the immobilisation efficiency on extracted, unfunctionalised material. The uptake of CALB by calcined and extracted material over 48 hours is shown below in Table 5.2.

Table 5.2 Effect of extraction on immobilisation of CALB onto SBA-15

Support	Time(h)	Enzyme offered (mg/g)	Immobilised (%)	Loading
SBA-15 (cal)	24	10	99	9.9
SBA-15 (cal)	48	10	100	10
SBA-15 (ex)	24	10	90	9.0
SBA-15 (ex)	48	10	97	9.7
SBA-15 (as prep)	24	10	21	2.1
SBA-15 (as prep)	48	10	23	2.3

From the results it can be seen that there is very little difference in the amount of enzyme immobilised by the extracted material compared to the calcined material, although the enzyme can be taken up into the pores more slowly.

The as-prepared material which has not had the template removed gave low uptake with 77% of the offered enzyme remaining in solution after 48 hours. This indicates that some adsorption takes place, either on the outer surface of the support material or as a result of partial extraction during the immobilisation process resulting in the removal of some surfactant and its replacement with enzyme.

5.4.2 Enzyme adsorption on 'additive-modified' SBA-15 materials

During the synthesis of SBA-15 it is possible to use additives to control the morphology of the resulting material. Alkanes, in this case decane, can be used to swell the micelles during the formation of SBA-15 (as described in chapter 3) causing the particles to change from the typical SBA-15 material to more branched particles as seen in Figure 5.10.

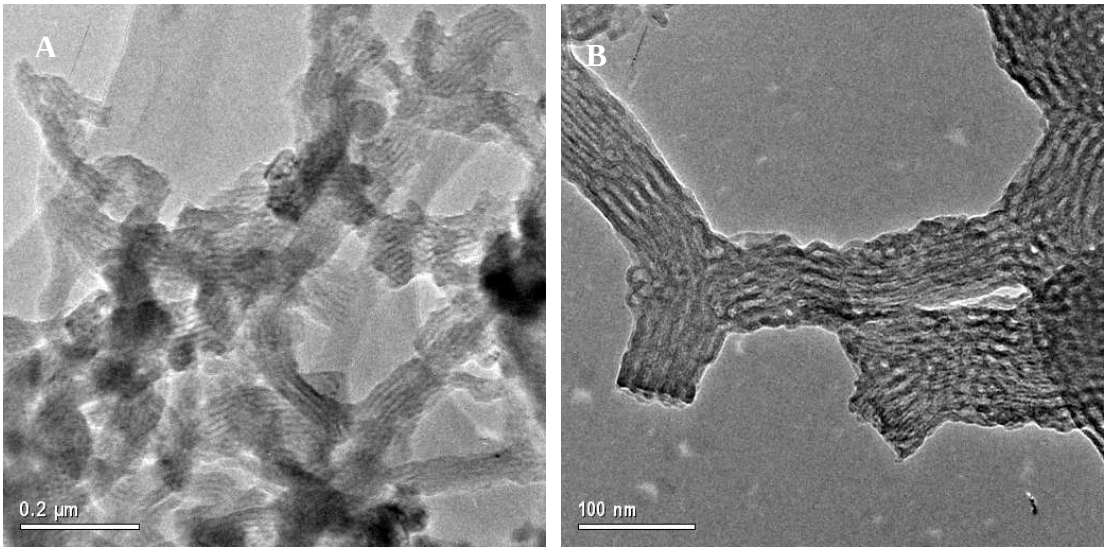

Figure 5.10 Effect of adding decane to SBA-15 synthesis in ratio of 5.8:1 (A) and 2:1(B)

As seen from the immobilisation results shown in Table 5.3 at a 10 mg/g loading 100% of the CALB offered was immobilised within the first 24 hours on all samples with decane ratios varying from 2 to 7.6:1.

Table 5.3 Calcined SBA-15 type material with decane: surfactant ratio shown in brackets

Support	Time(h)	Enzyme offered(mg/g)	Immobilised (%)	Loading (mg/g)
SBA-15 (7.6)	24	10	100	10
SBA-15 (5.8)	24	10	100	10
SBA-15 (2:1)	24	10	100	10

As seen in Figure 5.9, adding decane causes a change in the morphology of SBA-15 and so organic functional groups can be added to synthesis in addition to decane and the resulting materials can be seen in Figure 5.11 and are discussed in chapter 3.

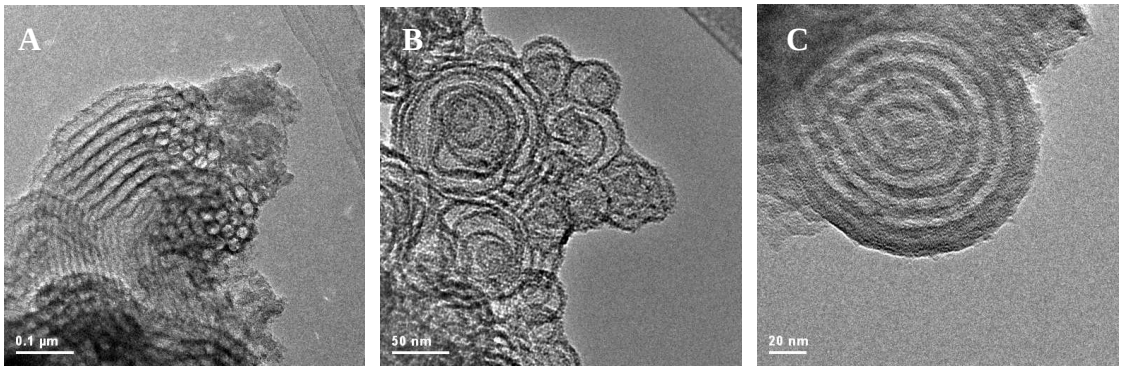

Figure 5.11 Effect of adding thiol and decane to SBA-15 synthesis; 2%SH 5.8(A), 7%SH 2:1(B), 7%SH 5.8:1(C)

The immobilisation of CALB on these materials are tabulated and shown in Table 5.4.

Table 5.4 Effect of decane and thiol on immobilisation

Support	Time(h)	Enzyme offered(mg/g)	Immobilised (%)	Loading (mg/g)
2%SH-SBA-15 (5.8)	24	10	71	7.1
2%SH-SBA-15 (5.8)	48	10	79	7.9
2%SH-SBA-15 (5.8)	168	10	99	9.9
7%SH-SBA-15 (5.8)	24	10	41	4.1
7%SH-SBA-15 (5.8)	48	10	42	4.2
7%SH-SBA-15 (5.8)	168	10	49	4.9
7%SH-SBA-15 (2)	24	10	25	2.5

7%SH-SBA-15 (2)	48	10	20	2.0
7%SH-SBA-15 (2)	168	10	36	3.6

When decane and 2% thiol are added this results in branched SBA-15 particles. This material has a slower uptake than unfunctionalised samples of similar morphology. Increasing the amount of thiol produces an 'onion ring' morphology (Figure 5.10-B and C) which shows a much lower uptake of enzyme. This is due to pore space being inaccessible when the material forms these onion rings, and the small micropores in the material are only accessible to nitrogen, as seen in chapter 3. The results of CALB uptake on these SBA-15 type materials are shown in Figure 5.12. Adding 7 mol % thiol and decane and changing the morphology from branched particles to onion rings strongly reduces the uptake of CALB.

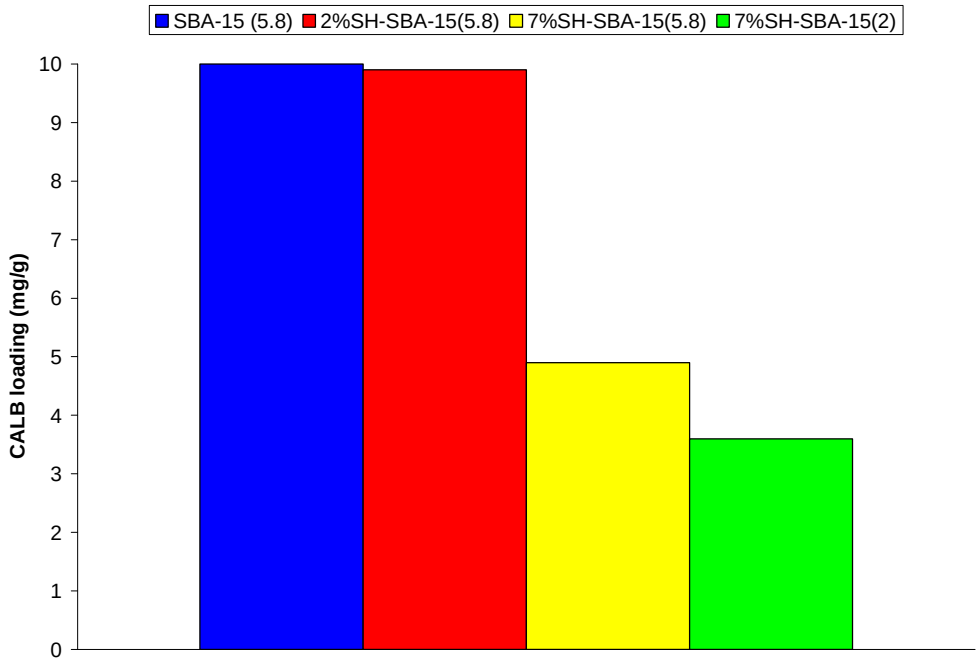

Figure 5.12 CALB uptake in SBA-15 type materials prepared in presence of decane when offered 10mg/g enzyme (number in bracket indicating weight ratio of decane to surfactant)

5.5 Enzyme immobilisation on cubic Ia-3d silicas

KIT-6 is a three dimensional mesoporous silica with Ia-3d symmetry consisting of 2 separate channel networks. The immobilisation of CALB was carried out in the same way as with SBA-15 described in section 5.5. The effect of template removal and pore size are

tabulated below (Table 5.5). Two materials synthesised in chapter 3 were selected, the KIT-6 100 material and KIT-6 130 material.

Table 5.5 CALB loading on KIT-6 type materials

Support	Pore Size (nm)	Time (h)	Enzyme offered (mg/g)	Immobilised (%)	Loading (mg/g)
Large pore (as prep)	/	48	10	18	1.8
Large pore (as prep)	/	144	10	20	2.0
Large pore (calcined)	8	24	10	100	10
Med pore (calcined)	6	24	10	100	10
Med pore (calcined)	6	48	50	53	26.5
Med pore (calcined)	6	144	50	81	40.5

In an as-prepared sample the pores remain blocked by presence of the surfactant used to synthesise the material, so as shown above when 10 mg/g enzyme (in solution) is added to 100 mg of mesoporous material only 20% of the enzyme offered is immobilised. Upon repeating this immobilisation using calcined samples of material with pore diameter 6 and 8 nm 10 mg/g can be completely immobilised as there is a much larger pore volume available. With the medium pore calcined material increasing the loading to 50 mg/g still results in a relatively high immobilisation of over 40 mg/g.

5.5.1 Immobilisation on Ia-3d materials synthesised at low temperature

Repeating the synthesis procedure used to give SBA-15, but at low temperature and with the addition of thiol and decane, a material with Ia-3d symmetry (and a pore size of 8 nm) is produced (STA-11). This material is closely similar to large pore KIT-6. The immobilisation data shown in Table 5.6 is comparable to the uptake seen in typical SBA-15 material (Table 5.1) with 100% uptake at a 10 mg/g loading and ~90% at 50 mg/g loading for both materials, which is higher than achieved for the KIT-6 materials.

Table 5.6 Immobilisation of CALB on STA-11 Ia-3d material (extracted)

Time(h)	Enzyme offered (mg/g)	Immobilised (%)	Loading
24	10	99	9.9
24	20	99	19.8
48	30	99	29.7
48	40	81	32.4
96	40	95	38
48	50	77	38.5
96	50	90	45

5.5.2 Increasing loading on KIT-6 material

The uptake of CALB on the large pore KIT-6 material by gradually increasing the loading from 10 to 50 mg/g (Table 5.7) was examined in more detail. At low enzyme loadings the uptake is complete within 24-48 hours and we see almost a 100% immobilisation of the enzyme offered. Increasing the loading to 40 mg/g only 45% is immobilised in the first 48 hours and it takes 168 hours to reach over 90% immobilisation. This trend is also seen for a 50 mg/g loading where a similar % of offered CALB is taken up by the solid over a period of 168 hours.

Table 5.7 KIT-6 material (calcined)

Time(h)	Enzyme offered(mg/g)	Immobilised (%)	Loading (mg/g)
24	10	99	9.9
24	20	97	19.4
48	20	99	19.8
48	30	94	28.2
72	30	94	28.2
48	40	45	18.0
96	40	75	30.0
168	40	92	36.8

48	50	50	25.0
96	50	65	32.5
168	50	91	45.5

A large pore KIT-6 material which has been functionalised with 5% thiol and subsequently extracted to remove the template has also been studied in terms of enzyme loading and subsequent catalytic activity and the immobilisation data can be seen in Table 5.8.

Table 5.8 Large pore 5% thiol KIT-6

Time(h)	Enzyme offered(mg/g)	Immobilised (%)	Loading (mg/g)
48	10	95	9.5
72	10	99	9.9
48	20	77	15.4
72	20	84	16.8
144	20	82	16.4
48	30	72	21.6
72	30	74	22.2
144	30	80	24.0
48	40	66	26.4
72	40	79	31.6
144	40	76	30.4
48	50	54	27.0
72	50	59	29.5
144	50	59	29.5
48	100	11	11.0
72	100	29	29.0
144	100	32	32.0

Like the unfunctionalised version almost 100% of the 10 mg/g enzyme offered was immobilised but with this material by increasing the enzyme offered, up to 100 mg/g, a more noticeable reduction in immobilisation was observed, due to the presence of

functional groups and residual surfactant decreasing the pore size from 8 to 6.5 nm, as observed from the nitrogen adsorption data.

Figure 5.13 compares uptake with enzyme offered for KIT-6 materials with and without thiol. The maximum uptake possible is shown in black.

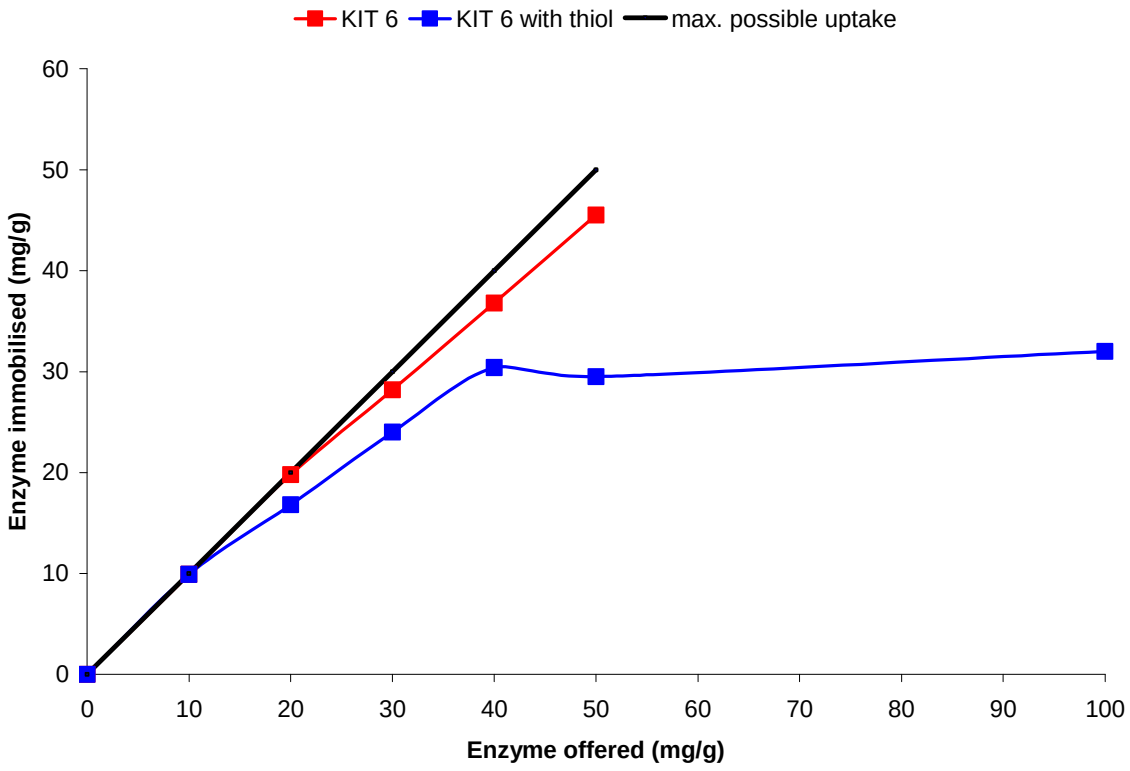

Figure 5.13 Enzyme loading on KIT-6 type material

In the case of the calcined KIT-6 material the uptake at concentrations from 10 to 50 mg/g are all close to the maximum possible indicating that the material has a large enough surface area and pore diameter to immobilise 50 mg/g. Uptake on the functionalised material appears to reach a maximum of approx 30 mg/g even when the amount offered is increased substantially (to 100 mg/g).

5.6 Cubic cage material – FDU-12

FDU-12 is a cubic mesoporous solid made up of large cavities connected by smaller connecting windows. For materials with cages up to 15 nm in diameter and varying window diameters the effects on enzyme immobilisation are shown in Table 5.9.

Table 5.9 Effect of pore size on enzyme immobilisation at 1% loading

Support	Window Size (nm)	Time(h)	Enzyme offered(mg/g)	Immobilised (%)	Loading (mg/g)
FDU-12 (50-100)	4	24	10	42	4.2
FDU-12 (50-100)	4	48	10	47	4.7
FDU-12 (50-100)	4	96	10	55	5.5
FDU-12 (15-100)	6	24	10	29	2.9
FDU-12 (15-100)	6	48	10	47	4.7
FDU-12 (15-100)	6	72	10	55	5.5
FDU-12 (15-100)	6	96	10	55	5.5
FDU-12 (50-140)	5	24	10	60	6.0
FDU-12 (50-140)	5	72	10	83	8.3
FDU-12 (50-140)	5	96	10	91	9.1
FDU-12 (15-140)	10-12	24	10	100	10

Typical FDU-12 synthesis (50-100) results in a cubic material with entrance windows approx 4 nm in size, which is on the limit of pore size able to immobilise CALB (3 x 4 x 5 nm) and even after 96 hours the support is only able to immobilise 55% of the CALB offered. As the enzyme is very close in size to the pore entrance then it is possible for the enzyme to become trapped and block the pore entrance therefore limiting the diffusion of the enzyme into the material. If the synthesis is altered by reducing the hydrolysis temperature (FDU-12 15-100) giving a solid with much larger cavities, the entrance windows remain similar giving a very comparable immobilisation of CALB (55% uptake). Increasing the acid erosion temperature gives materials with larger entrance windows (8-10 nm) and this allows a much greater uptake of enzyme with over 90% immobilisation after 96 hours for FDU-12 (15-140). The largest pore material (15-140) has entrance windows of between 6 and 12 nm and as CALB has dimensions of less than 5 nm there is no problem in all of the offered 10mg/g being immobilised within the pores after 24 hours. Figure 5.14 shows the maximum uptake of the 4 different FDU-12 materials and it is clear that by decreasing the hydrolysis temperature and increasing the acid erosion step (15-140) the entrance window is sufficiently increased to allow complete uptake of CALB.

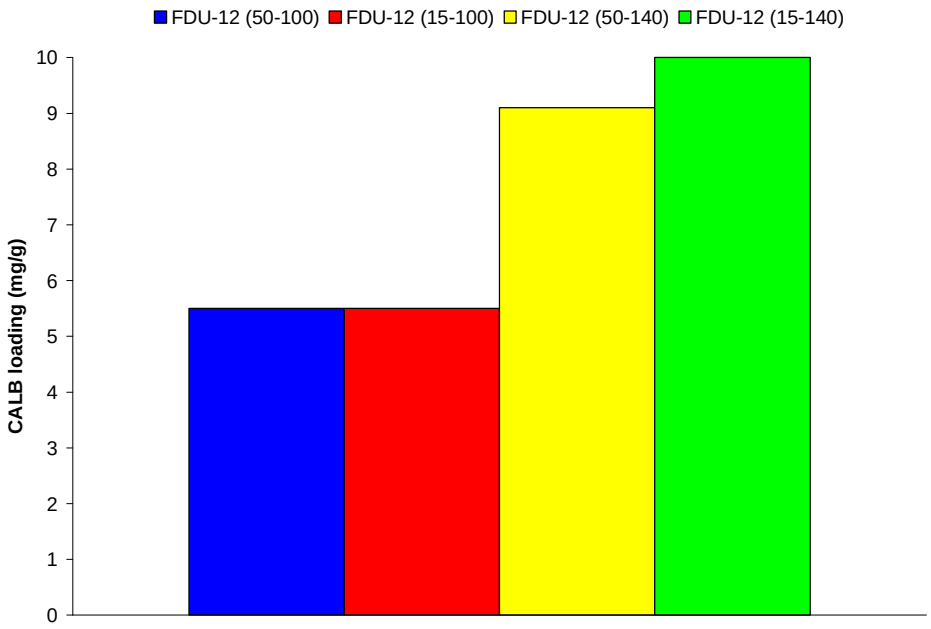

Figure 5.14 CALB uptake in FDU-12 type materials when offered 10mg/g enzyme

Functionalising FDU-12 materials prepared using the higher acid erosion temperature with a thiol group enables the effect of functionality on enzyme immobilisation to be examined and these are tabulated below (Table 5.10.)

Table 5.10 Effect of functionalising with thiol (med and large pore material)

Support	Window size (nm)	Time (h)	Enzyme offered (mg/g)	Immobilised (%)	Loading (mg/g)
FDU-12 (50-140)	6	24	10	60	6.0
FDU-12 (50-140)	6	72	10	83	8.3
FDU-12 (50-140)	6	96	10	91	9.1
5%SH-FDU-12 (50-140)	12	24	10	54	5.4
5%SH-FDU-12 (50-140)	12	72	10	80	8.0
5%SH-FDU-12 (50-140)	12	96	10	82	8.2
FDU-12 (15-140)	10-12	24	10	100	10
2%SH-FDU-12 (15-140)	8-10	24	10	85	8.5
2%SH-FDU-12 (15-140)	8-10	72	10	98	9.8
5%SH-FDU-12 (15-140)	8-10	24	10	73	7.3

5%SH-FDU-12 (15-140)	8-10	72	10	96	9.6
7%SH-FDU-12 (15-140)	8-10	48	10	98	9.8
7%SH-FDU-12 (15-140)	8-10	72	10	100	10

The large pore FDU-12 data shows that the material can be functionalised with 2, 5 and 7 mol % of thiol without a significant reduction in uptake.

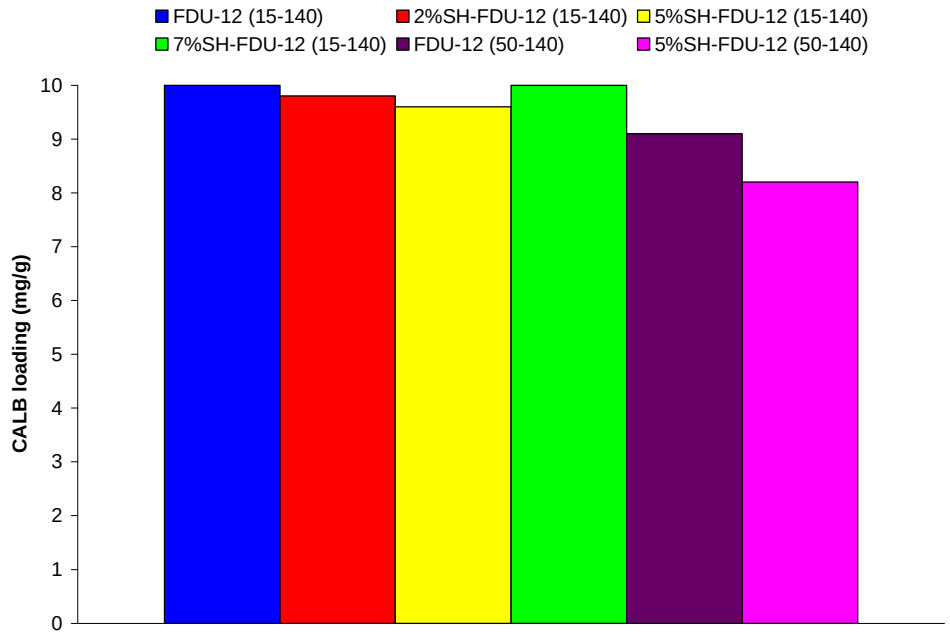

Figure 5.15 CALB uptake in FDU-12 and functionalised materials when offered 10 mg/g enzyme

5.6.1 Increasing loading on FDU-12 material

Enzyme immobilisation upon 15-140 FDU-12 material was studied by increasing the loading from 10 to 50 mg/g as shown in Table 5.11. Up to 30 mg/g there is almost complete immobilisation of all CALB offered but increasing this to 40 or 50 mg/g does not result in immobilisation above 33 mg/g.

Table 5.11 Increasing loading on large pore FDU-12 (15-140)

Time (h)	Enzyme offered(mg/g)	Immobilised (%)	Loading (mg/g)
72	10	98	9.8
168	10	100	10
72	20	93	18.6
168	20	95	19.0
72	30	87	26.1
168	30	90	27
72	40	73	29.2
168	40	80	32.0
72	50	59	29.5
168	50	66	33.0

The same can be carried out using a thiol-functionalised large pore FDU-12 (shown in Table 5.12) material but unlike the unfunctionalised material there is a much higher uptake at all loadings. (At 50 mg/g almost 20% more immobilisation occurs). The entrance sizes of both the functionalised and unfunctionalised material are both greater than 6 nm, which is larger than the size of CALB. The greater loading and immobilisation is attributed to the presence of thiol groups on the pore walls.

Table 5.12 Increasing loading on large pore 5% thiol functionalised FDU-12 (15-140)

Time (h)	Enzyme offered(mg/g)	Immobilised (%)	Loading (mg/g)
72	10	100	10
168	10	100	10
72	20	100	20
168	20	100	20
72	30	98	29.4
168	30	98	29.4
72	40	90	36
168	40	96	38.4

72	50	80	40
168	50	85	42.5

The effect of functionalising the FDU-12 material is shown in Figure 5.16 where the maximum possible loading is shown in black. FDU-12 reaches saturation at approx 30 mg/g whereas the thiol-functionalised material is seen to immobilise more than 42 mg/g.

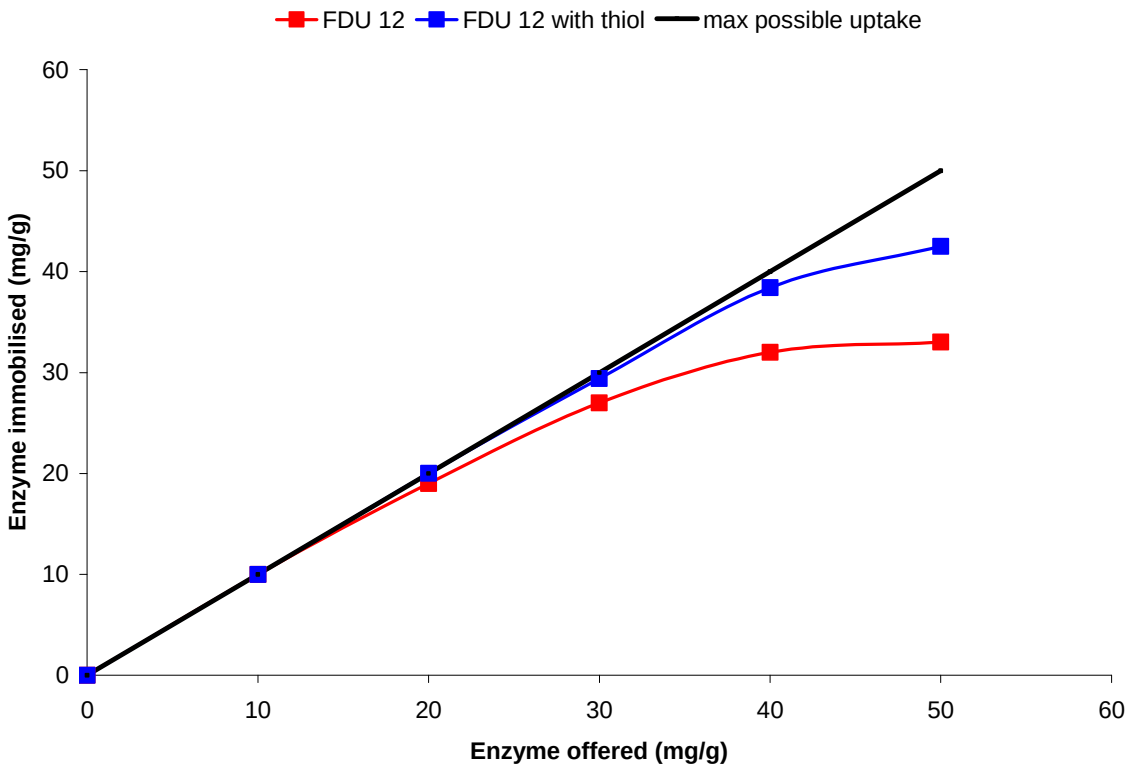

Figure 5.16 CALB loading on FDU-12 materials

5.7 Transesterification

From previous work on the transesterification of *R*-1-phenylethanol to *R*-1-phenylethyl acetate using CALB immobilised on SBA-15 materials by Smith **[26]** it was decided to investigate further the effects of modified SBA-15 materials and other pore topologies including KIT-6 and FDU-12 materials. The results obtained for SBA-15 and the free enzyme by Smith can be seen below in Table 5.13.

Table 5.13 Transesterification results for enzyme supported on calcined and extracted SBA-15 compared with free enzyme

Sample	Loading mg/g	Time min	(*R*)-1-PE %	(*R*)-1-PEA %	Rate µmol $min^{-1}g^{-1}$
SBA-15 (cal)	10	30	33.3	16.4	140
SBA-15 (ex)	10	30	31.5	18.8	170
SBA-15 (cal)	50	30	8.9	41.1	340
Chirazyme	1	30	49.7	0.4	0.3
CALB Powder dispersion	0.6	30	49.1	0.9	1.2

Both the calcined and extracted material at a loading of 10 mg/g show a much greater conversion of *R*-1-Phenylethanol to *R*-1-Phenylethyl acetate than when the equivalent amount of free enzyme is used to catalyse the reaction. This clearly shows the benefit of immobilisation of CALB in increasing the rate at which the R-1-phenylethanol can be converted to R-1-phenylacetate.

5.7.1 CALB supported on modified SBA-15

SBA-15 material modified using decane during the synthesis has been used to immobilise CALB at 10 mg/g in order to catalyse the transesterification of *R*-1-phenylethanol to *R*-1-phenylethylacetate (*R*-1-PEA). Once immobilisation of CALB onto the solids was complete the samples were washed with 1-propanol and MTBE before the substrate was added and the conversion to *R*-1-PEA was measured after 30 and 60 min to determine the conversion. Using 100 mg of support material and 5 mL of substrate, modified SBA-15

shows conversions of between 22 and 25% after 30 minutes, shown below in Table 5.14, also expressed as an 'initial rate' over the first 30 minutes.

Figure 5.17 also shows the conversion in the first hour of the reaction. The increase in initial rate from standard SBA-15 to material prepared by adding decane could possibly be explained by the greater external surface area as a result of the increased branching of the particles.

Table 5.14 Transesterification with calcined SBA-15 and modified SBA-15 supported CALB

Sample	Loading mg/g	Time min	(*R*)-1-PE %	(*R*)-1-PEA %	Rate $\mu molmin^{-1}g^{-1}$
SBA-15	10	30	33.3	16.4	140
SBA-15(2:1)	10	30	25.0	22.0	183.3
SBA-15(2:1)	10	60	19.8	28.3	
SBA-15(5.8:1)	10	30	26.2	21.4	178.3
SBA-15(5.8:1)	10	60	21.4	27.1	
SBA-15(7.6:1)	10	30	27.2	24.9	207.5
SBA-15(7.6:1)	10	60	20.9	27.8	

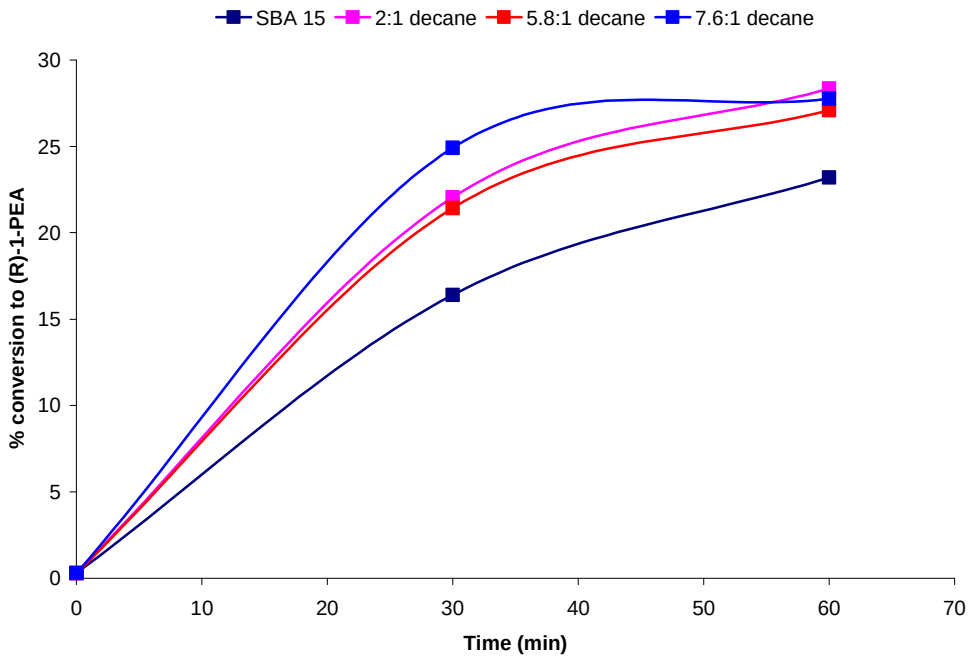

Figure 5.17 Conversion to (*R*)-1-PEA using CALB loaded SBA-15 type materials

For the previous samples initial rates were calculated based on the conversion of 1-phenylethanol to 1-phenylethyl acetate after 30 minutes using 100 mg of enzyme immobilised solid. The rate is based on the % conversion but it is possible that the initial rate is much faster at the beginning of the reaction i.e. the first 10-15 minutes and that the rate slows after this. As a result of this some of the samples were measured after 15 and 30 minutes, but earlier measurement was not deemed to be reliable.

5.7.2 SBA-15- increasing CALB loading

In the case of calcined SBA-15, the conversion after 15 minutes and also after 24 hours is shown in Table 5.15. At a loading of 10 mg/g there is a steady conversion to the product (after 24 hours the reaction has almost gone to completion, with a conversion of over 43% from a maximum 50% conversion (as the reaction is enantioselective)).

Table 5.15 Transesterification with calcined SBA-15 supported CALB

Sample	Loading mg/g	Time min	(R)-1-PE %	(R)-1-PEA %
SBA-15 (cal)	10	0	49.4	0.2
SBA-15 (cal)	10	15	37.2	12.4
SBA-15 (cal)	10	24 h	5.3	43.3

Looking at the same material, this time using solvent extraction to remove the surfactant rather than calcination, a similar CALB loading is achieved and an almost identical conversion results, with the % conversion within a percent of the calcined SBA-15 results, shown below in Table 5.16.

Table 5.16 Transesterification with extracted SBA-15 supported CALB

Sample	Loading mg/g	Time min	(*R*)-1-PE %	(*R*)-1-PEA %
SBA-15 (ex)	10	0	49.4	0.2
SBA-15 (ex)	10	15	36.1	13.2
SBA-15 (ex)	10	30	32.0	16.6
SBA-15 (ex)	10	24 h	5.9	42.8

By increasing the enzyme loading to 45 mg/g we observe a much faster conversion and we see almost complete conversion after 24 hours, as shown in Table 5.17.

Table 5.17 CALB at higher loading on calcined SBA-15

Sample	Loading mg/g	Time min	(*R*)-1-PE %	(*R*)-1-PEA %
SBA-15 (cal)	45	0	49.4	0.2
SBA-15 (cal)	45	15	17.9	31.0
SBA-15 (cal)	45	30	13.8	33.7
SBA-15 (cal)	45	24 h	0.0	48.9

The conversion to *R*-1-phenylethyl acetate for the three different materials can be seen in Figure 5.18 for the first 30 minutes of the reaction. There is not a significant difference between the calcined and extracted SBA-15 but increasing the loading on the calcined material gives a much faster conversion.

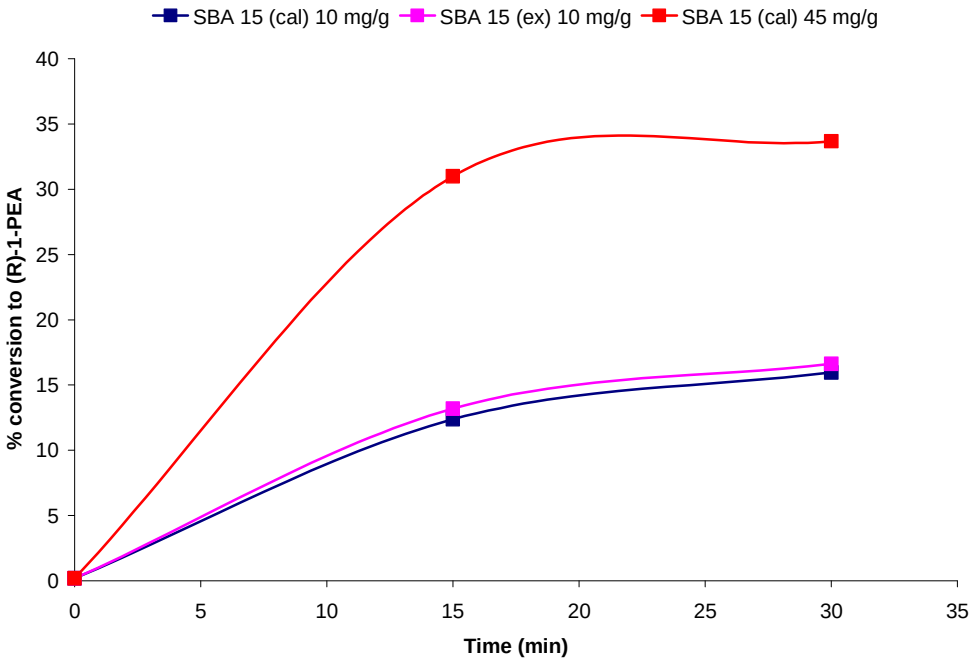

Figure 5.18 Conversion to *R*-1-PEA by SBA-15 supported CALB

5.7.3 KIT-6 material

KIT-6 is a cubic, 3D material composed of two interpenetrating, but not interconnecting channel systems. Medium pore (MP) (6 nm) and larger pore (LP) (8 nm) KIT-6 materials were used as supports for CALB in the transesterification. Table 5.18 shows the conversion to *R*-1-PEA for both materials, with the initial rate calculated based on the conversion after 30 minutes and as a function of increasing CALB loading on the large pore KIT-6. By increasing the CALB loading on the large pore KIT-6 a much faster conversion is observed (41% after 30 minutes).

Table 5.18 Transesterification with calcined KIT-6 supported CALB

Sample	Loading mg/g	Time min	(*R*)-1-PE %	(*R*)-1-PEA %	Rate $\mu molmin^{-1}g^{-1}$
MP KIT-6	10	30	24.7	28.5	237.5
MP KIT-6	10	60	19.7	32.0	
LP KIT-6	10	30	29.5	20.2	168.3
LP KIT-6	10	60	18.2	31.0	
LP KIT-6	28.2	30	10.4	38.2	318.3
LP KIT-6	28.2	60	6.2	43.4	
LP KIT-6	36.8	30	6.3	38.4	320
LP KIT-6	36.8	60	4.5	45.2	
LP KIT-6	45.5	30	8.2	41.0	347.5
LP KIT-6	45.5	60	3.5	46.0	

Figure 5.19 shows the conversion for these samples. KIT-6 (medium pore) shows higher conversion than SBA-15 when the enzyme loading is 10 mg/g but all conversions at higher loadings approach completion.

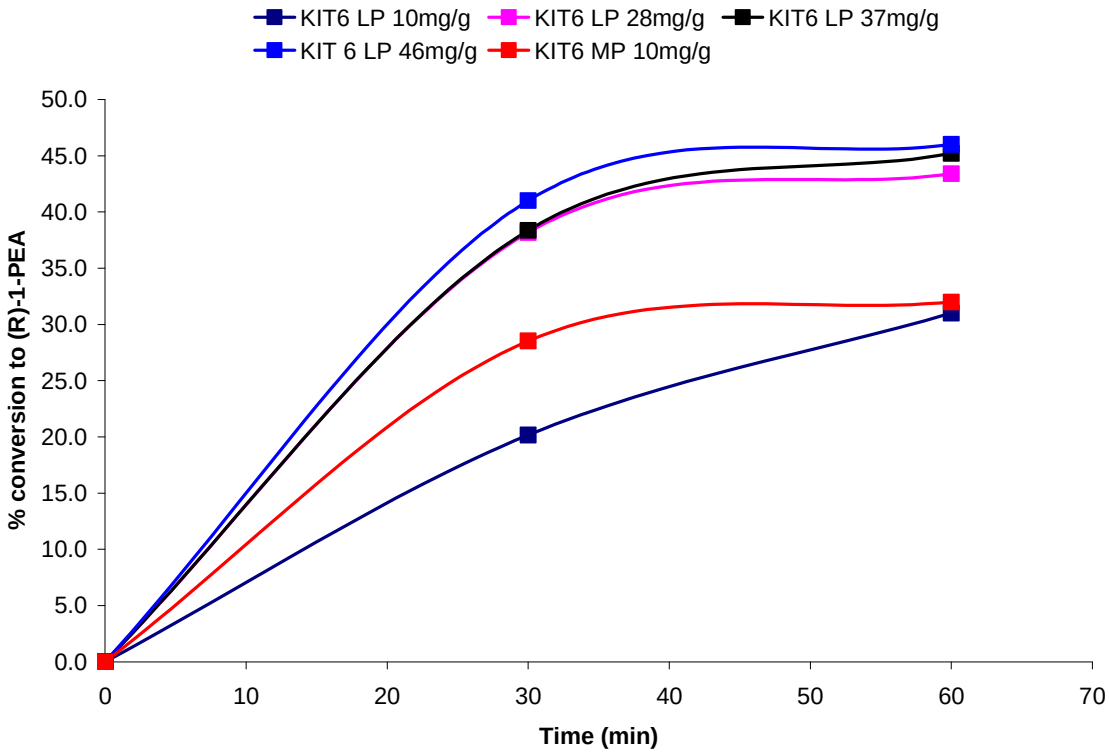

Figure 5.19 Conversion to *R*-1-PEA by KIT-6 supported CALB

5.7.4 Thiol functionalised KIT-6 material

Thiol-functionalised KIT-6 was also used as a support for CALB at different loadings as shown in Table 5.19 and Figure 5.20. These give conversions at 30 minutes similar to those observed for unfunctionalised KIT-6.

Table 5.19 CALB at higher loading on 5% thiol functionalised KIT-6

Loading mg/g	Time min	(*R*)-1-PE %	(*R*)-1-PEA %	Rate $\mu molmin^{-1}g^{-1}$
9.9	30	20.8	28.2	235
9.9	60	15.5	33.4	
16.4	30	21.8	27.2	226.7
16.4	60	16.8	32.4	
24.0	30	19.8	29.1	242.5
24.0	60	13.4	35.5	

30.4	30	14.2	35.1	292.5
30.4	60	13.0	37.0	
32.0	30	12.1	37.1	309.2
32.0	60	9.9	39.8	

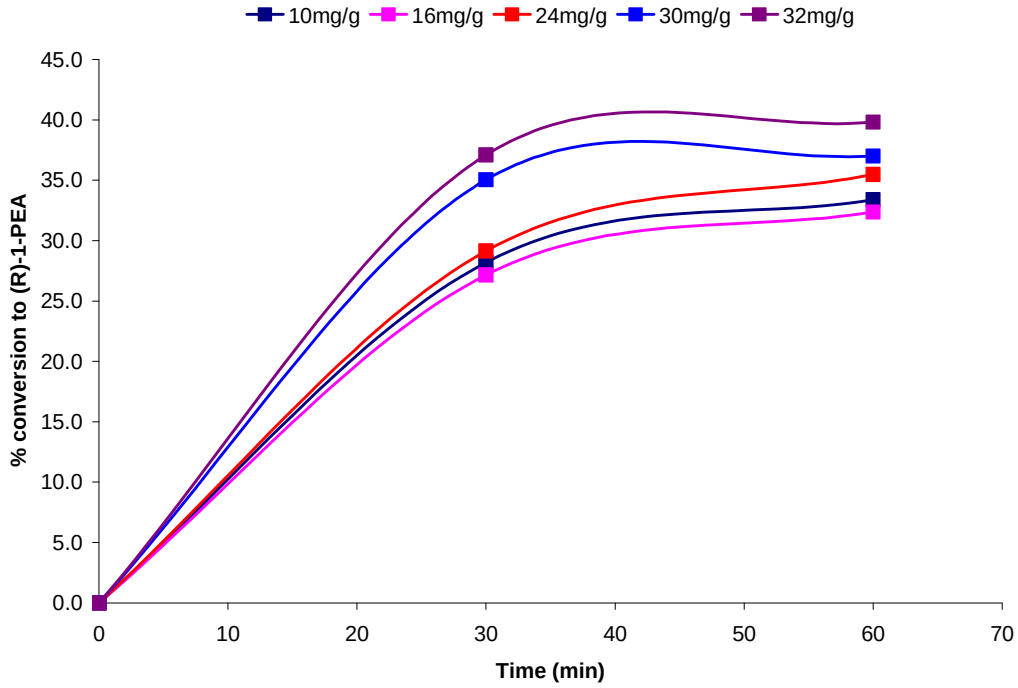

Figure 5.20 Conversion to *R*-1-PEA by 5% thiol functionalised KIT-6 supported CALB

5.7.5 Re-usability – Functionalised large pore KIT6

After the enzyme loaded support has been used to catalyse the transesterification reaction it is possible to centrifuge the sample, remove the solvent and wash the remaining solid with 1-propanol and MBTE. The transesterification can then be repeated with the addition of 5mL of fresh substrate and carried out as many times as required

Large pore KIT-6 material with 5% thiol which had been loaded with a range of differing enzyme concentrations was selected and the reaction was repeated 5 times using the same sample, with washings (as described above) carried out in between.

As can be seen Figure 5.21 even after catalysing the transesterification of 1-phenylethanol in five sequential 5 mL portions of substrate the same 100mg of enzyme loaded sample retains the same activity and produces consistent rates for each different enzyme loading.

This shows that the immobilised enzyme is bound tightly to the solid and does not lose any activity and so can be re-used many times.

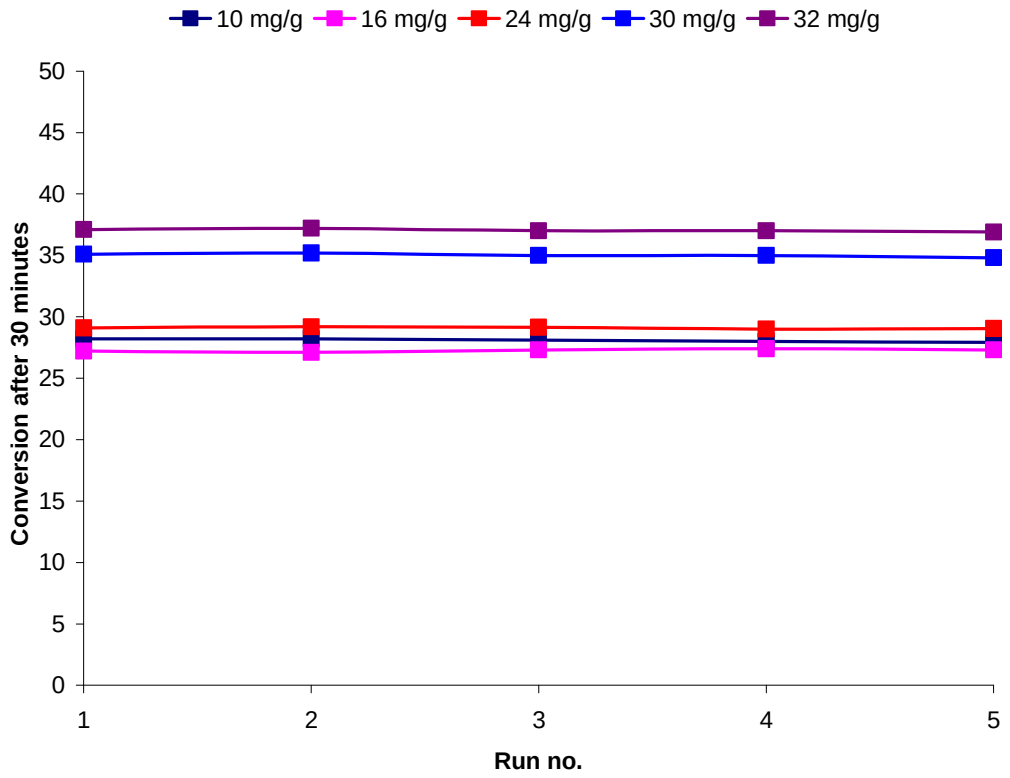

Figure 5.21 Reusability of thiol functionalised KIT-6 at varying CALB loadings

5.7.6 Increasing the thiol content of FDU-12 material

Large pore FDU-12 materials which have been synthesised with varying mol % thiol can be compared. The conversion rates after 30 and 60 minutes for these materials can be seen in Table 5.22.

Table 5.22 Effect of changing pore size and % thiol on conversion

Sample	Loading mg/g	Time min	(*R*)-1-PE %	(*R*)-1-PEA %	Rate $\mu molmin^{-1}g^{-1}$
2%SH -FDU-12 (15-140)	9.8	30	24.1	21.5	179.2
	9.8	60	14.9	32.3	
5%SH -FDU-12 (15-140)	9.6	30	19.9	29.3	244.2
	9.6	60	14.6	34.5	

7%SH -FDU-12 (15-140)	10	30	16.0	37.1	309.2
	10	60	11.2	38.1	

Following the % conversion rates for these 3 materials we can see in Figure 5.22 that after one hour that all three samples have converted a similar % of R-1-phenylethanol to R-1-phenylethyl acetate with values of 30-36% conversion. The main difference with these materials is the conversion after 30 minutes and the more noticeable difference in rate with the 2% thiol material converting 20% whereas the 7 mol% converts more than 35%. The 2% MPTES material shows a similar conversion and initial rate to the large pore KIT-6 material shown in section 5.7.4.

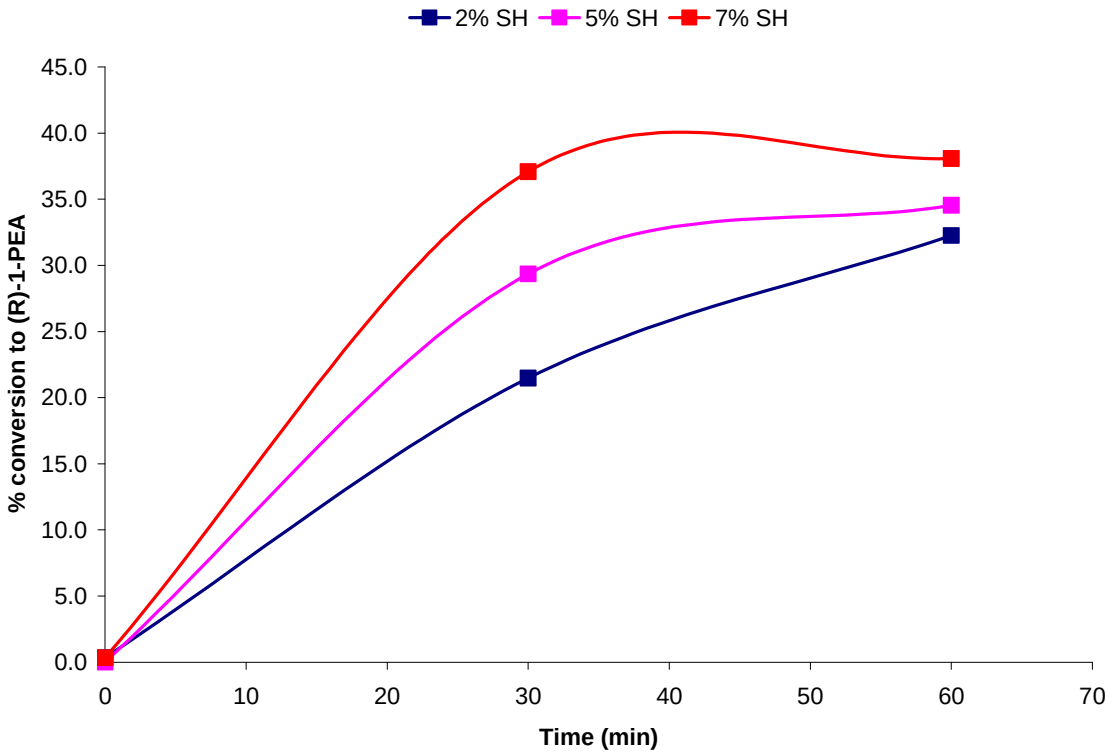

Figure 5.22 Effect of increasing mol % thiol on conversion rate

These three materials (2, 5, 7% thiol) all have a similar CALB loading and have all been extracted to remove the template and so the effect of the rate increase is either from the presence of the thiol groups or associated differences in the pore structure and not by a different loading of enzyme.

The data obtained from the SBA-15, KIT-6 and functionalised FDU-12 material can be seen below in Figure 5.23.

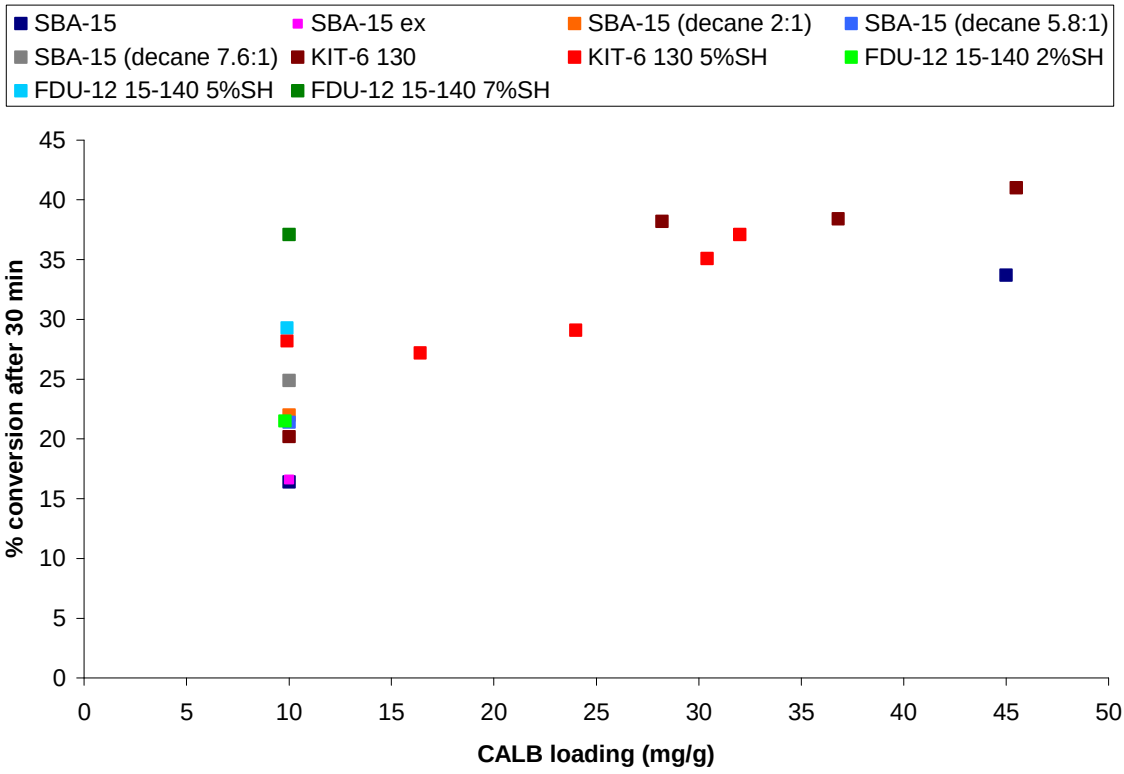

Figure 5.23 CALB loading vs. conversion

It can be concluded from these data that by increasing the loading within the same material an increase in loading increases the conversion and between the different solids differences in morphology and functionality have important effects. Standard SBA-15 is less efficient as a support, but increasing the external surface area and decreasing the particle size has a positive effect. KIT-6, with 3D connectivity appears to be more effective as a catalyst than standard SBA-15, but the effect is small and within the range of variability between samples. FDU-12 with different thiol contents shows very different initial conversion rates, suggesting that the pore structure itself is not the rate limiting factor.

5.7.7 FDU-12 with variable loading of CALB

Two further series of transesterification reactions were performed, on a large cage FDU-12 (15-140) material and its thiol-functionalised analogue, FDU-12 (15-140) 5%SH. Due to limited availability of these mesoporous substrates only 50 mg of supported catalyst were used in these experiments, although the quantities of substrate and solvent were kept the same. The loadings of CALB were from 10-33 mg/g for FDU-12 (15-140) and 10 – 42.5 for FDU-12 (15-140) 5%SH. Plots of the conversion and tabulated results are given below, Figures 5.24 and 5.25, Tables 5.20 and 5.21, and a combined plot is given in Figure 5.26 for conversions after 30 minutes.

Table 5.20 CALB at higher loading on FDU-12 15-140

Loading mg/g	Time min	(*R*)-1-PE %	(*R*)-1-PEA %
10	15	36.5	11.4
10	30	28.5	20.5
19	15	22.8	25.6
19	30	15.9	31.8
27	15	18.9	30.1
27	30	14.2	35.5
32	15	13.0	35.8
32	30	8.1	40.7
33	15	11.1	37.4
33	30	6.9	41.7

By increasing CALB loading using FDU-12 as a support we observe an increase in the rate of the conversion, as shown in Figure 5.21. There is a clear difference when the loading is doubled from 10 to 20 mg/g, followed by smaller increases in rate and conversion. The initial rate is also seen to triple as the CALB loading is increased to 33 mg/g.

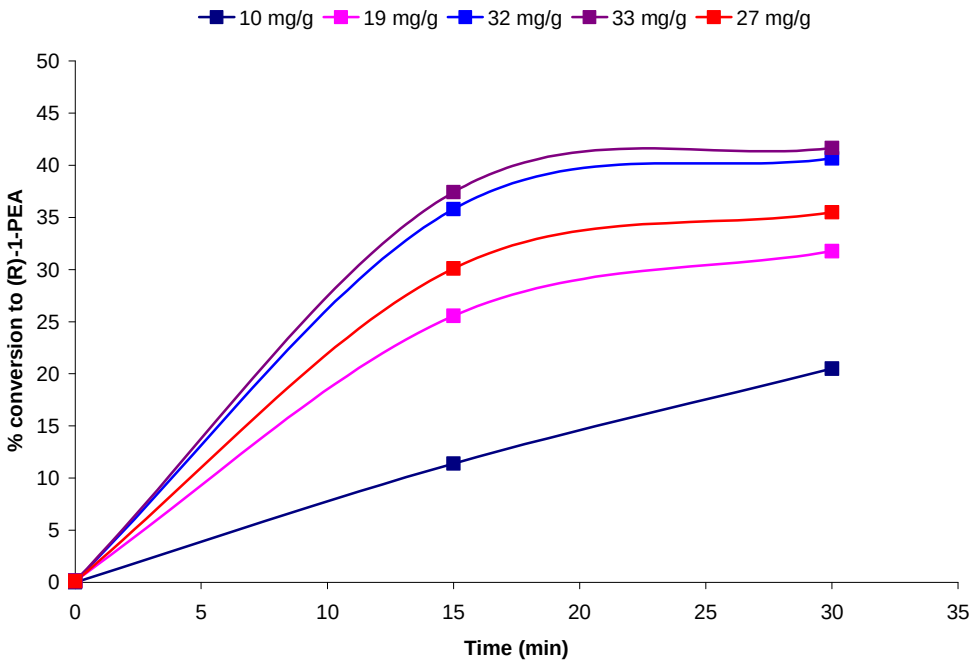

Figure 5.24 Conversion to *R*-1-PEA by large pore FDU-12 supported CALB

5.7.8 Thiol functionalised FDU-12

A series of functionalised large pore FDU-12 materials with increasing enzyme loading were also measured and the conversion calculated (Table 5.21).

Table 5.21 Conversion to *R*-1-PEA by 5% thiol functionalised FDU-12 15-140 material

Loading / mg/g	Time / min	(*R*)-1-PE / %	(*R*)-1-PEA / %
10	15	26.8	22.1
10	30	21.4	26.9
20	15	17.2	31.3
20	30	12.4	36.5
29.4	15	11.9	36.8
29.4	30	8.2	40.5
38.4	15	9.9	35.9
38.4	30	8.9	39.7
42.5	15	10.6	38.0
42.5	30	6.3	42.2

Figure 5.25 shows the effect of increasing the enzyme loading on the conversion measured after 15 minutes and an increase in conversion is observed as the loading is increased from 10 to 20 mg/g and again as it is increased to almost 30 mg/g. At this point a slight increase in conversion after 30 minutes is observed and in the case of material with a loading greater than 20 mg/g no clear increase in the conversion is seen if the reaction is allowed to continue to 30 minutes indicating that the reaction takes place within the first 15 minutes followed by a further slow conversion of the final phenyl ethanol to *R*-1-phenylethyl acetate.

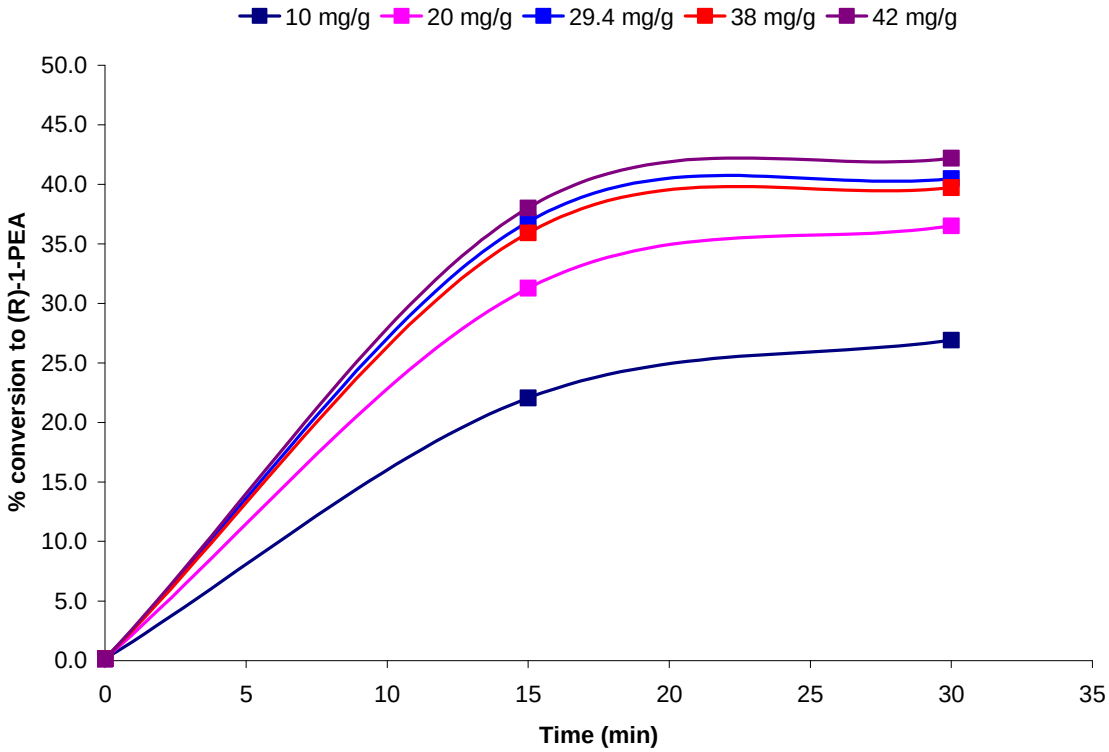

Figure 5.25 Conversion to *R*-1-PEA by 5% thiol functionalised large pore FDU-12 supported CALB

The FDU-12 materials can be compared in terms of enzyme loading and subsequent activity as shown in Figure 5.26. There is a slight difference between the two materials with the unfunctionalised FDU-12 showing a more closely linear trend in terms of increasing enzyme loading and subsequent initial rate. The functionalised FDU-12 material also exhibits a linear trend at lower enzyme loadings and show activity which is higher than the non functionalised material but as higher CALB loadings are reached no additional increase in rate is observed.

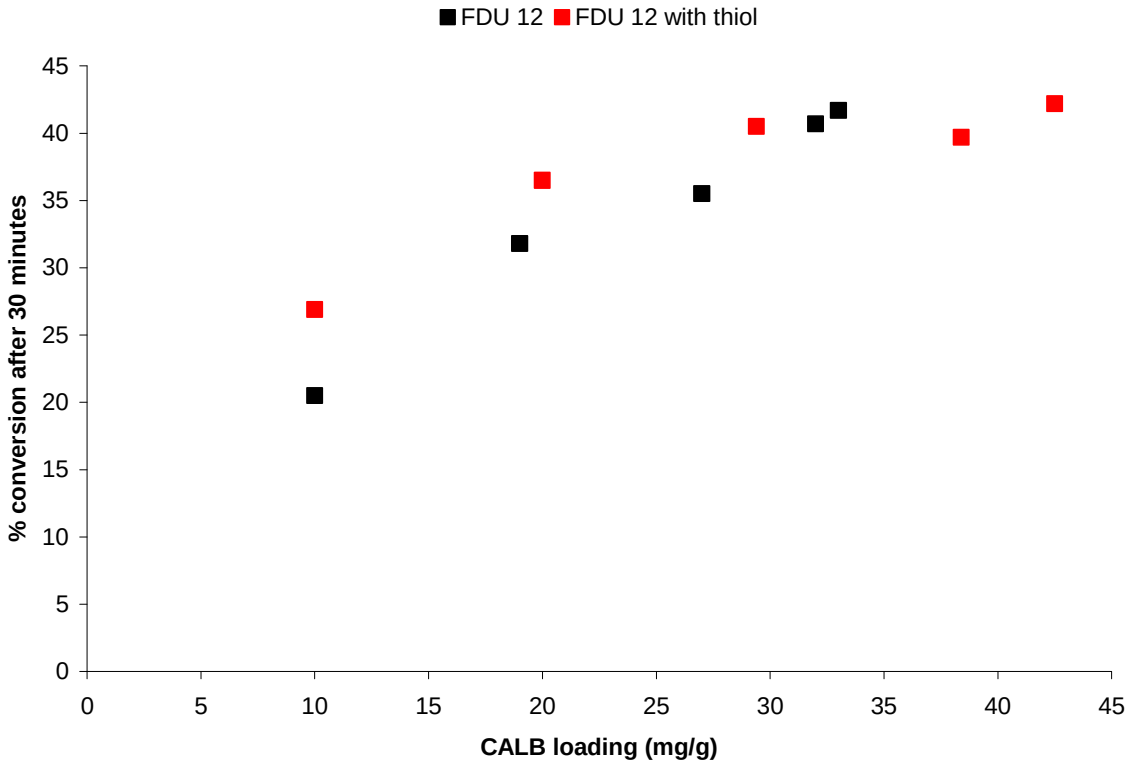

Figure 5.26 CALB loading vs. Initial conversion for FDU-12 and functionalised material

There is a clear increase in conversion with loading, as expected, but only a small difference in behaviour between the two sets of samples. At higher loading the reaction has already reached close to the complete conversion, so that initial rates will be strongly underestimated. It is noteworthy that high conversions are obtained with the reduced amount of catalyst, giving similar values to those observed previously with KIT-6 materials (figure 5.20 and 5.21). To understand the detailed kinetics of this reaction, and to separate the effects of diffusion and adsorption of substrate and product molecules through and onto the mesoporous solid from the reaction rate at the enzyme active site, a much more detailed chemical engineering study is required.

5.8 Conclusions

The mesoporous materials described in chapter 3 provide good support materials for the immobilisation of CALB with relatively fast uptake of enzyme and varying capacities. The enzyme is immobilised within the pore system, rather than on the surface, as shown by the low uptake of CALB by as-prepared materials. The uptake of CALB on both calcined and extracted SBA-15 proceeds readily, with 90% uptake of offered loadings of 50 mg/g in 24 hours. For the materials prepared in the presence of decane, the nanoparticulate SBA-15 readily takes up 10 mg/g when offered whereas the 'onion-ring' structures prepared in the presence of decane and thiol take up little CALB, even when calcined (and porous to nitrogen). The cubic Ia-3d 'STA-11' type material prepared via a low temperature (15 ^{o} C) synthesis gave excellent uptake properties, as expected on the basis of its channel structure (diameter 8 nm).

In the case of KIT-6, which also has the Ia-3d structure, but is prepared via a different route to STA-11, the uptake of CALB on the calcined form is efficient with similar uptake to that seen for SBA-15 at loadings of 50 mg/g. For the propylthiol-functionalised solid, the uptake of CALB is reduced, indicating that the addition of propyl thiol groups to the pore walls results in a decrease in pore size reducing the available pore space for immobilisation to take place. The stronger interaction with thiol groups could also retard the uptake. FDU-12 materials are prepared with 33 to 42.5 mg/g CALB, according to their method of preparation.

It has been previously shown that immobilised CALB is active for the enantioselective acylation of (*R*)-1-phenylethanol to (*R*)-1-phenylethyl acetate, without loss of selectivity upon binding. The activity of CALB immobilised within mesoporous silica shows a significantly higher activity when compared to free enzyme.

Using calcined SBA-15 as a support (CALB at 10 mg/g) the reaction almost goes to completion within 24 hours under the conditions used and a faster initial rate of reaction is observed for CALB immobilised on extracted SBA-15. Extracting the material leads to incorporation of hydrophobic groups which are expected to improve the rate of substrate diffusion through the support. By increasing the CALB loading a faster conversion of (*R*)-1-phenylethanol to (*R*)-1-phenylethyl acetate is seen.

Studies on KIT-6 demonstrate that by increasing the CALB loading a faster conversion with a 45 mg/g loading is observed, resulting in a conversion of 46% after 1 hour, close to the maximum 50% conversion possible. There appears to a point at which increasing the CALB loading has no effect on increasing the rate of reaction and this occurs at approx 30 mg/g. A similar trend is seen for propylthiol-functionalised KIT-6 material although at lower CALB loading a faster conversion is observed.

The reusability of the 5% thiol support is very good at all loadings of CALB, from 10 to 32 mg/g, which all show very little loss in activity after 5 uses.

FDU-12 materials show a similar increase in rate of conversion as the CALB loading is increased. Standard SBA-15 is less efficient as a support, but increasing the external surface area and decreasing the particle size has a positive effect. KIT-6, with 3D connectivity appears to be more effective as a catalyst than standard SBA-15, but the effect is small and within the range of variability between samples. FDU-12 with different thiol contents shows very different initial conversion rates, suggesting that the pore structure itself is not the rate limiting factor. To fully understand the different processes involved a detailed chemical engineering study is required to examine the effects of transport, adsorption and the rate of reaction.

5.9 References

[1] M. R. Stoner, D. A. Dale, P. J. Gualfetti, T. Becker, M. C. Manning, J. F. Carpenter, T. W. Randolph, *Enzyme Microb. Technol*., 2004, **34**, 114

[2] A. Manjon, J. L. Iborra, A. Arocas, *Biotechnol. Lett*., 1991, **13**, 339

[3] M. Ikunaka, *Catal. Today*, 2004, **96**, 93

[4] S. H. Bhosale, M. B. Rao, V. V. Deshpande, *Microbiol. Rev*., 1996, **60**, 280

[5] C. Lei, Y. Shin, J. Liu, E. J. Ackerman, *Nano Lett*., 2007, **7**, 1050

[6] A. M. Klibanov, *Anal. Biochem*., 1979, **93**, 1

[7] H. H. P. Yiu, P. A. Wright, *J. Mater. Chem.*, 2005, **15**, 3690

[8] A. Schmid, J. S. Dordick, B. Hauer, A. Kiener, M. Wubbolts, B. Witholt, *Nature*, 2001, **409**, 258

[9] R. A. Sheldon, *Adv. Synth. Catal*., 2007, **349**, 1289

[10] M. G. Sankalia, R. C. Mashru, J. M. Sankalia, V. B. Sutariya, *Eur. J. Pharamceut. Biopharamaceut.*, 2007, **65**, 215

[11] M. T. Reetz, *Adv. Mater*., 1997, **9**, 943

[12] M. T. Reetz, A. Zonta, J. Simpelkamp, *Biotechnol. Bioeng*., 1996, **49**, 527

[13] A. C. Pierre, G. M. Pajonk, *Chem.Rev.*, 2002, **102**, 4243

[14] S. Cohen, T. Yoshioka, M. Lucarelli, L. H. Hwang, R. Langer, *Pharm. Res*., 1991, **8**, 713

[15] R. V. Parthasarathy, C. R. Martin, *Nature*, 1994, **369**, 298

[16] X. Zhang, R. F. Guan, D. Q. Wu, K. Y. Chan, *J. Mater. Sci.: Mater. Med*., 2007, **18**, 877

[17] H. Jing, X. F. Li, D. G. Evans, X. Duan, C. Y. Li, *J. Mol. Catal. B: Enzym*., 2000, **11**, 45

[18] J.F.Diaz, K. J. Balkus, *J. Mol. Catal. B: Enzym*., 1996, **2**, 115

[19] H. Ma, J. He, D. G. Evans, X. Duan, *J. Mol. Catal. B: Enzym*., 2004, **30**, 209

[20] Y-J. Han, J. T. Watson, G. D. Stucky, A. Butler, *J. Mol. Catal. B: Enzym*, 2002, **17**, 1

[21] H. H. P. Yiu, P. A. Wright, N. P. Botting, *J. Mol. Catal. B: Enzym*., 2001, **15**, 81

[22] H. H. P. Yiu, P. A. Wright, N. P. Botting, *Microporous mesoporous Mater*., 2001, **44**, 763

[23] H. Takahashi, B. Li, T. Sasaki, C. Miyazaki, T. Kajino, S. Inagaki, *Chem. Mater*., 2000, **12**, 3301

[24] J. Uppenberg, N. Ohrner, M. Norin, K. Hult, G. J. Kleywegt, S. Patkar, V. Waagen, T. Anthonsen, T. A. Jones, *Biochemistry*, 1995, **34**, 16838

[25] J. Uppenberg, M. T. Hansen, S. Patkar, T. A. Jones, *Structure*, 1994, **2**, 293

[26] H. Frykman, N. Ohrner, T. Norin, K. Hult, *Tetrahedron Lett*., 1993, **34**, 1367

[27] V. Waagen, I. Hollingsaeter, V. Partali, O. Throstad, T. Anthonsen, *Tetrahedron-Asymmetry*, 1993, **4**, 2265

[28] G. Ping, J. M. Yuan, Z. F. Sun, Y. Wei, *J. Mol. Recognit.*, 2004, **17**, 433

[29] R. Ravindra, Z. Shuang, H. Gies, R. Winter, *J. Am. Chem. Soc*., 2004, **126**, 12224

[30] J. M. Moreno, J. V. Sinisterra, *J. Mol. Catal.*, 1994, **93,** 357

6. Drug delivery

6.1 Introduction

Mesoporous materials possess high surface areas, up to 1000 m^2/g, have adjustable pore sizes from 2-16 nm, a homogeneous pore structure and a high pore volume of up to 2.5 cm^3/g. A range of mesoporous silicas have been synthesised by different groups in the last 15 years including the MCM, SBA, MSU, FDU, KIT and STA series. All exhibit a variety of features which suggested their potential use as drug delivery systems, first examined with MCM-41 **[1]**. Typically drug administration via oral methods leads to an increase in drug concentration in the plasma followed by a decrease which shows a saw-tooth pattern as a function of time. Using a material which provides a controlled, sustained release is advantageous as the drug levels in the plasma would be kept more closely constant and lead to a more beneficial treatment. This initial work utilising MCM-41 as a drug delivery system for Ibuprofen has led to over 250 publications in the area of mesoporous materials and their use as drug delivery systems as shown in Figure 6.1.

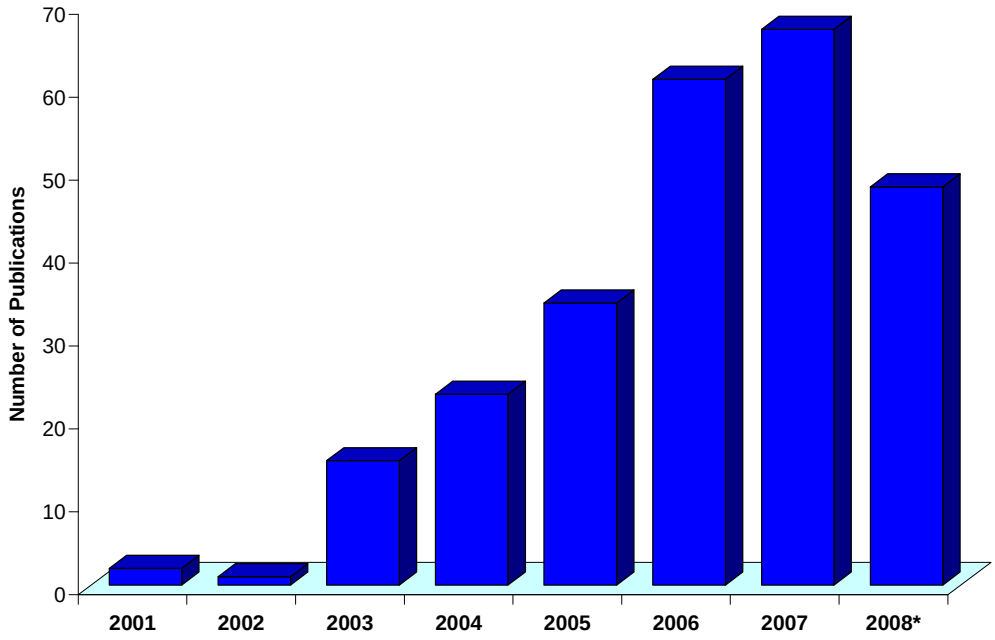

Figure 6.1 Statistics on recent publications in silica-based ordered mesoporous materials as drug delivery systems using Web of Science (ISI web of Knowledge [SM]) *2008 (results as of June 2008)

Mesoporous materials have two main uses as ceramic matrices; for bone tissue regeneration and as drug delivery systems **[2-4]**. Porous solids would be ideal if they could be designed as hosts for controlled and sustained release of drug molecules, some of which can be seen in Figure 6.2.

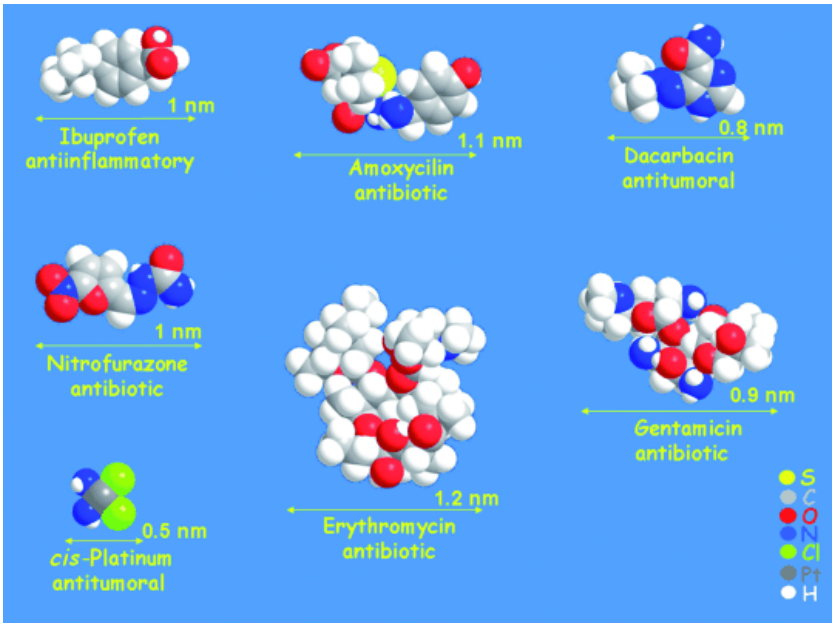

Figure 6.2 Molecules of several drugs with their sizes [5]

This could provide a material which could not only act as an implant for bone repair but also allow targeted delivery of drugs to prevent inflammation or infection after its insertion.

A drug delivery system (DDS) is said to be a framework structure which has the ability to control the rate and period of drug delivery (time-release dosage) and target a specific area of the body **[4]**. Unlike previous drug delivery methods a drug delivery system is designed to maintain desired drug release levels throughout the treatment period and prevent a saw-tooth release curve.

Much work has been carried out into the design of materials for DDSs by the Vallet-Regí research group **[4-6]**. They have investigated the effects of varying structure directing agents on MCM-41 and the adsorption and release of Ibuprofen and observed that the larger pore material released a higher percentage of the loaded drug. Increasing the pore size between 2.5 and 3.6 nm shows an increase in release rate which confirms that pore size is key in controlling drug delivery. This trend is not restricted to 2D hexagonal

structures but can also be seen in cubic 3D materials including MCM-48, as seen for Ibuprofen in Figure 6.3 and Erythromycin in Figure 6.4.

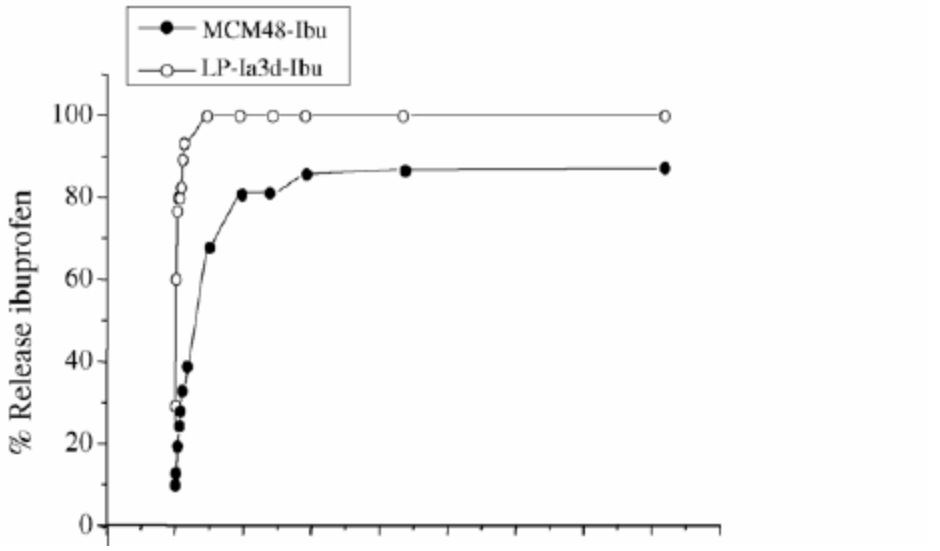

Figure 6.3 Erythromycin % release from MCM-48 and a large pore Ia-3d structure [7]

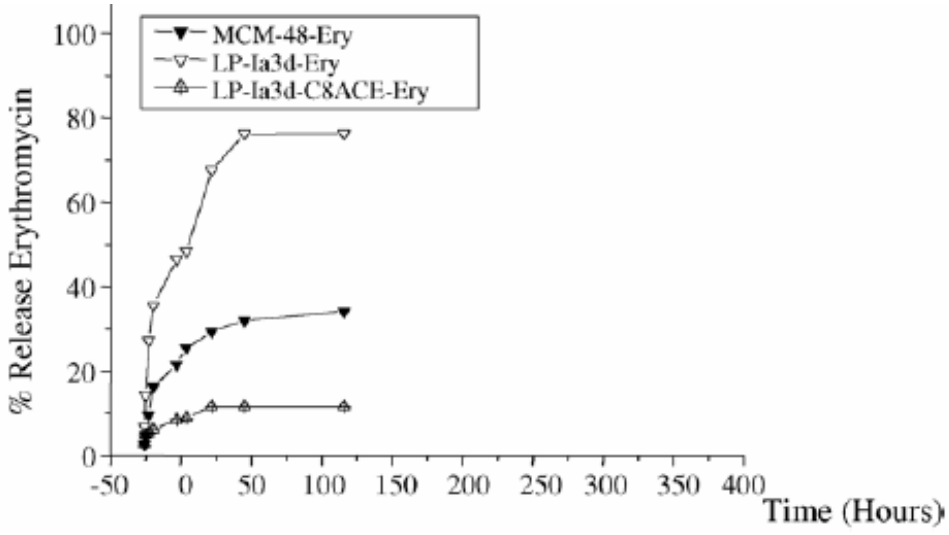

Figure 6.4 Ibuprofen % release from MCM-48 and a large pore Ia-3d structure [7]

For both drug molecules used in the release studies, Ibuprofen and Erythromycin, the larger pore Ia-3d materials exhibit a faster drug release profile than their small pore analogues **[7]**. Increasing the molecular size of the drug reduces the rate of release.

The adsorption and desorption behaviour of drug molecules on the mesoporous materials is determined not only by pore size but also by surface area. As long as the pore size is sufficient for ready adsorption of the molecules, then a higher surface area shows a higher

loading. Comparisons have been made between MCM-41 and SBA-15, which both possess the same 2D hexagonal structure and have surface areas of 1157 and 719 m^2/g respectively **[4]**. Alendronate was loaded into both materials and although MCM-41 has a smaller pore size, the increased surface area means that a maximum loading of 139 mg/g was achieved compared to 83 mg/g for SBA 15. This demonstrates that as long as the pore sizes of both materials are large enough to take in the drug molecule that surface area plays an important role in the total loading, indicating a strong surface attraction of the monolayer.

Incorporating the drug molecules into a mesoporous material is a very important aspect of the DDS. The most common method used is soaking the material in a concentrated drug solution which relies on the adsorptive properties of mesoporous materials and therefore pore size plays a key role **[5]**. By adding calcined mesoporous material to an aqueous solution this will promote the regeneration of OH groups on the pore walls which can then be used to bind to drug molecules as shown in Figure 6.5.

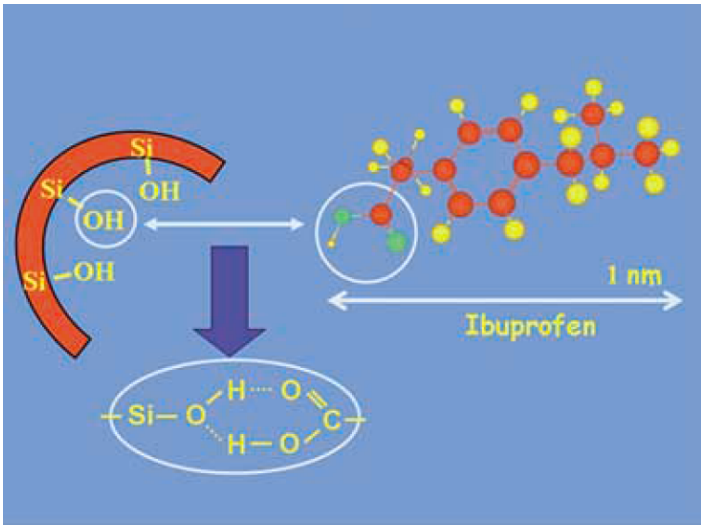

Figure 6.5 Interaction of the OH group of the silanol at the pore wall of the silica mesoporous material with the COOH group of the Ibuprofen

Controlling the release rate has been achieved by functionalising the large pore Ia-3d material with hydrophobic octyl hydrocarbon moieties which decreases the rate of release by a factor of 6 compared to that observed in calcined large pore Ia-3d material.

Andersson *et al.* **[8]** have studied drug adsorption and release characteristics of 2D hexagonal materials, MCM-41 and SBA-3 and the micellar cubic structure SBA-1 where cavities are connected through smaller windows. Their study focuses on additional parameters affecting the kinetic release including pore dimension, connectivity, and

geometry. They conclude that the presence of the one dimensional cage-like pore structure in SBA-1 is beneficial for a slow controlled release of Ibuprofen.

In addition to increasing the pore sizes of these materials, studies have been carried out into the functionalisation of the surface as a strategy for controlling drug delivery patterns. SBA-15 can be functionalised with alkyl chains **[9]** of varying lengths which increases the hydrophobicity of the materials and slows down the rate of degradation. A reason for this has been suggested by Otsuka *et al.*, in that the affinity between the drug adsorbed and the silica surface increases due to the addition of octadecyl chains.

6.1.1 Functionalisation for drug release

One of the most important features in the development of silica mesoporous materials for use as DDS is the functionalisation of the surface using organic groups. This is key to a controlled release of drug molecules and the high density of Si-OH groups provides scope for the grafting of functional groups using organic silanes ($(RO)_3SiR'$). Groups such as amines, thiols, carboxyls and chlorides can be used to link to drug molecules such as Gentamicin **[10]**, Ibuprofen **[7]**, bisphosphonates (as shown in Figure 6.6) **[11]**, Amoxicillin **[12]** and Erythromycin **[7, 9]** through ionic bonding or ester groups.

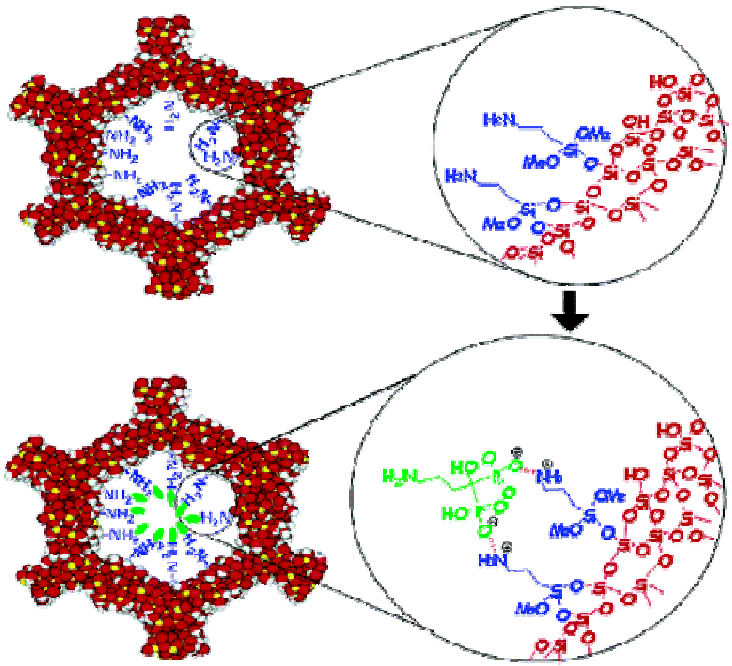

Figure 6.6 Alendronate adsorption on hexagonally ordered mesoporous silica functionalised with propylamine groups [11]

The group of Vallet-Regí has reported the functionalisation of MCM-41 and SBA-15 with amino groups to control Ibuprofen release **[13]**. Here it is the electrostatic interactions between the Ibuprofen carboxyl groups and the amino groups on the surface of the mesoporous material which have been confirmed by NMR spectroscopy.

There is still debate as to which method of functionalisation is preferred, post-synthesis or *in situ* functionalisation, with post synthesis functionalisation after template removal being reported to give better results by the groups of Vallet-Regí and Song **[14, 15]**. However *in situ* functionalisation using a co-condensation method leads to a higher degree of order and more uniform functional group distribution compared to post-synthesis or solvothermal methods **[16,17]**.

Rather than functionalising the surface in order to increase drug-surface interactions and bonding it is also possible to functionalise with hydrophobic species. Instead of binding specifically to the drug molecule the hydrophobicity of the surface impedes the drug release from the material *via* weaker dispersive interactions. This is believed to be important in the interaction of thiols with proteins (G. M. Smith, PhD Thesis, University of St Andrews 2008).

6.1.2 Drug loading

Impregnation of materials with drug molecules is the most common method of drug loading. This is carried out by adding the mesoporous material, in powder or compact form, to a solution of drug of known concentration. Various methods of loading and release have been studied including loading the drug into powdered material and releasing also from powder form **[10]**. Alternatively the loading can be carried out onto powder that is subsequently pressed into discs using uniaxial and isostatic pressure **[1]**. Finally, loading and release can be carried out on pre-pressed pieces of compacted material. The difference in the type of material used for loading and release is reflected by the results with the powder material having the highest drug loading due to the more accessible channel network. When the material is compressed the release is much slower which can be attributed to either narrowing or closing of pores which prevents the drug molecules from leaving as rapidly and can prevent release of all the drug loaded. Factors such as pH, temperature, drug solubility, size and polarity must be considered when loading drug molecules. If polar drug molecules such as Amoxicillin are to be adsorbed into a silica matrix, for example, then a polar solvent must be used, such as water, and conversely if a

non-polar drug like Ibuprofen is used then an apolar solvent, for example hexane, is required.

6.1.3 Analysis of drug loading

Several methods are used to determine whether or not drug loading has been successful. Nitrogen adsorption can be carried out on the materials before and after loading, indicating if there has been a reduction in surface area and pore volume due to the occupation of the channels and cavities by the drug molecules. For example when Ibuprofen has been loaded onto MCM-41 we see a reduction of surface area and pore volume from 1157 m^2/g and 0.98 cm^3/g to 688 m^2/g and 0.39 cm^3/g respectively **[1]**. This trend is repeated for other mesoporous materials and drug molecules.

Difficulties arise when characterizing mesoporous materials using typical powder diffractometers because only a few broad reflections are produced and at very low scattering angles. XRD is useful however, to confirm highly ordered mesoporous structures before and after drug loading.

6.1.4 Using larger drug molecules e.g. proteins

When the guest molecules are in the region of 1-2 nm, for example Ibuprofen **[1]** and Alendronate, then the mesoporous material used as a host matrix need only have pore sizes sufficient to adsorb these molecules. If we want to expand the range and size of molecules that can be taken up by mesoporous materials, for example proteins, then we need to look at methods of enlarging pore diameters **[18-26]**.

Serum Albumins are major components of plasma proteins present in humans and many mammals and are assembled from a single amino acid chain. One protein in this family is of particular interest, Bovine Serum Albumin (BSA) **[27,28]** as it has the ability to carry many drugs to sites of pharmacological action. It is an order of magnitude larger than common drug molecules (Ibuprofen) with an approximate size being 10 nm in length and 6 nm width (Figure 6.7).

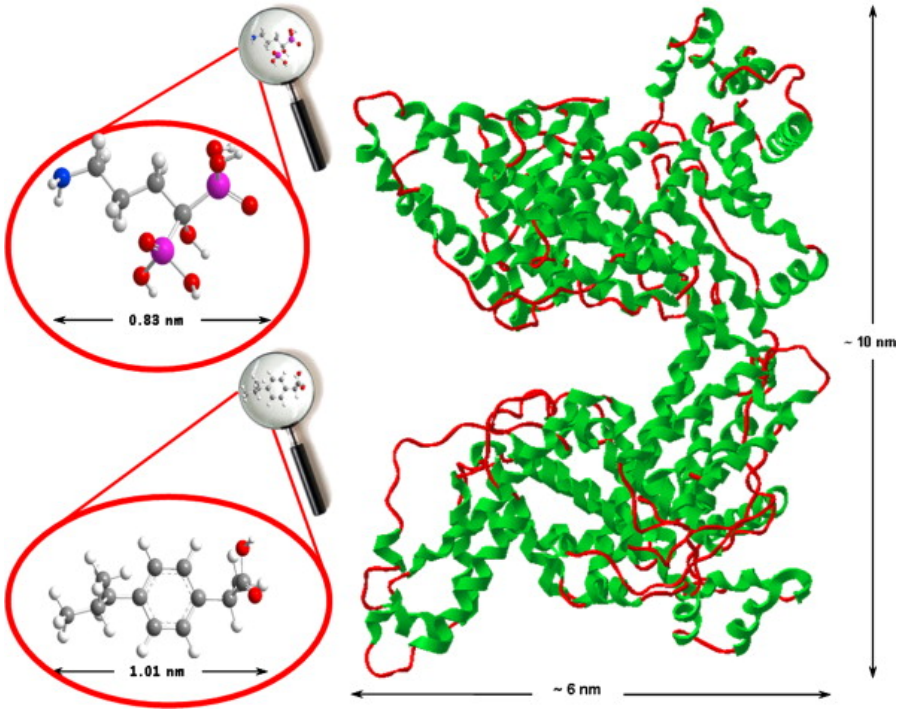

Figure 6.7 Comparison in size between Alendronate (0.83 nm), Ibuprofen (1.01 nm) and BSA (6 nm) [29]

Typical syntheses of SBA-15, MCM-41 and MCM-48 give materials with pore sizes (ca. 4 nm) that are not large enough for the uptake of BSA. Methods have been developed for the tailoring of pore sizes of varying different materials including adding a swelling agent **[19]**, using surfactant blends **[23,24]** increased hydrothermal treatment time, changing both the hydrolysis and hydrothermal temperature **[30]**. Also using a mixture of surfactants has been shown to increase pore size and provide the opportunity to fine tune the pore size on a nanometre level.

Studies have been carried out with BSA on SBA-15 material with pore diameter ranging from 8.22 to 11.4 nm, both with and without functionalisation with amine groups **[29]**. The increase in pore size and subsequently mesopore volume is carried out by extension of the hydrothermal treatment time from 1 d to 7 d. The largest pore diameter was achieved after 7 d and the highest pore volume after 3 d. Functionalisation of the pore walls decreased the pore diameter in relation to the length of the functional group used.

Upon increasing the pore diameter the amount of protein loading also increased, as shown in Figure 6.8. For amine-modified SBA-15 a similar trend can be observed. The presence of amine groups on the pore walls (which can interact with the amide groups of the BSA) increases the tendency of the mesoporous material to retain the protein within the pores.

Functionalising the surfaces for protein adsorption post synthesis reduces pore size and volume, so a material with a sufficiently large pore diameter must be used so that when the pore size is reduced by the additional groups it is still large enough to allow the protein to pass freely in the channels.

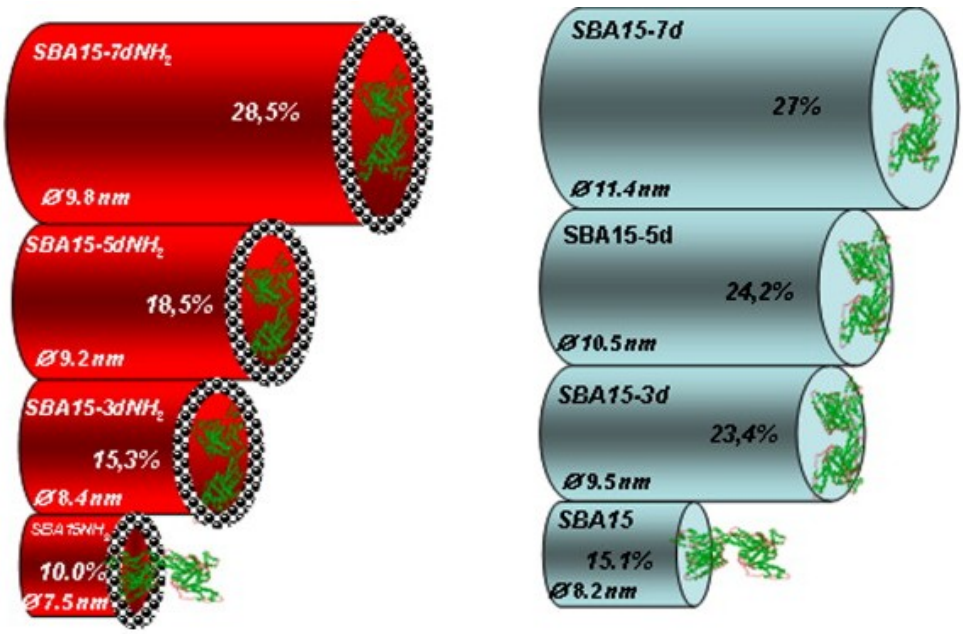

Figure 6.8 Loading of BSA on pure silica SBA-15 and amine-functionalised SBA-15 with increasing pore sizes [29]

Release of the protein from mesoporous materials is very dependent on the pore size and functionalisation of the surface as shown in Figure 6.9. With pure siliceous materials a sharp burst of release can been observed with 90% of the adsorbed material being released in the first 24h and the remaining protein is released linearly until complete delivery after 192h. In comparison when the material has been functionalised the release is never complete and the % release varies between 25% for functionalised SBA15 with pore size 7.5 nm and 9.8 nm to 60% release for functionalised materials with pore sizes of 8.4 and 9.2 nm.

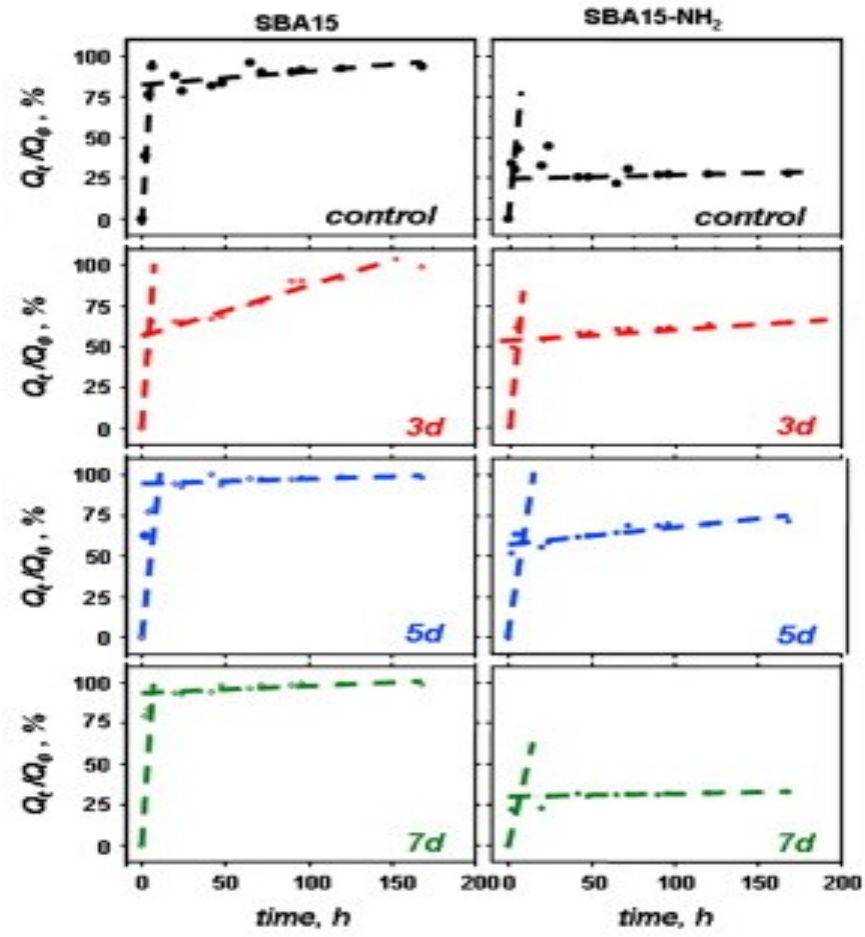

Figure 6.9 Dependence of mesopore diameter and amine functionalisation in the release of BSA from pure silica SBA-15 and amine functionalised SBA-15 ordered mesoporous matrices, shown as protein released versus time as a function of the total protein loaded

These studies using mesoporous materials for protein adsorption open up the field for further research in this area, with the possibilities of using different mesoporous materials to try and control the release rate. One possibility of using large proteins such as BSA in drug delivery is to add peptides into the globular structure of BSA for delivery to a particular living tissue.

6.2 Drug release Materials

A series of KIT-6 and FDU-12 materials was prepared in as-prepared, calcined, extracted and thiol-functionalised form (synthesis described in chapter 3).

The samples used in this study are shown below in table 6.1.

Table 6.1 Samples used for drug delivery study

Synthesis	Functional group	Channel/Cage diameter (nm)	Window size (nm)	Template removal	Abbreviation used
KIT-6		7	6	calcined	K100C
KIT-6		/	/	as prepared	K130AP
KIT-6		9	8	extracted	K130EX
KIT-6		9	8	calcined	K130C
KIT-6	5% thiol	6.5	6	extracted	K130FEX
KIT-6	5% thiol	/	/	as prepared	K130FAP
FDU-12		16	10-12	calcined	F15-140C
FDU-12	5% thiol	12	8-10	extracted	F15-140FEX
FDU-12		10	8	calcined	F50-140C
FDU-12	5% thiol	12-16	12	extracted	F50-140FEX

6.2.1 KIT- 6 materials

Two KIT-6 materials were prepared with different channel diameters, a medium pore sample and larger pore sample with channel diameters of 6 and 8 nm respectively as determined from the desorption branches of N_2 adsorption isotherms and therefore a minimum estimate. TEM images of these materials can be seen in Figure 6.10 showing an ordered porous material and in the case of the larger pore material the cubic Ia-3d morphology can be observed.

A functionalised version of the large pore material was prepared using thiol to functionalise the surface, which causes a decrease in the pore diameter to 6.5 nm. Samples were rendered porous by either extraction or calcination and compared in drug delivery experiments with as-prepared material where no template removal step was used.

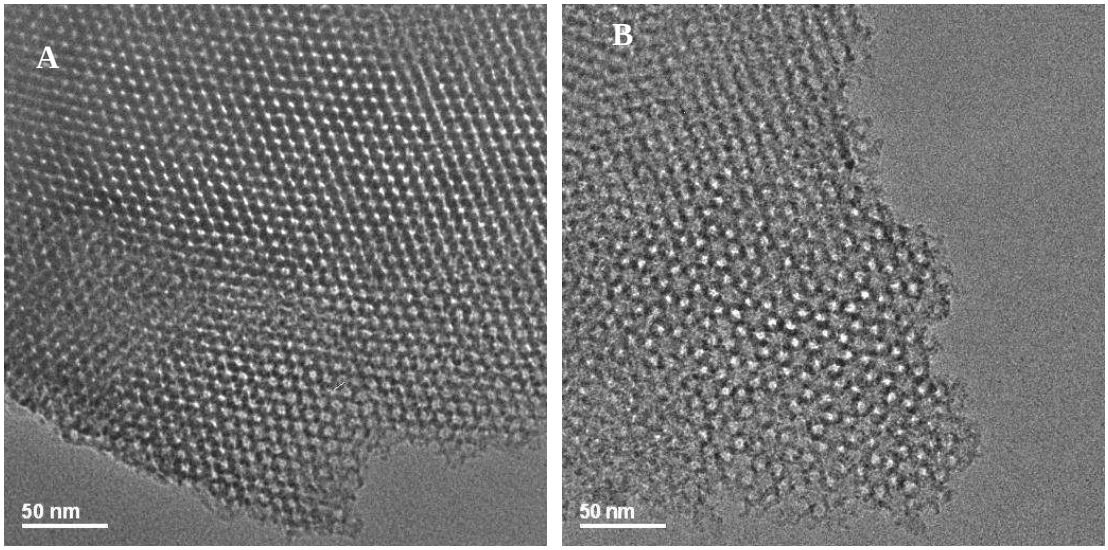

Figure 6.10 Medium and large pore KIT-6 synthesised at 100 °C (A) [110] axis view and 130 °C (B) [111] axis view

6.2.2 FDU-12 Material

FDU-12 with space group Fm3m and containing cages connected by necks/channels was prepared (as described in chapter 3). Four samples were chosen for examination using two different synthesis temperatures both with and without thiol. A material was synthesised, denoted FDU-15-140, which from nitrogen adsorption data was shown to have cavities of at least 16 nm and windows ranging from 4 to 12 nm, and by looking at TEM images we can see these large pores shown in Figure 6.11. This material can also be functionalised with thiol groups and is shown to retain its ordered porous morphology and pore diameter.

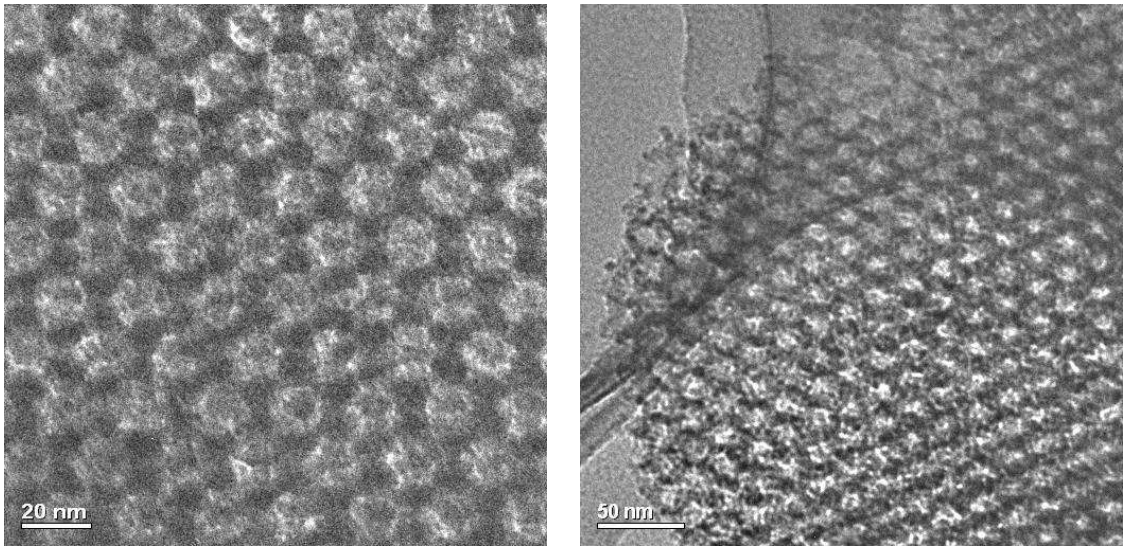

Figure 6.11 FDU-12 (15-140) (A) and thiol functionalised FDU12 (F15-140FEX) (B)

By increasing the hydrolysis temperature from 15 to 50 ^{o}C it is possible to synthesise a material of the same morphology (Figure 6.12) but with pores slightly smaller. Upon functionalisation and extraction the adsorption isotherm, shown in chapter 3.7 shows adsorption at a higher P/P_o a therefore a larger pore with windows of 12 nm.

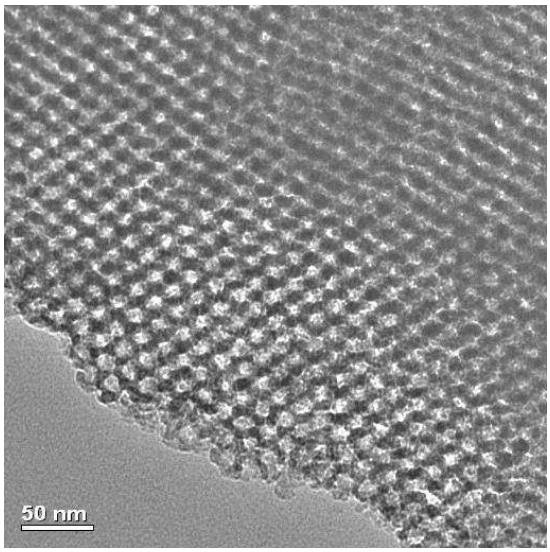

Figure 6.12 FDU-12 (50-140)

6.3 BSA loading and release measurements

Powdered KIT-6 and FDU-12 samples were loaded with BSA (98% Aldrich) by soaking them in a 0.9% saline solution of BSA (200 mg/mL) with continual stirring for 24 h at room temperature **[29]**. This solution was buffered at pH 4.75 using acetic acid and sodium acetate. This pH was chosen as the isoelectric point of BSA is 4.7 and so we will see the greatest interaction and adsorption at this pH. During this loading process it is possible that partial extraction of surfactant may occur as the surfactant may dissolve in the buffer solution. A ratio of 1:8 (by weight) of mesoporous solid:BSA was used. Powder BSA-loaded samples were recovered by centrifugation and left to dry at 37 ^{o}C in a vacuum oven to ensure complete removal of all solvent. 100 mg of BSA loaded samples were compacted into discs (13 mm x 3 mm) as shown in Figure 6.13 under uniaxial pressure (0.5 MPa) followed by isostatic pressure (0.1 MPa).

Fig 6.13 BSA loaded discs (13 mm x 3 mm)

The *in vitro* drug delivery assay was carried out by suspending the sample discs in a 0.9% NaCl solution buffered at physiological pH 7.4 at 37 ^{o}C in an orbital shaking oven, shown in Figure 6.14.

Figure 6.14 Orbital shaking oven: Sample vials indicated by arrow, held in place using an adhesive surface and shaken horizontally.

The BSA concentration in the liquid phase was evaluated by high pressure liquid chromatography (HPLC) using a Waters Alliance 2695 separation module, at 313K oven temperature. The mobile phase consisted of 20 wt % acetonitrile and 80 wt % of water (chromatography water, Aldrich). The flow rate was 1 mL min^{-1} and the injection volume was 10 µL. HPLC results obtained are an average of two pills prepared for each material.

6.4 Characterisation

Materials were characterised both prior to and after drug loading by Fourier transform infrared spectroscopy (FTIR), transmission electron microscopy (TEM), X-ray diffraction (XRD), thermogravimetric analysis (TGA), N_2 adsorption and elemental analysis.

FTIR was carried out on a Nicolet Nexus spectrometer in the range of 4000-400 cm^{-1}. The FTIR spectra were recorded at room temperature on the sample directly. TEM images from calcined KIT-6 and FDU-12 samples were obtained using a JEOL 2011 transmission electron microscope at 200 kV. Thermogravimetric (TG) analysis was performed between 30 and 700 ^{o}C at a heating rate of 5 ^{o}C/min (under gentle flow of air) using a Perkin-Elmer Pyris Diamond TG analyzer. Surface area and pore size were determined from N_2 adsorption/desorption isotherms obtained at -196 ^{o}C on a Micromeritics ASAP2020. For all samples 30-50 mg of material was degassed at 120 ^{o}C for 2 hours under a vacuum

before measuring the isotherms. Elemental analysis was performed on a Macroanalyzer Leco CNS-2000-I.

6.4.1 Nitrogen Adsorption

Nitrogen adsorption measurements were performed on materials before and after BSA loading to determine to what extent the protein was present in the pores (Table 6.2).

Table 6.2 Results obtained from nitrogen adsorption before and after protein loading

Sample	BET m^2/g	Channel or window diameter (nm)	Pore volume cm^3/g	BET m^2/g	Channel or window diameter (nm)	Pore volume cm^3/g (BJH ads)
1. K100C	**638**	**6**	**0.95**	**192**	**7.3**	**0.42**
2.K130AP	**133**	**7.4**	**0.37**	**47.1**	**7.3**	**0.114**
3.K130EX	**451**	**8.2**	**1.07**	**133.48**	**7.5**	**0.304**
4. K130C	**646**	**8.0**	**1.32**	**68.1**	**7.0**	**0.143**
5. K130FEX	**507**	**6.5**	**1.03**	**160.3**	**4.3**	**0.211**
6. K130FAP	**92**	**6.6**	**0.204**	**19.0**	**6.5**	**0.0414**
7. F-15-140C	**380.2**	**10.2**	**0.87**	**83.7**	**10.7**	**0.234**
8. F15-140FEX	**290**	**8.8**	**0.64**	**82.57**	**7.4**	**0.176**
9. F50-140C	**192**	**4.8**	**0.25**	**13.2**	**7.4**	**0.022**
10.F50-140FEX	**348**	**12.9**	**0.96**	**26.9**	**5.8**	**0.038**

Results from table 6.2 showing the effects of BSA loading on BET and pore volume can be seen in graphs (Figure 6.15 and 6.16) and it is clear for all samples that there is a decrease in both surface area and pore volume. It can be seen that in general (with the exception of the as-prepared materials) the surface area and pore volume of the KIT-6 materials are higher than those of the FDU-12 materials.

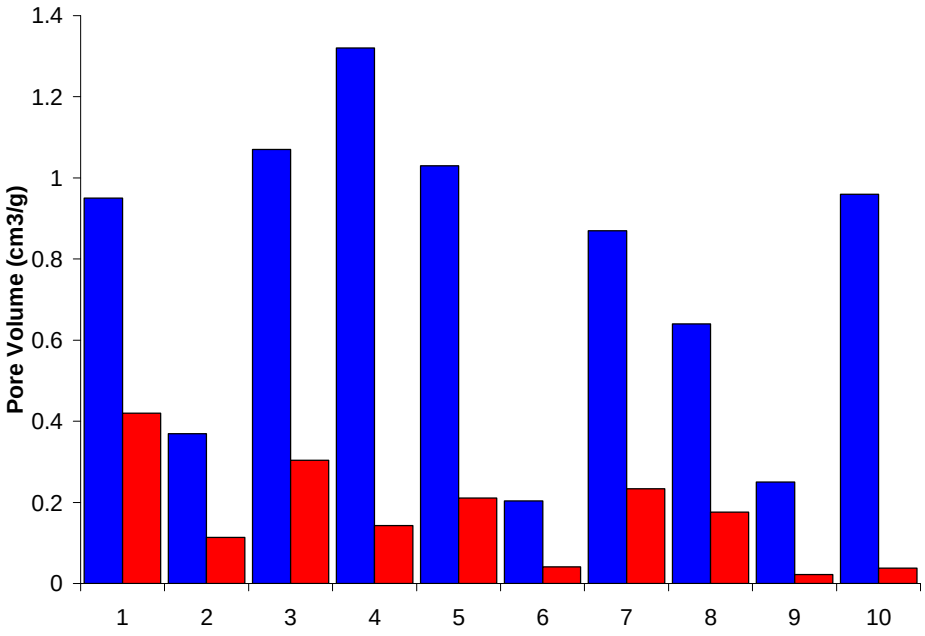

Figure 6.15 Pore volume before and after BSA loading,
1-KIT-6 med pore (cal) 2-KIT-6 large pore (as prep) 3-KIT-6 large pore (ex) 4-KIT-6 large pore (cal) 5-KIT-6 large pore 5%SH (Ex) 6-KIT-6 large pore 5%SH (as prep) 7-FDU-12 15-140 (cal) 8-FDU-12 15-140 5%SH (ex) 9-FDU-12 50-140 (cal) 10-FDU-12 50-140 5%SH (Ex)

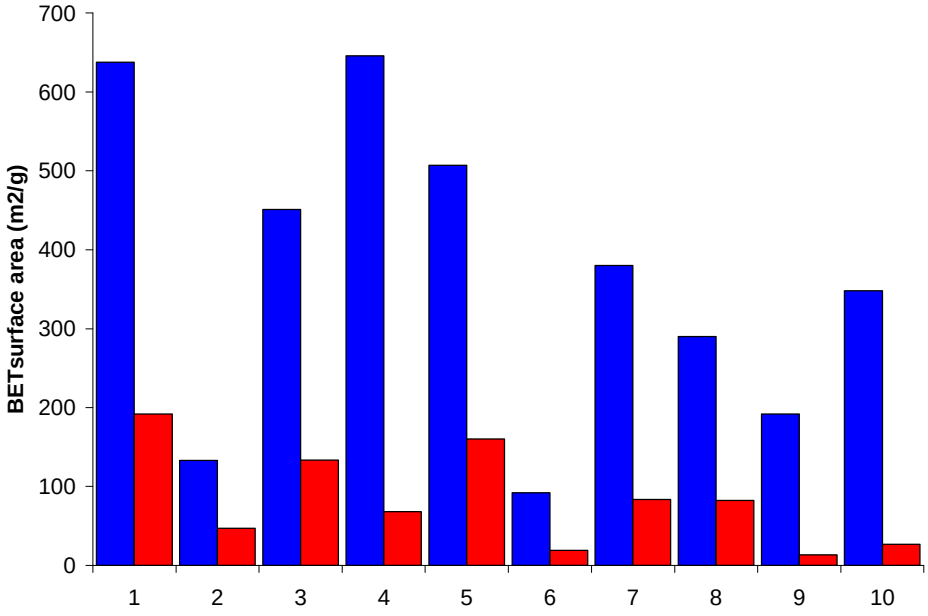

Figure 6.16 BET surface area before and after BSA loading
1-KIT-6 med pore (cal) 2-KIT-6 large pore (as prep) 3-KIT-6 large pore (ex) 4-KIT-6 large pore (cal) 5-KIT-6 large pore 5%SH (Ex) 6-KIT-6 large pore 5%SH (as prep) 7-FDU-12 15-140 (cal) 8-FDU-12 15-140 5%SH (ex) 9-FDU-12 50-140 (cal) 10-FDU-12 50-140 5%SH (Ex)

Comparison of the adsorption isotherms before and after loading shows a major reduction in the available/accessible pore volume (to N_2). This could be due to complete blocking of some channels either by adsorption at the surface or in the channels for KIT-6, where for the calcined and extracted large pore KIT-6 isotherm shapes are the same before and after BSA loading. For the calcined large pore KIT-6 material the surface area shows a dramatic decrease after loading and a large drop in pore volume can be seen. The nitrogen adsorption isotherm of the material prior to loading (Figure 6.17) gives an uptake of over 800 cm^3/g and a sharp, steep capillary condensation between 0.7-0.8 P/P_o. A pore size of 8 nm is obtained from the adsorption branch of the isotherm. Once the BSA has been loaded and the samples dried in a vacuum oven, nitrogen adsorption gives a much lower uptake, less than 100 cm^3/g. A small hysteresis loop is observed at the same position and pore size is only seen to be reduced by 1 nm to 7 nm suggesting the structure remains intact.

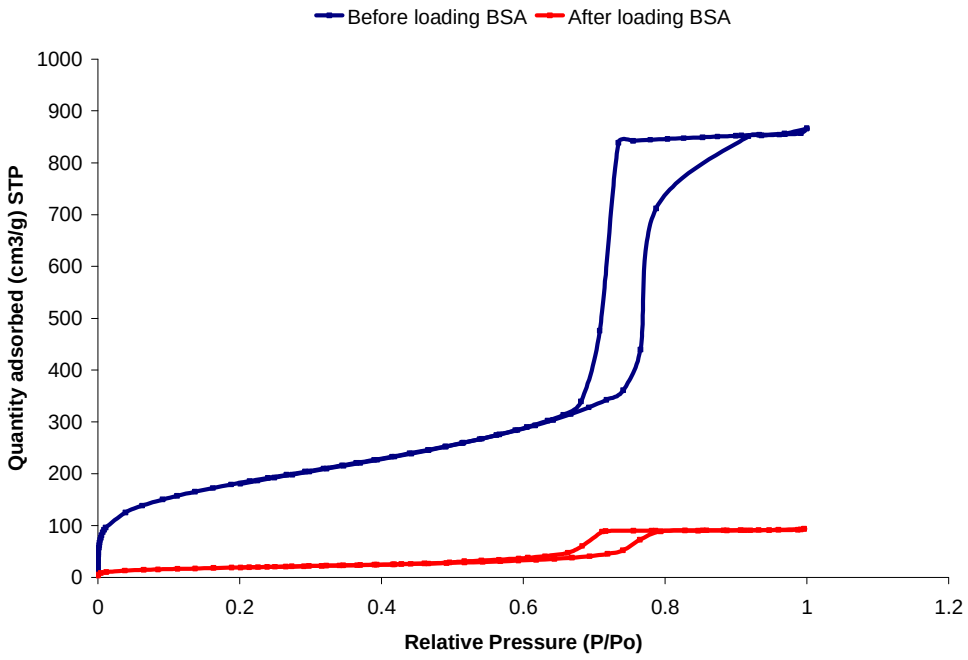

Figure 6.17 Isotherm of calcined large pore KIT-6 material before and after BSA loading

For an extracted large pore KIT-6 sample a similar trend can be followed but for this material not such a large decrease in surface area and pore volume is observed indicating a lower level of BSA uptake. The pore diameter is reduced by approx 1 nm and the nitrogen uptake decreases from 700 to 200 cm^3/g as seen in Figure 6.18.

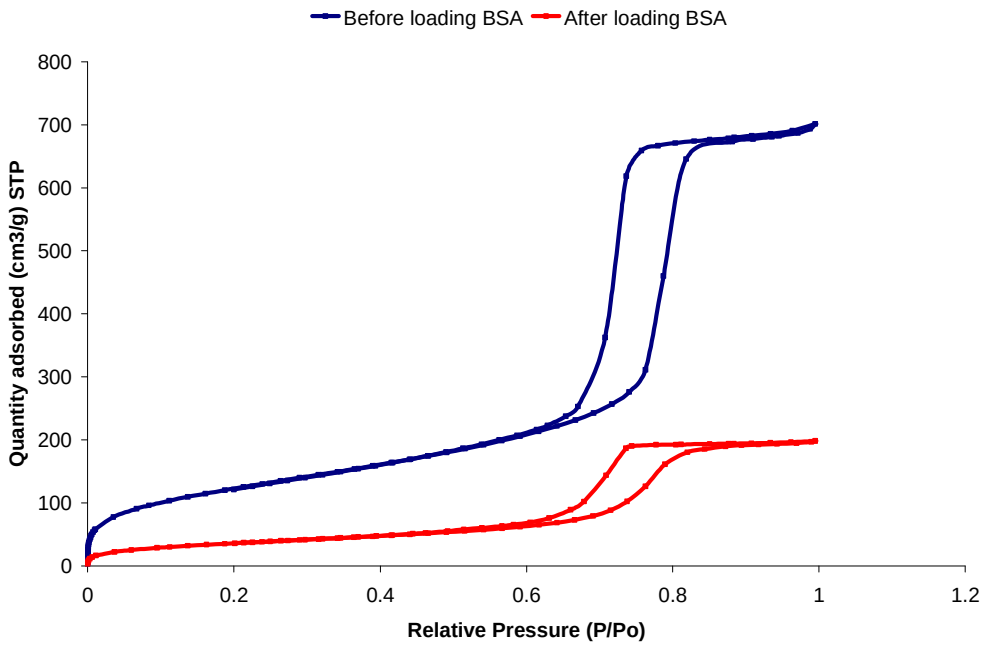

Figure 6.18 Isotherm of extracted large pore KIT-6 material before and after BSA loading

For functionalised KIT-6 the shape of the isotherm has changed (Figure 6.19), confirming that at least some of the BSA is definitely within the channels. A decrease in surface area, pore size and pore volume is also observed. Unlike previous samples, where the isotherm of BSA loaded samples have capillary condensation occurring in the same position, the isotherm seen in this case is much broader and occurs at a lower $P/P_{o,}$ indicating some reduction in channel dimensions.

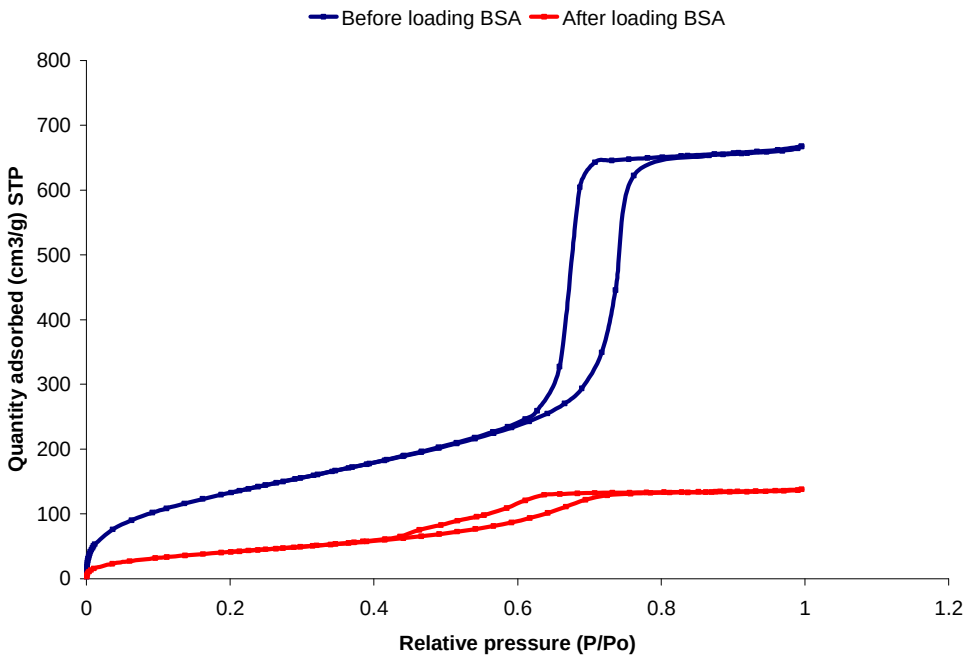

Figure 6.19 Isotherm of functionalised extracted (K130FEX) KIT-6 material before and after BSA loading

FDU-12 materials also exhibit reduced surface area and pore volume when loaded with BSA. For the FDU-12 15-140 material a reduction in surface area is observed and pore volume decreases. As seen in Figure 6.20 the isotherm for FDU-12 15-140 material is shown to have a reduced uptake of nitrogen when BSA is present within the material but the hysteresis loop is shown to occur at approximately the same position. It may be that much of the protein fills pores near the outer surfaces, leaving residual open space within the centre of the particles similar to unloaded samples.

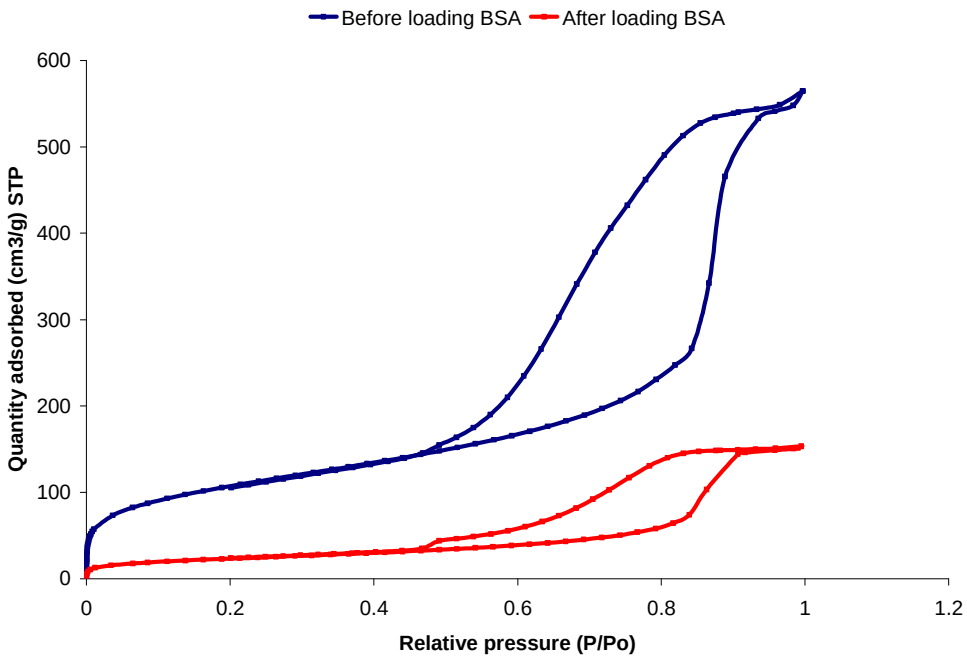

Figure 6.20 Isotherm of FDU-12 15-140 material before and after BSA loading

For the isotherm of functionalised extracted FDU-12 50-140 material, the isotherm of which shows the largest window size, the shape has strongly changed, confirming that BSA has entered the pores. Functionalised FDU-12 50-140 material has a very high uptake of BSA as seen by the disappearance of the hysteresis loop seen from the adsorption/desorption isotherm (Figure 6.20a). In particular the adsorption of nitrogen at higher partial pressures is strongly reduced.

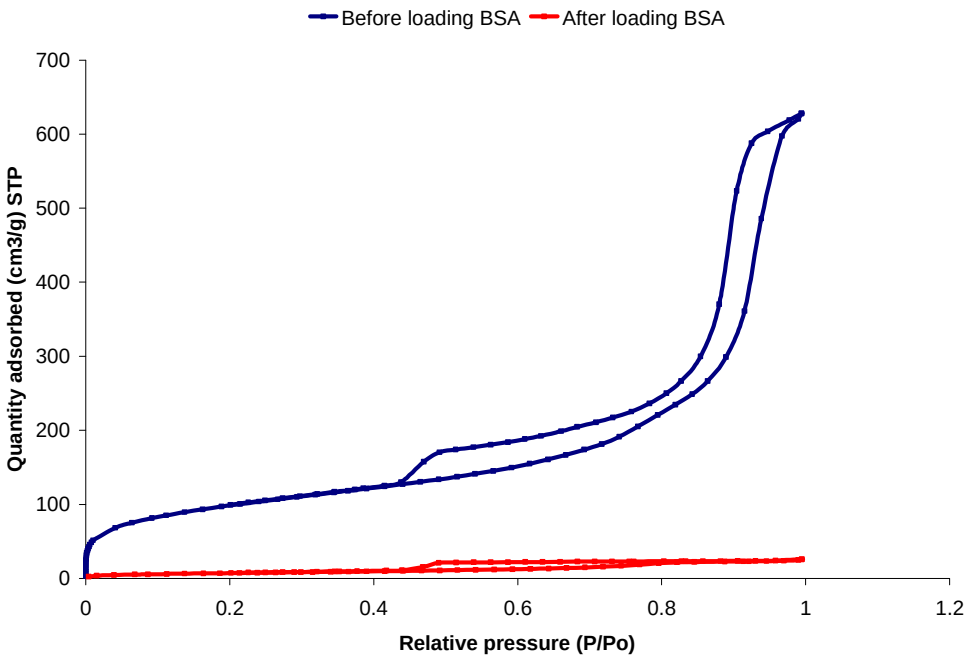

Figure 6.20a Isotherm of functionalised extracted FDU-12 50-140 material before and after BSA loading

6.4.2 Thermogravimetric Analysis - KIT-6

Thermogravimetric analysis was carried out on calcined and extracted samples of large pore KIT-6 both before and after BSA loading (Figure 6.21).

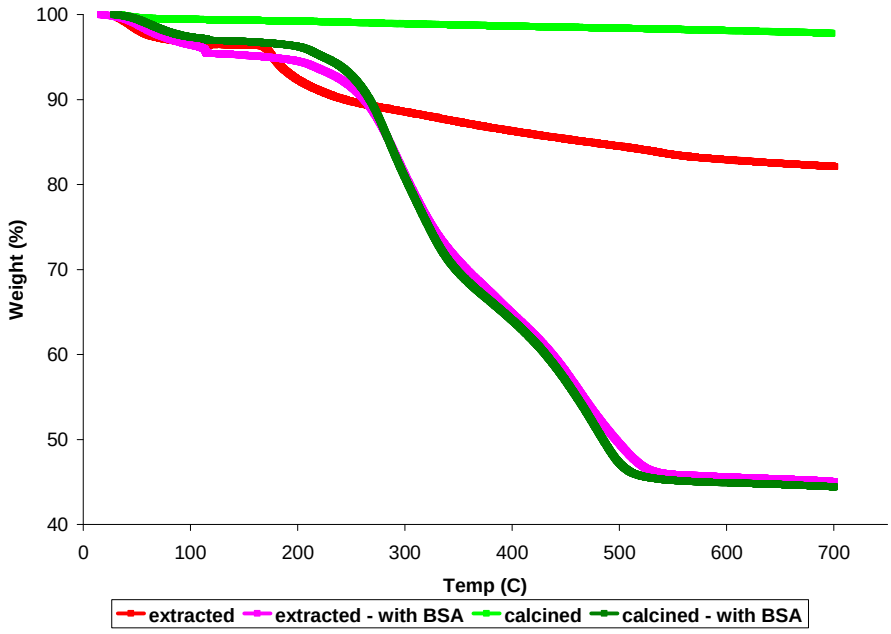

Figure 6.21 TGA trace for large pore KIT-6 samples (calcined, extracted) before and after BSA loading.

With the calcined material there is very little weight loss as the temperature is ramped up to 700 ^{o}C. After the loading of BSA there is a loss of 55% of the sample weight as the sample is heated from 250 ^{o}C to 500 ^{o}C, attributed to BSA loaded in the sample and solvent from the drug loading process. An extracted KIT-6 gives a total weight loss of 17% and after BSA loading a total of 55% of the weight of the sample is lost.

The as-prepared sample (Figure 6.22) exhibits a loss of 40% of the sample weight, which can be attributed to the decomposition and burning out of the surfactant. The majority of the weight loss is rapid and occurs between 150 and 200 ^{o}C, due to surfactant with a small loss due to the removal of the physically adsorbed water up to 150 ^{o}C. When the as-prepared material which has been loaded with BSA undergoes thermal analysis there is a small decrease in weight up to 200 ^{o}C followed by a gradual loss in weight between 200 and 500 ^{o}C. In the case of the BSA-loaded material an additional 15% by weight of the sample is lost compared to the as-prepared material before loading. The greater weight loss from the BSA-loaded material suggests that some of the BSA must be at the surface, because even if the surfactant were replaced by BSA, it would not be replaced by a larger amount (by weight). This is the same for all the KIT-6 as-prepared samples with added BSA.

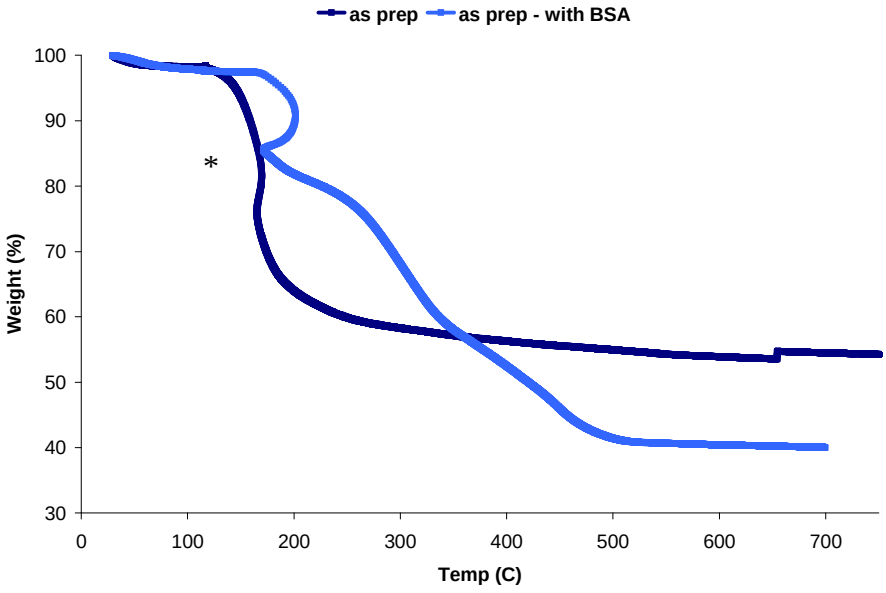

Figure 6.22 TGA trace for large pore KIT-6 samples (as prepared) before and after BSA loading. The reason for the section of the TGA indicated by '*' results from the heating rate being too fast to permit complete combustion of all the surfactant

The thiol-functionalised as-prepared material exhibits a very similar TGA trace (Figure 6.23) to the unfunctionalised as-prepared material with a sharp loss in weight between 150 and 200 ^{o}C prior to the BSA loading and a more gradual but greater loss in weight after the loading.

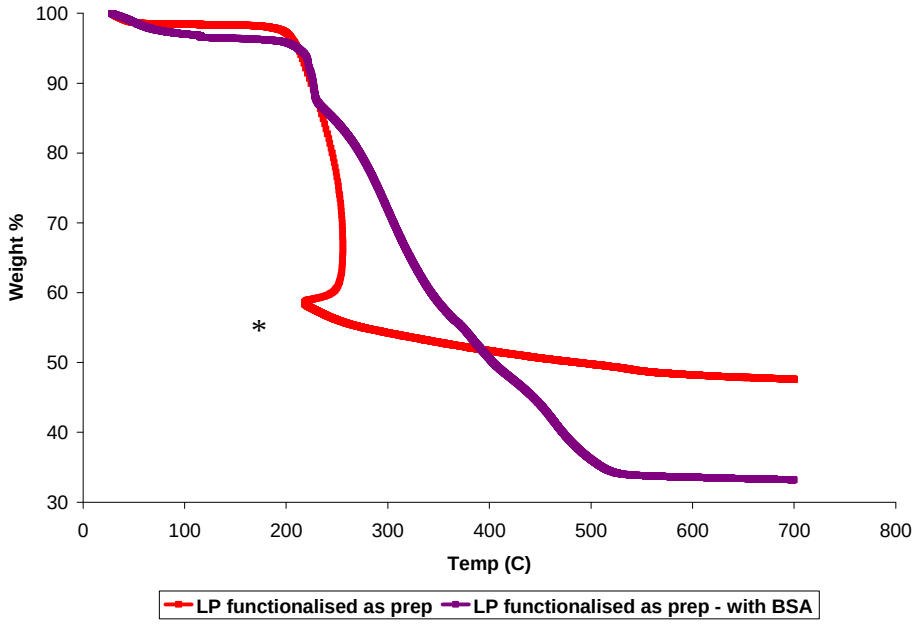

Figure 6.23 TGA trace for K130 functionalised KIT-6 samples (as prepared) before and after BSA loading. The reason for the section of the TGA indicated by '*' results from the heating rate being too fast to permit complete combustion of all the surfactant

TGA of the extracted, functionalised KIT-6 (Figure 6.24) shows that up to 20% of the sample weight is lost on heating to 700 ^{o}C indicating that surfactant remains and functional groups. Addition of BSA results in a slower and greater loss of weight.

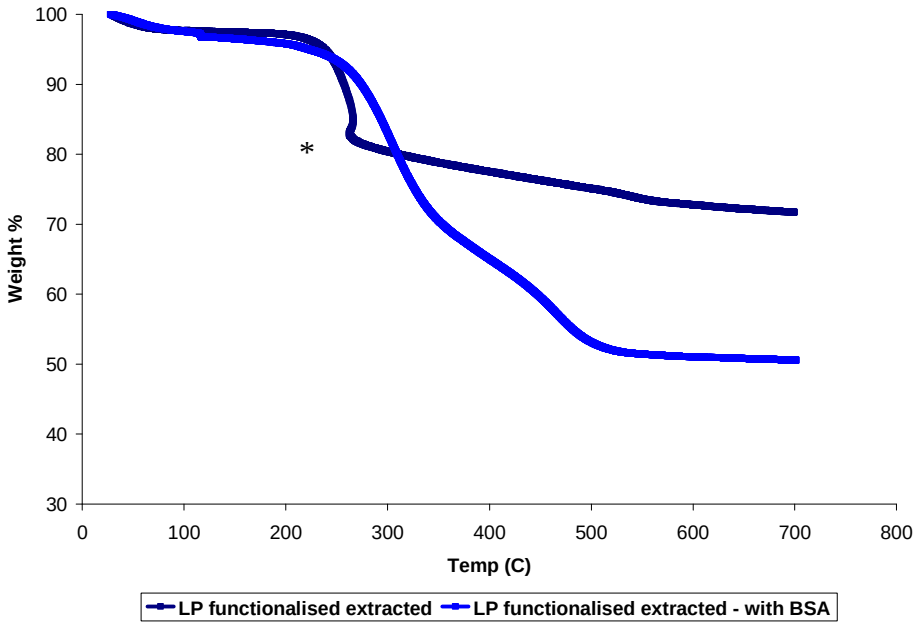

Figure 6.24 TGA trace for K130 functionalised KIT-6 samples (extracted) before and after BSA loading. The reason for the section of the TGA indicated by '*' results from the heating rate being too fast to permit complete combustion of all the surfactant

6.4.3 Thermal Gravimetric Analysis – FDU-12

The TGA traces of the 15-140 and 50-140 FDU-12 material with and without thiol are shown in Figures 6.25 and 6.26 respectively before and after BSA loading. In all cases the weight loss of the sample is greater after BSA loading with the 50-140 5%SH FDU-12 material showing the largest weight loss (60%) compared to the unfunctionalised 50-140 FDU-12 material which has a weight loss of 35% after BSA loading.

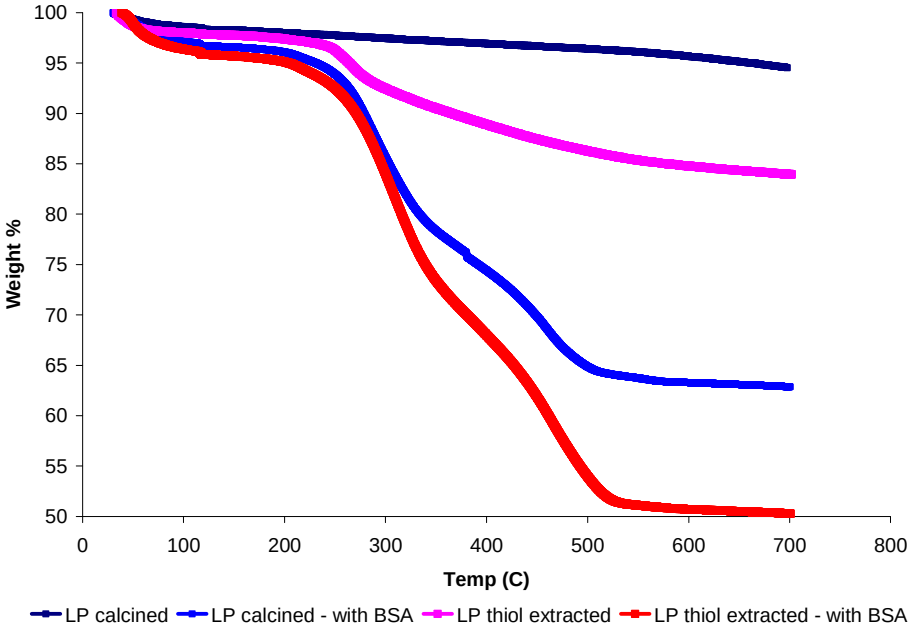

Figure 6.25 TGA FDU-12 15-140 material

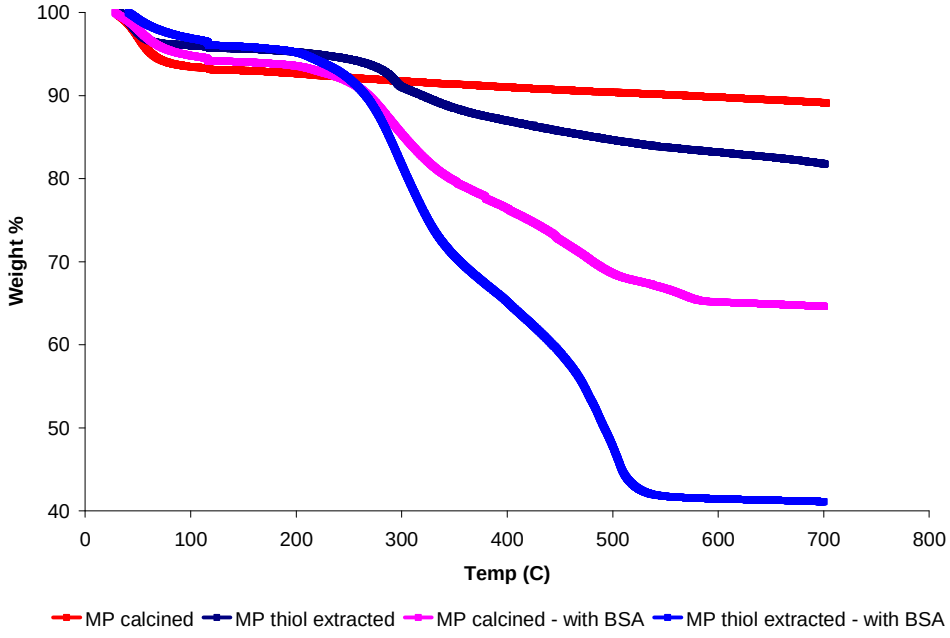

Figure 6.26 TGA FDU-12 50-140 materials

6.4.4 FTIR

The FTIR spectra of all KIT-6 samples show the presence of Si-O/Si-O(H) by a broad vibration band at 1000 cm^{-1}as shown in Figure 6.27. The spectra produced by the BSA loaded samples all indicate the presence of BSA by the appearance of additional peaks at 1500-1600 cm^{-1}, due to C=O and C-N bonds, expected at 1550-1650 and 1600 cm^{-1} respectively. The as-prepared sample both before and after BSA loading additional peaks are present at 2800 cm^{-1} this is the region that indicates the presence of C-H groups and is a result surfactant remaining within the structure. For extracted and calcined samples in which the surfactant has been removed these peaks are strongly reduced or are removed. There is also a suggestion that the C-H band due to surfactant is reduced upon BSA loading, suggesting that some removal of surfactant occurs.

The presence of BSA in the loaded samples was evaluated by TGA and elemental analysis and a combination of these was used to determine the % BSA present.

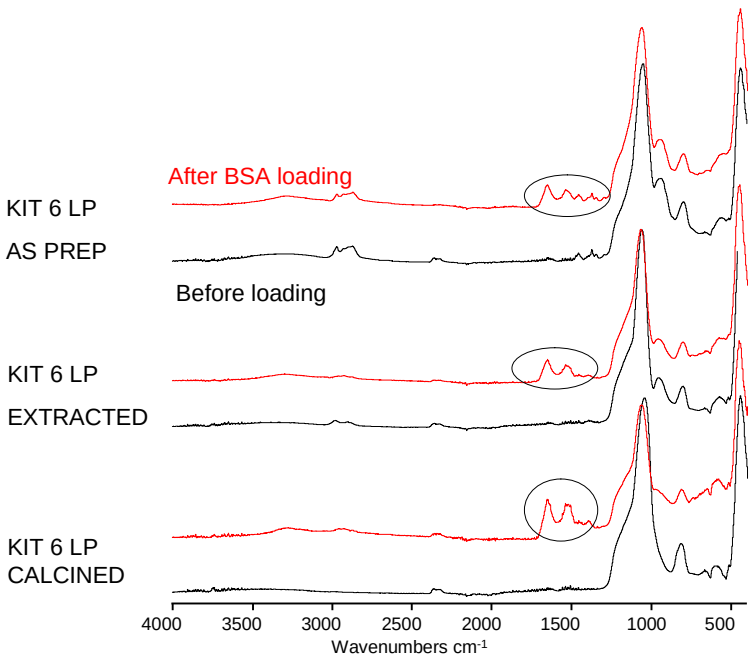

Figure 6.27 FTIR for KIT-6 materials before (black) and after (red) BSA loading

The FTIR spectra for the FDU-12 samples show very similar results with additional peaks at 1500-1600 cm^{-1} after the addition of BSA as shown in Figure 6.28. In the case of functionalised samples it is difficult to confirm the presence of sulfur groups within the

sample as the large peak at 1000-1200 cm^{-1} masks any peaks that would be visible. Therefore CHNS analysis must be used to confirm the presence of sulfur groups.

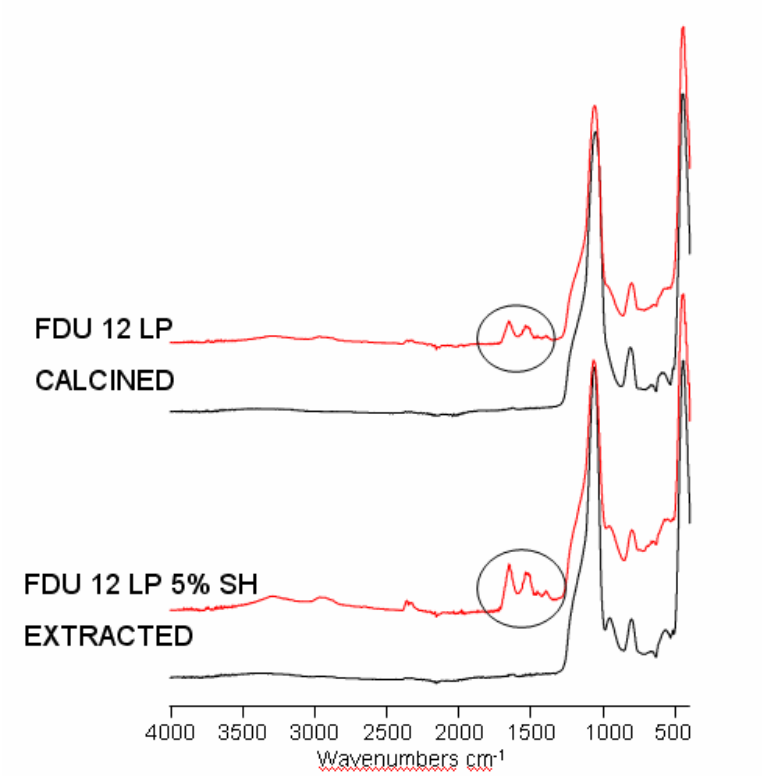

Figure 6.28 FTIR for 15-140 FDU-12 materials before (black) and after (red) BSA loading

6.4.5 CHNS

Analysis was performed on samples before and after BSA loading to determine the extent of loading (Table 6.3).

Table 6.3 CHNS results for materials before (black) and after (blue) BSA loading and also BSA

Sample	%C	%H	%N	%S	%C	%H	%N	%S
1. KIT-6 (100) - calcined		**0.31**			**15.35**	**2.98**	**4.69**	**0.47**
2. KIT-6 (130) - as prep	**23.95**	**4.57**			**30.74**	**5.05**	**4.07**	**0.46**
3. KIT-6 (130)- extracted	**5.73**	**1.94**			**24.50**	**3.86**	**6.82**	**0.76**
4. KIT-6 (130)- calcined		**0.38**			**25.17**	**4.04**	**7.80**	**0.84**
5. KIT-6 (130) 5%SH - ex	**12.45**	**2.98**		**1.34**	**21.19**	**3.72**	**3.98**	**1.68**
6. KIT-6 (130)5%SH – as prep	**28.33**	**5.13**		**1.06**	**33.84**	**5.52**	**4.63**	**1.26**
7. FDU-12 15-140 - calcined		**0.46**			**17.62**	**2.98**	**5.39**	**0.60**
8. FDU-12 15-140 SH -ex	**5.11**	**1.62**		**0.98**	**24.09**	**3.88**	**6.65**	**1.44**
9. FDU-12 50-140 - calcined	**0.18**	**1.27**			**14.10**	**2.73**	**4.35**	**0.47**
10. FDU-12 50-140 SH - ex	**6.18**	**1.88**		**1.53**	**26.76**	**4.33**	**7.39**	**1.86**
**** BSA**	**50.24**	**6.83**	**15.38**	**1.62**				

These data confirm that samples functionalised with thiol groups have sulfur present, prior to BSA loading. BSA contains sulfur-containing amino acids such as cysteine therefore by adding BSA to a material there will be an increase in the nitrogen and sulfur content. As seen in Table 6.3 none of the samples contain any nitrogen prior to BSA loading and so the increase in %N can be used to determine the quantity of BSA loaded, as the BSA will be the only source of nitrogen within the sample. CHNS confirms a much higher loading for the large pore KIT-6 materials which have been extracted and calcined and also the thiol extracted FDU-12 materials. By performing CHNS on a sample of BSA we can use the data to estimate the loading (in mg) of BSA on each sample as seen in Table 6.4.

Table 6.4 Loading of BSA on each sample

Sample	BSA loading (mg per 100mg solid)
1. KIT-6 (100) - calcined	**30.04**
2. KIT-6 (130) - as prep	**22.79**
3. KIT-6 (130)- extracted	**42.89**
4. KIT-6 (130)- calcined	**50.91**
5. KIT-6 (130) 5%SH - ex	**21.43**
6. KIT-6 (130)5%SH – as prep	**17.83**
7. FDU-12 15-140 - calcined	**35.73**
8. FDU-12 15-140 SH -ex	**36.50**
9. FDU-12 50-140 - calcined	**28.35**
10. FDU-12 50-140 SH - ex	**36.51**

Pore size, functionalisation and method of surfactant removal have an effect on the BSA loading that can be achieved (Table 6.4). By comparing the effects of pore size, in the case of KIT-6 material, a calcined large pore (8 nm) material can take up 50 mg whereas the smaller pore material (6 nm) only has 30 mg of BSA present in a 100 mg sample. For the large pore KIT-6 sample which has been extracted a slightly lower BSA loading of 43 mg per 100 mg is observed, due to the slightly lower pore volume and decreased surface area. If the material has not been calcined or extracted so that most of the surfactant remains within the pores we see that there is still an uptake of BSA of 22% which can be attributed either to the adsorption of BSA onto the outer surface or by replacing surfactant in the loading step, as previously described. It is observed that even the as-prepared materials show some pore volume (Figure 6.15 and 6.16). In the ‘as-prepared’ form by adding thiol groups the BSA uptake is lowered to 18% from 22% but when this material is extracted to render the material porous a significant increase in BSA uptake is not seen. From nitrogen adsorption data the pore size of this material is seen to decrease from 8 nm to 6.5 nm and these additional functional groups may hinder the uptake of any protein within the pores.

On FDU-12 a different trend in BSA loading is observed. The FDU-12 15-140 calcined (entrance 8-12 nm) material shows a 36% loading of BSA. When this material is functionalised and extracted the loading remains almost identical, unlike the decrease seen with a functionalised KIT-6 sample. As the synthesis is changed to produce FDU-12 50-140 material a change in BSA uptake is observed with a slightly lower BSA uptake seen.

For the functionalised material, which has much larger cavities and entrance windows (20 and 12 nm respectively) an uptake of 36 mg/ 100 mg of solid is observed.

6.5 Summary

BSA has been loaded *via* solution onto 10 different mesoporous support materials. These materials are of two different cubic morphologies, KIT-6 – a bicontinuous channel material with 2 different pore networks and FDU-12 – a cage material consisting of large cavities connected by smaller entrance windows. These materials have a range of pore sizes, functional groups and have had the surfactant removed using different methods. Nitrogen adsorption and FTIR has been performed on materials before and after BSA loading to show qualitatively that BSA is present in all materials whilst TGA and CHNS analysis has been used to quantitatively determine the level of BSA loading on each material. Increasing the pore size of KIT-6 shows an increase in BSA loading whilst functionalising FDU-12 (both pore sizes) increases the loading of BSA, most noticeably in the FDU-12 50-140 functionalised material which has a large entrance window.

6.6 Drug release results

After the sample discs loaded with BSA were prepared they were suspended in a saline solution (0.9% NaCl solution buffered at physiological pH 7.4) and placed in an orbital oven at 37 ^{o}C to initiate the drug release. Samples of the solution were taken at selected times over a period of a week and tested for BSA concentration using HPLC. Figure 6.29 shows the BSA concentration (mg/mL) present in the saline solution at various times during the drug release for a selection of support materials. The same volume of saline solution (0.3 mL) was removed each time. A greater amount of BSA is released by the KIT-6 material shown here. In the following graphs the concentrations are normalised in terms of the quantity of BSA loaded on each material to enable the release behaviour of the different mesoporous supports to be compared more readily.

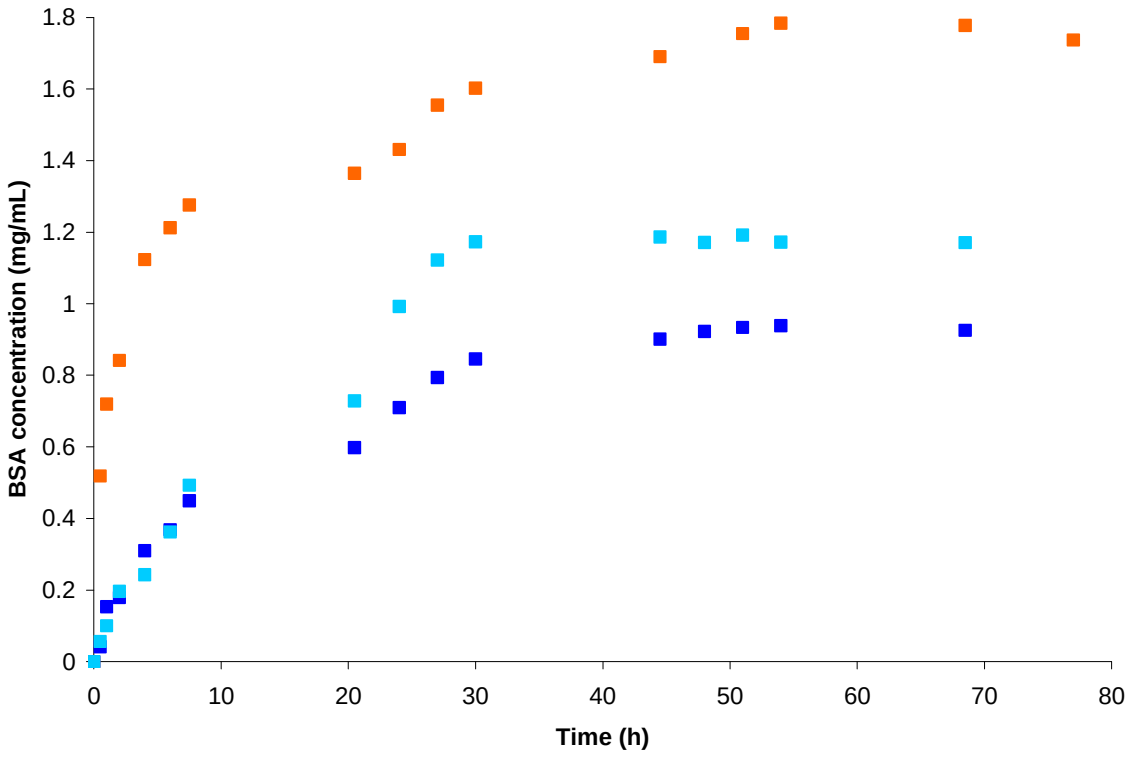

Fig 6.29 BSA concentration in saline solution as a function of time
KIT-6 130 (cal) FDU-12 15-140 (cal) FDU-12 15-140 5%SH (extracted)

The elemental analysis (CHNS) results were used to estimate the amount of BSA present in each sample so that BSA release normalised against the amount loaded can be plotted against time as shown in Figure 6.30.

(For some of the materials it appears that more BSA has been released into the saline solution than was thought to be loaded into the material which produces results indicating a greater than 100% release of BSA. It is possible that the low BSA concentrations of between 0 and 2 mg/mL obtained from HPLC results have a certain margin of error).

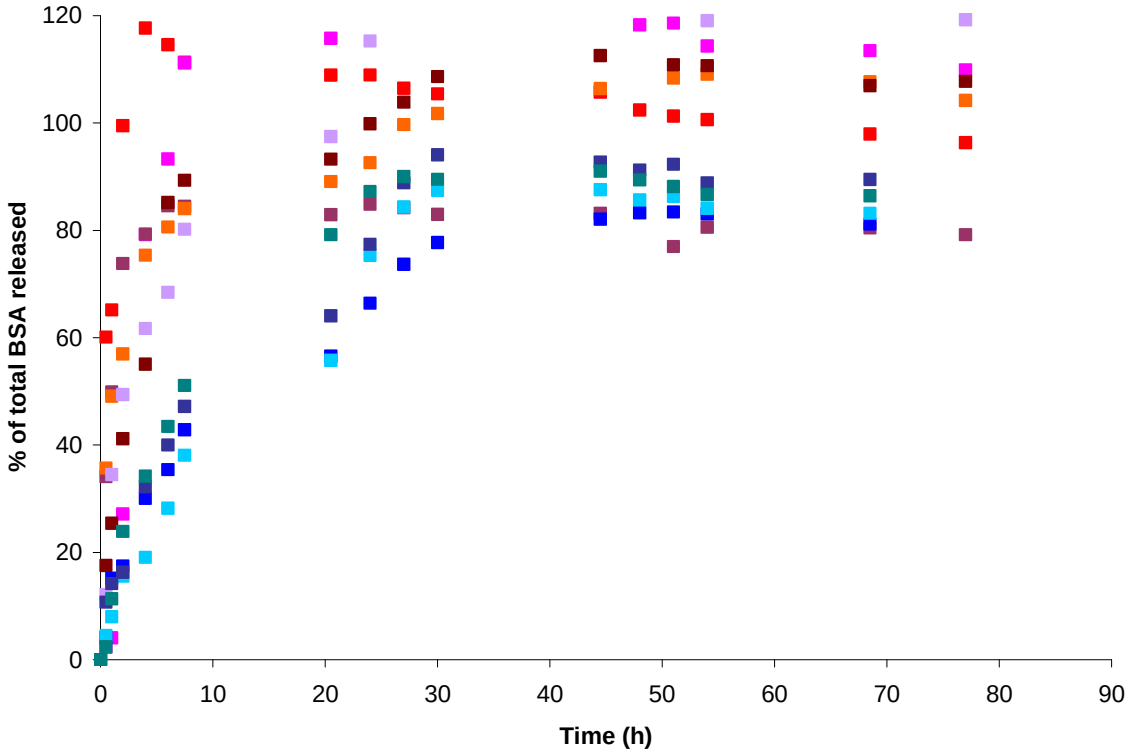

Figure 6.30 BSA release in terms of % loaded
1. KIT-6 100 (cal) 2. KIT-6 130 (as prep) 3. KIT-6 130 (ex) 4. KIT-6 130 (cal) 5. KIT-6 130 5%SH (Ex) 6. KIT-6 130 5%SH (as prep) 7. FDU-12 15-140 (cal) 8. FDU-12 15-140 5%SH (ex) 9. FDU-12 50-140 (cal) 10. FDU-12 50-140 5%SH (Ex)

All materials show release levels off by 30 hours as the maximum amount of BSA loaded has been released, followed by a steady level of BSA present in the SBF (Figure 6.30). The first 30 hours of release are shown in Figure 6.31. In the case of the KIT-6 type materials the materials exhibit a 'burst' profile where at least 80-90% of the adsorbed protein is released within the initial 5 hours of testing and the remaining adsorbed protein is linearly released up to the final level of release at 30 hours. This trend is observed for all KIT-6 materials regardless of functionality present or template removal method.

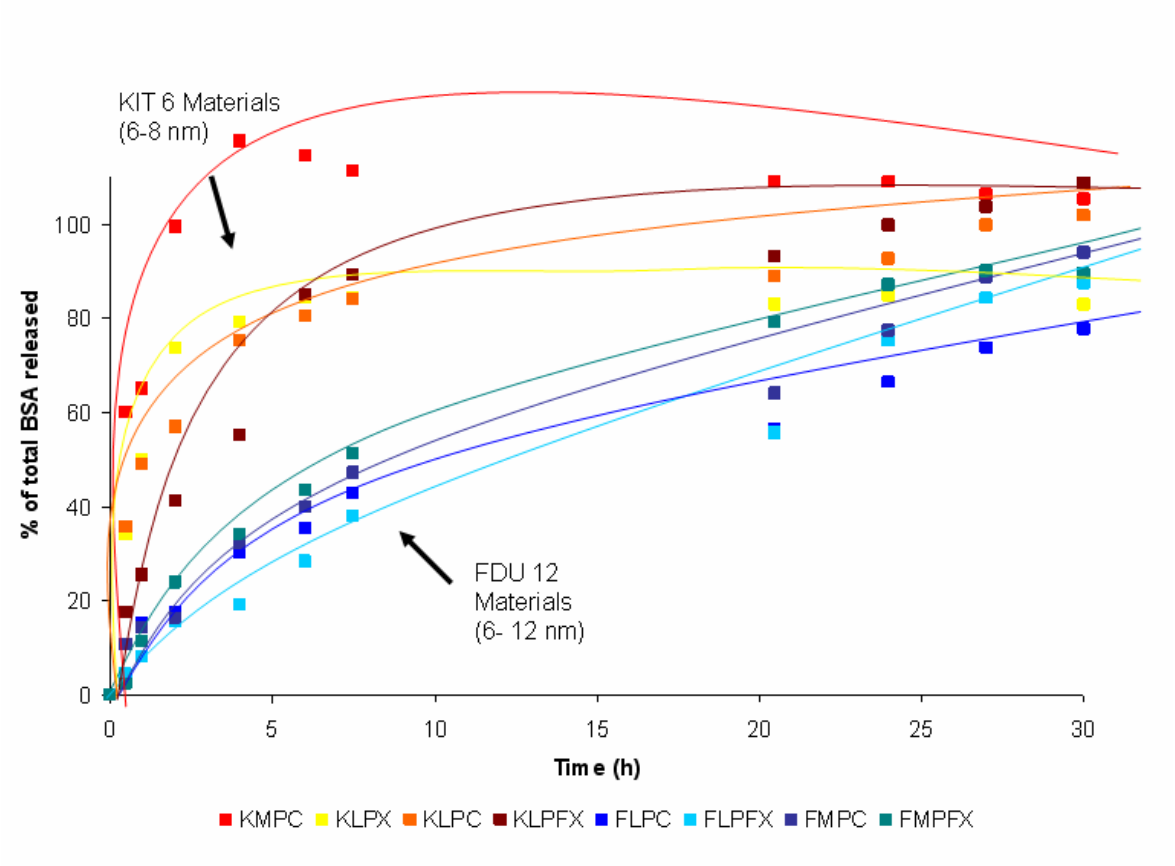

Figure 6.31 Release profile of all calcined and extracted materials
1. KIT-6 100 (cal) 3.KIT-6 130 (ex) 4. KIT-6 130 (cal) 5. KIT-6 130 5%SH (Ex) 7. FDU-12 15-140 (cal) 8. FDU-12 15-140 5%SH (ex) 9. FDU-12 50-140 (cal) 10. FDU-12 50-140 5%SH (Ex)

In contrast the FDU-12 type material shows a smaller initial burst with <35% of the adsorbed protein released after the first 5 hours followed by a linear release resulting in 75-95% of BSA release after 30 hours. In the case of FDU-12 materials a maximum release of 80-90% of adsorbed protein is achieved, even after 70 hours, which indicates that some of the protein remains trapped within the matrix. Again there appears to be no effect of thiol functionalisation in terms of slowing down the protein release.

The release profiles of the FDU-12 50-140 and KIT-6 100 sample are shown in Figure 6.32 where the different rates of drug release can be compared. Plotting the release of the materials on the same graph shows clearly the difference in the way the BSA is released into the simulated body fluid. The KIT-6 material releases 100% of the BSA loaded within the first few hours whereas it takes at least 30 hours for complete release of BSA from the FDU-12 material.

It is possible to conclude that the release is much slower from the FDU-12 materials than the KIT-6 materials. This is independent of template removal method or whether the material is functionalised or not. The pore structure has a strong influence on the release profile of the BSA and it is likely that the protein can become 'stuck' in the connecting windows between the cages of FDU-12.

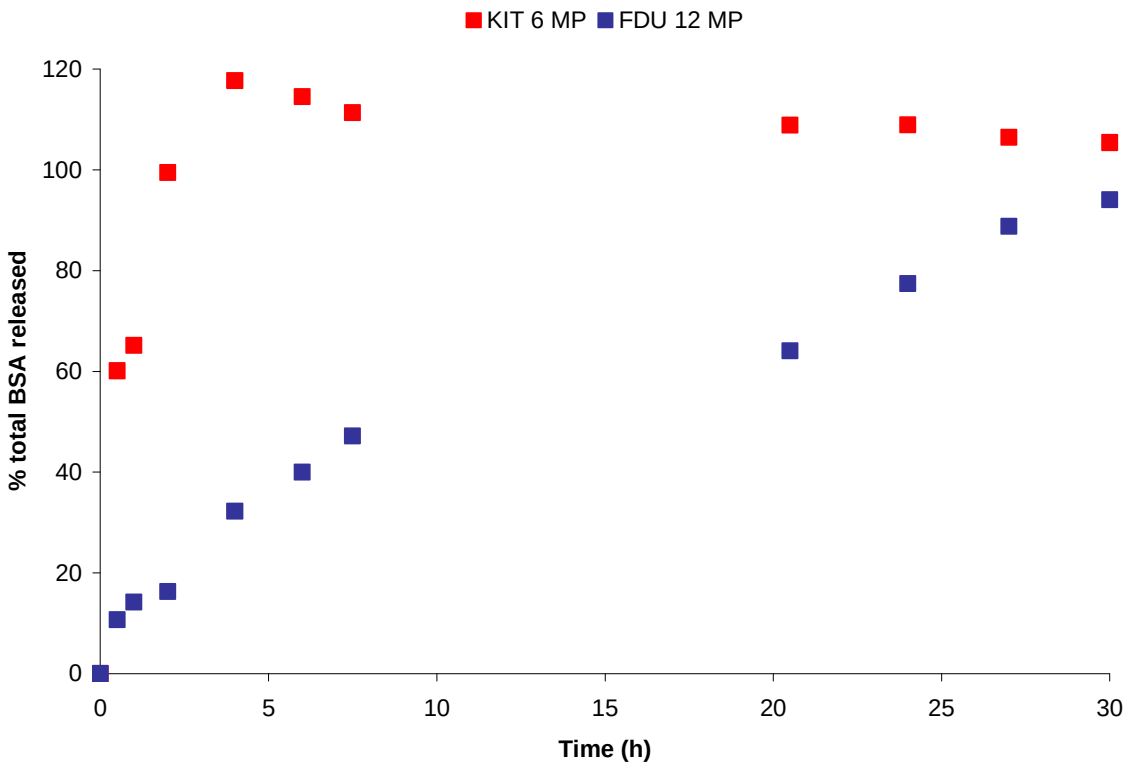

Fig 6.32 Comparing 50-140 FDU-12 and medium pore KIT-6

6.7 Conclusions

BSA has been loaded onto 10 different mesoporous support materials. These materials are of two different cubic morphologies, KIT-6 – a bicontinuous channel material with 2 different pore networks and FDU-12 – a cage material containing large cavities connected by smaller entrance windows. These materials have a range of pore sizes, functional groups and have had the surfactant removed using different methods. Nitrogen adsorption and FTIR has been performed on materials before and after BSA loading to show qualitatively that BSA is present in all materials whilst TGA and CHNS analysis has been used to quantitatively determine the level of BSA loading on each material. Increasing the pore size of KIT-6 shows an increase in BSA loading whilst functionalising FDU-12 (both pore sizes) increases the loading of BSA, possibly as functionalising the 'medium' pore material results in an increased pore size.

From the release profiles seen we can see there is a clear effect on the rate of release by the morphology of the support material. The channel materials (KIT-6 type) show a rapid release of BSA with most of the protein released within 5 hours whilst the FDU-12 material exhibits a more closely linear release over 30 hours. As KIT-6 possesses cylindrical channel systems there should be no change in the pore size throughout the whole materials. This results in the BSA being allowed to freely enter and exit the material without being trapped by smaller entrance windows. FDU-12 being a cage structure with large cavities connected by smaller windows does not have homogenous pore channels through out the material and the BSA takes longer to leave the material.
It is possible that the release of the BSA could be further slowed by incorporation of $–NH_2$ rather than thiol groups, which have little effect, despite the presence of sulfur in BSA.

6.8 References

[1] M. Vallet-Regí, A. Ramila, R.P. del Real, J. Perez-Pariente, *Chem. Mater*., 2001, **13**, 308

[2] M. Vallet-Regí, F. Balas, M. Colilla, M. Manzano, *Drug Metabolism Letters*, 2007, **1**, 37

[3] M. Vallet-Regí, L. Ruiz-Gonzalez, I. Izquierdo-Barba, J. M. Gonzalez-Calbet, *J. Mater. Chem*., 2006, **16**, 26

[4] M. Vallet-Regí, F. Balas, D. Arcos, *Angew. Chem. Int. Ed*., 2007, **46**, 7548

[5] M. Vallet-Regí, *Chem. Eur. J*., 2006, **12**, 5934

[6] M. Vallet-Regí, F. Balas, M. Colilla, M. Manzano, *Solid state sciences*, 2007, **9**, 768

[7] I. Izquierdo-Barba, A. Martinez, A.L. Doadrio, J. Perez-Pariente, M. Vallet-Regí, *European journal of pharmaceutics and biopharmaceutics*, 2005, **26**, 365

[8] J. Andersson, J. Rosenholm, S. Areva, M. Linden, *Chem. Mater*., 2004, **16**, 4160

[9] J.C. Doadrio, E.M.B. Sousa, I. Izquierdo-Barba, A.L. Doadrio, J. Perez-Pariente, M. Vallet-Regí, *J. Mater. Chem*., 2006, **16**, 462

[10] A.L. Doadrio, E.M.B. Sousa, J.C. Doadrio, , J. Perez-Pariente, I. Izquierdo-Barba, M. Vallet-Regí, *Journal of controlled release*, 2004, **97**, 125

[11] F. Balas , M. Manzano, P. Horcajada, M. Vallet-Regí, *J. Am. Chem. Soc*., 2006, **128**, 8116

[12] M. Vallet-Regí, J.C. Doadrio, A.L. Doadrio, I. Izquierdo-Barba, J. Perez-Pariente, *Solid state ionics*, 2004, **172**, 435

[13] M. Manzano, V. Aina, C.O. Arean, F. Balas, V. Cauda, M. Colilla, M.R. Delgado, M. Vallet-Regí, *Chemical engineering journal*, 2008, **137**, 30

[14] B. Munoz, A. Ramila, J. Perez-Pariente, I. Diaz, M. Vallet-Regí, *Chem. Mater*., 2003, **15**, 500

[15] S.W. Song, K. Hidajat, S. Kawi, *Langmuir*, 2005, **21**, 9568

[16]W. Zeng, X.F.Qian, J. Yin, Z.K. Zhu, *Mater. Chem. Phys*., 2006, **97**, 437

[17] W. Zeng, X.F.Qian, Y.B. Zhang, J. Yin, Z.K. Zhu, *Mater. Res. Bull*. 2005, **40**, 766

[18] J.L. Blin, C. Otjacques, G. Herrier, S. Bao-Lian, *Langmuir*, 2000, **16**, 4229

[19] M. Kruk, M. Jaroniec, A. Sayari, *Microporous mesoporous Mater*., 2000, **35**, 545

[20] E. Prouzet, T.J. Pinnavaia, *Angew. Chem*., 1997, **36**, 516

[21] P.J. Branton, J. Dougherty, J.W. White, G. Lockhart, *Characterisation porous solids IV*, 1997, **668**, 60

[22] T. Kimura, Y. Sugahara, K.J. Kuroda, *J. Chem. Soc. Chem. Commun*, 1998, **55**, 559

[23] B. Smarsley, S. Polarz, M. Antonietti, *J. Phys. Chem B.*, 2001, **105**, 10473

[24] K.M. Ryan, N.B. Coleman, D.M. Lyons, J.P. Hanrahan, T.R. Spalding, M.A. Morris, *Langmuir*, 2002, **18**, 4996

[25] M. Kruk, V. Antochshuk, M. Jaroniec, A. Sayari, *J. Phys. Chem B.*, 1999, **103**, 10670

[26] S.A. El-Safty, T. Hanaoka, F. Mizukami, *Chem. Mater*., 2005, **17**, 3137

[27] S. Sugio, A. Kashima, S. Mochizuki, M. Noda, K. Kobayashi, *Protein Eng*., 1999, **12**, 439

[28] Protein Data Bank PDB ID#1ao6 (http://www.rcsb.org/).

[29] M. Vallet-Regí, F. Balas, M. Colilla, M. Manzano, *Prog. Solid State Chem.*, **2007**, doi: 10.1016/j.progsolidstchem.2007.10.002

[30] J. Fan, C. Yu, J. Lei, Q. Zhang, T. Li, B. Tu, W. Zhou, D. Zhao, *J. Am. Chem. Soc*., 2005, **127**, 10794

7. General Conclusions and Outlook

7.1 General Conclusions

The synthesis of a range of mesoporous silicas has been achieved and the materials characterised via microscopy, nitrogen adsorption measurements, diffraction, TGA and elemental analysis. Materials of unusual morphology including branched and 'onion ring' particles were synthesised along with mesoporous materials with hexagonal symmetry p6mm and cubic materials with Ia-3d and Fm3m symmetry.

The pore size of the cubic Ia-3d material was increased by utilising a greater hydrothermal treatment temperature and these materials were successfully functionalised using mercaptopropyltriethoxysilane.

A low temperature method published during the course of this thesis was used to synthesise the mesocage FDU-12 with larger cavities and entrance windows both with and without the *in situ* co condensation of propyl thiol siloxanes.

Two FDU-12 materials of different entrance window size were selected for protein adsorption using a range of proteins spanning 17 to 160 kDa. From these results the size of the protein adsorbed onto the support material and the pore diameter of the support material itself were shown to have an effect on the ability to adsorb the protein and the speed at which this occurs. The entrance window of the support material must be at least the size of the protein to allow complete uptake within the pores.

Within 240 hours the large pore material, of entrance size 6 to 12 nm, is able to adsorb the smaller 4 proteins (myoglobin, CALB, BSA and β –Galactosidase) completely, even at higher concentrations, whereas the small pore material is only able to adsorb 100% of the smallest protein offered (myoglobin) and then only at lower protein concentrations (0.02 – 0.06 g/g).

These mesoporous materials provide suitable support materials for the immobilisation of CALB with relatively fast uptake of enzyme and varying capacities according to the pore structure. The enzyme is thought to be immobilised within the pore system, rather than on the surface, by comparison with the much lower uptakes of CALB by as-prepared materials.

The immobilisation behaviour of CALB on calcined and extracted SBA-15 is similar. The calcined material shows highly efficient uptake of up to 45 mg/g. In the case of KIT 6 material we see that adding propyl thiol groups to the large pore material reduces the uptake of CALB, possibly due to the resulting decrease in pore size from the addition of functional groups to the pore walls. With the FDU-12 cage materials we observe that the addition of thiol actually increases the maximum uptake of CALB.

Immobilised CALB is highly active for the enantioselective acylation of (R)-1-phenylethanol to (R)-1-phenylethyl acetate, without loss of selectivity upon binding. The activity of CALB immobilised within mesoporous silica shows a significantly higher activity when compared to free enzyme.

By increasing the CALB loading on all support materials a faster conversion of (R)-1-phenylethanol to (R)-1-phenylethyl acetate is observed. At a low CALB loading of 10 mg/g a significant difference in the conversion obtained after 30 minutes by changing the support material is observed. CALB on standard SBA-15 is seen to show the lowest initial conversion rate and by changing the morphology of the support from a cylindrical pore system to a cubic material an increase in conversion after 30 minutes for both FDU-12 and KIT-6 is observed. If these two cubic materials are functionalised with 5 mol % thiol an even greater increase in initial conversion is seen. This increase could either be due to the thiol groups on the pore walls which bind to the enzyme ensuring a good distribution throughout the channel allowing the reaction to take place faster or it may be that extracting the material leads to incorporation of hydrophobic groups which improve the rate of substrate diffusion through the support. A more detailed chemical engineering study is required to determine the full effects of transport, diffusion and loading.

BSA was loaded onto 10 different mesoporous support materials of two different cubic morphologies, KIT-6 – a bicontinuous channel material with 2 different pore networks and FDU-12 – a cage materials consisting of large cavities connected by smaller entrance windows. Increasing the pore size of KIT-6 shows an increase in BSA loading whilst functionalising FDU-12 (both pore sizes) increases the loading of BSA.

The release of the BSA into a simulated body fluid can be followed and there is a clear effect on the rate of release by the morphology of the support material. The channel materials (KIT-6 type) show a rapid release of BSA in the first few hours with most of the

BSA released within 7 hours whilst the FDU-12 materials all exhibit an initial burst followed by a linear release over 30 hours. As KIT-6 consists of a series of two cylindrical channel systems there should be no change in the pore size throughout the whole materials. This results in the BSA being allowed to freely enter and exit the material without being trapped by smaller entrance windows. FDU-12 being a cage structure with large cavities connected by smaller windows does not have homogenous pore channels throughout the material and this is possibly why the BSA takes longer to leave the material.

7.2 Outlook

The studies described here, and those documented in recent literature, have proved that mesoporous solids provide suitable supports for the uptake and release of proteins with advantages over amorphous silicas. Future studies will aim to develop these materials as multifunctional enzyme-bearing hosts for catalysis and to understand in detail the roles of diffusion, adsorption and reaction at the active site. For drug delivery, the requirement will be to tailor pore morphology, particle size and surface properties for specific applications.